NUCLEAR ENERGY RESEARCH INITIATIVE

U.S. Department of Energy – Nuclear Energy Research Initiative
Award No. DE-FC07-06ID14737
Project No. 06-058

Engineered Materials for Cesium and Strontium Storage

Final Technical Report

2006 to 2009

April 14, 2010

Contact: Dr. Sean M. McDeavitt
Texas A&M University
Department of Nuclear Engineering
Look College of Engineering
3133 TAMU
College Station, TX 77843-3133
(979) 862–1745 (Phone) (979) 845–6443 (FAX)
mcdeavitt@tamu.edu

Overview

Closing the nuclear fuel cycle requires reprocessing spent fuel to recover the long-lived components that still have useful energy content while immobilizing the remnant waste fission products in stable forms. At the genesis of this project, next generation spent fuel reprocessing methods were being developed as part of the U.S. Department of Energy's Advanced Fuel Cycle Initiative. Oee of these processes was focused on solvent extraction schemes to isolate cesium (Cs) and strontium (Sr) from spent nuclear fuel [1-3]. Isolating these isotopes for short-term decay storage eases the design requirements for long-term repository disposal; a significant amount of the radiation and decay heat in fission product waste comes from Cs-137 and Sr-90. For the purposes of this project, the Fission Product Extraction (FPEX) process is being considered to be the baseline extraction method.

The objective of this project was to evaluate the nature and behavior of candidate materials for cesium and strontium immobilization; this will include assessments with minor additions of yttrium, barium, and rubidium in these materials. More specifically, the proposed research achieved the following objectives (as stated in the original proposal):

1) Synthesize simulated storage ceramics for Cs and Sr using an existing lab-scale steam reformer at Purdue University. The simulated storage materials will include aluminosilicates, zirconates and other stable ceramics with the potential for high Cs and Sr loading.
2) Characterize the immobilization performance, phase structure, thermal properties and stability of the simulated storage ceramics. The ceramic products will be stable oxide powders and will be characterized to quantify their leach resistance, phase structure, and thermophysical properties.

The research progressed in two stages. First, a steam reforming process was used to generate candidate Cs/Sr storage materials for characterization. This portion of the research was carried out at Purdue University and is detailed in Appendix A. Steam reforming proved to be too rigorous for efficient The second stage of this project was carried out at Texas A&M University and is Detailed in Appendix B. In this stage, a gentler ceramic synthesis process using Cs and Sr loaded kaolinite and bentonite clays was developed in collaboration with Dr. M. Kaminski at Argonne National Laboratory.

The detailed research reports are attached as Appendices to this report. These include an MSNE thesis from Purdue University (Appendix A) and a PhD thesis from Texas A&M University. A brief summary of the results is provided below as well.

Research Summary

Steam Reforming Experiments: Aqueous precursor solutions containing cesium and strontium nitrates ($CsNO_3$ and $Sr(NO_3)_2$) were combined with solid powder reactants (e.g., kaolin ($Al_2Si_2O_5(OH)_4$), carbon, and titanium oxide). In the first year of this project, steam reforming produced cesium aluminosilicate ($CsAlSi_2O_4$) and strontium carbonate ($SrCO_3$) as stable reaction products but only a fraction of the Cs and Sr reagents were actually immobilized in the final ceramic product. This was due, in part, to the high flow rate of steam and the short residence time of the reagents through the process vessel.

The final experiments were performed using a modified scheme that relied on reactions between H_2O and various solid reagents but the internal energy of the system was reduced by switching to a low flow rate argon cover gas along with a low-flow systaltic pump to inject Cs and Sr bearing solutions. Vaporized water from the feed solution provided the requisite oxygen and hydrogen to the synthesis reactions. The system was used to synthesize cesium aluminosilicate ($CsAlSi_2O_4$) and strontium carbonate ($SrCO_3$) but the effectiveness was poor. Some experiments produced negligible reaction products and unreacted strontium nitrate was frequently observed in the product. Further, in the final tests with titanium oxide, it became clear that the system was not able to synthesize titanate and zirconate ceramics without going to much higher temperatures. In the end, the steam reforming option was set aside due to poor efficiency in the high energy system and ineffective conversion in the low energy system.

Clay-Loading/Sintering Experiments: A new strategy for waste form synthesis was developed in conjunction with ANL during a summer internship in 2008. In this method, nitrate solutions containing cesium, strontium, barium and rubidium based on the expected FPEX effluent concentrations are loaded into aluminosilicate clays and converted into ceramic pellets via high temperature sintering. The simulated waste solution is prepared with the concentrations of Cs, Sr, Ba, and Rb increased to their solubility limit to minimize volume. The simulated waste solution is mixed with the clay to produce a slurry that is heated at low temperature and dried into a waste loaded powder. This powder is pressed into a pellet and sintered to produce a solid pellet.

The variables being explored include the type of clay, the waste loading of the solution (and thus the final waste form), and the sintering time and temperature. Experiments were performed using (1) bentonite clay loaded with a simulated waste solution and (2) kaolin clay loaded with dry nitrate salts. The sintering temperatures were varied from 1100 to 1400 °C and the waste concentrations varied from 18 to 30 mass percent Cs, Sr, Ba, Rb. In the initial experiments it was observed that the kaolin samples expand and crack extensively upon sintering when loaded with dry nitrates. Further, the bentonite samples densify into a strong monolith upon sintering between 1100°C and 1300°C; sintering at 1400°C caused local melting and vitrification. These initial tests with bentonite revealed that higher temperatures (i.e., 1300°C) produced higher densities but that there was also significant in mass loss during sintering above 1200°C. Therefore, the current focus of our research is to optimize the waste loading and sintering conditions to minimize mass loss while achieveing high density.

The simulated waste stream was prepared using a dilute nitric acid solution containing non-radioactive cesium and strontium introduced into the solution by dissolving nitrate salts. Rubidium and barium were also added because they are likely components of the waste stream due to their similar chemical behavior. The simulated waste solution was mixed with the natural mineral bentonite, which was previously proposed as a nuclear waste immobilization matrix [4]. Bentonite clay was loaded with waste ions in concentrations ranging from approximately 16 mass percent to 32 mass percent total waste ions. The simulated liquid waste was added to the clay to the desired concentration and the slurry was dried to a powder. The powder was pressed into a pellet and sintered at temperatures ranging from 700°C to 1400°C. Because of the known behavior of aluminosilcates, the anticipated products were alkaline earth feldspars and pollucites

of cesium and rubidium. Pollucite is an aluminosilicate which has been considered as a Cs-137 waste form material [5].

The simulated waste solution was prepared by mixing dilute nitric acid with nitrate salts of cesium, strontium, barium, and rubidium. The metal ion ratios were chosen to mimic the Department of Energy's proposed Fission Product Extraction (FPEX) process stream [6]. The nitrate concentration in the simulated waste solution was increased to the point of saturation in order to minimize the volume of liquid required to load the clay. The molar amounts in solution were 0.054M Ba, 0.061M Cs, 0.033M Sr, and 0.015M Rb which corresponds to a solution concentration ~2.5 times higher than the expected FPEX product stream. The addition of the ions in aqueous form was selected to simulate a wet clay loading process. Liquid simulated waste addition and drying was repeated until the desired waste ion concentration was reached. The dry powders were then crushed, homogenized, and pressed to ~45 MPa, and sintered with a heating rate of 5°C per minute and a 12 hour hold at the sintering temperature.

Differential Scanning Calorimetry (DSC) Data

Differential Scanning Calorimetry (DSC) analyses with in situ mass loss measurements were completed using loaded but unsintered bentonite clay powders. The sintered samples noted above displayed some mass loss during densification which was consistent with the loss of water and nitrates from the loaded clay structure. The DSC measurements confirmed this phenomenon. The object is to determine a threshold temperature below which the waste elements will not be appreciably expelled from the clay as it sinters. As part of this effort, neutron activation analysis was used to quantify the concentrations of waste elements in the final monoliths and transmission electron microscopy will be used to assess structure and overall uniformity of the proposed waste material.

Samples of the loaded-but-unsintered bentonite clay were heated to observe mass changes and heat evolution up to 1450°C with a Netzsch STA 409. The instrument performs simultaneous Thermo-Gravimetric Analysis (TGA) and Differential Scanning Calorimetry (DSC). Samples masses of 20 to 40 mg were loaded into a weighed alumina crucible, placed on the sensitive TGA balance (±40μg), and subjected to a controlled heating program under an argon cover gas. Figure 1 shows an example of the DSC/TGA data revealing transitions during heating. For each change in the rate of mass loss an endothermic/exothermic transition was visible in the DSC curve.

The initial endothermic peak in Fig. 1 coincides with the vaporization of loosely bound water which corresponds to a steep drop in mass, which is consistent with previously reported data [7]. The second endothermic reaction began at approximately 525°C. This coincides with the dehydroxylation mass loss (or, the removal of structural water from the crystalline system), which was also previously observed in cation loaded bentonite [8]. After this, a gradual exothermic transition is notable until the DSC trace peaks between 800°C and 875°C. The final endothermic trend continued as the temperature increased (except in samples where bloating occurred) until melting.

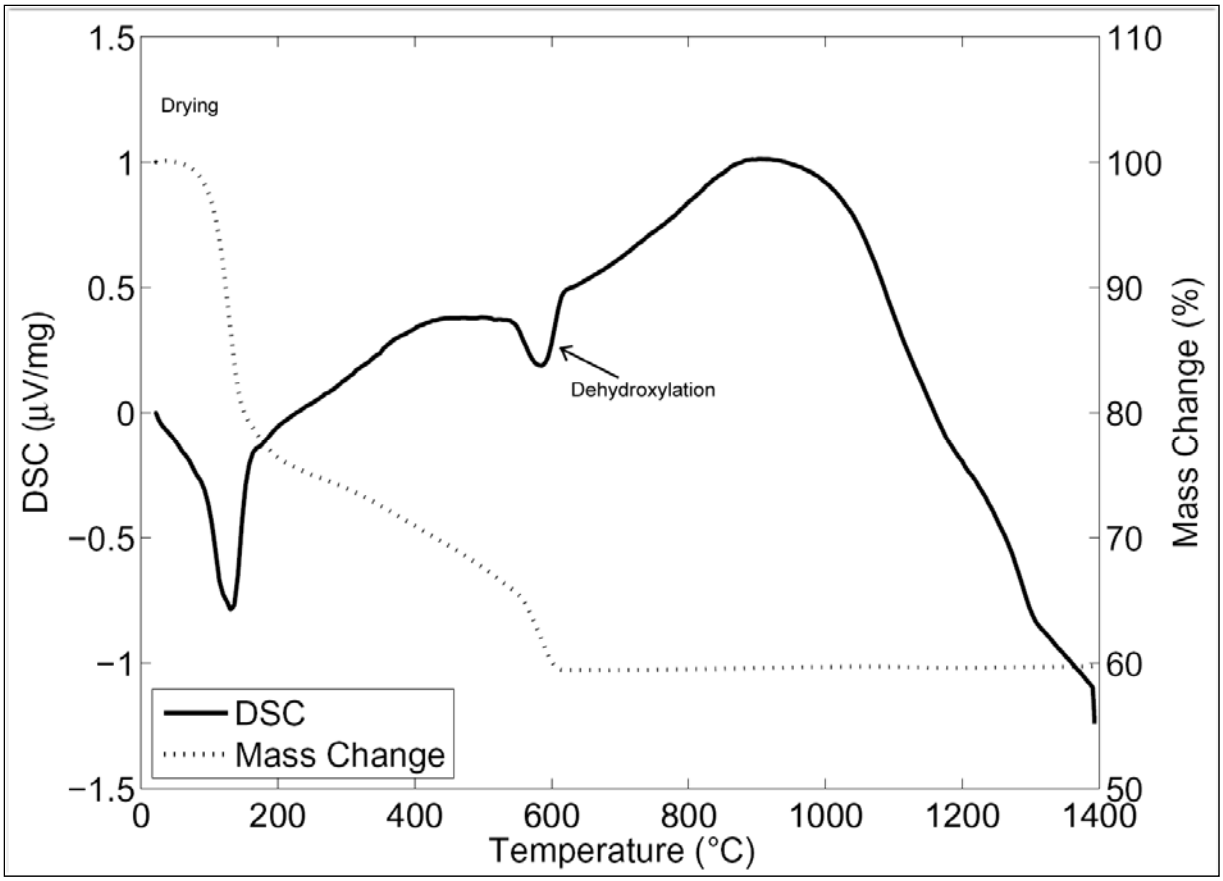

Figure 1. Percent mass change and heat flux vs. temperature for bentonite clay loaded with 22 wt% total waste ions (Cs, Sr, Ba, and Rb).

The mass loss traces quantified by the TGA data elucidate the meaning of the two DSC endotherms in that the major changes in mass loss rates are clearly related to the consumption of energy (such as a phase change), which is also consistent with the data seen for pure bentonite clay [7,9]. As noted above, each significant mass loss corresponds to the liberation of water bound within the structure to a different degree (dashed line Fig.1). The final mass loss occurred during dehydroxylation, at approximately 525°C. Balek found that after dehydroxylation the clay becomes an amorphous material, known as meta-montmorillonite [8]. Kaminski et al found the final release of nitrates also coincided with the release of dehydroxylation water [10].

X-ray Diffraction Data

Crushed samples of the sintered ceramic products were prepared for X-Ray Diffraction (XRD) analysis. The powder size and morphology was certified using a calibrated Hirox optical microscope (Model KH 1300). The XRD equipment used was a Bruker-AXS Advanced Bragg Brentano X-Ray Powder Diffractometer, with a D8 Goniometer (Texas A&M University Chemistry Department). Samples were analyzed with copper radiation at 40 kV and 40 mA, with a step size of 0.015 degrees (2θ), and a scan speed of 0.1 seconds per step. Representative data from samples containing 32 wt% total waste ions and sintered at 700°C, 800°C, 1000°C, and 1200°C are shown in Fig. 2.

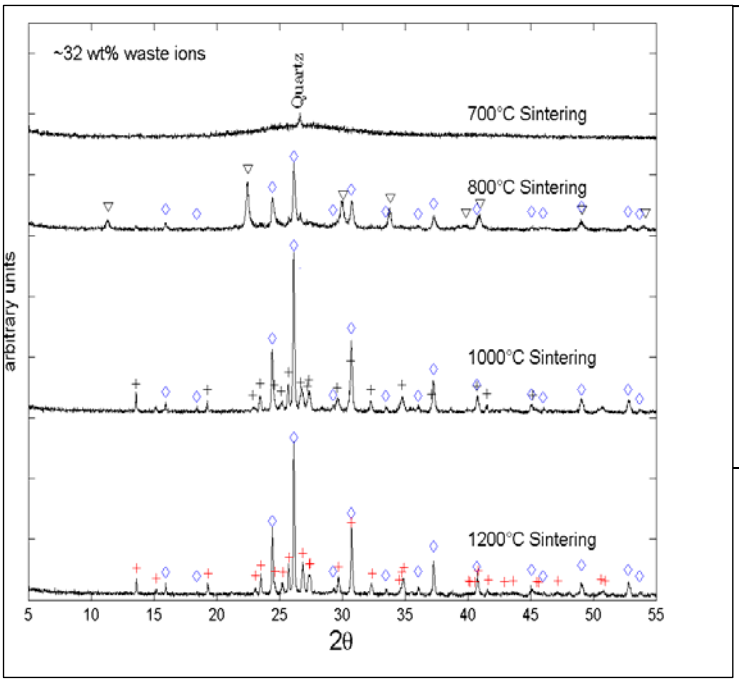

▽ refers to barium aluminum silicate $Ba(Al_2Si_2O_8)$ PDF 1-088-1048, a hexagonal barium feldspar; and ◊ refers to cesium aluminum silicate (pollucite) $CsAlSiO_4$ PDF 47-0471; + refers to barium strontium aluminum silicate $Ba_{.75}Sr_{.25}Al_2Si_2O_8$ PDF 38-1451, and + refers to barium strontium aluminum silicate $Ba_{0.5}Sr_{0.5}Al_2Si_2O_8$ PDF 38-1452.

Figure 2. X-ray Diffraction patterns from waste-loaded sintered bentonite at various temperatures(32 wt% total waste ions).

The data in Fig. 2 at 700°C shows an amorphous hump from 20 to 30 2θ with only the quartz impurity peak visible (top Figure 1), consistent with the observations above. The data in Fig. 2 at 800°C confirm the formation of the cesium aluminum silicate pollucite (CsAlSiO4) and a hexagonal barium feldspar (Ba(Al2Si2O8)). The data at temperatures at or above 1000°C no longer display the hexagonal feldspars, but the monoclinic forms were clearly evident. The transformation from a hexagonal layered structure, to the monoclinic three dimensional configuration required higher energy to enable restructuring, hence the higher sintering temperatures were necessary to development those phases. The XRD pattern attributed to pollucite increased in intensity with higher sintering temperature (Fig. 2). At 1000°C a high silica cesium aluminum silicate (Cs4Al4Si20O48) was detected but only in the sample with the lower, 22 wt% waste concentration (not shown). Monoclinic feldspars of barium and strontium were observed in samples sintered at 1000°C (i.e., Ba.75Sr.25Al2Si2O8 and Ba0.5Sr0.5Al2Si2O8). The data at 1200°C displayed only two obvious crystallization spectrums, pollucite and a 50:50 barium to strontium atom ratio monoclinic feldspar (Fig. 2).

Processing and Structural Observations

Sintering loaded bentonite powders at 700°C and 800°C created brick-like samples with open porosity and a multicolored brown-red appearance. These samples were brittle and easily pulverized. This is in contrast to samples generated at 1000°C and higher, where the product samples had less porosity and a uniform coloration and exhibited high toughness akin to glass and other solid ceramics. Sample densities were ~2 g/cm3 when sintered at 1000°C and densification reached a maximum level of ~3 g/cm3when the sintering temperatures were 1100°C. The endothermic heat flux above 1000°C seen in Fig. 1 connotes an energy consuming

reaction occurring, this is consistent viscous sintering, which is also consistent with the higher density and reduced porosity. At 1200°C, sintering caused the samples with lower waste loadings to slump and crack. When sintered at 1200°C the cesium had formed pollucite crystals, and the barium and strontium had formed lath shaped crystals up to 10 micrometers long (Figure 3). The lowest loading, 15 wt% waste ions, swelled and became a pumice-like foam material. At the 32 wt% ion loading the pellets were hard smooth and a uniform grey color. At the highest sintering temperature tested, 1400°C, the samples completely melted.

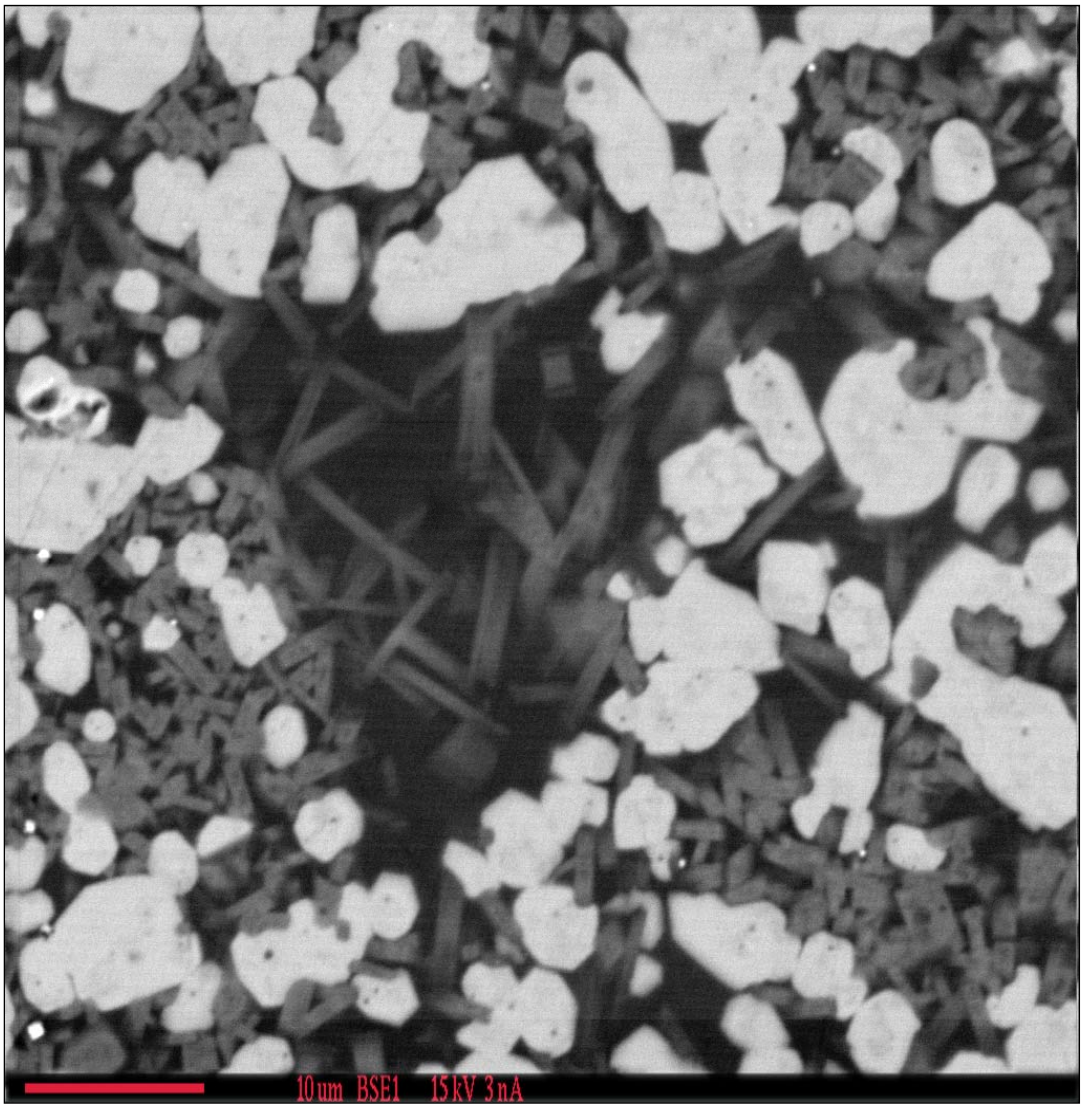

Figure 3. Backscattered electron image of bentonite sintered at 1200°C displaying three phases (bar = 10μm).

Final Comments

The information reported here represents selected highlights from the results of the final year of this project. The Appendices contain a more complete presentation of the processing methods developed and the behavior of this new waste form material. This NERI Project is complete, but the development of bentonite as a waste host may continue under future research funding.

REFERENCES

[1] T.A. Todd, T.A. Batcheller, J.D. Law, R.S. Herbst, Cesium and Strontium Separation Technologies Literature Review, in, Idaho National Engineering and Environmental Laboratory, 2004.

[2] C.W. Forsberg, Rethinking high-level waste disposal: Separate disposal of high-heat radionuclides (90Sr and 137Cs), Nuclear technology, 131 (2000) 252 - 268.

[3] C. Pereira, G.F. Vandegrift, M.C. Regalbuto, A. Bakel, D. Bowers, A.V. Gelis, A.S. Hebden, L.E. Maggos, D. Stepinski, Y. Tsai, Lab-Scale Demonstration of the UREX+ 1a Process Using Spent Fuel, Waste Management, 7.

[4] L.P. Hatch, Ultimate disposal of radioactive wastes, in, BNL-1345, Brookhaven National Lab., 1953.

[5] D.M. Strachan, W.W. Schulz, Glass and ceramic materials for the immobilization of megacurie-amounts of pure cesium-137, in, 1976.

[6] C.L. Riddle, J.D. Baker, J.D. Law, C.A. McGrath, D.H. Meikrantz, B.J. Mincher, D.R. Peterman, T.A. Todd, Fission product extraction (FPEX): Development of a novel solvent for the simultaneous separation of strontium and cesium from acidic solutions, Solvent Extraction and Ion Exchange, 23 (2005) 449-461.

[7] M. Onal, Y. Sarikaya, Thermal behavior of a bentonite, Journal of Thermal Analysis and Calorimetry, 90 (2007) 167--172.

[8] V. Balek, Z. Malek, S. Yariv, G. Matuschek, Characterization of montmorillonite saturated with various cations, Journal of Thermal Analysis and Calorimetry, 56 (1999) 67--76.

[9] R.E. Grim, W.F. Bradley, Investigation of the effect of heat on the clay minerals illite and montmorillonite, Journal of the American Ceramic Society, 23 (1940) 242--248.

[10] M.D. Kaminski, C.J. Mertz, M. Ferrandon, N.L. Dietz, G. Sandi, Physical properties of an alumino-silicate waste form for cesium and strontium, Journal of Nuclear Materials, 392 (2009) 510-518.

APPENDIX A

ENGINEERED STORAGE FORMS FOR THE IMMOBILIZATION OF RADIOACTIVE CESIUM AND STRONTIUM FROM SPENT NUCLEAR FUEL

A Thesis

Submitted to the Faculty

of

Purdue University

by

Luis Humberto Ortega

In Partial Fulfillment of the

Requirements for the Degree

of

Master of Science in Nuclear Engineering

August 2006

Purdue University

West Lafayette, Indiana

TABLE OF CONTENTS

Page

LIST OF TABLES

LIST OF FIGURES

ABBREVIATIONS

AFC	Advanced Fuel Cycle
ANL	Argonne National Laboratory
DOE	Department of Energy
DU	Depleted Uranium
EPA	Environmental Protection Agency
FPEX	Fission Product EXtraction
GAC	Granular Activated Carbon
HEPA	High Efficiency Particulate Air
HLW	High Level Waste
INTEC	Idaho Nuclear Technology and Engineering Center
LAW	Low Activity Waste
LLW	Low Level Waste
MACT	Maximum Achievable Control Technology
NPP	Nuclear Power Plant
PVC	Poly Vinyl Chlorides
SNF	Spent Nuclear Fuel
SRBSR	Savannah River Bench-Top Steam Reformer
SRRW	Steam Reforming Radioactive Waste
SYNROC	SYNthetic ROCk
THORTT	Thor Treatment Technologies
TRU	Transuranics
UREX	Uranium EXtraction
WIPP	Waste Isolation Pilot Plant
XRD	X-Ray Diffraction

GLOSSARY

kaolin	A mineral source of kaolinite, a layered silicate $Al_2Si_2O_5(OH)_4$.
SYNROC	"Synthetic Rock" a ceramic waste form which incorporates radioactive waste into its crystal structure, invented by Doctor Ted Ringwood of Australian National University in 1978.
syngas	Hydrogen rich gas mixed with carbon monoxide and other gases in various proportions created by steam reforming of organics.
transmutation	Transformation of one isotope to another by one or a series of nuclear reactions.
transuranic	Elements with an atomic number greater than 92 (uranium).
zeolite	Any of various hydrous aluminum silicate minerals whose molecules enclose cations of sodium, calcium, potassium, strontium and other cations in their cage-like structure.
Wigner energy	Energy that accumulates in a crystal structure from the dislocations caused by neutron bombardment.

ABSTRACT

Ortega, Luis H. M.S.N.E., Purdue University, August, 2006. Engineered Storage Forms for the Immobilization of Radioactive Cesium and Strontium from Spent Nuclear Fuel. Major Professor: Sean McDeavitt.

Cesium and strontium (Cs: $T_{1/2} = 30.07a$; Sr: $T_{1/2} = 28.78a$) bearing radioactive wastes are particularly serious radioactive hazards. The motivation for waste form development is a desire to immobilize these isotopes and isolate them from the biosphere. In addition, the potential for putting into effect an advanced fuel cycle which separates these isotopes from the bulk of the spent nuclear fuel is a driving force for research to find cheaper and safer ways to treat these potential new cesium and strontium bearing wastes. The separation of these elements is being considered because the majority of the heat load and radiation coming off spent nuclear fuel for the first 100 years comes from cesium and strontium. Steam reforming may be an effective way to treat these cesium and strontium wastes without the high temperatures associated with vitrification and other processes which can volatilize the radioactive elements. Although Steam Reforming Radioactive Waste (SRRW) is not done at low temperatures, ~ 700 °C steam reforming may be simpler and have lower energy requirements than other methods. The treatment of the waste will destroy solvents whether the wastes are organic or dilute nitric acid-based with the addition of a carbon source. The addition of minerals during the steam reforming process, such as alumina and silica, should create a rigid backbone. If reacted with metal oxides, the waste should bind in ways analogous to natural geologic forms. This can create a durable waste form suitable for sequestration. A simulated FPEX waste stream was created. The waste consisted of cesium and/or strontium nitrate dissolved in nitric acid. This waste was reacted with kaolin and carbon at ~ 700 °C under a fluidizing

flow of steam or argon. Silica beads were also added to the steam experiments as a starter material. Under steam a glass-like material was created with cesium and strontium loadings of 2.77 and 0.11 mass %, respectively. Argon experiments created cesium aluminum silicate ($CsAlSiO_4$) and strontianite ($SrCO_3$).

1. INTRODUCTION

Cesium and strontium (Cs: $T_{1/2} = 30.07a$; Sr: $T_{1/2} = 28.78a$) bearing radioactive wastes are particularly serious radioactive hazards; both have high activities with biological absorbance characteristics. Strontium has chemical behavior similar to that of calcium and cesium is chemically similar to sodium and potassium. The motivation for the waste form development explored here is a desire to immobilize these isotopes and isolate them from the biosphere. Cesium is particularly troublesome due to its volitization potential and the ease with which it travels through aqueous matter. In addition, the potential for an advanced fuel cycle (AFC) being put into effect which separates these isotopes from the bulk of the spent nuclear fuel (SNF) is driving research to find effective ways to treat these potential new cesium and strontium bearing wastes. The separation of these isotopes is being considered, because the majority of the heat load and radiation coming off SNF for the first 100 years comes from ^{137}Cs and ^{90}Sr. Once separated, something must be done with this unique new waste. Steam reforming may be an effective way to treat these cesium and strontium wastes without the high temperatures associated with vitrification and other processes which can volatilize the radioactive elements. Although Steam Reforming Radioactive Waste (SRRW) is not done at low temperatures,$\sim$ 700 °C steam reforming may be a simpler and cost effective means to treat this radioactive material. Assuming tritium, iodine, and mercury are not in the waste, the off-gas should be workable in a safe manner without large amounts of secondary waste. If these volatiles are present in the waste feed, they will be in the off-gas. In this case, scrubbing will be necessary to adequately deal with them. The waste feed will consist of the chemicals used to remove the isotopes from the spent fuel and any impurities that will be carried along. With the addition of a carbon source, steam reformer waste treatment will

destroy solvents whether the wastes are organic or dilute nitric-acid based. The addition of the minerals silica and alumina in the form of kaolin during the steam reforming process creates a rigid backbone to bind the hazardous isotopes. These steam reformed products will have structures analogous to natural geologic forms.

Alternate compositions may be possible with steam reforming. The addition of metal oxides such as iron, titanium, and zirconium to the process feed will alter the waste product mineralogy, and may have beneficial catalytic effects. These oxides can be substitutions or additions to the silica and alumina in the process feed to create varied molecular structures. We are attempting to mimic rocks which are naturally robust. The suitability of these forms will need to be tested for effectiveness as sequestration vehicles. Qualities for comparison are the effects of radiation, physical stress, and how exposure to water changes the immobilization of isotopes (leachability of the waste form). Leach tests to determine how well the isotopes stay trapped in a waste form under aqueous conditions are necessary. A comparison is made among the different compositions to determine the most effective immobilization technique. The final waste form structural determination requires the weighing of different factors such as the total production cost of the method, safety considerations, and the amount of secondary waste generated. A waste form is chosen by determining which characteristics are most important for the waste form to have, and by finding a balance between them.

1.1 Background & Motivation

The Department of Energy (DOE) is funding the Advanced Fuel Cycle Initiative, and is currently investigating methods to treat spent nuclear fuel in a sustainable manner while shortening the extremely long half lives characteristic of the isotopes. The current policy is to take entire fuel bundles after sufficient cooling and ship them to Yucca Mountain in Nevada for deep geologic burial. The repository is not yet open, but current estimates see it being filled by 2015.[1] After reaching this limit, the

repository will require new legislation to extend the legal capacity of the mountain. Eventually another site will be necessary. If current nuclear generation is not replaced as plants age and become decommissioned the current method will suffice. On the other hand if the United States continues to produce nuclear power and it builds new nuclear power plants (NPP)s, a fuel cycle with separation, transmutation and recycle is an alternative worthy of analysis. An AFC will reduce waste volume and shorten the half lives of some of the troublesome isotopes while providing burnable fuel for future power generation. The DOE is exploring these goals.

1.1.1 AFCI

Chemical separations are the foundation of reprocessing, and determining the extent and exact method is currently under investigation. To begin, the ultimate fate of each isotope or group of isotopes with similar properties must be determined.

The bulk of the spent fuel is depleted uranium (DU) ∼95.6%. DU can be treated as low level waste, so it does not require deep geologic burial. The next largest fraction consists of stable isotopes and the short-lived fission products at ∼3.3%. Once these are separated they are not a radiation hazard but may still be chemically toxic. The next fraction includes plutonium and the long-lived fission products at ∼0.95%. These can be incorporated into new mixed oxide fuel or transmuted to shorten their half lives. Transmutation can also be used for the minor actinides and other long-lived fission products ∼0.15%. Each of these portions of spent fuel can be treated separately. The end result is less volume for high level waste disposal, shorter half-lives after transmutation, and recycled energy producing fuel. Of the long-lived isotopes, some will not be suitable for transmutation due to half-lives that are not long enough to justify the process. Two primary examples are ^{137}Cs and ^{90}Sr at approximately 30 years.[2]

The radioactivity of the HLW is of primary concern during repository design. The activity of the waste will determine the heat generation and temperature. Water

exists as moisture in the soil. Temperature limits are set to keep water from boiling inside the repository. Lowering the overall activity will allow more waste into the repository without exceeding these temperature limits.

To maintain low temperatures inside the repository active cooling with fans has been proposed. Eventually the fans will be turned off after the decay heat goes down to a level where the active cooling is no longer necessary. To further reduce the activity during the initial years of operation the removal of cesium and strontium will make a substantial reduction.

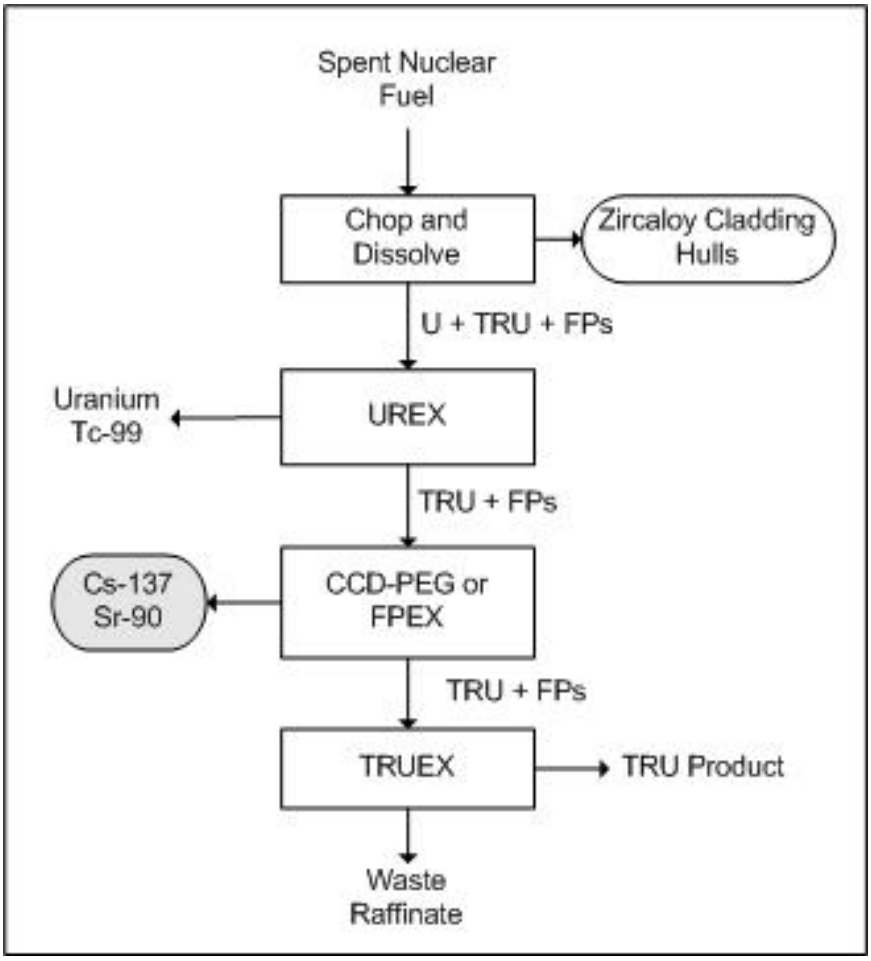

Figure 1.1. Advanced Fuel Cycle Initiative

To accomplish

The AFCI aqueous reprocessing methods incorporate sequential solvent extraction schemes to separate uranium and selected fission products from dissolved spent nuclear fuel. Figure 1 shows a high level flow diagram with three sequential steps having the acronyms UREX, CCD-PEG or FPEX, and TRUEX. These three steps are briefly defined below, but the process functions are (in order) 1) the recovery of uranium and technetium (UREX), 2) the recovery of cesium and strontium (CCD-PEG or FPEX), and 3) the recovery of the transuranic (TRU) isotopes (TRUEX). The step that is germane to this proposal is the recovery of cesium and strontium and CCD-PEG and FPEX are the acronym names for the two process options being developed at INL.

The acronym UREX stands for Uranium Extraction, which is a solvent extraction process that removes high purity uranium and technetium in three steps: Extraction/Scrub, Technetium Strip, and Uranium Strip. The first step extracts uranium and technetium from the dissolved fuel using 30 volIn the scheme shown in Fig 1, Cs and Sr isotopes are removed from the process stream following the UREX step and before the TRUEX step. As stated earlier, the motivation for removing these isotopes from the waste stream is that their radiation and decay heat levels are very high which may result in storage limitations when designing a repository packing scheme. Removing these relatively short lived isotopes to a separate decay storage facility will extend the capacity of a deep high level waste repository (i.e., Yucca Mountain). The longest lived Cs and Sr isotopes are Cs-137 (t1/2=30.07 y: 0.66 MeV and 0.514 MeVmax -) and Sr-90 (t1/2=28.78 y: 0.546 MeVmax -) so their activities remain relatively high for 90 to 120 years (i.e., 3 to 4 half lives). The two isotopes generate a major portion of the decay heat in spent nuclear fuel over the first 100 years of storage, but then they are essentially gone. Removing Cs and Sr for decay storage will reduce the short term heat load on a repository waste form and therefore enable a higher waste packing density. The two Cs/Sr extraction processes being developed under the AFCI program are 1) the cobalt dicarbollide/polyethelyne glycol (CCD/PEG) solvent extraction process [3] and 2) the crown ether/calixarene fission product extraction process (FPEX)

[4]. The basis for CCD/PEG was established through collaborative research between the Idaho National Engineering and Environmental Laboratory and the Khlopin Radium Institute in Russia [5,6]. In brief, the CCD component enables the extraction of Cs and the PEG component enables the extraction of Sr. Coming out of this process, Cs and Sr are strongly complexed within the organic components of these solvents. Following this extraction, the Cs and Sr complexes are re-stripped away from the organic using either DTPA (Diethylenetriaminepentaacetate) and guanidinium carbonate or methylamine carbonate. The FPEX process is named for its function (fission product extraction process) instead of the primary chemical solvents [4]. The process nominally uses a crown ether/calixarene (other calixarenes are being considered) solvent to simultaneously extract cesium and strontium from a nitric acid solution. This relatively new process has been demonstrated to extract both cesium and strontium simultaneously from 1 M nitric acid solutions at ambient temperature. If FPEX development is ultimately successful, the precursor for steam reforming will be a simple dilute HNO3 solution. In summary, at the time of this proposal, there are 3 potential precursors that may contain the Cs and Sr isotopes: 1) guanidinium carbonate/DTPA solution, 2) methylamine carbonate/DTPA solution, and 3) dilute nitric acid solution. Each of these have advantages and drawbacks that are part of the final process selection. For example, the guanidinium carbonate/DTPA solution would have a large waste stream, the methylamine carbonate/DTPA components may perhaps be recycled, and the dilute nitric acid solution comes from a new process that is not fully developed. Therefore, all three precursor options will be considered at the outset of this program. If a precursor option is eliminated by process selection in the AFCI program, it will be eliminated from this program. On the other hand, the material synthesis data generated in this proposal may be used to assist the process selection. (In other words, we will explore whether a suitable storage form can be made from a given precursor?)

1.2 Objective

The goal of this study is to test the creation of a simulated radioactive waste form with steam reforming. The waste is a simulant that may be created in an AFC scenario. The methodology of an AFC has been under investigation for many years, but is not finalized. Using advice from researchers[3,4] and literature dealing with cesium and strontium separation methods[5] candidate waste streams for treatment are assumed, then simulated with non-radioactive surrogates.

The waste form created in the fluidized bed steam reformer is tailored by adding specific amounts of mineral additives to trap cesium and strontium. The target products are chosen to mimic geologic forms. The analogs are common sources of cesium and strontium found in natural rocks. Assuming the forms found in nature are in a stable configuration, reactants were chosen to favor the production of these naturally occurring forms, pollucite $CsAlSi_2O_6$ for cesium, and strontianite $SrCO_3$, Sr-feldspar and Sr-brewsterite for strontium. To make this possible alumina and silica are added to the waste simulant along with carbon to drive out excess nitrate and oxygen. SiO_2 or spheres are also added to the initial waste simulant mixture to serve as nucleation points for waste solid formation. The reaction tube is constructed out of alumina, as is one of the reactants tested. To avoid coating the inside of the alumina tube with the reaction product, the seed beads supply a reaction surface with a higher Gibbs free energy of formation than the alumina tube which initiates formation of the product. The final product is a granular solid with the cesium and strontium isotopes embedded in the silica alumina matrix.

2. NUCLEAR WASTE MANAGEMENT SURVEY

Radioactive materials require special treatment to keep the material from entering the environment. A waste package or waste form not only protects the environment from contamination with radioactive isotopes, but also protects the waste from reactive elements in the environment that may destroy or degrade the waste containment. Waste forms are engineered to encase specific waste types according to how they will ultimately be stored. These emplacements are in above ground tombs, deep burial underground, or under the ocean. Some considerations when designing a radioactive waste treatment are the following:

- Waste chemistry
- Isotope half lives
- Chemistry of emplacement
- Thermal conductivity
- Thermal stability
- Radiation durability
- Chemical stability
- Structural durability
- Proliferation risk
- Process safety
- Process cost

This is by no means a complete list. Politics and other factors play a large role determining how and where waste will be treated. Each circumstance requires a

solution tailored to the waste type and requirements needed. The focus here is on aspects that affect the engineering of the physical waste package or waste form. The following are some common methods to deal with radioactive waste immobilization. Steam reforming of radioactive wastes (SRRW) is a relatively new technique. The focus of this study is SRRW, therefore this process covered in greater detail here.

2.1 Steam Reforming

Steam reforming for the treatment of waste volume reduction has been employed by various industries. Organic waste or biomass from varied sources can be converted to a usable energy source by steam reforming.[6] The pyrolysis of biomass is done at relatively low temperatures $300 - 500\,^{\circ}\mathrm{C}$ producing a volatile matter which reacts with steam to produce a hydrogen rich synthesis gas. It has been shown that steam reforming is an effective way to treat simulated waste consisting of naphthalene and o-dichlorobenzene in order to test its effectiveness treating polyaromatic hydrocarbons and halogenated aromatics.[7]

Steam reforming applied to radioactive waste treatment is a relatively new process. Different types of waste are being tested and the products created are being analyzed to determine the effectiveness of these waste forms. Recently steam reforming has been chosen for the treatment of sodium bearing waste in Idaho,[8] in a project treating almost one million gallons of Department of Energy (DOE) radioactive waste. The DOE tested five technologies for the task: direct vitrification, cesium ion exchange with grout, calcination with Maximum Achievable Control Technology (MACT) upgrades, direct evaporation, and steam reforming. Steam reforming was chosen for its ability to handle nitrates and potential for use in other types of low level wastes. Another reason cited was the lower disposal cost of the individual waste streams. THOR Treatment Technologies (THORTT), a United States joint venture between Sweden's nuclear services firm, Studsvik, and the U.S.'s Washington Group International will perform the steam reforming.

J. Bradley Mason is the primary inventor of the methods employed by THORTT. The principle patents are U. S. Patent No. 6,280,694 B1 Single Stage Denitration[9] and U. S. Patent No. 6,084,147 Pyrolytic Decomposition of Organic Wastes.[10] Testing and research into steam reforming technology has progressed continuously in the last decade and has been performed with various types of wastes.

One resource that covers the basic principles of steam reforming applied to radioactive waste treatment is published by the CRC Press, *Hazardous and Radioactive Waste Treatment Technologies Handbook (2001).* Process operation, chemistry and some of the waste types treated are covered in this publication. The case studies described include: pharmaceutical waste, NPP mixed waste, Ethylene Diamine Tetraacetic Acid ($C_{10}H_{16}N_2O_8$), NPP fuel pool waste, soil clean-up and the reactivation of Granular Activated Carbon (GAC).[11]

Motivation to steam reform waste is rooted in the desire to avoid incineration. Site licenses for incinerators are difficult to obtain, and the difficulty of dealing with products of incomplete combustion drive exploration into other means to treat wastes.[12] Galloway and Thermolytica proposed steam reforming instead of incineration for different types of troublesome wastes on site with relatively small steam reformers.[12] In 1993 Galloway, working for Synthetica (formerly Thermolytica), demonstrated the destruction of organics and decomposition of nitrates in Hanford's storage tank wastes.[13] In this process the waste surrogates were soaked into alumina beads which were top fed into a reactor vessel that was injected with 600 °C steam. A screw at the bottom extracted the reacted beads and deposited them into a bucket elevator which recycled them back to the top of the reformer. The off-gas is directed into a higher temperature, 1100 °C chamber for further detoxification.

ThermoChem continued this line of work acquiring DOE contract DOE/MC/32091-97/C0789, *Steam Reforming of Low-Level Mixed Waste.* This work included among the test surrogates a cesium chloride doped resin. The test was run at $\sim$ 565 °C with a silica sand starter bed which ran for five hours. These experiments demonstrated that cesium could be trapped in a steam reformed solid product, and the organics,

chlorine and sulfur, could be separated and further decomposed, while accomplishing significant volume and mass reductions.[14] In 2001 Duratek tested volume reduction of low level waste surrogates (ion exchange resin and Poly Vinyl Chlorides (PVC)) with steam reforming. The resulting product was an ash-like residue with weight reduction ratios of 200 for ion exchange resin and 50 for PVC.[15]

Recent work treating radioactive waste with steam reforming has focused on tank wastes. The following references are some examples; Hanford Low Activity Waste (LAW),[16] DOE tank waste denitration and immobilization,[17] INTEC's sodium bearing waste[18], and disposition of tank 48H organics at the Savannah River Site.[19] These and other sources are covered in sections 2.1.1-2.1.5.

The materials created in these processes are mineralized zeolite-like compounds. The benefit these forms provide is their capacity to encase undesirable isotopes within their crystal structure. The reaction temperatures and conditions make the waste form durable and water insoluble.[20]

2.1.1 Industrial Process Description

In recent years SRRW and the products created by this process have been presented by THORTT and Jantzen in their technology reports[21,22] and in various conference proceedings and papers. The technology has been presented at Waste Management conferences from 2003 through 2006. In 2006 J. B. Mason *et al* report being selected to treat DOE sodium bearing tank waste at Idaho National Laboratory.

The work done by Mason *et al* is primarily focused on tank wastes which are mostly liquids but some of the wastes can also be considered sludges. The waste feed enters the reactor, where it is mixed with the additional reactant additives. These additives are used to destroy the nitrate/nitrite and organics that may be present and also create a solid suitable for waste disposal. The additives may include but are not limited to carbon in the form of sugar or granulated activated carbon, clay, silica and/or catalysts.

The product is a silica alumina cage-like structure with the targeted isotopes and some heavy metals trapped inside. This method's ability to destroy the solvent without prior treatment, whether organic or acidic, reduces the treatment's complexity and therefore increases the safety. Fewer steps lower cost and reduce the possibility of radiation exposure in a intermediate pre-processing step.

The process is a two-stage steam reformer system, which operates under a vacuum at $650 - 750$ °C. The first stage is a fluidized bed vessel. The reactants and waste are introduced into the bed which is fluidized with superheated steam. In the fluidization process the reactants and waste are intermixed and allowed to react. The reactions that occur are (1) the evaporation of liquids, (2) the destruction of organics, (3) nitrates and nitrites are converted to nitrogen gas and (4) the reactive chemicals are embedded in a stable solid waste product. The second stage's focus is oxidation. Once in the second stage, any carbon particulates are destroyed as well as any organics that are not fully decomposed. These are converted to carbon dioxide and solid calcium compounds. The off-gases are then cooled and filtered. A High Efficiency Particulate Air (HEPA) filter is the final step before release of the off-gas which consists mostly of water vapor and carbon dioxide.

2.1.2 Sodium Bearing Tank Waste

In 2003 Marshall, Soelberg and Shaber reported in INEEL/EXT-03-00437 the details of a bench-scale demonstration which steam reformed a non-radioactive sodium bearing waste simulant.[18] I will briefly cover their experiment focusing on the reactants, operational conditions and the main findings.

The waste feed was simulated to mimic waste from tank WM-180 at Idaho Nuclear Technology and Engineering Center (INTEC). Rhenium was added to the waste simulant as a substitute for technetium and naturally occurring isotopic compositions of the other elements were used. The waste is typical of the accumulated products of decades of SNF processing at INTEC. Approximately one million gallons of radioac-

tive acidic sodium bearing waste (SBW) is stored at INTEC awaiting treatment. Large amounts of waste raffinates have been calcined and exist as powders at INTEC also. The search for alternate treatments was motivated by the fact that the calcination process does not reach MACT. As a result of these trials, steam reforming was chosen to treat the waste.[8]

Test objectives:

1. Show that fluidized bed reformation can treat SBW without agglomeration of bed particles or de-fluidization
2. Characterize the composition of the products
3. Characterize the composition of the off-gas
4. Determine the fate of Cs and Re (Tc surrogate) and Hg speciation
5. Quantify nitrate destruction and NO_x emissions

The reactor operation is at negative pressure to lower the risk of harmful chemicals leaking out of the system. The temperature range is from $\sim 670 - 695$ °C with a maximum reactor surface temperature of ~ 750 °C.

The system is a two stage process connected by a cyclone filter to remove particles larger than 15μm which were collected in a drum. The externally heated first stage is the main dryer/ reactor which is made of inconel. The bottom half, or bed section, is six inches (15.24 cm) in diameter and 30 inches (76.2 cm)tall, and is connected by a reducer to the upper freeboard section which is 12 inches (30.48 cm) in diameter and five feet (1.524 m) tall. The finer particles and gases exit the top and enter the cyclone filter. After cyclone filtering, the gases and fine particulates enter the second stage. The second stage completes the oxidation reactions and filters further. The final step is the off-gas system which monitors composition and does the final scrubbing and mercury removal if necessary.

The waste simulant feed was mixed with sucrose and activated carbon before entering the reactor, with a sucrose-to-feed ratio of 1 pound to each liter. The feed is

injected into the reactor bed, which is loaded with alumina along with an iron oxide catalyst (with an alumina to catalyst ratio of 10:1). The purpose of these additives is to reduce the nitrate to nitrogen and carbon oxides.

This experiment produces three separate particle fractions, one from the main fluidized bed, another from the cyclone, and finally the smallest particles are collected in the last stage. The fluidized bed particles were $\sim$800μm spheroids, with nodules protruding from the base sphere. The cyclone particles were in the tens of μm range, while the filter catch particles were less than or equal to 25μm. The estimates were made by observing the micrographs included in the report.

The off-gas analysis was done without considering N_2 since it was added at several steps in the process. What they found after normalization was mostly H_2O (76%), and carbon monoxide averaged 1.3% and methane 0.1%. The NO_x was over 98% destroyed.

The cesium and rhenium found in the scrub solution were 0.003% and 0.01% respectively, so most of these elements were embedded in the waste form product. Mercury was recovered in the off-gas GAC column (76.1%) and in the scrub solution with less than 1%; none was found in the waste product. It was noted that this was a test demonstration and in a production scale facility performance improvements would be made.

At another location, the Savannah River National Laboratory, a Bench-Top steam reformer (SRBSR) was built and various waste simulants have been tested, including sodium bearing tank waste. Tests were performed with changes in co-reactants, such as using different clays and BB carbon versus GAC. The resulting products were analyzed using X-ray diffraction (XRD) to identify the phases present.

Four-hour sodium bearing waste experiments on the SRBSR found that using Sagger clay creates two phases, a nepheline and a carnegietite phase. When operated for 48 hours, the more stable nepheline and sodalite phases are created. With Troy clay and excess NaOH, the stable phases were created after running for four hours. The excess base has the side effect of creating Na_2CO_3 from the NaOH reacting

with the CO_2. Possible complications could be the short reaction time and low stoichiometric reactants (2× vs. 3.2×). The use of BB carbon destroyed over 98% of the off-gas NO_x, and doubts about the need for using a catalyst were raised.[23]

2.1.3 Low Activity Tank Waste

In December of 2001 at Hazen Research Inc. of Golden, Colorado, fluidized bed steam reforming experiments were conducted with a Hanford tank AN-107 LAW simulant.[22] Studvik THOR^{sm} developed the process. Jantzen's 2002 report WSRC-TR-2002-00317[16], and McGrail *et al* report in PNWD-3288 (2003) the process details which are briefly summarized here.[24]

The waste simulant was spiked with rhenium and stable ^{133}Cs as surrogates for ^{99}Tc and ^{137}Cs respectively. Coal was added to promote de-nitration; kaolin clay was added along with excess SiO_2; and iron oxide was added as a catalyst. Runs were at $\sim 715 - 735$ °C. Some of the attributes listed for the waste form created via steam reforming are as follows:

- Robust technology that accommodates a wide range of feeds and additives including high sulfate concentrations
- Continuous operation
- Durability superior to vitrification
- Radionuclide substitutes Re and ^{133}Cs released at a rate lower than that of sodium (<2 g/m^2)
- Temperatures low enough to avoid vaporization of radionuclides but high enough to destroy organics with the aid of catalysts
- Acid free off-gases, SO_4^{-2}, F^-, and Cl^- in waste form
- Waste form cage-like structures that trap radionulides anions

- Mineral phases of the waste forms are known to have survived for millions of years in surface environments
- When they alter, mineral phases' cage-like structures become zeolites which are also known to hold anions and radionuclides

The objectives of the study were (1) to explore the feasibility of the fluidized bed, (2) describe the mineral phases in the waste form, and (3) test the durability of the waste form. Comparisons of the waste form to vitrification, and ceramic and hydroceramic waste forms were also done. The methods applied were ASTM C1285-97, and Environmental Protection Agency (EPA) Toxic Characteristic Leaching Procedure.

Findings demonstrated the sodium release was <2 g/m^2 and the Re and Cs were an order of magnitude lower; SO_4^{-2} retention in the waste form was 100%. The report noted the durability of the steam reformed waste form to exceed that of vitrified LAW. The primary products are sodium aluminosilicates, which are anhydrous feldspathoid phases. These cage-like structures typical of sodalite and nosean minerals hold the radionuclides and anions inside. Other phases found:

- Nosean $Na_8Al_6Si_6O_{24}(SO_4)$
- Nepheline $NaAlSiO_4$
- Corundum Al_2O_3
- Hematite Fe_2O_3
- Magnetite Fe_3O_4

The organic portion of the reactants was converted to CO_2 and H_2 with an efficiency of over 99%. Acids in the off-gas were mostly all removed in the scrubber system, leaving only <2.5 ppm SO_x downstream. Less than 4 to 8% of the acidic gases were volatized. The waste form held >91% of the SO_4^{-2}, >93% Cl^-, and >92% of the F^-.

In summary, the product created held high concentrations of sulfate, an ability which vitrification lacks. The durability of the steam reformed product was also more durable than vitrified waste. The process was found to be MACT compliant, with the anions trapped in the waste form. The cage-like mineral phases produced are similar to natural forms that are known to have survived for millions of years.

Hanford LAW was also treated with steam reforming at the Savannah River National Laboratory with a SRBSR.[23] The tests varied the types of co-reactants and temperatures as well as test duration. Three types of clay were used, OptiKasT, Sagger, and Troy. Two sources of carbon, BB and GAC, were also tested. The temperatures used were either 650 or $\sim$ 725 °C. The products were similar to those in the Colorado tests done by Hazen Research Center Inc. Use of BB carbon was found to be superior to GAC. The different temperatures had no appreciable effect on the destruction of NO_x nor did the type of clay. The optimum NO_x destruction was found statistically to be BB carbon with no catalyst.

2.1.4 Organic Tank Waste

At the Savannah River Site (SRS) in-tank processing was employed to remove ^{137}Cs from HLW supernates. The organic chemicals employed were monosodium titanate (MST) and sodium tetraphenylborate (NaTPB). The product of concern here is the precipitated CsTPB, which was diluted to create 250,000 gallons of $\sim$0.53 wt% Cs. To investigate the feasibility of a steam reforming process, crucible tests were excecuted at SRS.[19] The objectives and results are outlined in Report WSRC-TR-2003-00352, Rev 0 are briefly covered below.

The objectives of the study were as follows:

1. Destruction of TPB, antifoam, and nitrate at $650 - 725$ °C with sugar
2. Formation of Na_2CO_3 for subsequent vitrification
3. Formation of Na_2SiO_3 or Na_4SiO_4 for subsequent vitrification

4. Assessment of the melting points of Na_2CO_3 and Na_2SiO_3
5. Optimization of the reductant amount to reduce the amount of reductant in the product
6. Demonstrate that tests in crucibles can duplicate a fluidized bed steam reformer

To prepare the simulant for the test, antifoam and Fe_2O_3 were added. Fe_2O_3 is used to determine the reduction to oxidation ratio ($Fe^{+2}/\sum Fe$). The simulant was made acidic with dry ice until pH of ∼9.5 was reached to turn NaOH to Na_2CO_3. These steps are to create a atmosphere similar to that in a fluidized bed steam reformer. Sucrose was added to reduce the nitrates, and the stoichiometric ratio of [C]:[N] of 0.97 was varied within the test matrix from none, and 1/2× to 1×. Also, test reaction times were varied from 1/2, 3, and 48 hours. Temperatures used were 650 and ∼ 725 °C. The feed was dried to a thick paste and put in Al_2O_3 crucibles then sealed with a nepheline ($NaAlSiO_4$) gel. The gel was melted to seal the crucible before the reaction started creating an airtight reaction chamber. The crucibles were then placed in a calibrated furnace at the desired temperature.

Results:

- TPB and antifoam were destroyed in all samples
- >99% of nitrate was destroyed with 1× stiochiometry sugar
- Total Organic Carbon analysis did not find any reductant in the product
- The desired Na_2CO_3 product melted at 980 °C
- Tests seeking to produce either Na_4SiO_4 or Na_2SiO_3 resulted in different silicates being formed; this showed that Na_2O:SiO_2 ratios were incorrect
- Na_2CO_3 and Na_2SiO_3 melted at ∼ 980 °C and ∼ $1022 - 1049$ °C respectively
- Crucible tests demonstrated that complex reactions can be duplicated, especially a water gas shift as well as $\log p_{H_2O}/p_{H_2}$ and $\log p_{CO_2}/p_{CO}$

2.1.5 Transuranics and Graphite

Transuranics

The use of steam reforming for the treatment of TRU orphan wastes is proposed by THORTT.[25] The waste is kept inside 55 gallon drums which have been fitted with replacement lids that have a ceramic filter and inorganic seals. The seals and filters allow gas exchange but trap the radioisotopes and heavy metals that may be present. The drums are heated to between 650 and $\sim$ 750 °C leaving a carbon char with the radioactive and/or heavy metals. The gases enter a secondary stage steam reformer and scrubber. Here acids and volatized organics are converted to carbon dioxide, and water vapor. Downstream of the steam reformer is a wet scrubber where any acids or particulates are trapped concentrated and transferred into a 55 gallon drum that also can be pyrolized.

Graphite

THORTT proposes the treatment of moderator graphite with steam reforming.[26] The benefits listed include but are not limited to (1) a safe method to release Wigner energy in moderator graphite, (2) treatment of graphite and water slurries, (3) possible in situ moderator gasification and (4) other radioactive impurities can be separated (due to the low volume of off-gas creation). The primary benefit of this treatment compared to incineration is a tightly controlled containment to effectively reduce or eliminate the loss of hazardous or radioactive materials in the off-gas.

2.2 Waste Canisters

The spent fuel from a nuclear reactor is primarily UO_2 which is inherently unstable in aqueous systems. Inside a nuclear reactor the pelletized uranium oxide is encased in a zirconium cladding which keeps water from reacting with the fuel. Zirconium cladding works very well as long as it is kept intact. During fission the fuel

swells and gases are generated which add strain and stress to the fuel and cladding. These stresses lead to break up of the UO_2 pellet, and with time increase the likelihood of a cladding breach. This is usually manageable in the few years residence in a reactor, but for long term stability secondary measures must be employed to assure immobilization of the spent fuel. The current Yucca Mountain proposal has engineered special canisters for the long term containment of the spent fuel. These multiple barrier containers will hold entire fuel bundles inside for the duration of the decay process.

Waste canister methods employ layered defenses whose tasks include physical containment, radiation shielding, heat removal, and proliferation resistance suitable for sequestration. Most waste forms will have a canister, with the robustness of the canister depending on the durability of the waste form or on how the isotopes are immobilized. An initial waste treatment that immobilizes isotopes effectively will require less protection provided by the container. If the waste is in a relatively raw or unstable form the canister's requirements increase. The engineered canister complexity and cost will depend on what type of waste it is required to hold and the environment it will be expected to endure. After waste loading, a suitable area for sequestration must be chosen. Sequestration may be in an above ground cask or tomb, in deep sea burial, or in an underground repository. Underground repository geology may consist of salt beds or salt domes, volcanic tuff, basalt, or granite. Yucca Mountain is an example of volcanic tuff, while the Waste Isolation Pilot Plant (WIPP) is a salt bed repository. WIPP accepted its first waste shipment in 1999 and continues to operate.[27]

2.3 Vitrification

Radioactive waste immobilization via vitrification has an extensive history and worldwide usage.[28] Vitrification is generally done by taking glass frit and mixing it with the waste to be treated, then heating it until it becomes a liquid. The liquid is

then formed into the desired shape and cooled. Typical temperatures for vitrification are in $\sim 1000\ ^{\circ}C$ range. Various methods to vitrify waste have been developed. The encasement of radioactive waste in glass has been selected as the method for immobilizing high level waste in the WIPP. Vitrification processes have been thoroughly researched and tested.[29] Our focus is dealing with the complex chemistry of cesium.

The volatility of cesium in vitrification systems[30] has been under investigation and the question of how to deal with the issue has been solved in various ways. One method to aid retaining the volatiles is to cover the melt surface with a cold cap[31]. There are other methods to deal with volitization, the most prominent of these is to absorb the waste in some media such as zeolite,[32] ion exchange resin,[33] or crystalline silicotitanate,[34] and then vitrify the resulting compound. These treatments report reductions in the volitization of cesium during the vitrification process.

2.4 Grout and Concrete

The use of grout and concrete are usually limited to LLW and Intermediate Level Waste. They are favored for their low cost and simple application.[35] A drawback when applied to the immobilization of cesium-containing waste is the tendency for the cesium to stay in the aqueous region within the cementitious media.[36] To incorporate the cesium into the mineral phase, methods similar to what has been done to improve vitrification are applied. The use of zeolites or resins to first absorb the cesium bearing waste, then mixing with the concrete or grout, has shown improved leachability characteristics.[37]

2.5 Zeolites and Ion Exchange Materials

Zeolites and ion exchange materials can be used to solidify liquid waste or remove the radionuclides from a solution and trap them in the exchange medium.

The sorption of radioactive liquid wastes has been studied with the zeolite clinoptilolite for effectiveness in removing Cs and Sr isotopes.[38] The findings recommend

that concentrations should be below 3×10^{-9} mg/L and pH should be kept ~ 8. Kaolinite powders have also been investigated to reduce Cs and Sr emissions from high temperature processes.[39] This work displayed possible improvements to incineration and vitrification processes due to the kaolinite powder's ability to scavenge these metals from a vertical combustor.

In 1997 Pacific Northwest National Laboratory, operated by the DOE, was contracted to investigate radionuclide uptake of a number of different ion exchange materials. Their studies' conclusions noted that for ^{137}Cs, KCoHex (potassium cobalt hexacyanoferrate) and SZ-72 (modified zirconate) removed over 99% of the ^{137}Cs. These materials were developed by 3M and Texas A&M respectively. In the same study it was found that ^{90}Sr was most effectively removed with pharmacosiderite and sodium nonatitanate with an effectiveness greater than 99%. Both of these compounds were also developed at Texas A&M.[40]

The leachability of these ion exchange materials, or absorbers, can be improved, meaning the cesium and strontium can be held more effectively with the addition of a sintering step.[41] Similar improvements can be made by mixing the material with another binding agent.[36]

2.6 SYNROC

SYNROC or synthetic rock is a durable robust method to treat waste steams. The method was developed at the Australian National University and first described in 1978.[42] As the name implies, SYNROC is a synthetic rock, composed of titanium mineral assemblages to mimic natural rocks. The minerals are tailored to the type of waste being treated. The mineral oxide precursors are intimately mixed then slurried with the waste to be treated, calcined, then hot pressed into the final waste form. These waste forms are resistant to leaching even at elevated temperatures and can hold virtually all types of HLW. SYNROC is considered second to vitrification, but

has displayed superior mechanical behavior, was found to be more stable thermally, and can support higher loadings of certain types of waste as opposed to vitrification.[43]

2.7 Calcination

Calcination refers to the treatment of liquid radioactive wastes by heating to dryness. This method has been applied to various liquid wastes in different ways. A few examples,[27] are fluidized-bed calcination, pot calcination process, radiant heat-spray calcination, rotary ball-kiln calcination, and calcination in molten sulfur. These are effective techniques to remove liquids and reduce volume. The waste produced by these processes is usually in a powder or granular form. Once dry, the waste must be containerized in a method adequate to avoid dispersal into the environment. A container may also be needed to keep water from dissolving or moving the waste if no fixation is applied.

Proposed methods to improve calcination include mixing the calcine with Portland cement. Another method found to have better leachability performance than cement is the addition of metakaolin and a NaOH solution to the calcine followed by mild curing.[44] This waste form is also known as hydroceramic.

3. THEORY

The motivation to create a water insoluble form to trap radioactive wastes comes from existing wastes that require treatment, and the advent of potential new ways in which spent fuel may be processed. Particularly relevant is the fact that a new spent nuclear fuel cycle employing separation of cesium and strontium from the bulk waste will create a new radioactive waste problem. Once the separations are done, these new waste streams will require methods to make them suitable for transport and sequestration until no longer a hazard.

3.1 Solvent Destruction

The solvents used in the separation process will add waste volume and must somehow be dried or removed from the waste to render them manageable. With steam reforming, the solvents can be converted to gaseous species and the hazardous metals can be trapped in a solid mineral-like matrix where they can decay.

The methods to separate cesium and strontium from spent fuel are several[5] but we will look at two generalized categories here. One involves the use of non-specific organics, and the other dilute nitric acid solutions. When organics are used in the separation process the solvents must be destroyed. Under steam reforming conditions the possible reactions are listed in Table 3.1. When dilute nitric acid is solvent it too requires removal. The destruction of nitrate and nitrite under steam reforming conditions is outlined in Table 3.2.

The processes above remove the solvents which carry the radioactive isotopes. In our experiment the off-gas was vented without analysis. How complete the denitration is, or the exact composition of the exhaust gas is an important factor in any

Table 3.1
Organic reactions

$C_xH_y + xH_2O \longrightarrow xCO + (x + y/2)H_2$
$CO + H_2O \longrightarrow CO_2 + H_2$
$2CO + O_2 \longrightarrow 2CO_2$
$2H_2 + O_2 \longrightarrow 2H_2O$

Table 3.2
Nitrogen reactions

$NO_3 + 2C \longrightarrow NO + 2CO$
$NO_3 + C \longrightarrow NO_2 + CO$
$2NO_3 + 4C \longrightarrow N_2 + 2CO + 2CO_2$
$2NO_2 + 3C \longrightarrow N_2 + 2CO + CO_2$
$2NO + 2C \longrightarrow N_2 + 2CO$
$2NO + 2CO \longrightarrow N_2 + 2CO_2$
$2NO + 2H_2 \longrightarrow N_2 + 2H_2O$
$H_2O + C \longrightarrow H_2 + CO$

waste treatment, but we are primarily concerned with development of the waste form. In an industrial application of steam reforming technology, all streams including the off-gases must be accounted for. MACT compliance will require further treatment than our lab scale demonstration. To adequately treat monoxides and other undesirable volatiles in the exhaust gas, other steps must be applied. Not all gaseous isotopes will be treated adequately by the steam reforming process so special consideration will be required if radioactive gases are present in the feed.

Recycling waste gases through the fluidized bed will aid incorporating volatiles into the waste form. Complete oxidation to avoid the creation of carbon monoxide and nitrogen oxides may require treating the steam reformer off-gas in a secondary stage. In a secondary off-gas treatment, excess oxygen fed to the stream will push the reactions to completion.

Some volatile gases, such as mercury, may be better dealt with separately. Steam reforming will not be able to trap tritium (^3H) or ^{14}C, so these will not be treated

specifically. If these types of gases are present in the waste they should be removed before steam reforming.

3.2 Cesium and Strontium

The radioactive isotopes of cesium and strontium are high heat radionuclides. The FPEX (Fission Product Extraction) process has been developed specifically for the removal of cesium and strontium from the UREX (Uranium Extraction) process. The solvent proposed to remove cesium is 4',4',(5')-Di-(t-butyldicyclo-hexano)-18-crown-6 and to remove strontium Calix[4]arene-bis-(tert-octylbenzo-crown-6) is proposed. Once the elements are in the solvent the solvent will be washed with dilute nitric acid. The dilute nitric acid with dissolved cesium and strontium will require subsequent treatment. Another method to remove cesium and strontium from the UREX process stream is called the CCD/PEG (Chlorinated Cobalt Dicarbollide/Polyethylene Glycol) process. Once the elements are in the solvent, the solution will be washed with guanidine carbonate/ diethylenetriamine pentaacetic acid (DTPA). This process creates a highly radioactive organic liquid waste. Transportation requirements and repository facility restrictions will only allow solid forms, therefore at the bare minimum the solvents must be dried. Once dried the result may be a powder or reactive metals; both these results require additional treatment or specialized containers for transport.

All radioactive waste treatment methods or a combination of methods could be used to treat this waste. An ideal waste form will be durable under physical strains and stresses as well as chemically inert while resistant to radiation effects. Transmutation during radioactive decay will alter the waste composition. Table 3.3 displays the transformation of the cesium and strontium isotopes. Although a waste form that has all of these properties can be engineered, the cost to do so can become prohibative. A balance between effective treatment, cost, and safety must be achieved. And because each stage in a process dealing with these materials has to contend with pro-

tecting operators and technicians from intense radiation fields, reducing steps and the number of facilities both reduces cost and increases safety. For that reason a single step treatment of both cesium and strontium isotopes that combines the destruction of the carrier solvent would be beneficial.

Table 3.3
Cesium and strontium fission products[45]

		In discharge fuel 10^6 Ci/yr	
Radionuclide	$T_{1/2}$	150-day decay	10-yr decay
^{134}Cs	2.046 yr	5.83	0.228
^{135}Cs	3.0×10^6 yr	7.79×10^{-6}	7.79×10^{-6}
^{136}Cs	13.7 days	5.42×10^{-4}	0
^{137}Cs	30.0 yr	2.92	2.33
^{89}Sr	52.7 days	2.65	0
^{90}Sr	27.7 yr	2.09	1.65

We investigate steam reforming as a method to create a waste form that incorporates the isotopes in one step, at relatively low temperatures, with manageable secondary waste streams.

3.2.1 Pollucite

Pollucite ($CsAlSi_2O_6$) is the most common source of cesium found in nature. The approximate chemical composition of gem quality euhedral crystals have alkali metal weight percentages: Cs (32%), Na (2%), K (<1/2%), Rb (< 1/2%)[46]. To make a waste form, this chemical tolerance to impurities should be an asset. Pollucite has been touted as the most stable phase under repository conditions[47] and stability to radiation effects have been found to be reasonable. These characteristics are attributed to the zeolite nature of pollucite.[48] Zeolites are cage-like structures with empty spaces that allow for compaction and some molecular damage.

$CsAlSi_2O_6$ when composed of ^{137}Cs is transformed by radioactive decay, ^{137}Cs becomes ^{137}Ba under β^- decay:

$$Cs^{+} \xrightarrow{\beta^{-}} Ba^{2+}$$

The resulting ^{137}Ba is meta-stable and will quickly transform($T_{1/2}$= 2.6 min) to a stable configuration by giving off a 662 keV gamma. This process will deform the structure over time. To determine the overall suitability will depend on concentration of ^{137}Cs and the waste form's final structure. Investigations of pollucite for waste storage have shown good leach rates, low solubility and good thermal stability while conceding uncertainties in radiation stability and transmutation effects.[49] ^{137}Cesium doped pollucite (synthesized from colloidal silica solution with stoichiometric amounts of cesium and aluminum nitrates which was stirred and dried, then calcined at 793–813 K followed by grinding, compaction at 250 Pa, and finally sintering) has been observed for β^{-} radiation effects on the long-range and local structure of pollucite.[50] The study above was not able to observe the γ effects due to small sample size but found swelling and distortion of the lattice. This may not be identical to a steam reformed pollucite product, but suggests waste product testing with active cesium will eventually be necessary to determine overall suitability of the waste form. ^{137}Cs, ^{135}Cs, and ^{133}Cs will not be separated due to near identical chemical behavior. ^{135}Cs gives off a 0.21 MeV β^{-} which decays to ^{135}Ba with $T_{1/2}$= 2.3 $\times$ 10^{6} years, and ^{133}Cs is stable.

The creation of pollucite, Figure 3.1 in our experiment, is assumed to occur according to the following:

$$2CsNO_3 + 4SiO_2 + Al_2O_3 + 5C \longrightarrow Cs_2Al_2Si_4O_{12} + N_2 + CO_2 + 3CO$$

The molar Gibbs free energies of formation for pollucite have been determined for differing compositions Table 3.4. The composition of our waste form will not have the exact same composition of any of the forms shown. Naturally occurring pollucite has sodium and rubidium in amounts that vary depending on the mineral's source. These energy values are for illustrative purposes and will only give a general range for the Gibb's free energy of formation for pollucite.

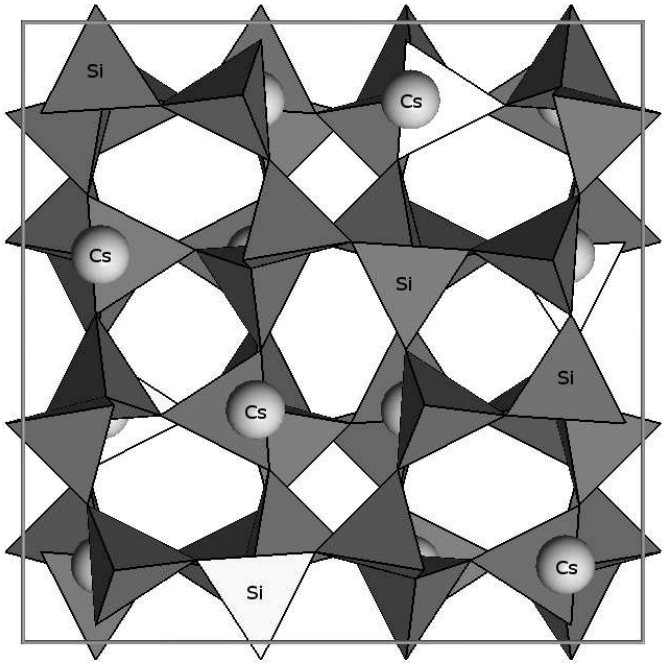

Figure 3.1. Pollucite unit cell

Table 3.4
Gibbs free energies of formation for pollucite (298.15 K)

Type	Chemical Composition	$\Delta_f G_m^\circ$(kJ mol^{-1})
Pollucite	$Cs_{0.65}Na_{0.185}Rb_{0.028}AlSi_2O_{5.863}OH_{0.137} \cdot 0.19H_2O$	-2919.9[51]
Pollucite I	$Cs_{0.77}Na_{0.14}Rb_{0.04}Al_{0.91}Si_{2.08}O_6 \cdot 0.34H_2O$	-2921[52]
Pollucite II	$Cs_{0.84}Na_{0.11}Al_{0.88}Si_{2.10}O_6 \cdot 0.17H_2O$	-2911[52]

3.2.2 Strontianite

Strontium carbonate or strontianite $SrCO_3$ is a natural source of strontium, another is celestite $SrSO_4$. We will not add sulfur to our reaction mixture so it will only be available in the individual reactant impurities so celestite creation should be minimal. Unlike cesium there are a number of possible outcomes for a steam reformed

product from reactants alumina and carbon added to strontium nitrate in nitric acid. Potential products (but not limited to this list) are strontium substituted feldspar, slawsonite, and Sr-brewsterite.

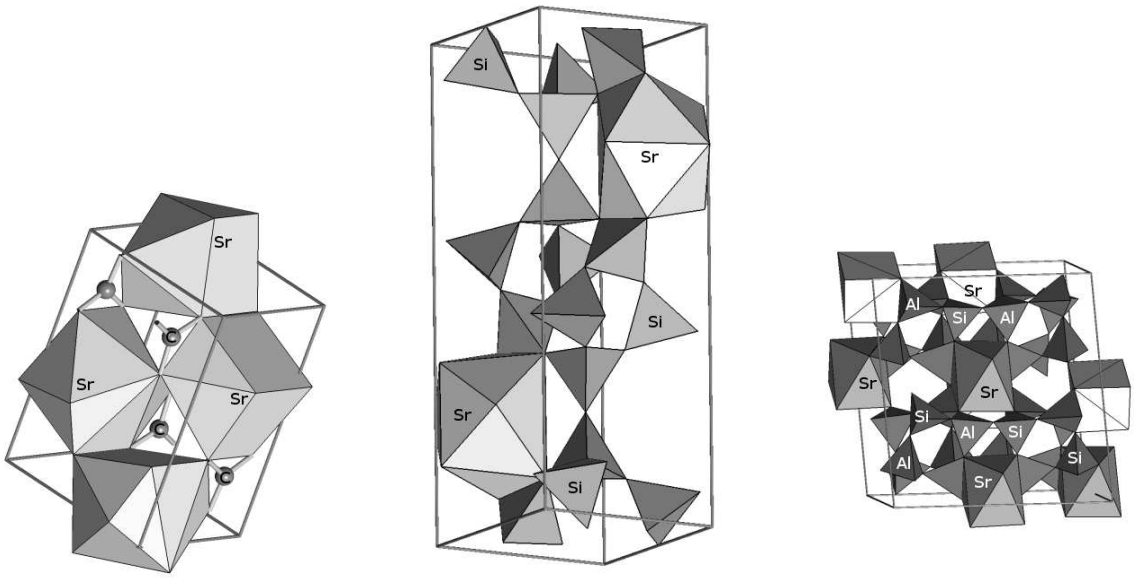

(a) Strontianite (b) Sr-brewsterite (c) Sr-feldspar

Figure 3.2. Strontianite Sr-feldspar Sr-brewsterite unit cells

The number of possible reaction paths strontium nitrate takes under steam reforming conditions makes a thermodynamic analysis out of the scope of this study. We have many avenues for potential research determining mechanisms and kinetic parameters when reacting strontium containing wastes. The addition of metal oxides can produce another series of potential products. Each of these radioactive waste treatments may have benefits yet unknown. To determine what a waste form structure is, the most logical way to begin is to know the composition of the waste stream. Once the half life and chemistry of the waste to be treated is known, the waste form characteristics can be defined. Knowing what is desired, such as the longevity and durability under the specific radiation of the waste, and what physical attributes are important, will guide the waste form design. A benefit of the lab scale steam reformer

is the relative ease of feed composition alteration, making it possible to customize the desired product with little or no modification to the apparatus.

4. METHODS

The work we have done consists of a very simple fluidized bed. The principle fluidized beds employ is a technique used to bring reactants energetically into contact with each other for mixing and subsequent interaction. Fluidization refers to the levitation of a mass of particles, or bed, by a fluid. In our case the carrier fluids are steam or argon. In our system, flow is maintained by a small pressure gradient $\leq$ 1 p.s.i. (6.895 kPa). The fluid carries the reactants and causes them to collide with each other. The intense mixing produces an effectively isothermal system with good mass transfer. The fluidized bed creates ideal conditions for reaction, mixing, drying and heat transfer.[53]

Two methods were tested in our study. Our reactants will be placed inside the fluidized bed initially, or injected after reaching the $\sim$ 700 °C reaction temperature. In the first run of experiments the test tube with the reactant solution is heated to the boiling point, then the steam flow is started. The steam is continuously blown through the bed until the experiment is finished. The fluidized bed is heated up to a reaction temperature of $\sim$ 700 °C, after reaching this temperature the system is held and allowed to react. After the desired reaction time is reached the heating furnace is turned off. Steam continues to flow through the system as the temperature decreases. After reaching approximately 300 °C the steam inlet is closed, and the steam generator is shut down. The entire system is allowed to cool for approximately 12 hours before sample removal and system examination.

Another trial was done with the waste feed added after reaching the reaction temperature. In these experiments only the dry reactants were placed in the reaction tube initially. Instead of steam, argon gas was used to fluidize the bed. The system was heated to the same final temperature of $\sim$ 700 °C under argon flow. After

reaching the reaction temperature the waste simulant was slowly injected into the reaction chamber.

4.1 Apparatus

The system we created for waste treatment experimentation is completely enclosed in a chemical hood with the exception of the steam generator (Figure 4.1). The system consists of a closed end alumina tube 20″ (50.8 cm) long and 2″ (5.08 cm) in diameter. The tube is the reaction chamber which is heated by a clam-shell heater. The steam/argon inlet and outlet are 1/4″ (.635 cm) Inconel tubing to withstand the high heat and corrosive environment. The steam/argon inlet reaches down into the alumina tube to approximately 1″ (2.54 cm) above the bottom of the closed end. Method 2 employs a waste feed inlet, and does not require an outside steam source 4.2. The waste feed tube is an 1/8″ (.3175 cm) Inconel tube that reaches approximately three inches (7.64 cm) from the bottom of the alumina tube.

To keep the high heat from traveling outside the reaction zone, heat shields made out of A-286 stainless steel have been pressed to fit onto the steam/argon inlet tube. These shields effectively reduce temperatures at and above the test tube closure, protecting the gasket and supporting structure. Laying on top of the clam shell heater and wrapped around the alumina tube, a silica insulating matting is used to keep heat focused around the reaction area, and away from the rest of the apparatus. The fluidizing gas outlet and inlet tubes have pressure gauges, and thermocouples to monitor gas conditions before and after entering the reaction region. The temperature on the alumina reaction tube's surface at the reaction area is also monitored. In Method 2 a thermocouple inside the reaction tube was added.

After the steam/argon exits the alumina tube it goes through a particle trap which consists of concentric acrylic tubing to trap particles that may travel out of the reaction tube, a drain has been installed to remove excess condensation. After the particle trap, steam enters a heat exchanger made of 3/8″ (.9525 cm) finned copper

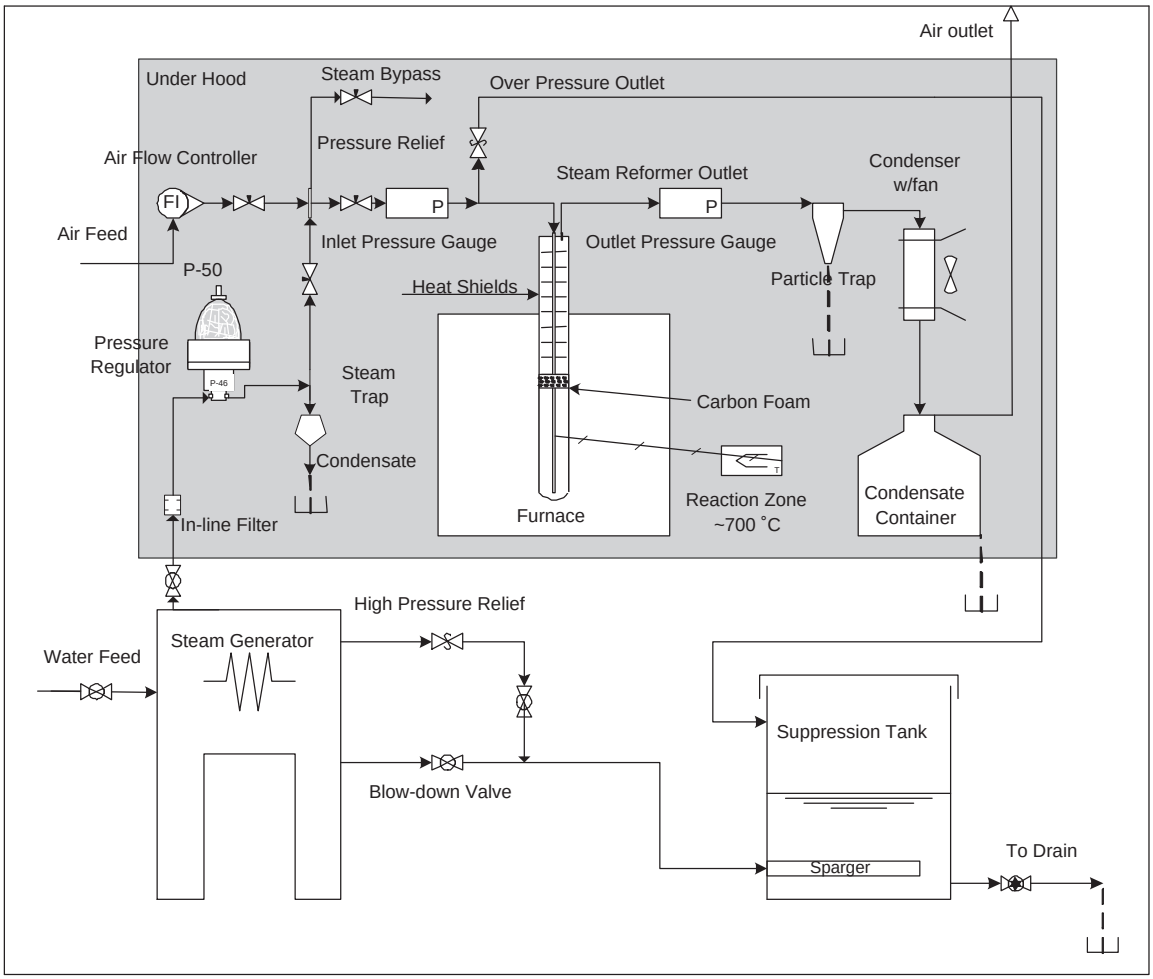

Figure 4.1. Steam reformer Method 1

tubing with a fan attached to cool and condense the steam which finally enters a condensate collection container, also with a drain and air vent tube that leads to the top of the hood. In Method 1 steam is provided by a Sussman MBA Electric Steam Generator (SG) fed by municipal supply water. The SG provided steam 45-55 p.s.i. (310-379 kPa), which was regulated down to 1 p.s.i. (6.895 kPa)). In Method 2 steam is provided by the waste solution itself. The argon for Method 2 is fed from a pressurized bottle, which is regulated down to 5 p.s.i. (34.5 kPa), then lowered further with a needle valve.

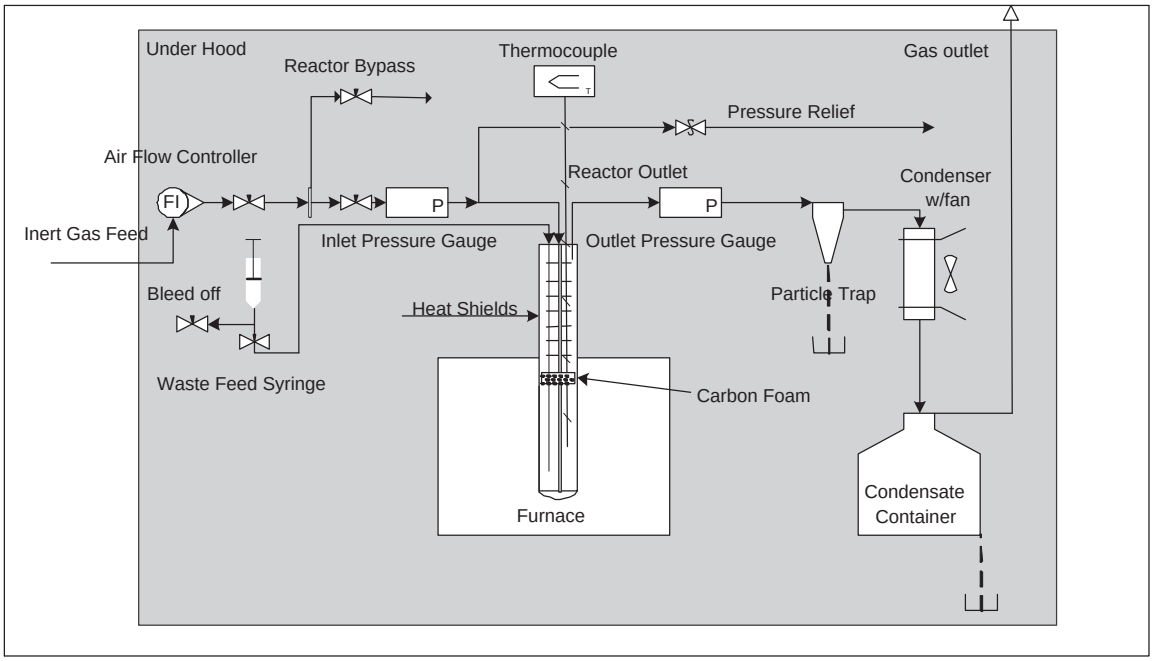

Figure 4.2. Steam reformer Method 2

4.2 Chemical Feed

The reactants chosen have been selected to simulate a potential radioactive waste in the event of a AFC where the removal of cesium and strontium is employed. The exact method of separation is not yet determined, but we have chosen the FPEX process stream. In the FPEX process the final product stream contains the cesium and strontium dissolved in nitric acid. To simulate this waste steam cesium nitrate ($CsNO_3$) and/or strontium nitrate ($Sr(NO3)_2$) were dissolved in dilute nitric acid. The nitric acid plus nitrate make up the waste simulant. No radioactive isotopes are used in this study.

The waste simulant solution was reacted with minerals to create a solid waste form. The minerals are either added to the waste solution, then heated to the reaction temperature (Method 1). Or the minerals were placed in the reactor vessel at the start, fluidized with argon, and then the waste feed was injected at the reaction

temperature. In addition to the mineral additives a carbon source is added for nitrate destruction.

The minerals we have chosen are in the form of Kaolin, which is a mixture of silica and alumina with an approximate formula $Al_2Si_2O_5(OH)_4$. The carbon source is granular activated carbon and/or carbon foam. In Method 1 a starter material, in addition to the kaolin, was added to the waste solution. SiO_2 beads were added to provide a reactive surface for the waste form creation to initiate. The SiO_2 beads were of a size range 800-1000 μm.

The stoichiometry was tailored to create cesium and/or strontium aluminum silicates. This mineral structure was chosen only as a basis. For the cesium experiments the target material chosen was pollucite, $Cs_2Al_2Si_4O_{12}(H_2O)$. In experiments with strontium, slawsonite was the assumed product, $SrAl_2Si_2O_8$. Typically it was attempted to produce 1 gram of mineral product at a time. To create one gram, stiochiometric amounts of nitrate were dissolved in dilute nitric acid, 0.276 M HNO_3. The waste feed was reacted with kaolin, $Al_2Si_2O_5(OH)_4$ and carbon. The limiting reactants in the cesium experiments were the cesium itself, and the SiO_2 in the kaolin; this is due to the 2:1 ratio of Si:Al ratio in pollucite. In experiments with strontium, the $Sr(NO_3)_2$ to kaolin ratio was 1:1. The amount of carbon added was one $\sim$1 mole of carbon to $\sim$1 mole nitrate in the first experiments, but was actually in excess after Experiment 1 with the addition of carbon foam to the top of the reaction zone. SiO_2 beads were added in varied amounts, 0 grams in experiments 9 and 10, and from 0.25 to 1.0 grams in all previous experiments; this is detailed in Results.

4.3 Operation

4.3.1 Method 1

To begin, the reactants are mixed and put inside the reaction tube. To the lowermost heat shield, a circular section of carbon foam is added to reduce the amount of reactant particles that carry over. The tube is then attached and sealed in position

under a support plate centered inside the clam shell heater. Inlet and outlet tubing is attached to the tube seal in a fixed position. Silica pad insulation is placed above the heater and surrounding the alumina tube; a pad insulation is also placed under the clam shell heater.

The steam generator sparge tank is filled between 2/3 and 3/4 full. The steam generator emergency pressure relief outlet valve is opened and the steam blow down valve is closed. The municipal inlet water supply valves are opened. The steam pressure upper bound is set to 45 p.s.i. (310 kPa). The reactor main steam inlet valve is opened; the steam inlet needle valve is closed. The reaction air feed inlet valves are all closed. The steam generator is turned on.

The variac power controller is switched on and set to 30-50% . The temperature at the reaction area on the alumina tube is continuously monitored. The temperature is increased by increasing the variac outlet percentage. The heating rate was initially kept below 5 °C per minute, but after some problems the rate was lowered to $2 - 3$ °C per minute. The reaction tube outlet and inlet gas temperature is monitored as the reaction region temperature increases. The temperature of these tubes should be at or near ambient until the liquid in the reaction tube begins to boil. At this point the steam generator should be pressurized and ready to provide steam to the reactor. The needle valve inlet is opened allowing steam into the reactor tube.

Steam is continuously fed to the system. The particle trap is observed to keep the condensation from filling the trap; once the water level in the trap exceeds $3/4''$ (1.905 cm) it must be drained. All water drained must be collected and treated as hazardous chemical waste. Additionally the condensation collection container may require draining occasionally during operation, this water also must be collected as waste.

The reaction area temperature is increased until reaching 700 °C at this point the temperature is stabilized by monitoring and adjusting the current appropriately. The minimum temperature is 700 °C, while the maximum temperature is 725 °C. The

reaction temperature is held at this range for the desired time for reaction, typically one hour.

Once the predetermined time duration is satisfied, the heat is reduced and steam is eventually shut off. To keep the particles from agglomerating, gas flow should be kept running till $\sim$ 300 °C. The water inlet to the steam generator is closed. The emergency pressure relief outlet valve is closed. The blow down valve is opened carefully, wearing gloves or holding an insulating pad, because it will be very hot, and slowly, allowing the remaining steam to enter the sparging tank. Once the steam generator is completely drained, the sparging tank may be also drained into the sewer.

After cooling down for approximately 12 hours the sample may be removed for examination.

4.3.2 Method 2

After analysis of samples created by Method 1 (discussed in Results) the system design was changed. The most significant decision was to feed the reactants to the reactor after reaching the reaction temperature.

To improve the design an 1/8″ (.3175 cm) Inconel feed tube and a syringe, as well as a internal thermocouple were added to the system. The use of an inert gas (argon) was chosen as the fluidizing medium instead of steam. The silica beads used in Method 1 were omitted.

The alumina tube is first loaded with kaolin and carbon. The reactants are fluidized with argon gas and heated to $\sim$ 700 °C at a rate of $\sim$ 3 °C per minute. The waste is loaded into a syringe attached to the 1/8″ (.3175 cm) feed tube. After reaching the reaction temperature, the waste is injected into the heated tube. No other source of steam is necessary due to the water in the waste feed. Once all the waste is injected, the temperature is slowly reduced ($\sim$ 3 °C per minute). When the temperature is lower than 300 °C the gas flow is shut off. The current is slowly lowered, and

when the lower current no longer decreases the cooling rate, it is completely shut off. After a 12 hour cool off period the samples are ready for removal.

5. RESULTS

5.1 Method 1

The first experiments were done with steam generated from the municipal water supply. The water was filtered with a general purpose rust and sediment filter. The waste simulant and reactants were all mixed initially, and placed inside the reaction tube. The tube was slowly heated to boiling, then steam was fed into the reaction tube to fluidize the reactants.

5.1.1 Experiment 1

Table 5.1
Experiment 1 Reactants

Reactant	Amount	Form
$CsNO_3$	0.610 g	dissolved in 100 ml 0.276 M HNO_3
kaolin	0.885 g	0.1–4 μm powder
carbon	1.10 g	$\leq$ 40 μm activated charcoal
SiO_2	1.01 g	800–1000 μm spheres

Result: 0.91 grams product, a mixture of silica beads (<0.10 g coated Figure 5.1) and loose powder.

Experiment 1 Discussion

During this experiment the control of steam flow was very difficult. During the entire experimental run the flow had to be adjusted with the inlet needle valves. The reactor tube inlet pressure fluctuated from 0.5–2 p.s.i. (3.45–13.79 kPa). The particle trap collected a large amount of reactants. During this run the voltage percentage

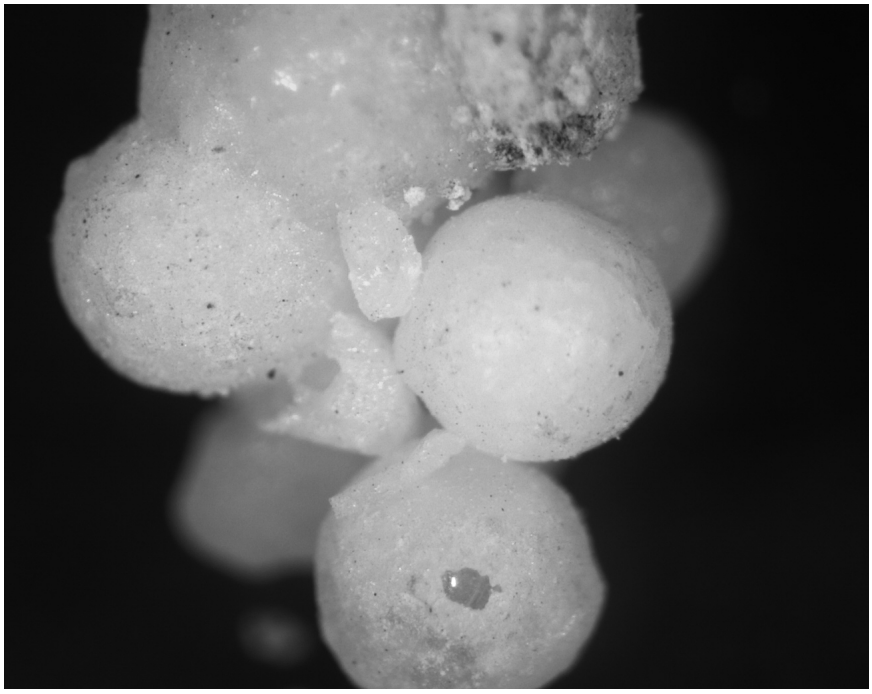

Figure 5.1. Experiment 1 Product

was held at 100% for about two and a half hours, recording a peak test temperature of 719 °C.

Determined to install a pressure regulator. The regulator was ordered to specifically reduce the steam generator pressure of 45–55 p.s.i. (310–379 kPa) down to 1–5 p.s.i. (6.90–34.47 kPa). In addition to the pressure regulator a carbon foam plug was attached to the bottom of the lower most heat shield. The carbon foam adds an additional source of carbon, and aids in the prevention of reactants blowing out of the reaction vessel.

5.1.2 Experiment 2

Result: 0.91 grams of solid product. The product was a dark grout like material, Figure 5.2. No silica beads remained. No information could be assessed from the XRD analysis.

Table 5.2
Experiment 2 Reactants

Reactant	Amount	Form
$CsNO_3$	0.60 g	dissolved in 100 ml 0.276 M HNO_3
kaolin	0.88 g	0.1–4 μm powder
carbon	0.99 g	$\leq$ 40 μm activated charcoal
SiO_2	1.09 g	800–1000 μm spheres

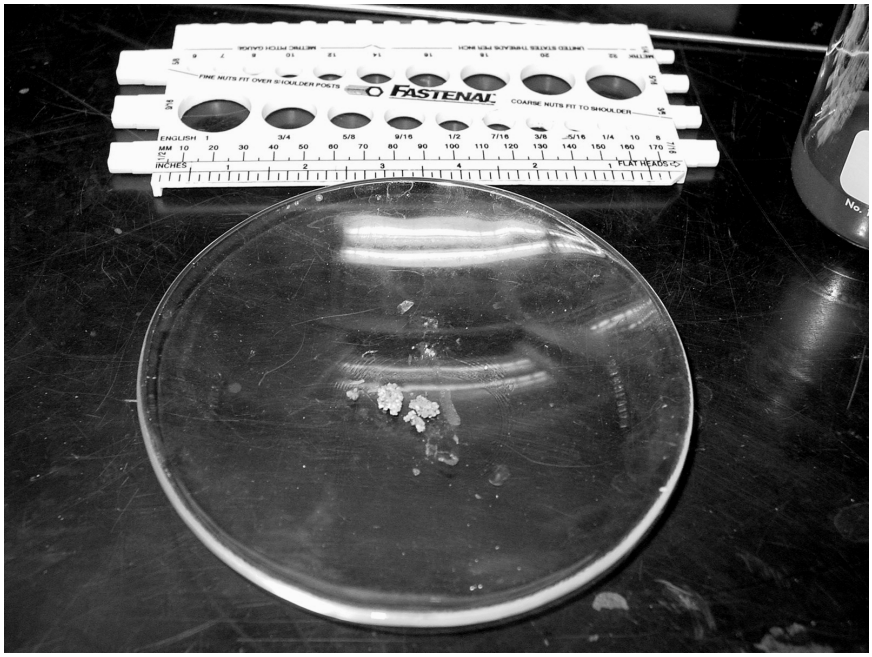

Figure 5.2. Experiment 2 Product

Experiment 2 Discussion

The silica beads were consumed in this experiment. To take advantage of this, the silicon oxide from the beads was included in the Experiment 3 stoichiometry. The voltage percentage was held at 100% for about one hour reaching a maximum temperature of 721 °C.

Table 5.3
Experiment 3 Reactants

Reactant	Amount	Form
$CsNO_3$	1.24 g	dissolved in 100 ml 0.276 M HNO_3
kaolin	0.885 g	0.1–4 μm powder
carbon	1.0 g	$\leq$ 40 μm activated charcoal
SiO_2	1.01 g	800–1000 μm spheres

5.1.3 Experiment 3

Result: Tube broke at $\sim$ 441 °C, the current voltage was at 90%.

Experiment 3 Discussion

This experiment was stopped after the first hour due to a clog in the steam inlet line. The pressure regulator has a pin hole opening which lowers the steam pressure. Particles in the water supply were making it to the regulator, clogging the outlet hole. A 1/4″ (0.635 cm) inline filter was installed. The filter was installed after the steam generator and before the regulator. The steam generator vessel is cast iron, and rust is visible in the water after draining the system after experiments. This may be the source of the particles clogging the feed line. This adjustment caused a one week delay.

5.1.4 Experiment 4

Table 5.4
Experiment 4 Reactants

Reactant	Amount	Form
$CsNO_3$	1.22 g	dissolved in 100 ml 0.276 M HNO_3
kaolin	0.80 g	0.1–4 μm powder
carbon	1.0 g	$\leq$ 40 μm activated charcoal
SiO_2	0.50 g	800–1000 μm spheres

Result: Tube broke at ~ 444 °C, the current voltage was at 85%.

Experiment 4 Discussion

Half as many SiO_2 beads were used in this experiment. During this experimental run a brown gas was visible in the condensate container at ~ 264 °C.

5.1.5 Experiment 5

Table 5.5
Experiment 5 Reactants

Reactant	Amount	Form
$CsNO_3$	0.645 g	dissolved in 100 ml 0.276 M HNO_3
kaolin	0.255 g	0.1–4 μm powder
carbon	0.51 g	≤ 40 μm activated charcoal
SiO_2	0.105 g	800–1000 μm spheres

Result: Tube broke, not realized until after shut down. The highest temperature reading was 727 °C at a current voltage of 90%. Small amount of product recovered, 0.09 g.

Experiment 5 Discussion

After considering all the reasons for the continued problems with tubes breaking, the assumption was made that water was entering the tube and flashing. Possible sources of water are the feed itself, or water condensing downstream and flowing back down into the reaction tube. In an attempt to limit condensation within the system these steps were taken, (1) added a steam trap, (2) increased and added insulation to most of the inlet and outlet tubing, and (3) lowered the particle trap.

The steam trap is a condensate collection vessel with a float operated valve to release water that condenses in the feed line. The steam trap was installed just before the reaction tube entrance.

While waiting for new alumina tubes to continue with the experiments, a test was done on the system without any chemicals. With a used, and expendable tube, the steam trap and other modifications were tested. In the dry run experiment the test tube did not rupture, and the voltage percentage never exceeded 70% with a maximum temperature of 670 °C.

Another possible reason the alumina tubes kept breaking may have been a sudden reaction occuring. A spontaneous gereration of hot gases could fracture the tube if this were occuring. To aid the reaction a small amount of iron oxide, to act as a catalyst, was added in the next experiment.

5.1.6 Experiment 6

Table 5.6
Experiment 6 Reactants

Reactant	Amount	Form
$CsNO_3$	0.66 g	dissolved in 100 ml 0.276 M HNO_3
kaolin	0.26 g	0.1–4 μm powder
carbon	0.505 g	$\leq$ 40 μm activated charcoal
SiO_2	0.25 g	800–1000 μm spheres
Fe_2O_3	<0.01 g	Powder

Result: Test tube broke during cool down. There was a clean break at the furnace-to-insulation transition. Due to the placement of the break the product was salvaged. A significant amount of product was recovered, 0.27 g of coated particles, Figure 5.3 and 0.165 g of powder. Temperature reached a maximum reading of 724 °C, at a current voltage of 70%. Chemical analysis determined the sample to be 3 mass percent cesium.

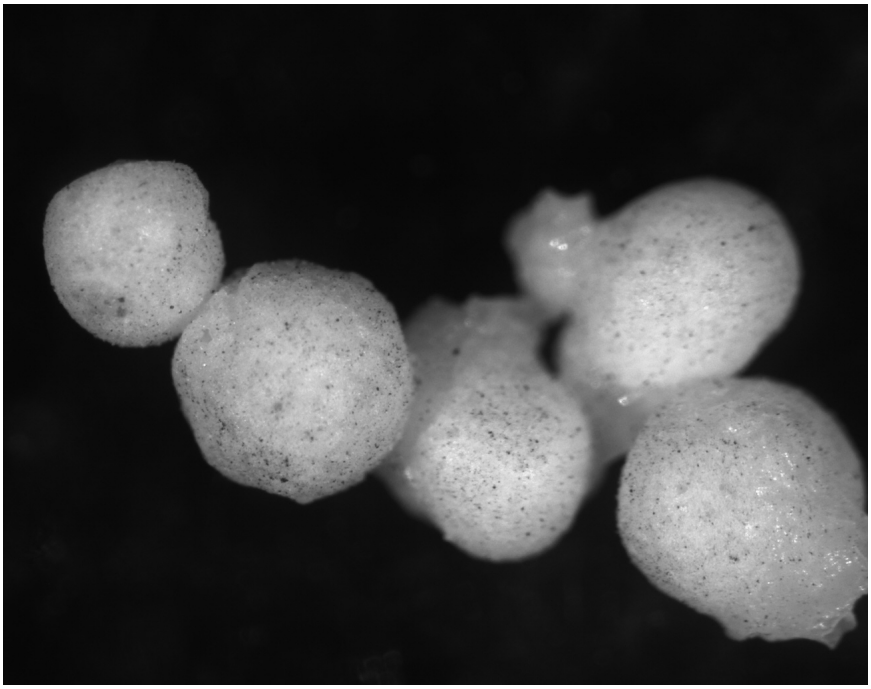

Figure 5.3. Experiment 6 Product

Chemical Analysis

ANL chemical analysis was done on the sample with ICP/OES and ICP-MS* Table 5.7.

Table 5.7
Experiment 6 Chemical Analysis

Metal	Al	Si	Ca	K	Na	Cs*
Mass percent	1.91	27.4	12.0	0.58	10.9	2.77

Experiment 6 Discussion

An XRD analysis of the product, Figure 5.4, found the peaks characteristic of sodium calcium silicate. XRD could not confirm or deny the presence of pollucite in the sample.

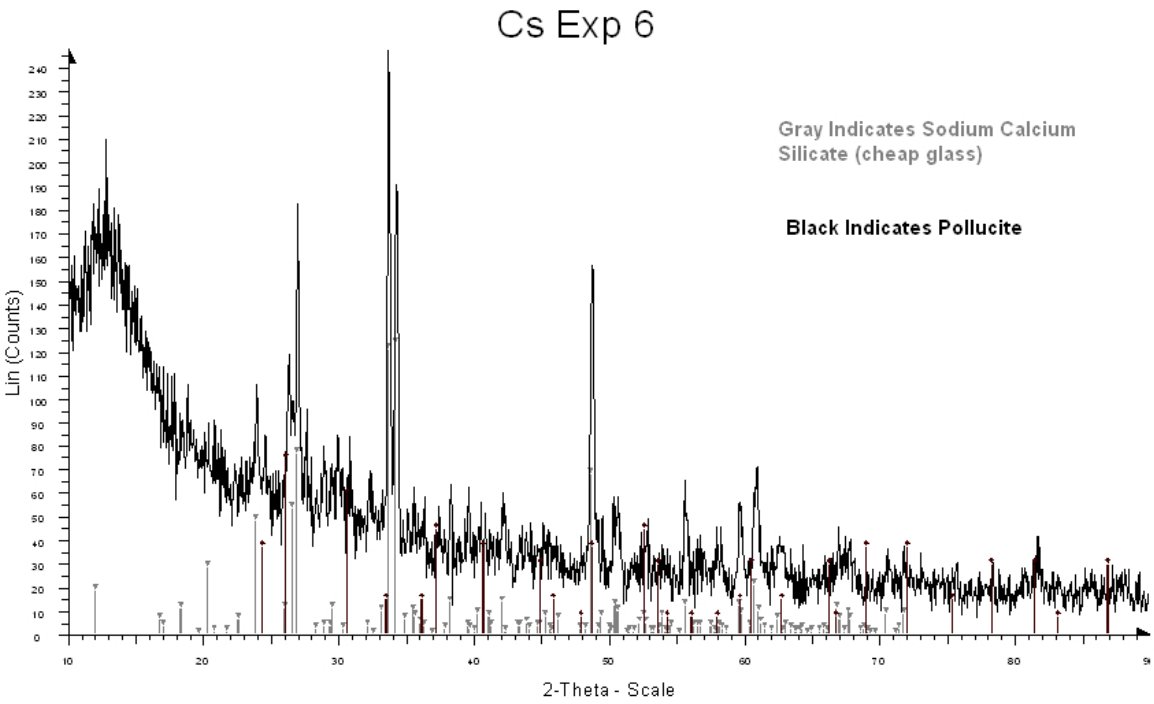

Figure 5.4. Experiment 6 XRD

After experiment 6 was completed, the appearance of the product was very encouraging. This was the first of only two samples shipped to ANL for chemical analysis. Determined to attempt a strontium experiment without catalyst next.

5.1.7 Experiment 7

Table 5.8
Experiment 7 Reactants

Reactant	Amount	Form
$Sr(NO_3)_2$	0.70 g	dissolved in 100 ml 0.276 M HNO_3
kaolin	0.50 g	0.1–4 μm powder
carbon	0.50 g	$\leq$ 40 μm activated charcoal
SiO_2	0.50 g	800–1000 μm spheres

Result: A very clean white product was created. Reached a maximum temperature reading of 730 °C, at a current voltage of 74%. A sample was sent to ANL for analysis.

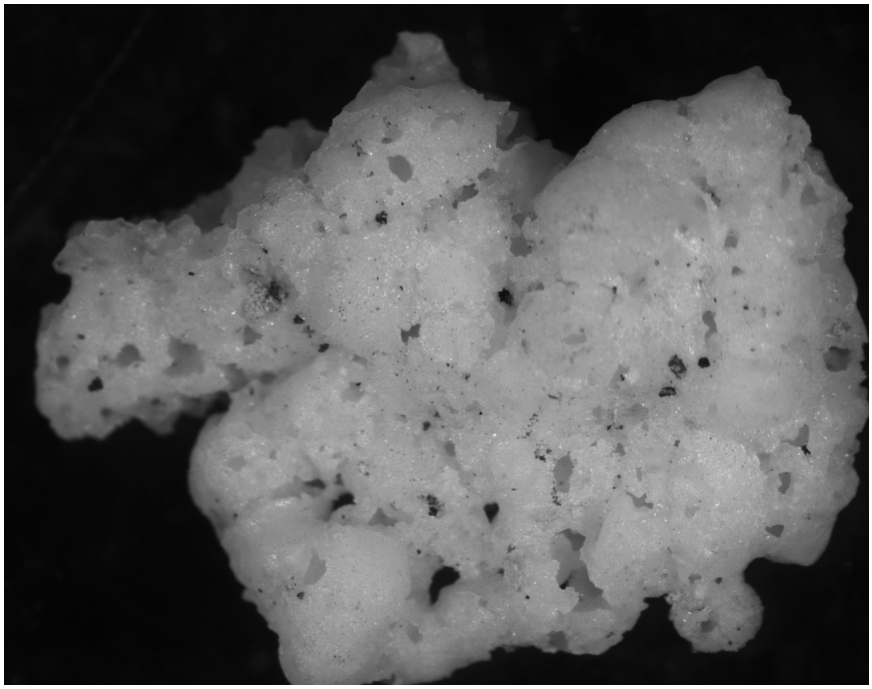

Figure 5.5. Experiment 7 Product

Chemical Analysis

ANL chemical analysis was done on the sample with ICP/OES twice, Table 5.9.

Table 5.9
Experiment 7 Chemical Analysis

Metal	Al	Si	Ca	K	Na	Sr
Mass percent (1)	1.49	29.5	12.3	0.67	11.3	0.11
Mass percent (2)	1.51	29.4	12.5	0.67	11.3	0.12

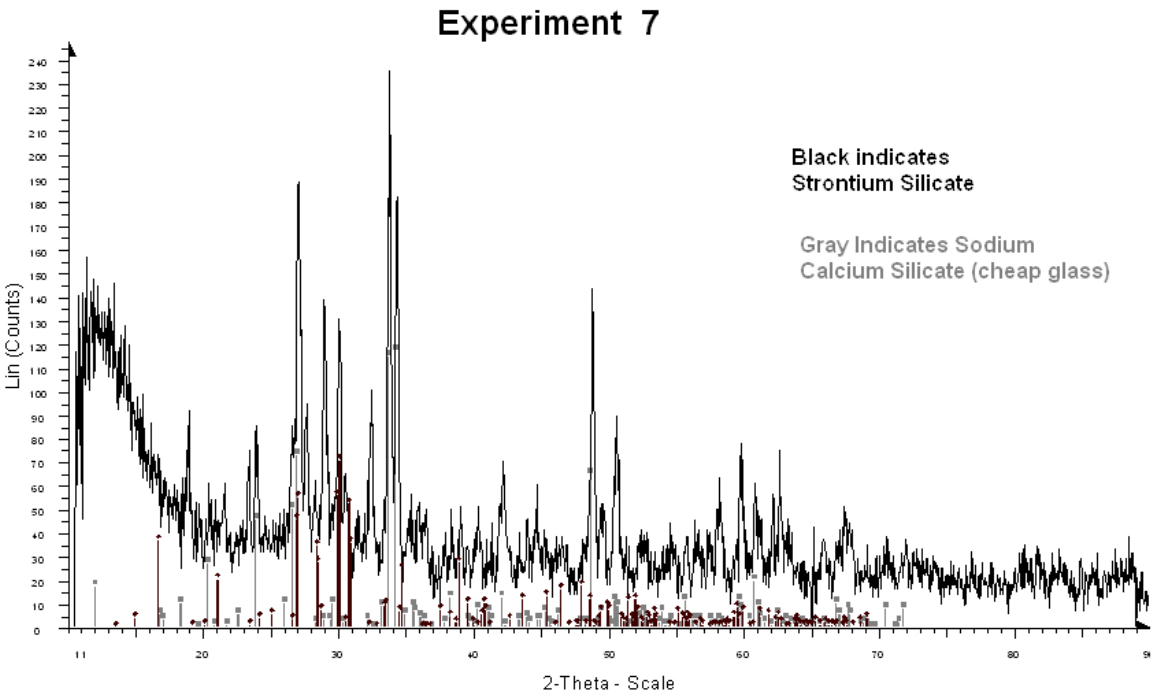

Figure 5.6. Experiment 7 XRD

Experiment 7 Discussion

The product sample under an optical microscope appeared to have completely changed the silica beads, Figure 5.5. The spherical shape is distorted and appears porous. ANL chemical analysis found only a very small amount of strontium in the sample, ∼0.11 mass percent, Table 5.9. Determined to run cesium mixed with strontium experiment next. From conversations with J. Tripp[3] chose a 3:1 cesium to strontium ratio.

5.1.8 Experiment 8

Result: Product was in separate fractions: one had large agglomerated white pieces, Figure 5.7, another mixed portion of smaller agglomerates mixed with uncoated particles. The last two portions were powders that appeared to be unreacted

Table 5.10
Experiment 8 Reactants

Reactant	Amount	Form
$CsNO_3$	0.62 g	dissolved in 100 ml 0.276 M HNO_3
$Sr(NO_3)_2$	0.22 g	dissolved in 100 ml 0.276 M HNO_3
kaolin	0.605 g	0.1–4 μm powder
carbon	0.505 g	$\leq$ 40 μm activated charcoal
SiO_2	0.67 g	800–1000 μm spheres

clay and an ash-like material. The maximum temperature reached was 724 °C at a current voltage 68%.

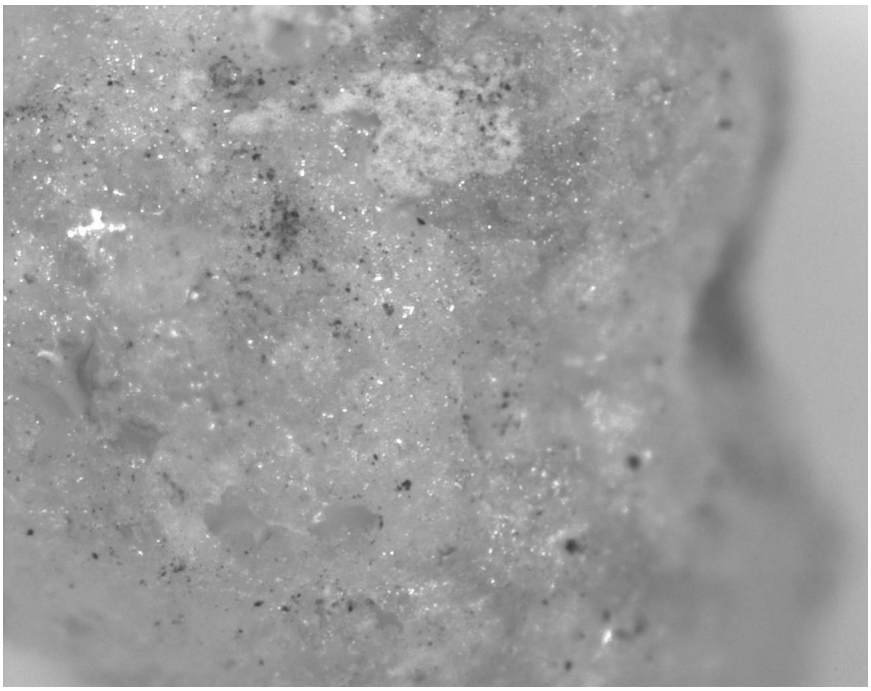

Figure 5.7. Experiment 8 Product

Experiment 8 Discussion

Results from the chemical analysis done at ANL on Experiment 7's product were received after this experiment. The levels of strontium were extremely low, ∼1/10

of 1%. The XRD data from Experiments 6, 7, and 8 were very similar Figure A.1. Assumed that Experiment 6 (cesium) would have similar results, and also be low. Assumed the strontium, or cesium may be in a amorphous phase of the material, or very little is present. The primary product appeared to be a glass like material, sodium calcium silicate. Determined the system required modifications to improve performance.

5.2 Method 2

Due to low strontium loading found in Experiment 7, and XRD data that showed little difference between experiments, the system was changed. The lack of strontium in the product may be due to the steam carrying it out of the reaction area. Argon was chosen to fluidize the powder reactants until reaching the reaction temperature. After reaching the reaction temperature, the waste simulant was injected into the hot vessel pre-loaded with the co-reactant powders. The silica beads were omitted.

5.2.1 Experiment 9

Table 5.11
Experiment 9 Reactants

Reactant	Amount	Form
$CsNO_3$	0.70 g	dissolved in 60 ml 0.276 M HNO_3
kaolin	1.125 g	0.1–4 μm powder
carbon	0.35 g	$\leq$ 40 μm activated charcoal
argon	continuous	inert gas

Result: Created about one gram of product. The product was a gray powder with white specs Figure 5.8. The maximum temperature reached was 729 °C at current voltage of 64%.

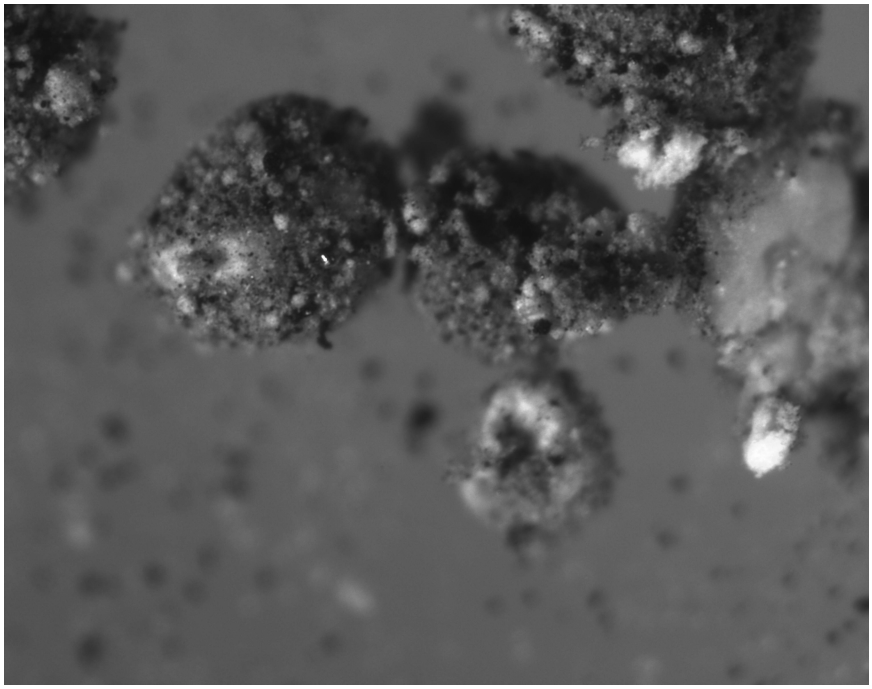

Figure 5.8. Experiment 9 Powder

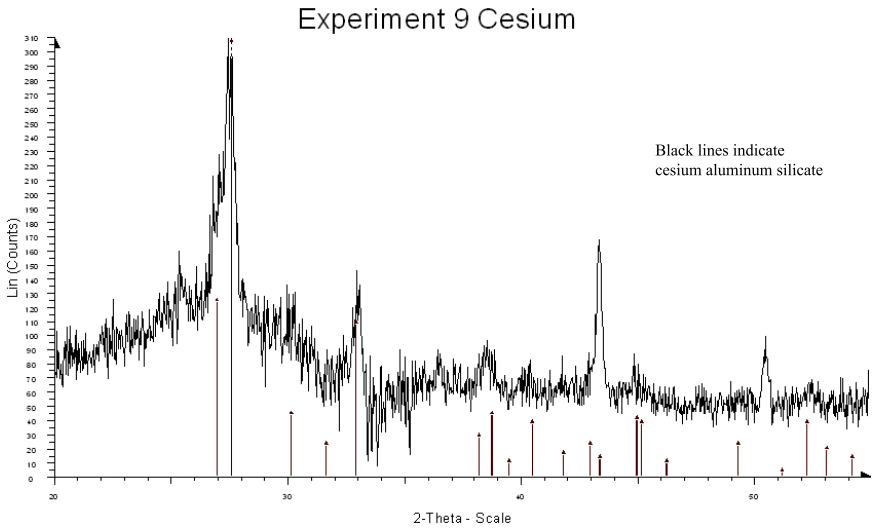

Figure 5.9. Experiment 9 XRD

Experiment 9 Discussion

XRD analysis found strong evidence for the presence of cesium aluminum silicate, Figure 5.9. Determined XRD data may be improved with a higher yield. To improve

the yield the amount of strontium nitrate was be doubled in Experiment 10, Table 5.12.

The initial calculations assumed pollucite,$CsAlSi_2O_6$ as the product. After these experiments, cesium aluminum silicate ($CsAlSi_2O_4$), appears to be more pronounced in the XRD data.

5.2.2 Experiment 10

Table 5.12
Experiment 10 Reactants

Reactant	Amount	Form
$Sr(NO_3)_2$	1.37 g	dissolved in 130 ml 0.276 M HNO_3
kaolin	1.010 g	0.1–4 μm powder
carbon	0.50 g	$\leq$ 40 μm activated charcoal
argon	continuous	inert gas

Result: Created 0.95 grams of product. Most was (0.810 g) a speckled powder; the remainder was in the form of solid pale yellow granules, Figure 5.10. Maximum temperature reached was 727 °C at a current voltage of 66%.

Experiment 10 Discussion

XRD of the gray loose powder found the characteristic peaks of strontianite were well pronounced, Figure 5.11. The white granules were ground up and also analyzed under XRD, but the granules did not display any crystal structure.

Initially, the assumption was that the large pieces were the waste product. During crushing they were soft, and pulverized easily in to a fine dust.

In future work the stoichiometry must be adjusted from slawsonite to strontianite. Strontianite is a water insoluble material, but dissolves in carbonic acid.

Figure 5.10. Experiment 10 Powder and Granule

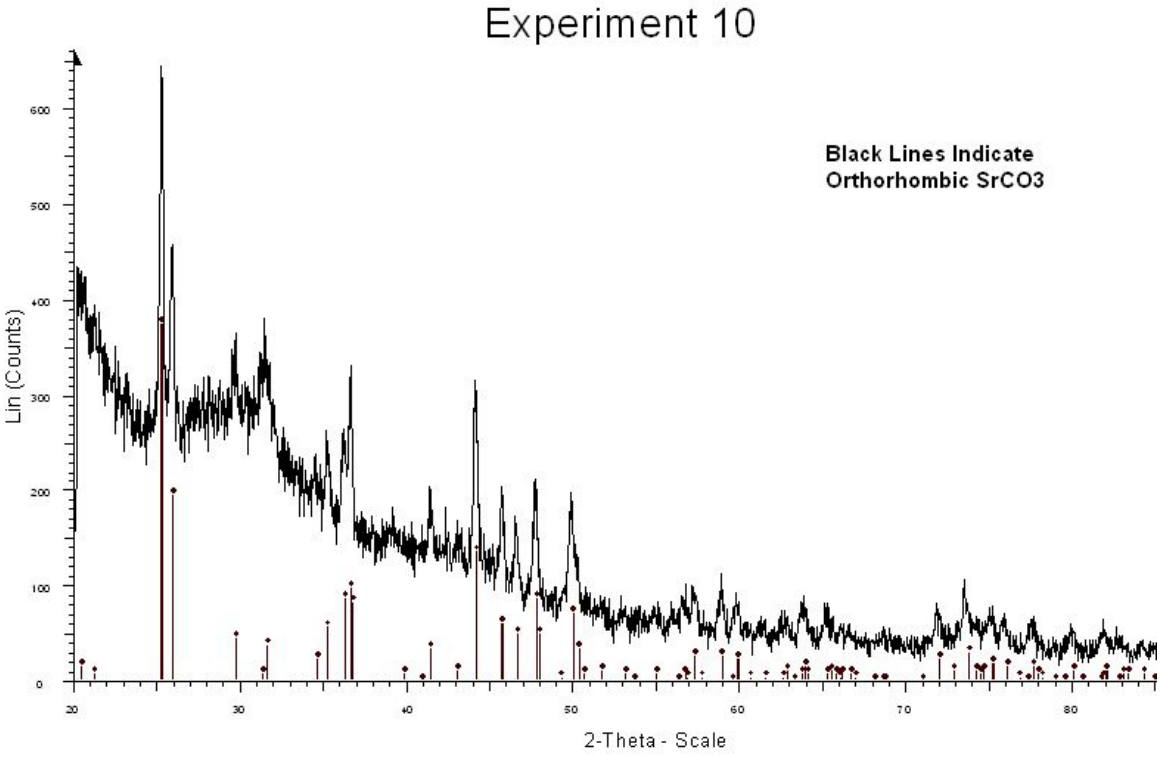

Figure 5.11. Experiment 10 XRD

6. SUMMARY

This study is an attempt to apply steam reforming to a potential AFC waste stream. The waste stream would come from the FPEX process that removes cesium and strontium from SNF. The elements will be dissolved in a dilute nitric acid solution. Steam reforming has been applied to many types of existing tank wastes, and has created solid mineral products.

The goal of this study was to test the feasibility of converting the liquid cesium and/or strontium bearing waste into a water insoluble solid. A waste simulant was prepared by dissolving cesium and/or strontium nitrate (non-radioactive) in dilute nitric acid. This simulant was reacted with silica (SiO_2) and alumina (Al_2O_3) at approximately 700 °C. These oxides were both supplied in the form a kaolin. Kaolin is a mineral clay powder, that consists of approximately 50:50 silica to alumina. In addition to the kaolin, the simulated waste was also reacted with carbon to destroy the nitrate. The first experiments were carried out with silica beads to nucleate the formation of the waste product. One experiment had an iron oxide added as a catalyst.

Two methods were employed. Both methods used an alumina tube as the reaction vessel. The vessel was heated with a resistance heater up to $\sim$ 700 °C. In the first experiments, Method 1 (Experiments 1-8) all the reactants were loaded into the tube initially (kaolin, carbon, and silica beads), then fluidized with steam until the reaction temperature was reached. After holding the system at the desired reaction temperature, the entire system was allowed to cool. XRD analysis found evidence of Sodium calcium silicate present in the product. Cesium was found in the silicate at 2.77 mass percent, and the strontium loading was $\sim$0.11 mass percent, Figure C.1. To increase the loading and improve system reliability, the process was changed.

Under the second method (Experiments 9 and 10) argon gas was employed as the fluidizing gas, and the silica beads were omitted. The method the feed and reactants were loaded into the system was also changed. Instead of loading all the reactants at the beginning, only the dry powders were pre-loaded into the reaction tube. The temperature was raised to the reaction temperture while agitating the powders with argon gas. The simulated waste feed was injected into the system after reaching the reaction temperature. Two forms were identified in the second method's products, cesium aluminum silicate ($CsAlSiO_4$) and strontianite ($SrCO_3$). Both forms are water insoluble powders.

The first experiment created a few coated beads. Initially it seemed like a simple fine tuning of the process would achieve greater yields. Each subsequent experiment prompted changes in the process, but overall the progress limited. Experiment 2 created a grout-like material that was uncharacteristic of all other samples; XRD did not show anything above the background signal noise. The temperature readings may have been in error in the first experiments (the temperature may have been much higher than 700 °C). In the early experiments only the temperature of the surface of the reaction tube was monitored inside the furnace. The voltages were high, up to 100% to achieve the >700 °C temperature. One of the changes done to the system for Method 2, was the addition of an internal thermocouple. The voltage necessary to reach the reaction temperature never exceeded 80% after this modification.

Experiments 3, 4, 5, and 6 all broke their reaction tubes. Experiment 6, due to the nature of the break, left a recoverable product. The Experiment 6 product was shipped to ANL for chemical analysis, as was Experiment 7. After low loading was confirmed with the preliminary results, product shipments to ANL for analysis were halted.

Chemical analysis done at ANL on the products from Experiments 6 and 7 found sodium, potassium, and calcium. These elements are from the composition of the silica beads. XRD analysis on Experiments 6, 7, and 8 also found the crystal structure similar to that of soft glass (sodium calcium silicate) was dominant. The silica beads

were not been pure silica, but glass beads. This fact was not discovered until after the testing was done.

The Method 1 XRD results (Figure A.1) show very little variation in the crystal structure of the product. The cesium and strontium present may be in an amorphous phase within the solid, or due to such low concentration, their presence in the crystalline form may not raise appreciably above the noise in the XRD signal.

The setup was changed after repeated test tube ruptures and poor loading. The source of the problems seemed to be the steam. After employing methods to reduce condensation in the feed line, test tube breakage was reduced, but not eliminated. Cesium and strontium may have been carried out of the reaction area along with the steam. A source of reactant carry over may have been the duration of time to heat the system to the desired reaction temperature while under the flow of the steam. The steam may have washed the reactants out before reaching the desired reaction temperature.

The following changes were made to the process, (1) switching to argon gas as the fluidizing medium, (2) omitting the silica beads, and (3) feeding the waste simulant to the system after reaching the reaction temperature. Implementation of these changes had significant results. The most obvious is the form of the product. The product was primarily a powder after the changes. Method 1 created coated, or reacted beads.

The resulting powders had identifiable crystalline products under XRD analysis. The first attempt with the new set-up was with cesium (Experiment 9, 5.2.1). The XRD analysis displayed peaks characteristic of cesium aluminum silicate ($CsAlSiO_4$). There were also peaks from an unidentified phase, or phases. The second attempt with strontium (Experiment 10, 5.2.2), was carried out with twice the amount of waste simulant used in previous experiments. This created a powder with a strong XRD signal corresponding to strontium carbonate, or strotianite ($SrCO_3$). Stontianite is the second most abundant natural form of strontium found in nature. Strontianite is water insoluble except under acidic conditions.

Both powder products display two separate particle phases under magnification. A mixture of gray and white particles was observed in both samples. Further analysis is necessary to determine the differences and compositions of each phase.

7. RECOMMENDATIONS

The products created in this study have not been tested for suitability as waste forms. To determine if the elements are immobilized effectively specialized testing is necessary. Leachability tests to test how well immobilized the elements are in the product is necessary to determine which steps are necessary to reach a final waste form. In a addition to leachability, the physical durability must be tested also. The product of the Method 2 experiments is a powder, this may be an effective precursor to other forms, but not suitable as final waste form. A radioactive powder has proliferation risks, and would require special handling.

A basic understanding of the thermodynamics involved is necessary for any industrial scale-up of this process. Determining what temperature, and the reaction energies involved during the conversion is essential to the understanding of the processes involved in the reactions. Thermodynamic information could be determined with differential scanning calorimetry testing done on the products.

Product variations should be explored. With modifications to the feed conditions, and changing the reactants other compounds could be created. Using different oxides, instead of silica or alumina, such as zironium and titanium oxides may be suitable candidates for further study. The use of differing fluidization gases may also be an effective way to alter product chemistry. The range of possible products could create an array of potential waste forms, or precursors to waste forms to test.

In our tests the liquid waste was completely dried, but the amount of cesium and strontium in the condensate, and off-gas streams were not measured. To create a full scale process, a thorough analysis of the conversion yield will be mandatory. In addition, identification of all products created will be necessary.

The experiments done here employed a 20″ (50.8 cm) alumina tube. An inert steel reactor will solve most of the breakage issues that developed during this study. A high nickel alloy, such as Inconel or A286 stainless steel would be a stronger reaction vessel. The configuration should also be altered. In a fluidized bed an increasing diameter region creates a gas velocity gradient. A small diameter inlet increasing to a wide diameter outlet causes the gas to enter at a high velocity that decreases along the path to the exit. The decreasing velocity will carry particles up until the gas will no longer support them. The region will have the largest, heavier particles lowest in the reaction region and the lighter smaller particles toward the top. Eventually the particles will grow to size no velocity will carry them, at this point they fall out of the reaction region. The kaolin used in this study is of a small particle phase (0.4-4 μm). Small particles improve reaction rates, but tend to be carried easily along a pressure gradient. Larger particles may improve fluidizantion, and reduce reactant carry over. Experimentation with reactants of differing particle sizes (larger), may improve fluidization, and would make higher flowrates possible.

LIST OF REFERENCES

LIST OF REFERENCES

[1] R. G. Bennett. Alternatives to direct SNF disposal: Advanced nuclear fuel cycles, 2003.

[2] C. W. Forsberg. Rethinking high-level waste disposal: Separate disposal of high-heat radionuclides ^{90}Sr and ^{137}Cs. *Nuclear Technology*, 131(2):252 – 268, 2000.

[3] Julia Tripp, October 2005.

[4] Candido Pereira, September 2005.

[5] T. A. Todd, T. A. Batcheller, J. D. Law, and R. S. Herbst. Cesium and strontium separation technologies literature review. Technical Report INEEL/EXT-04-01895, Idaho National Engineering and Environmental Laboratory, March 2004.

[6] M. J. Jr. Antal. Synthesis gas production from organic wastes by pyrolysis/steam reforming. In *Energy From Biomass and Wastes*, pages 495–523, Washington, DC, USA, 1978. Inst of Gas Technol, Chicago, IL.

[7] D.N. Bangala, N. Abatzoglou, J.P. Martin, and E. Chornet. Catalytic gas conditioning: Application to biomass and waste gasification. *Industrial & Engineering Chemistry Research*, 36(10):4184–4192, 1997.

[8] F. Thecla. Steam cleaning at Idaho. *Nuclear Engineering International*, 50(615):42–44, 2005.

[9] B. J. Mason. Patent: Single stage denitration, August 2001.

[10] B. J. Mason. Patent: Pyrolytic decomposition of organic wastes, July 2000.

[11] T. R. Galloway, M. Cage, and T. Snyder. *Hazardous and Radioactive Waste Treatment Technologies Handbook*, chapter 4.3 Application of steam-reforming to various types of radioactive waste. CRC Press, 2003.

[12] T. R. Galloway. Destroying hazardous waste on site– avoiding incineration. *Environmental Progress*, 8:176–185, August 1989.

[13] T. R. Galloway, R. G. Dosch, and J. L. Sprung. Destruction of organics and decomposition of nitrates in UST wastes by steam reforming. In *Waste Management Conference*, Tuscon, AZ, 1993. American Nuclear Society.

[14] G. E. Voelker, W. G. Steedman, and R. R. Chandran. Steam reforming of low-level mixed waste. Technical Report DOE/MC/32091-97/C0789, ThermoChem Inc., December 1996.

[15] K. Arai, T. Makita, Y. Endo, and D. Weigle. Volume reduction of low level wastes by steam reforming. In *8th International Conference on Radioactive Waste Management and Environmental Remediation*, volume 1 of *Proceedings of the International Conference on Radioactive Waste Management and Environmental Remediation, ICEM*, pages 447–449, Bruges, Belgium, 2001. American Society of Mechanical Engineers.

[16] C. M. Jantzen. Engineering study of the Hanford Low Activity Waste (LAW) steam reforming process (U). Technical Report WSRC-TR-2002-00317, Rev.0 SRT-RPP-2002-00163, Rev.0, Savannah River Technology Center, July 2002.

[17] M. J. Cowen, B. Mason, and D. Schmoker. Steam reforming technology for denitration and immobilization of DOE tank wastes. In *Waste Management '04*, Tucson, AZ, 2004.

[18] D. W. Marshall, N. R. Soelberg, and K. M. Shaber. THOR^{SM} bench-scale steam reforming demonstration. Technical Report INEEL/EXT-03-00437, Idaho National Engineering and Environmental Laboratory Environmental Research & Development, May 2003.

[19] C. M. Jantzen. Disposition of tank 48H organic slurry by Fluidized Bed Steam Reforming (FBSR) (U). Technical Report WSRC-TR-2003-00352, Rev. 0, Savannah River Technology Center, September 2003.

[20] C. M. Jantzen. Characterization and performance of Fluidized Bed Steam Reforming (FBSR) product as a final waste form. In *Ceramic Transactions*, volume 155 of *Ceramic Transactions*, pages 319–329, Nashville, TN, United States, 2004. American Ceramic Society, Westerville, OH 43086-6136, United States.

[21] THOR^{SM} steam reforming process for hazardous and radioactive wastes. Technical Report TR- SR02-1, Rev. 1, THOR Treatment Technologies, LLC, 2002.

[22] C. M. Jantzen. Characterization and performance of Fluidixed Bed Steam Reforming (FBSR) product as a final waste from (U). Technical Report WSRC-MS-2003-00595, Revision 0, Westinghouse Savannah River Company, 2003.

[23] P. R. Burket, J. C. Marra, J. M. Pareizs, and C. M. Jantzen. Evaluation of Fluidized Bed Steam Reforming (FBSR) technology for sodium bearing wastes from Idaho and Hanford using the Bench-top Steam Reformer (BSR) (U). Technical Report WSRC-TR-2004-00560 Rev. 0, Savannah River National Laboratory, February 2005.

[24] B. P. McGrail, H. T. Schaef, P. F. Martin, D. H. Bacon, E. A. Rodriguez, D. E. McCready, A. N. Primak, and R. D. Orr. Initial suitability evaluation of steam-reformed low activity waste for direct land disposal. Technical Report PNWD-3288 WTP-RPT-097, Rev 0, Battelle, Pacific Northwest Division, January 2003.

[25] B. J. Mason, J. McKibbin, Schmoker D., and P. Bacala. Pyrolysis/steam reforming technology for treatment of TRU orphan wastes. In *Waste Management*, Tucson, AZ, 2003.

[26] J. B. Mason and D. Bradbury. Patent: Process for the treatment of radioactive graphite, September 2003.

[27] J. H. Saling and A. W. Fentiman. *Radioacitve Waste Management 2nd Edition*. Taylor & Francis, New York NY, 2002.

[28] J. L. McElroy, W. J. Bjorklund, and W. F. Bonner. Waste vitrification: A historical perspective. In *The treatment and handling of radioactive wastes*, pages 171–177, Richland, Wash., April 1982.

[29] D. F. Bickford and R. Schumacher. Vitrification of hazardous and radioactive wastes. *Ceramic Engineering and Science Proceedings*, 16(2):1 – 10, 1995.

[30] H. Kamizono. Volatilization of cesium and ruthenium from high-level waste glass. In *High Level Radioactive Waste Management*, pages 1115 – 1118, Las Vegas, NV, USA, 1990.

[31] N.E. Bibler, T.L. Fellinger, S.L. Marra, R.J. O'driscoll, J.W. Ray, and W.T. Boyce. Tc-99 and Cs-137 volatility from the DWPF production melter during vitrification of the first macrobatch of HLW sludge at the Savannah River site. *Materials Research Society Symposium - Proceedings*, 608:697 – 702, 2000.

[32] M. A. Schiffhauer, D. E. Carl, and L. E. Rykken. Design of a high-level waste pretreatment process for the purpose of vitrification. In *Waste Management '86*, pages 479 – 487, Tucson, AZ, USA, 1986.

[33] T. N. Jr. Sargent, T. J. Overcamp, D. F. Bickford, and C. A. Cicero-Herman. Vitrification of cesium-laden organic ion-exchange resin in a stirred melter. *Nuclear Technology*, 123(1):60 – 66, 1998.

[34] M. K. Andrews. Glass formulation development and testing for the vitrification of cesium-loaded (CST). *Proceedings of the Air & Waste Management Association's Annual Meeting & Exhibition*, 1997.

[35] D. G. Bennett, J. J. W. Higgo, and S. M. Wickman. Review of waste immobilization matrices. Technical Report 0126-1, Galson Sciences Limited, December 2001.

[36] J.V. Hanna, L.P. Aldridge, and E.R. Vance. Cs speciation in cements. *Materials Research Society Symposium - Proceedings*, 663:89 – 96, 2001.

[37] R. Neilson Jr., P. Kalb, M. Fuhrmann, and P. Colombo. Solidification of Ion Exchange Resin Wastes in Hydraulic Cement. In *The treatment and handling of radioactive wastes*, pages 497–503, Richland, WA, April 1982.

[38] N. V. Elizondo, E. Ballesteros, and B. I. Kharisov. Cleaning of liquid radioactive wastes using natural zeolites. *Applied Radiation and Isotopes*, 52:27–30, 2000.

[39] J. Yoo, T. Shinagawa, J. P. Wood, W. P. Linak, D. A. Santoianni, C. J. King, Y. Seo, and J. O. L. Wendt. High-temperature sorption of cesium and strontium on dispersed kaolinite powders. *Environmental Science and Technology*, 39:5087–5094, 2005.

[40] G. N. Brown, K. J. Bontha, J. R.and Carson, R. J. Elovich, and J. R. DesChane. Comparison of inorganic ion exchange materials for removing cesium, strontium, and transuranic elements from k-basin water. Technical Report PNNL-11746, Pacific Northwest National Laboratory, October 1997.

[41] H. Mimura, T. Hirabayashi, and M. Ozawa. Leachability and thermal properties of ceramic solid forms immobilizing cesium and/or strontium. In *International Conference - Nuclear Energy for New Europe, Proceedings*, pages 615 – 622, Portoroz, Slovenia, 2003.

[42] K.D. Reeve and A.E. Ringwood. The SYNROC process for immobilizing high-level nuclear wastes. *Radioactive Waste Management. Proceedings of an International Conference*, pages 307 – 24, 1984.

[43] I. W. Donald, B. L. Metcalfe, and R. N. J. Taylor. Review the immobilization of high level radioactive wastes using ceramics and glasses. *Journal of Materials Science*, 32:5851–5887, 1997.

[44] Yun Bao, S. Kwan, D.D. Siemer, and M.W. Grutzeck. Binders for radioactive waste forms made from pretreated calcined sodium bearing waste. *Journal of Materials Science*, 39(2):481 – 488, 2004.

[45] M. Benedict, T. H. Pigford, and H. W. Levi. *Nuclear Chemical Engineering Second Edition*. McGraw-Hill Inc., New York NY, 1981.

[46] R.E. Newnham. Crystal structure and optical properties of pollucite. *American Mineralogist*, 52(9-10):1515 – 1518, 1967.

[47] K. Yanagisawa, M. Nishioka, and N. Yamasaki. Immobilization of cesium into pollucite structure by hydrothermal hot-pressing. *Journal of Nuclear Science and Technology*, 24(1):51 – 60, 1987.

[48] E. R. Vance, B. E. Scheetz, M. W. Barnes, and B. J. Bodnar. Studies of pollucite. *Materials Research Society Symposia Proceedings*, 6:31 – 35, 1982.

[49] D. M. Strachan and W. W. Schulz. Characterization of pollucite as a material for long-term storage of cesium-137. *American Ceramic Society Bulletin*, 58(9):865 – 8, Sept. 1979.

[50] N.J. Hess, F.J. Espinosa, S.D. Conradson, and W.J. Weber. Beta radiation effects in ^{137}Cs-substituted pollucite. *Journal of Nuclear Materials*, 281(1):22 – 33, 2000.

[51] K. O. Bennington, R. P. Beyer, and G. K. Johnson. Thermodynamic properties of pollucite (a cesium-aluminum-silicate). *Report of Investigations - United States, Bureau of Mines*, pages 22 –, 1983.

[52] L. P. Ogorodova, L. V. Melchakova, and I. A. Kiseleva. Calorimetric study of natural pollucite. *Informational Bulletin of the Annual Seminar of Experimental Mineralogy, Petrology and Geochemistry*, July 2003.

[53] M. Pell. *Gas Fluidization*, volume 8 of *Handbook of Powder Technology*. Elsevier Science Publishers B. V., 1990.

APPENDIX

APPENDIX A
XRD RESULTS METHOD 1

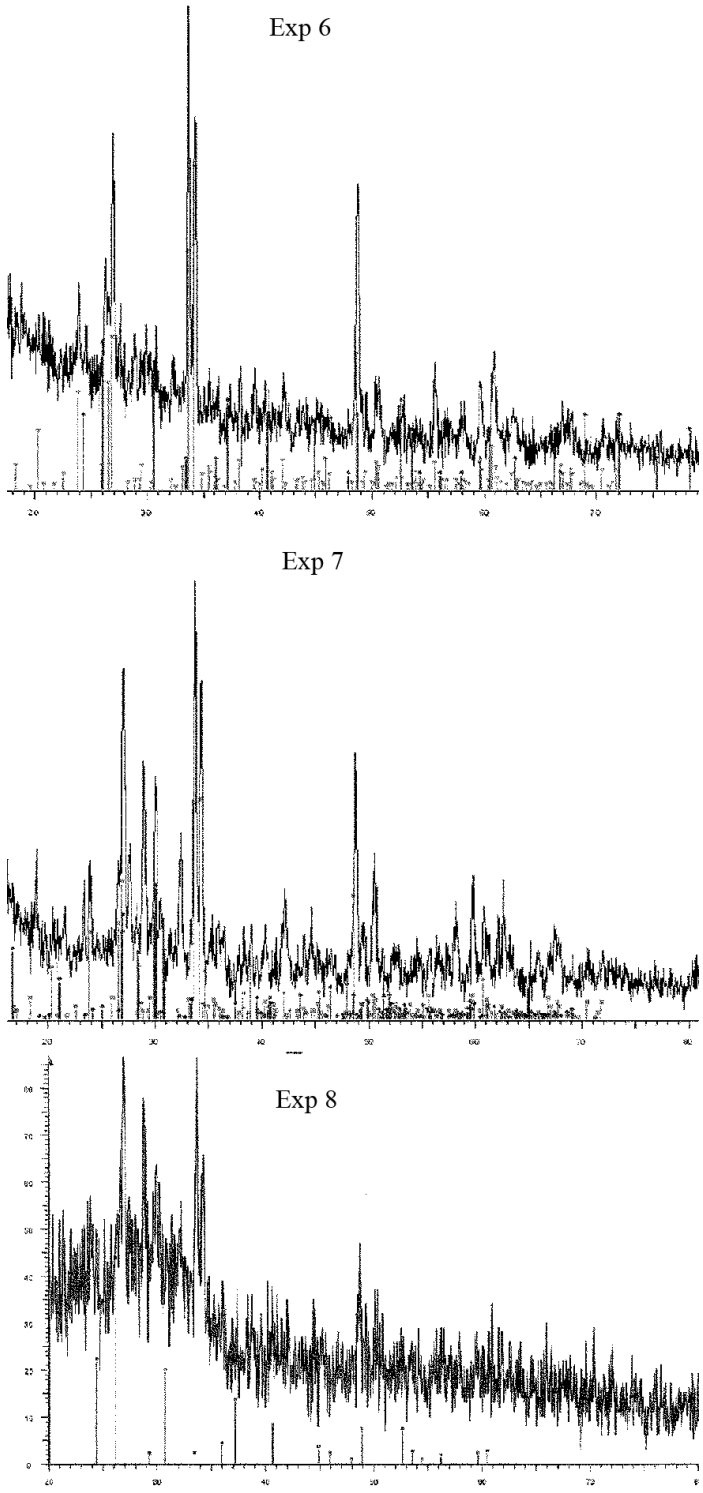

Figure A.1. XRD Method 1

APPENDIX B
APPARATUS IMAGES

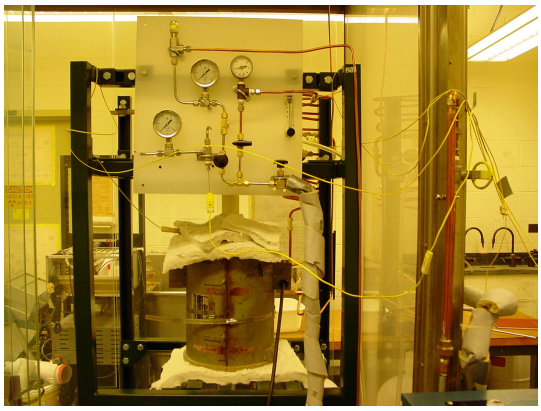

(a) Front

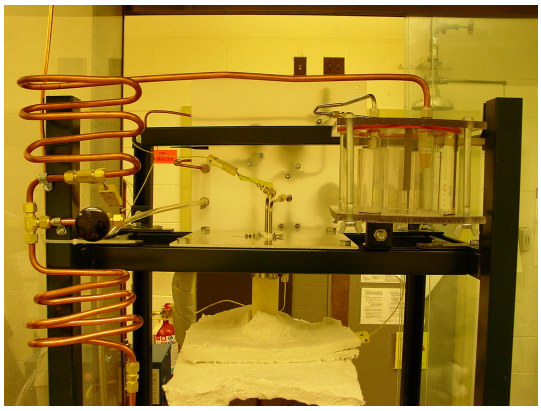

(b) Particle Trap

Figure B.1. Method 1 Apparatus Images (1)

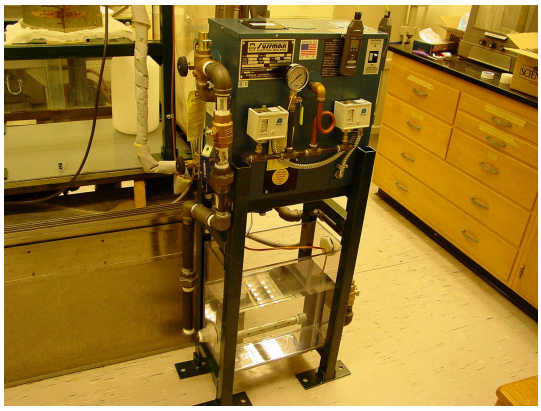

(a) Steam Generator & Sparger Tank

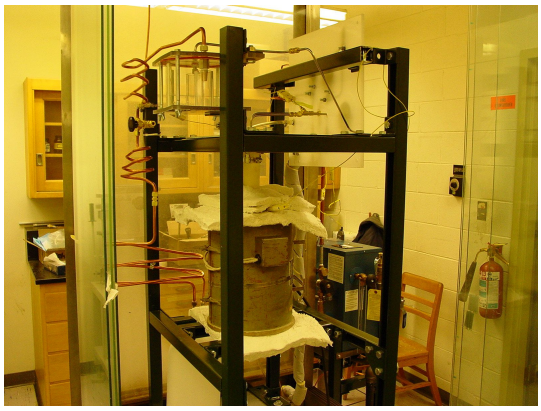

(b) Rear View

Figure B.2. Method 1 Apparatus Images (2)

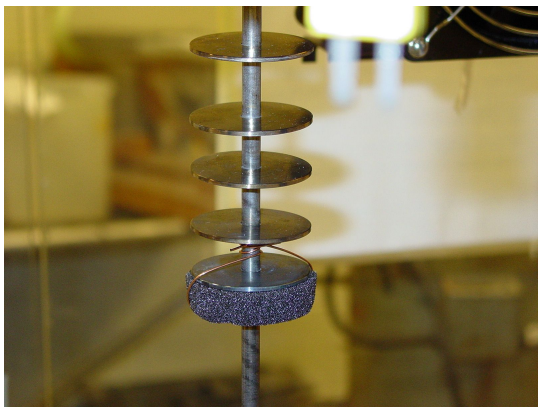

(a) Carbon Foam

(b) Pressure Regulator

Figure B.3. Method 1 Changes

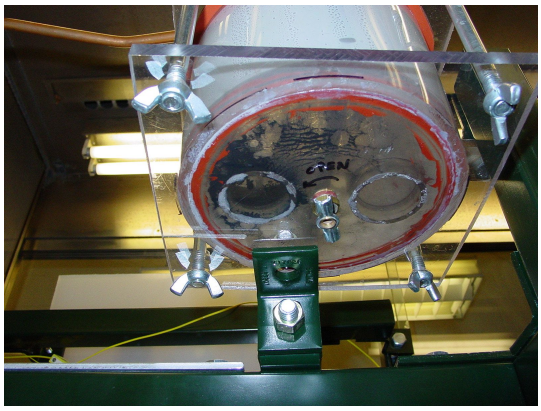

(a) Reactant Carry-over Exp. 1

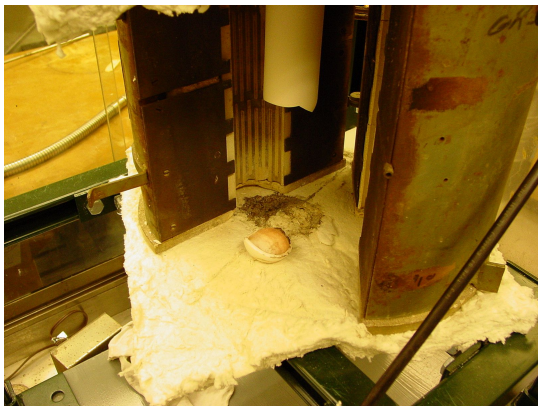

(b) Tube Break Exp. 3

Figure B.4. Method 1 Results Images

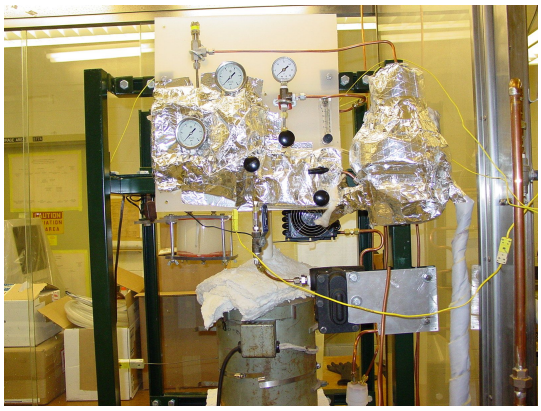

(a) Steam Trap

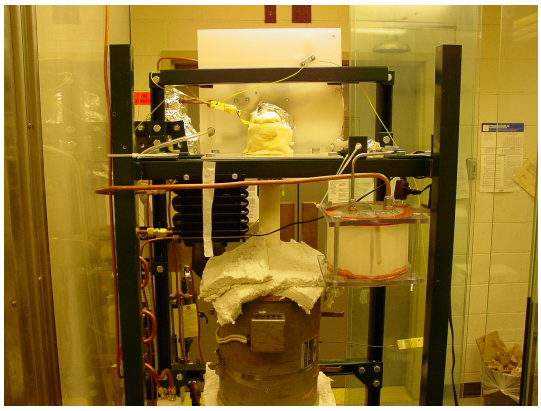

(b) Particle Trap (lowered)

Figure B.5. Method 1 Apparatus Changes (2)

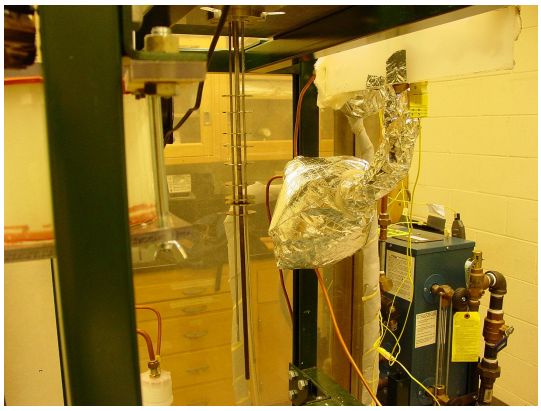

(a) Method 2 Tubing

(b) Feed Syringe

Figure B.6. Method 2 Apparatus Images

APPENDIX C
ANL RESULTS

Date Received: 06/13/2006
Date Reported: 06/28/2006
Sample Material: Metal Oxide
Submitted By: Luis Ortega Purdue University

ANALYTICAL CHEMISTRY LABORATORY
Argonne National Laboratory
Argonne, IL 60439

REPORT OF ANALYTICAL RESULTS

Analysis: ICP/OES, ICP-MS*
Reporting Units: Weight%
Uncertainty: +/-5% of reported value for majors and +/-10% for minors.

Analyst(s): Y. Tsai
S. Naik

Submitter's Sample No.	ACL Sample No.	Al	Si	Sr	Ca	K	Na		*Cs		
Exp 6	06-0154-01	1.91	27.4	<0.1	12.0	0.58	10.9		2.77		
Exp 7	06-0154-02	1.49	29.5	0.11	12.3	0.67	11.2		na		
Exp 7	06-0154-02D	1.51	29.4	0.12	12.5	0.67	11.3		na		

NOTE: na - not analyzed.

NOTE: Unused sample material will be returned to the Client. When making future inquiries regarding this report, please reference the ACL sample number(s) above. For further information about the results reported here, please call D. Graczyk at extension 2-3489.

Reference(s): Notebook 2140, p. 127. ICP Spec. No.-60569. ICP Instrument Data Files-061606, 061606B. SN#2164, p. 73.

Copies To: L. Leibowitz
L. Ortega
sn:06/28/06 D. Graczyk
jl:07/06/06 V. Sullivan
ACL File

Page 1 of 1

Figure C.1. ANL Chemical Analysis Results

APPENDIX D

CHEMICAL & EQUIPMENT LISTS

Table D.1
Chemical List

Description	Formula	Manufacturer	Product Number
Cesium Nitrate	$CsNO_3$	Aldrich	289337-50G
Strontium Nitrate	$Sr(NO_3)_2$	Fluka	85900
Kaolin	$Al_2Si_2O_5(OH)_4$	Sigma-Aldrich	K7375-500G
69.7% Nitric Acid	HNO_3	Mallinckrodt	1409-04
Activated Charchoal	C	Fluka	05120
Silica Beads	SiO_2	FPEX CertiPrep	2160
Red Iron Oxide	Fe_2O_3	Fisher Scientific	S93241

Table D.2
Equipment List

Description	Manufacturer	Model
Steam Generator	Sussman	MBA 3
Pressure Regulator	Jordan Valve	MK 61
Steam Trap	Spirax Sarco	FT1-15
Electric Furnace	Arthur S. LaPine & Co.	M-2012
Variac	Staco Energy	3PN1510B

APPENDIX B

SINTERED BENTONITE CERAMICS FOR THE IMMOBILIZATION OF CESIUM- AND STRONTIUM-BEARING RADIOACTIVE WASTE

A Dissertation

by

LUIS HUMBERTO ORTEGA

Submitted to the Office of Graduate Studies of
Texas A&M University
in partial fulfillment of the requirements for the degree of

Doctor of Philosophy

December 2009

Major Subject: Materials Science and Engineering

SINTERED BENTONITE CERAMICS FOR THE IMMOBILIZATION OF CESIUM- AND STRONTIUM-BEARING RADIOACTIVE WASTE

A Dissertation

by

LUIS HUMBERTO ORTEGA

Submitted to the Office of Graduate Studies of
Texas A&M University
in partial fulfillment of the requirements for the degree of

Doctor of Philosophy

Approved by:

Chair of Committee,	Sean M. McDeavitt
Committee Members,	Bill Bachelor
	Michael D. Kaminski
	Lin Shao
	Karen Vierow
Head of Department,	Tahir Cagin

December 2009

Major Subject: Materials Science and Engineering

ABSTRACT

Sintered Bentonite Ceramics for the Immobilization of Cesium- and Strontium-Bearing Radioactive Waste. (December 2009)
Luis Humberto Ortega, B.S.Ch.E., New Mexico State University; M.S.N.E., Purdue University
Chair of Advisory Committee: Dr. Sean M. McDeavitt

Cesium and strontium are two primary heat sources in the first 300 years of spent nuclear fuel's decay, specifically isotopes Cs-137 and Sr-90. While various schemes to remove these isotopes have been developed, this study has focused on nitric acid based liquid waste. The simulated waste was prepared from nitrate salts of stable ions. These ions were limited to cesium, strontium, barium and rubidium. The ratios of these ions in the waste simulant were based on the Fission Product EXtraction (FPEX) process [1] under development by the U.S. Department of Energy (DOE). The waste liquid was added to natural bentonite clay incrementally with drying steps between each addition. The dry powder was pressed and then sintered at various temperatures. The maximum loading tested is 32 wt. percent waste, which refers to 13.9 wt. percent cesium, 12.2 wt. percent barium, 4.1 wt. percent strontium, and 2.0 wt. percent rubidium. Lower loadings of waste were also tested. The final solid product was a hard dense ceramic with a density that varied from 2.12 g/cm3 for a 19% waste loading with a 1200 °C sintering temperature to 3.03 g/cm3 with a 29% waste loading and sintered at 1100 °C.

Differential Scanning Calorimetry and Thermal Gravimetric Analysis (DSC-TGA) of the loaded bentonite displayed mass loss steps which are consistent with water losses in pure bentonite. Water losses are complete after dehydroxylation at ~650°C. The final nitrate release has also been found to occur at this step [2]. The onset of

viscous sintering was found at ~1100°C. The ceramic melts at temperatures greater than 1300°C.

Pollucite crystals were detected at 800°C in samples with 32 wt% waste, and in all sinterings above 800°C. Hexacelsian, a hexagonal feldspar formed at 800°C but was no longer detectable at sinterings >1000°C. At 1000°C and above, barium and strontium form monoclinic feldspars.

A glass eutectic formed at 1100°C with the barium and strontium feldspars. At 1200°C, barium and strontium feldspar crystals are apparent within the glass eutectic phase. The glass region was found to have a higher concentration of strontium than barium, while the feldspar crystals had higher barium concentrations than strontium. Pollucite phases were found to segregate from the glass eutectic and form crystals with low to undetectable levels of barium and strontium.

Leach rates determined by a simplified TCLP procedure found sintering to temperatures greater than 1100°C was necessary to keep strontium levels below 100 ppm. Strontium had leach rates higher than all other metal ions immobilized in the ceramic. Stoichiometric calculations found alumina to be the limiting reactant, Bahat found barium crystallizes aggressively with respect to strontium [3]. Strontium and barium formed feldspars with various atomic ratios, a 50:50 barium to strontium phase detected at 1000 and 1200°C, as well as a 75 atom% barium to 25 atom% strontium at 1000°C.

Light flash analysis found thermal diffusivities of the ceramic to be comparable to those of strontium and barium feldspars as well as pollucite. Thermal conductivity improved with lower porosity. Porosity was reduced with higher sintering temperatures, and was minimized in 1200°C sinterings. Ceramics with waste loadings less than 21 wt% displayed slump which increased as the waste concentration was reduced. Waste loading above 21 wt% produced smooth uniform ceramics when sintered >1100°C.

I am very fortunate to have a loving family and friends who gave their unwavering support, my sister and her husband Mary Helen and Terry Ormseth, my mother and father Maria Elena and James Resley, and my uncle Guillermo Ortega; my close friends Andy Walter, Red Knaak, Frank Williams, Matt Murawski, Flint Taylor, Michael Robbins, Mike Aussem, Sarah Harcum, Barry Goode, Matt Hartman, Rob Cruz, Edith Cassell and Karie Badgley. I would also like to thank God for everything.

ACKNOWLEDGMENTS

I would like to thank my adviser Sean McDeavitt for his patience and support throughout this process, without his experience and suggestions this would have not been possible. I would also like to thank my committee for their time and attention to detail, Bill Batchelor, Karen Vierow, Lin Shao and especially Michael Kaminski whose guidance has been immeasurable.

Researchers whose individual expertise helped collect the data before you are Ray Guillemette for his work with the electron microprobe, Latha Vasudevan for neutron activation analysis, Nattamai Bhuvanesh for x-ray powder diffraction, Yefen Tsai and Robert Taylor for inductively coupled plasma mass spectroscopy.

For their assistance in the lab I would like to thank Carol Mertz for her help finding materials and equipment, Grant Helmreich for running the light flash analyzer, Julie Borgmeyer for her help with the toxicity leach procedure and assisting Dr. Guillemette, and Daren Malik and Jeff Hausaman for their help with the differential scanning calorimeter.

I would like to thank Kevin Hogan for his help making the data presentable. I would like to thank Aaron Totemeier for his LaTeX work as well as his friendship and overall support in this entire process. This work required the assistance of dozens of other people to complete, I am grateful to all of them.

This work has been funded by the Advanced Fuel Cycle Initiative (AFCI) and the Nuclear Energy Research Initiative (NERI) Award No. DE-FC07-06ID14737 Project No. 06-058, under the United States Department of Energy Office of Nuclear Energy.

NOMENCLATURE

CTE	Coefficient of Thermal Expansion
EDS	Energy Dispersive Spectroscopy
FPEX	Fission Product Extraction Process
ICP-MS	Inductively Coupled Plasma Mass Spectroscopy
UREX	uranium extraction process
WDS	Wave Dispersive Spectroscopy

TABLE OF CONTENTS

Page

LIST OF TABLES

LIST OF FIGURES

FIGURE Page

FIGURE Page

1. INTRODUCTION

Proposed advanced fuel cycles may separate cesium and strontium isotopes to reduce the heat load on the bulk of used nuclear fuel [4]. Once removed the cesium and strontium require treatment. The focus of this work investigates the immobilization of this potential waste stream with sintered clays. In addition to the cesium and strontium, barium and rubidium are also in the waste stream due to similar chemical properties. We prepared a simulated waste stream by dissolving nitrate salts of each metal in a dilute nitric acid solution. Our simulated waste solution was mixed with the natural mineral bentonite, a smectite clay. Bentonite clay consists primarily of montmorillonite with small amounts of quartz. Montmorillonite has a layered aluminosilicate structure composed of alternating sheets of alumina and silica. An alumina octahedral sheet resides between two silica tetrahedral sheets. Between these repeating silica-alumina-silica layers are metal cations and water, and within the silica and alumina there are hydroxyl groups (Figure 1.1). A typical formula unit may be as follows: $(Na,Ca)_{0.33}(Al,Mg)_2(Si_4O_{10})(OH)_2nH_2O$ where the cation species and concentrations vary from source to source.

The clay was loaded with waste ions in concentrations ranging from approximately 16 mass percent to 32 mass percent total waste ions. The theoretical maximum was based on the mineral pollucite $(Cs,Na)_2Al_2Si_4O_{12}(H_2O)$. Pollucite is an aluminosilicate with the same alumina-to-silica ratio as montmorillonite, and cesium constitutes ~30 mass percent or ~32 mass percent when sodium is replaced by cesium. In this document clay loadings are occasionally referred to as a percentage of the theoretical maximum, where 100% refers to a target of 30 mass percent waste ions. The liquid simulated waste was added to the clay to the desired concentration, then the liquid waste-clay slurry was dried to a powder. The powder was then pressed into a pellet and sintered. Sintering temperatures were varied from 700 to

1400 °C, while the waste concentrations varied from approximately 50% to 100% of the theoretical maximum.

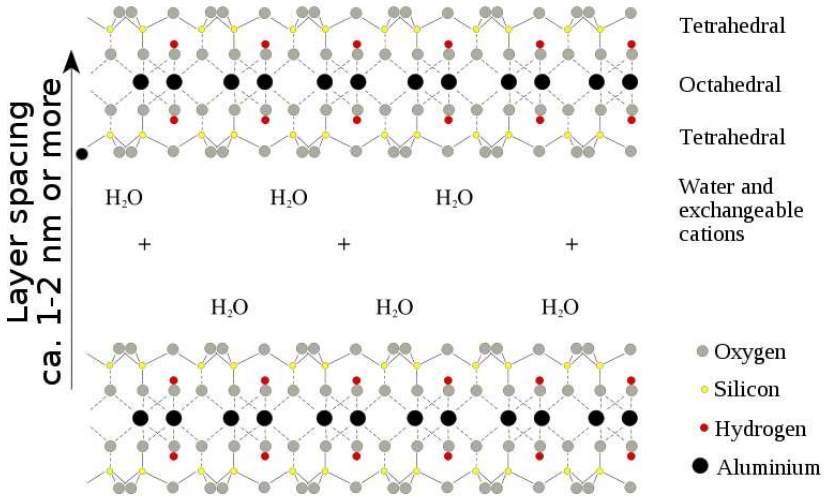

Fig. 1.1. Montmorillonite clay

1.1 Objective

The potential waste stream is a highly radioactive acidic liquid. How to stabilize this liquid is a problem that can be solved in various ways. The considerations required to make an efficient and economical solution are several. The primary criteria is the immobilization of the ions. These metals must be bound tightly in the final matrix due to their radiotoxicity as well as their chemical hazards; *i.e.* water soluble barium compounds are poisonous. The resulting matrix may be exposed to moisture which may be acidic or alkaline. The radioactivity creates multiple problems. The heat given off during the decay process, if great enough, can melt the material if the geometry and loading are not carefully thought out. The radiation can damage the structure as well. The isotopes themselves change chemically as they under go decay. Other considerations are economic, logistic, as well as processing safety.

High temperatures require energy that comes at cost, similarly with processes requiring high pressures. Processes with intermediate steps, especially those involving powders create safety issues. The simpler the process the more economical. Each step with a highly radioactive material requires automation; fewer steps reduce cost considerably.

An ideal waste form will be mechanically and chemically stable, will withstand radiation damage, be dense, and sufficiently thermally conductive. Processing should have minimal steps, and if there are powders involved they should be continuously consolidated to avoid a large holdup of an easily dispersible hazardous substance. Although daunting, these issues are manageable.

Due to the nature of this waste solution, containing only the alkali metals and alkaline earth metals, the reactants can be chosen to target a specific outcome. Using natural aluminosilicate minerals as examples of stable compounds, we chose these forms as prospective hosts for the waste ions. Bentonite clay primarily consists of silica and alumina, and for this reason bentonite clay was chosen as a reactant. The silica and alumina become the building blocks for the objective minerals.

Alumino-silicates have been produced from clay before. Sorrell found strontium, barium and lead sulfates could be heated with kaolin clays to produce feldspars [5]. Spitsyn looked at roasting bentonite specifically for the immobilization of strontium [6]. Investigations by Strachan and Shultz done on pollucite, a cesium bearing alumino-silicate, for radioactive waste storage found good leach rates, low solubility and thermal stability. They conceded uncertainties in pollucite's radiation stability and transmutation effects [7]. They proposed the use of pollucite for cesium-137 immobilization derived from CsCl, or $CsCO_3$ reacted with montmorillonite at 970 K [8]. Vance used high pressures and temperatures to convert a sol to pollucite for use as a Cs-137 immobilization matrix also [9]. Cs-137 doped pollucite was synthesized from a colloidal silica solution with stoichiometric amounts of cesium and aluminum nitrates, which were stirred and dried, then calcined at 793–813 K, fol-

lowed by grinding, and compaction at 250 Pa, and finally sintering. The pollucite was observed for β^- radiation effects on the long-range and local structure [10]. The study was not able to observe the γ effects due to small sample size but found swelling and distortion of the lattice.

Cs-137 is transformed by β^- decay into Ba-137:

$$Cs^{+} \xrightarrow{\beta^-} Ba^{2+}$$

The resulting Ba-137^m is meta-stable and will quickly transform($T_{1/2}$= 2.6 min) to a stable configuration by giving off a 662 keV gamma-ray. Cs-137, Cs-135, and Cs-133 will not be separated during reprocessing due to their near identical chemical behavior. Cs-135 gives off a 0.21 MeV β^- which decays to Ba-135 with $T_{1/2}$= 2.3 × 10^6 years, and Cs-133 is stable.

Sr-90 is a pure beta emitter, with a half life of 28.8 years. Sr-90 decays with a 0.546 MeV β^- yielding an Y-90 atom, which also β^- decays with a half life of 64 hours, giving off a 2.28 MeV β^- leaving a stable Zr-90 atom. Thus:

$$Sr^{+2} \xrightarrow{\beta^-} Y^{+3} \xrightarrow{\beta^-} Zr^{+4}$$

The goal of the present study is to produce mineral compounds embedded with ions of cesium, strontium, barium and rubidium. Concentration of the total waste will be varied, but the ratios of individual ions will be kept the same. Sintering temperatures will be varied from 700 to 1400 °C. These products will be characterized and a preliminary assessment of their properties will then be made. This baseline study can lead to further research into their potential as radioactive waste forms.

2. BACKGROUND AND MOTIVATION

The fate of used nuclear fuel in the United States is uncertain due to the shelving of Yucca Mountain the proposed nuclear waste repository [11]. There have been many proposed methods to sequester used nuclear fuel. Deep geologic burial in basalt, salt, and tuff have all been extensively investigated. Due to the difficulty in approval of a geologic site, dry storage in casks with or without a retrievable option are currently being investigated as well. An option that has potential to recycle isotopes with energy content as well as reduce the amount high level radioactive waste is reprocessing.

The Department of Energy (DOE) has been funding the Advanced Fuel Cycle Initiative, and various researchers are currently investigating methods to treat spent nuclear fuel in a sustainable manner [4]. The policy in the USA had been to take entire fuel bundles after sufficient cooling and ship them to Yucca Mountain in Nevada for deep geologic burial. The repository is not yet open, and the future of the project is uncertain. If the United States continues to produce nuclear power and it builds new nuclear power plants, a fuel cycle with separation, transmutation and recycle is an alternative worthy of analysis. An advanced fuel cycle will reduce waste volume and transmute long lived isotopes to ones with shorter half lives, as well as provide burnable fuel for future power generation.

2.1 Advanced Fuel Cycle Initiative

Chemical separations are the foundation of reprocessing, and determining the extent and exact method is currently under investigation. To begin, the ultimate fate of each isotope or group of isotopes with similar properties must be determined.

Nuclear fuel at 33,000 MWD/MT and 10 years of cooling is ~95.6 mass% depleted uranium. The next largest fraction consists of stable isotopes and the short-lived fission products at ~3.3 mass%. Once these are separated they are not a radiation

hazard but may still be chemically toxic. The next fraction includes plutonium and the long-lived fission products at ~0.95 mass%. These can be incorporated into new mixed oxide fuel or transmuted to isotopes with shorter half-lives. Minor actinides and other long-lived fission products ~0.15 mass% can also be transmuted. Each of these portions of spent fuel can be treated separately. The end result is less volume for high-level waste disposal, shorter half-lives after transmutation, and recycled energy producing fuel [12]. Of the long-lived isotopes, some will not be suitable for transmutation due to half-lives that are not long enough to justify the process. Two primary examples are ^{137}Cs and ^{90}Sr at approximately 30 years [13].

The radioactivity of the high level waste is of primary concern during repository design. The activity of the waste will determine the heat generation and resulting temperature. Water exists as moisture in the soil. In a cold repository design temperature limits are set to keep water flowing through the repository, preventing a hold up of water above the repository from flooding the repository as it cools [14]. Lowering the overall activity will allow more waste into the repository without exceeding these temperature limits.

To maintain low temperatures inside the repository, active cooling with fans has been proposed [14]. Eventually the fans will be turned off after the decay heat goes decreases a level where the active cooling is no longer necessary. The removal of cesium and strontium will make a substantial reduction in the activity during the initial years of operation.

The AFCI aqueous reprocessing methods (UREX+) separate used nuclear fuel into different fractions [15]. These fractions are then treated according to the nature of the particular isotopes they contain. A general overview of the AFCI is shown in Figure 2.1. The three primary steps, Uranium Extraction (UREX), Chlorinated Cobalt Dicarbollide/Polyethylene glycol (CCD-PEG) or FPEX, and Transuranic Extraction (TRUEX) are briefly outlined below.

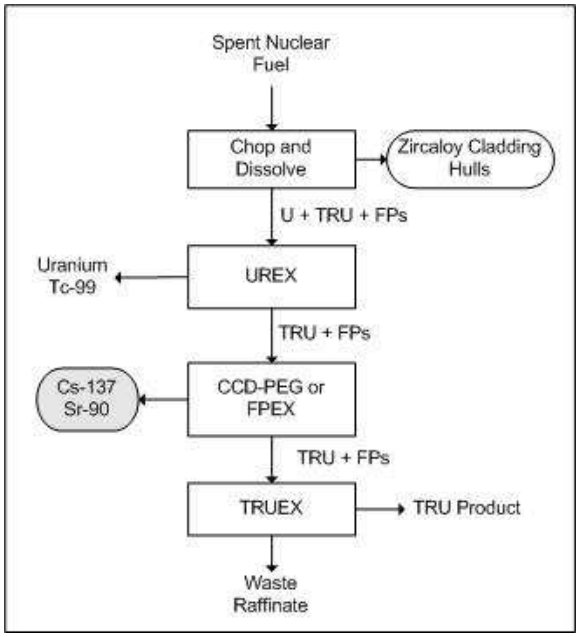

Fig. 2.1. Advanced Fuel Cycle Initiative

In the UREX process, high purity uranium and technetium are recovered in three steps. In the first step uranium and technetium are extracted with a 30 vol% tributyl phosphate in n-dodecane solvent. In the next step technetium is extracted from the loaded solvent. The third step strips the uranium from the technectium strip solvent [16]. The remaining transuranics and fission products then go on to either the CCD-PEG or FPEX processes.

2.2 Cesium and Strontium Separation

The FPEX (Fission Product Extraction) process has been developed specifically for the removal of cesium and strontium from the UREX process. There are several cesium and strontium fission products in spent fuel (Table 2.1 which will also be extractd with the Cs^{137} and the Sr^{90}, along with barium and rubidium. The solvent proposed to remove strontium is 4',4',(5')-di-(t-butyldicyclo-hexano)-18-crown-6, and

to remove cesium calix[4]arene-bis-(tert-octylbenzo-crown-6) is proposed. Once the elements are in the solvent the solvent will be washed with dilute nitric acid. The dilute nitric acid with dissolved cesium and strontium will require subsequent treatment [17]. Another method to remove cesium and strontium from the UREX raffinate, is called the CCD/PEG (chlorinated cobalt dicarbollide/polyethylene glycol) process, where the CCD is employed for the removal of cesium, and PEG for strontium [18]. For further separation techniques involving cesium and strontium see [19]. Once the elements are in the solvent, the solution will be washed with guanidine carbonate/ diethylenetriamine pentaacetic acid (DTPA). This process creates a highly radioactive liquid waste. Transportation requirements and repository facility restrictions will only accept solid forms. Therefore at the minimum the solvents must be dried. Once dried the result may be a powder or reactive metals, both requiring additional treatment or specialized containers for transport.

An ideal waste form for these waste streams will be durable as well as chemically inert while resistant to radiation effects. Transmutation during radioactive decay transforms cesium with a $^{+}1$ oxidation state to barium at $^{+}2$. Strontium decays from an oxidation state of $^{+}2$ to zirconium at $^{+}4$. These chemical changes will alter the waste composition by changing the bonding symmetry due to different ionic radii, and ionic charge.

Table 2.1
Cesium and strontium fission products [20]

		In discharge fuel 10^6 Ci/yr	
Radionuclide	$T_{1/2}$	150-day decay	10-yr decay
^{134}Cs	2.046 yr	5.83	0.228
^{135}Cs	3.0×10^6 yr	7.79×10^{-6}	7.79×10^{-6}
^{136}Cs	13.7 days	5.42×10^{-4}	0
^{137}Cs	30.0 yr	2.92	2.33
^{89}Sr	52.7 days	2.65	0
^{90}Sr	27.7 yr	2.09	1.65

Uranium-fueled 1000-MWe PWR, 3-year fuel life.

3. RADIOACTIVE WASTE MANAGEMENT

The United States' long term strategy for the fate of commercial spent nuclear fuel is undetermined. Currently most spent fuel remains at the site where the power was generated. A repository has been started in Nevada's Yucca Mountain but legislative issues have left the entire project in question. When this study was initiated the problems associated opening Yucca Mountain were already evident. The prospect of exhausting the space to store spent fuel, leading to a second repository motivated the search for methods to limit waste volume. The DOE's Advanced Fuel Cycle Initiative was investigating methods to reuse isotopes with energy content, transmute long-lived nuclides into isotopes with shorter half-lives, and find ways to reduce volume as well [4]. the waste packing is limited by the heat generated by the radioactive decay. If the total heat load can be reduced, space can be saved. The removal of cesium and strontium could reduce repository size to <20% of current estimates [13]. The cesium and strontium will require immobilization once separated from the bulk of the spent nuclear fuel.

3.1 Alumino-Silicates

Bentonite has been proposed as a waste immobilization matrix as early as 1953 [21]; Hatch cited several of bentonite's benefits, such as cation exchange capacity (~1 meq per gram of clay), and a structure that, when sintered to 1000 °C, becomes inert and no longer able to exchange cations. Other characteristics are the stability of the material, its abundance, its ability to be formed into any desired shape and withstand high temperatures. Barney reported the use of several clays for radioactive waste immobilization by hydrothermal reactions at mild temperatures (up to 100 °C) [22]. Surrounding waste canisters with bentonite to retard the migration of radionuclides in the groundwater was proposed more recently [23, 24]. A novel use for bentonite was proposed by Papachristodoulou *et al* in the decontamination of ruminants [25].

While effective as a generic radioactive waste immobilization matrix, bentonite appears ideally suited for wastes containing alkali and alkaline earth metals when combined with sintering. The bentonite contains the necessary molecular building blocks for pollucite, as well as strontium feldspar. Rubidium and barium both have very similar chemistry to their chemical group counterparts, cesium and strontium respectively and so will have similar reaction products forming rubidium substituted pollucite and barium feldspars.

Natural pollucite and these feldspars survive over geologic time scales, as strontium feldspars are used as geologic chronometers [26]. For this reason synthetic analogs of these aluminosilicate minerals have been studied extensively for radioactive waste treatment. A few methods to produce pollucite include hydrothermal synthesis [27], using an arc melter [28], high temperature treament of high alumina containing cement mixed with silica fume [29], heating of electrorefiner salt with glass frit to produce a high cesium content glass bonded ceramic [30], and from sintering expanded natural perlite [31]. Konovalov and others used high temperature synthesis, where a highly exothermic metal-to-oxide transformation fuels the mineral synthesis. These reactions are Fe_2O_3 + Al to incorporate cesium into pollucite, and Ti + MoO_3 for strontium into sphene ($CaTiSiO_5$) [32]. Pereira synthesized pollucite from CsCl and chabazite by melting at 700°C for waste chloride immobilization [33].

Vasil'eva *et al* were able to produce both pollucite and strontium feldspar products via solid state crystallization at 700-900 °C of coal fly ash cenospheres [34], as well as Mimura and Akiba by calcination of Cs-mordenite Sr-zeolite [35], Bogdanova and others achieved the similar products with zeolite containing rocks [36]. Zimmer and others treated a complex waste simulant with numerous chemical species with a sol-gel technique where pollucite, as well as barium and strontium feldspars were in the final matrix [37]. Each of these has similarities to this study, the use of alumino silicates to immobilize cesium and strontium, but none incorporated a FPEX waste solution, neither did they use bentonite specifically. In our work we simulated an

acidic waste solution with barium and rubidium as well as the cesium and strontium. Only one of the previous studies had these species incorporated in their waste, but all were in low levels in conjunction with several other elements (Zimmer). The addition of the wastes to the immobilizing matrix in these aforementioned studies is of greatest difference to our study, most employed contacting the solutions with the absorbing zeolite, where we dried off the waste solution with heat. The reason we did this was to mimic a process close to an engineering solution. This way the effect of a highly concentrated acid has on the bentonite during processing can be observed, as well as an opportunity to document any gross volitization occurring. When contacting the absorber with the waste solution the loading is limited to the cation exchange capacity of the particulur zeolite, cenosphere etc. The greatest benefit to drying the solution onto the bentonite, is the loading concentration is not limited by the cation exchange capacity. Our limit will have to be determined by experiment to determine at what concentration leachability becomes unacceptably high.

The work mentioned above and throughout this document, which has focused on pollucite for Cs-137 immobilization has been motivated by the low leachability of pollucite. Pollucite has been shown to have leach rates from 3×10^{-4} to 2.2×10^{-6} g/m$^2 \cdot d$ [38]. Anchell found this is due to self diffusion rates to be ~0 [39]. Anchell noted findings by Barrer and Rees which showed that when pollucite (Cs-analcite) is finely crushed and dispersed in a NaCl solution the cation exchange rate is 1.74×10^{-17} cm^2/sec (at 25°C self diffusion of Na^+ in glass is 10^{-17} cm^2/sec) [40]. Although low, he recommended minimizing the surface area of these waste forms to counter this issue. Hess found β^- damage to stoichiometric ^{137}Cs doped pollucite structure slightly increased the volume from 0.5 - 1 % [10]. A study performed by Argonne and Pacific Northwest National Labs interrogated ^{137}Cs pollucite sources for transmutation effects on the pollucite structure [41]. They found minimal damage even in a sample that had decayed 20 years, corresponding to a decay of 16% of

the ^{137}Cs transmuting to ^{137}Ba. However the initial ^{137}Cs mass fraction was 0.0375 which is relatively low.

Thermodynamic properties of pollucite and the feldspars of Sr and Ba were calculated by two methods. Natural pollucite data was calculated by Ogorodova and others [42], the feldspars were synthesized by Chernyshova and his colleagues [43]. The heat capacities cited here were plotted on a mass basis along with our results for comparison (Figures 5.9, 5.10, 5.11) Heats of formation and Gibb's free energies are listed in Table 3.1. Heat capacity for the natural pollucite:
$Cs_{0.84}Na_{0.11}Al_{0.88}Si_{2.10}O_6{\cdot}0.17H_2O$

$$C^{\circ}_{p,m} = 131.37 + 181.97 \times 10^{-3}T - 11.84 \times 10^{5}T^{-2}JK^{-1}mol^{-1}(\pm 0.36\%) \tag{3.1}$$

at 298.15610K [42].

Heat capacity for the sythetic Sr and Ba feldspars:
$SrAl_2Si_2O_8$

$$C_p = 269.59 + 5.784 \times 10^{-2}T - 5.833 \times 10^{6}T^{-2}JK^{-1}mol^{-1} \tag{3.2}$$

at 250-1000K [43].

$BaAl_2Si_2O_8$

$$C_p = 261.05 + 6.640 \times 10^{-2}T - 5.2568 \times 10^{6}T^{-2}JK^{-1}mol^{-1} \tag{3.3}$$

at 250-1000K [43].

Table 3.1
Thermodynamic properties of natural pollucite, and synthetic Sr-feldspar, and Ba-feldspar at T = 298.15 K

Mineral	$-\Delta_f H^\circ_m$ (kJ mol^{-1})	$-\Delta_f G^\circ_m$ (kJ mol^{-1})	Reference
Pollucite I$^\clubsuit$	3104 ± 13	2921	[42]
Pollucite II$^\heartsuit$	3090 ± 14	2911	[42]
Sr-Feldspar ($SrAl_2Si_2O_8$)	4248	4023.75	[43]
Ba-Feldspar ($BaAl_2Si_2O_8$)	4244.30	4021.87	[43]

$^\clubsuit Cs_{0.77}Na_{0.14}Rb_{0.04}Al_{0.91}Si_{2.08}O_6{\cdot}0.34H_2O$ (molar mass = 294.15×10^{-3} kg mol^{-1})

$^\heartsuit Cs_{0.84}Na_{0.11}Al_{0.88}Si_{2.10}O_6{\cdot}0.17H_2O$ (molar mass = 295.88×10^{-3} kg mol^{-1})

These minerals display low Coefficients of Thermal Expansion (CTE). Yanse reported the thermal expansion coefficient for pollucite 1.3×10^{-6}/°C (23-1000 °C) [44]. Barbeeri reported the CTE for Ba-feldspar to be 2.29×10^{-6}/°C from 20-1000°C (CTE for borosilicate glass 0.75×10^{-4} 300-500°C [45]) , and melting points of 1760 and 1650°C for Ba-feldspar and Sr-feldspar, respectively. Beall found that barium and strontium feldspars to be thermally stable above 1400°C with a melting point just below 1700°C. He also determined that these feldspars could have their coefficients of thermal expansion adjusted by 30-50 $\times 10^{-7}$/°C with the addition of accessory phases: for example The CTE could be lowered by the addition silica rich glass [46]. Adding glass requires heating to the liquidous temperature, which for borosilicate glass is 1050°C [47].

3.2 Other Waste Forms

Spent fuel and radioactive waste must be isolated from the environment. In the following sections a brief review of engineered barriers that will be employed in conjunction with sequestration. Sequestration may be in an above ground cask or tomb, as well as natural barriers such as deep sea burial, or in an underground repository. An underground repository's geology may consist of salt beds or salt domes, volcanic tuff, basalt, or granite. Yucca Mountain is an example of volcanic tuff, while the Waste Isolation Pilot Plant (WIPP) is a salt bed repository (WIPP accepted its first waste shipment in 1999 and continues to operate [48]).

The spent fuel from a nuclear reactor is primarily UO_2 which is inherently unstable in aqueous systems [49]. Inside a nuclear reactor the pelletized uranium oxide is encased in a zirconium cladding which keeps water from reacting with the fuel. During fission the fuel swells and gases are generated which add strain and stress to the fuel and cladding [50]. These stresses lead to break up of the UO_2 pellet, and with time increase the likelihood of a cladding breach [51]. This is usually manageable in the 24 months residence in a reactor [48], but for long term stability secondary measures must be employed to assure immobilization of the spent fuel. The current Yucca Mountain proposal has engineered special canisters for the long term containment of the spent fuel. These multiple barrier containers will contain entire fuel bundles for thousands of years. The purpose of these waste canisters include physical containment for shipping and handling, radiation shielding, and to isolate the waste from the natural barriers [52].

3.2.1 Vitrification

Radioactive waste immobilization via vitrification has an extensive history and worldwide usage [53] and testing [54]. During vitrification glass frit is mixed with the waste to be treated and heated until it becomes a liquid. The liquid glass is

transferred to a container, where it forms the final shape and cools. Various types of nuclear waste have been vitrified, one example is high level tank waste from Hanford. Hanford waste was vitrified at 1150°C for 2.5 h to produce a borosilicate glass. Once the waste glass has been manufactured it is transferred to a repository. High level radioactive waste glass shipments have been accepted at the WIPP for long term isolation [55, 56].

The high temperatures required for vitrification may volatilize low melting point waste constituents, such as cesium and technetium. The volatility of cesium, and the various mitigation methods in vitrification systems have been investigated by Kamizono [57]. One technique employed to aid retaining the volatiles is to cover the melt surface with a cold cap [58]. A slurry is fed to the top of the melter forming a crust on the surface of the melt pool, this crust or cold cap reduces the amount of volatiles that escape the melt [59]. Other methods to reduce or eliminate volatility include absorbing the waste in a media, such as a zeolite [60], ion exchange resin [61], or crystalline silicotitanate [62], and then vitrify the resulting compound. These treatments report reductions in the volitization of cesium during the vitrification process.

3.2.2 Grout, Concrete and Geopolymers

The use of grout and concrete are usually limited to low level waste and intermediate level waste. They are favored for their low cost and simple application [63]. A drawback when applied to the immobilization of cesium-containing waste is the tendency for the cesium to stay in the aqueous region within the cementitious media [64]. To incorporate the cesium into the mineral phase, methods similar to what has been done to improve vitrification are applied. The use of zeolites or resins to first absorb the cesium before mixing with the concrete or grout improved leachability characteristics [65]. Geopolymers are primarily amorphous solids produced by mixing alumino-silicates with concentrated alkali solutions. Their application to the

immobilization of radioactive waste has been tested by Perera and others [66, 67]. By mixing fly ash or metakaolinite with alkali solutions and polymerizing at 90 °C they found 1 wt% cesium and strontium could be effectively immobilized.

3.2.3 Zeolites and Ion Exchange Materials

Zeolites and ion exchange materials can be used to remove the radionuclides from a solution and trap them in the exchange medium. The sorption of radioactive liquid wastes has been studied with the zeolite clinoptilolite to remove Cs and Sr isotopes [68]. Researchers recommend concentrations below 3×10^{-9} mg/L and pH should be kept ~ 8. Kaolinite powders have also been investigated to reduce Cs and Sr emissions from high temperature processes [69]. This work displayed possible improvements to incineration and vitrification processes due to the kaolinite powder's ability to scavenge these metals from a vertical combustor.

In 1997 Pacific Northwest National Laboratory under the Department of Energy was contracted to investigate radionuclide uptake of a number of different engineered inorganic ion exchange materials from 105-KE Basin water. The study concluded that KCoHex (potassium cobalt hexacyanoferrate) and SZ-72 (modified zirconate) removed over 99% of the ^{137}Cs. In the same study they found ^{90}Sr was most effectively removed with pharmacosiderite and sodium nonatitanate with an ability to absorb greater than 99% of the strontium from the basin water [70]. The stability against leaching of these ion exchange materials, or absorbers, can be improved with the addition of a sintering step [71]. Similar improvements can be made by mixing the material with another binding agent, *i.e.* cement [64]. Mimura and Akiba were able to produce cesium and strontium loaded ceramic solids from zeolites. To have a consistent particle size in their feed, they first pulverized and sieved mordenite and Zeolite A. The mordenite was saturated with cesium, and the zeolite A was saturated with strontium as well as both cesium and strontium. The ions were dissolved in 1 M nitrate solutions. These were filtered and dried at 250 °C then cold isostaticly

pressed at 78 MPa followed by calcination at 1200 °C. The final products consisted of pollucite ($CsAlSi_2O_6$) and strontium feldspar ($SrAl_2Si_2O_8$) [35].

3.2.4 SYNROC

SYNROC or synthetic rock is a durable robust method to treat waste steams. The method was developed at the Australian National University, and first described in 1978 [72]. As the name implies, SYNROC is a synthetic rock, composed of titanium mineral assemblages to mimic natural rocks. The minerals are tailored to the type of waste being treated, such as perovskite for strontium, and hollandite for cesium immmobilization. The mineral oxide precursors are intimately mixed then slurried with the waste calcined, then hot pressed into the final waste form. These waste forms are resistant to leaching even at elevated temperatures and can hold virtually all types of high level waste. SYNROC is considered second to vitrification, but has displayed superior mechanical behavior, was found to be more stable thermally, and can support higher loadings of certain types of waste as opposed to vitrification [73].

The immobilization of cesium in hollandite melts was investigated by Carter and others [74]. They prepared samples via an alkoxide route, where molar quantities of the required alkoxides are dissolved in water with the necessary nitrates. The solution was then dried and calcined in air at 750 °C for two hours. These were melted in Pt crucibles in air at 1450-1550 °C. They found ~7.5 wt % Cs_2O could be prepared with Cr^{3+}, Ni^{2+}, Zn^{2+} or Co^{2+} resulting in hollandite ceramics with PCT-B normalized Cs leachate concentrations <0.2 g/L. The PCT-B leach procedure requires sample powders to be within 75-150μm, which are then ultrasonically washed prior to testing. The leach test requires holding 1 g of powder in 10 ml of de-ionized water for 7 days at 90°C, the resulting leachate solution is analyzed for suspended ion concentrations. Their work continued with a hot isostatic pressing (HIP) route which reduced the processing temperatures. Instead of melting in air, the powders were heated to 1275 °C at 30 MPa for an hour. These experiments also incorporated strontium with

cesium resulting in a 12 wt % loadings. A SYNROC rich in the mineral rutile was also tested for the immobilization of Tc [75].

A report by Tripp and Maio [76] concluded Synroc would be an effective cesium and strontium immobilization method, but would not rule out steam reforming as an alternative. The drawbacks of the SYNROC process are complex preprocessing, the stoichiometry must be tailored to produce the desired final minerals, and the sintering is done at high temperatures and pressures.

3.2.5 Steam Reforming

Steam reforming is a waste treatment method where a liquid waste is injected into a fluidized bed along with the necessary co-reactants at an elevated temperature. [Steam is added or is part of the feed stream.] Typical co-reactants are different types of clay which provide silica and alumina, and carbon sources to facilitate organic and/or nitrate destruction. The products are solid alumino-silicates [77].

Steam reforming of various types of radioactive waste, including tank wastes [78, 79], radioactive graphite [80], and low level mixed wastes [81], have been tested among others. Radioactive waste treatment with steam reforming has been applied to cesium and strontium bearing separation product solutions as well. Tripp *et al* found strip solutions from several cesium and strontium separation methods could be converted to solids forms, without volatization of cesium while destroying the organics and nitrates in the process. The final product was a leach resistant aluminosilicate. The product does have a water soluble fraction of cesium and strontium, the quantity depends on which process feed was used. The peak concentrations of unmineralized product, or water soluble solids were 22% for cesium and 10% for strontium. Another issue of concern is the production $<\mu$m particles [82].

3.2.6 Calcination

Calcination refers to the treatment of liquid radioactive wastes by heating to oxide. This method has been applied to various liquid wastes in different ways. A few examples are fluidized-bed calcination, pot calcination, radiant heat-spray calcination, rotary ball-kiln calcination, and calcination in molten sulfur [48]. These are effective techniques to remove liquids and reduce volume. The waste produced by these processes is usually a powder or granular form. Once dry, the waste must be containerized in a method adequate to avoid dispersal into the environment. A container may also be needed to keep water from dissolving or moving the waste if no fixation is applied.

A method to immobilize calcine from low level sodium- aluminum- and zirconium-bearing waste, involved mixing the calcine with Portland cement, blast furnace slag, and fly ash, researchers found the product reduced volume and met leach requirements [83]. Another method found to improve leachability and performance is the addition of metakaolin and a NaOH solution to the calcine followed by mild curing, which produced a durable solid [84]. This waste form is known as hydroceramic.

4. EXPERIMENTAL METHOD AND ANALYSES

Simulated waste was prepared from stable isotopes of cesium, strontium, barium and rubidium. Nitrates of each metal were dissolved in dilute nitric acid. Then this solution was added to bentonite clay. Bentonite clay was used as received (American Colloid Company of Belle Fourche, SD provided Volclay HPM-20, 425 mesh) The composition reported by American Colloid was SiO_2 = 69.56%, Al_2O_3 = 20.69%, MgO = 2.70%, Fe_2O_3 = 4.85%, CaO = 1.30%, Na_2O = 2.43%, K_2O = 0.30%. The loss-on-ignition was 4.80%. The specific gravity was 2.6 and the pH of a 2% solid suspension was 8.5-10.5 [2]. Laboratory-supplied deionized water was used for all experiments, except for TCLP where purchased deionized water was used instead.

4.1 Sample Preparation

The first step was to create a simulated waste liquid. The waste liquid was then added to the bentonite clay. The bentonite clay and waste solution were dried to a powder, the powder was then pressed into pellets to be sintered. Pellets were sintered at various temperatures and waste concentrations.

4.1.1 Simulated Waste

The FPEX process stream will produce a strip solution of dilute nitric acid containing cesium, strontium, barium and rubidium ions. Cesium and strontium are the primary targets of immobilization, while the rubidium and barium are co-extracted due to their similar chemistry. The quantities of waste ions in the proposed waste stream are relatively dilute. Ion ratios of Cs:Rb of 3340:537 and Sr:Ba of 1180:3100 were used in the simulated waste. The ion quantities were 2:1 Cs to Sr by mass in the solution. These were provided by ORIGEN simulations of the UREX process raffinate developed by Argonne National Laboratory [85]. Nitrates of the required

Table 4.1
Simulated waste solution composition

Component	Qty	MW	moles/L
HNO_3 70%	103.97 ml	63.01	1.64
$Ba(NO_3)_2$	14.183 g	261.34	0.054
$CsNO_3$	11.90 g	194.91	0.061
$RbNO_3$	2.27 g	147.47	0.014
$Sr(NO_3)_2$	6.88 g	211.63	0.033

ions were chosen for the waste simulant. The nitrates were dissolved into a dilute nitric acid solution. The ion concentrations of these metal ions were increased to the point of saturation in order reduce the volume of liquid required to process (Table 4.1). To completely dissolve the nitrates the salts were stirred with a magnetic bar for ~24.

4.1.2 Bentonite Waste Loading

The concentrated waste solution was added to the clay then stirred, the water was driven off by placing the beacker in an oil bath at approximately 110°C. The process was repeated until the desired concentration metal ions was reached. The clay was mixed as the waste solution heated to dryness to prevent hot spots and to homogenize the powder.

The clay waste concentrations were based on the mineral pollucite. Pollucite is a natural source of cesium, which contains silicon and aluminum oxides. This mineral has had extensive study as cesium immobilization compound [7–9,38]. In addition to cesium, natural pollucite also contains sodium; if we assume sodium can be replaced by cesium the potential cesium content is approximately 42 mass %. 30 % was

chosen as a theoretical maximum loading for the clay based on the amount of alumina available to produce pollucite and feldspars from the cesium, rubidium, barium, and strontium. Various percentages of the pollucite based theoretical maximum were chosen as loadings for comparison.

After reaching the desired waste content, the dried clay powder was ground by mortar and pestle. A small amount of loaded unsintered clay was allotted for differential scanning calorimetry and thermal gravometric analysis, as well as a reserve. The powder was then axially pressed to 2000 lbs in a 5/8" die (~6500 psi) to create a green puck. The pucks were then sintered.

4.1.3 Sintering

The sintering temperatures were varied from 700°C to 1400°C. The ramp rates were held constant at 5° per minute for all sinterings. Once reaching the desired temperature, samples were soaked for 12 hours. Cooling was initially controlled to 5 °C per minute but eventually the cooling rate decreased to a much slower natural rate.

4.2 Analyses

After samples were prepared a series of analyses were performed to characterize the material properties.

4.2.1 Bulk Properties

Masses and dimensions of the pucks before and after sintering were collected for comparison. The true volume was calculated with a Quantachrome helium pycnometer. A sample was placed in a known volume and pressurized, a working gas enters the empty space including the open porosity, in this case helium up to ~0.117 MPa.

Next a valve is opened allowing the gas to be shared with another known volume. With the initial pressure and the final pressure the sample volume can be calculated using an expression of Boyle's law (4.1)

$$V_p = V_c - V_r \times ((P_1/P_2) - 1) \tag{4.1}$$

where V_p is the sample volume, V_c is the sample cell volume, V_r is the reference cell volume, P_1 is the pressure in the sample cell and sample, and P_2 is the pressure after opening the connecting valve between the sample cell and the reference cell. With the volume of the sample, and its meaured mass the true density can be determined. By comparing the true density to the bulk density, the porosity is calculated(4.2).

$$Porosity\ \% = (1 - (bulk\ density/true\ density) \times 100 \tag{4.2}$$

Bulk density was calculated by measuring the sample dimensions. The color and changes in shape, such as slump and cracking were also noted.

4.2.2 Differential Scanning Calorimetry and Thermal Gravimetric Analysis

Unsintered bentonite clay samples were subjected to a controlled heating rate in a Netzsch STA 409 PC *Luxx* simultaneous thermal analysis instrument, with Proteus Software. The instrument performs a thermal gravimetric analysis (TGA), as well as differential scanning calorimetry (DSC) on each sample in tandem over a specified heating profile. The sample is loaded into an alumina crucible of know mass, which then is set on a sensitive balance. The balance resolution is 2μg, while the error in mass changes in our process is ~40μg. Along with the sample an empty, but identical alumina crucible of known mass was loaded as a reference. Heat flux is measured with a pair of thermocouples attached to bottom of each of the crucible mounting points. The reference signal is subtracted from the sample to obtain endothermic and exothermic rates and transitions.

The heating rate was 5° per minute from room temperature to 1400 °C. Argon flowed at 50 ml/min to act as a cover gas. Before analysing the samples, the heating

program was run with empty crucibles to create a baseline signal. The baseline signal contained the weight and thermal behaviour due to the crucible as well as any buoyancy effects resulting from the flow of the cover gas. The baseline was then subtracted from the data acquired from the samples. This step corrects for instrument trends, leaving only data due to the samples. Each sample was 20–50 mg.

4.2.3 Light Flash Analysis

Thermal diffusivity and specific heat were measured with a Netzsch Light Flash Analyzer (LFA) 447 *NanoFlash* instrument. Disc samples were first cut and ground to 2 mm ±0.06 mm thick and 12.7 ±0.14 mm in diameter for 800–1000°C; 700°C specimens were prepared identically except they were 15.4 mm square. The instrument used a short light pulse from a xenon lamp to heat the the bottom side of the sample. An infra-red sensor measured the temperature change on the opposing side as a function of time. Thermal diffusivity is determined using the half-time method (4.3) [86].

$$\alpha = 0.1388 \times d^2/t_{1/2} \tag{4.3}$$

Where α is the thermal diffusivity, d is the sample thickness, and $t_{1/2}$ is the time to reach half the maximum temperature. The system applies mathematical regression routines to adjust for radial and facial heat losses, as well as finite pulse effects. The specific heat C_p is simultaneously measured on the same specimen. With the known density ρ the thermal conductivity λ can be calculated (4.4).

$$\lambda(T) = \alpha(T) \times C_p(T) \times \rho(T) \tag{4.4}$$

4.2.4 X-ray Powder Diffraction

The x-ray powder diffraction (XRD) was done by the Texas A&M University Chemistry Department's X-ray Diffraction Laboratory. The instrument used was a Bruker-AXS Advanced Bragg-Brentano X-Ray Powder Diffractometer. Specifications and operating parameters are listed in 4.2.

Table 4.2
Bruker-AXS D8 Advanced Bragg-Brentano X-Ray Powder Diffractometer

Specifications	
D8 Goniometer	
Lynxeye Position Sensitive Detector	
Copper X-ray Radiation	
Software: EVA, Bruker AXS Inc.	
Database: PDF-2, International Center for Diffraction Data (ICDD)	
Operating parameters	
Power	40 kV, 40 ma
Step size	0.015 degree 2θ
Scan Speed	0.1 seconds per step

Samples were prepared for XRD by pulverizing briefly (≤1 minute) in a WIG-L-BUG (Model 3110B) grinding mill with a steel ball bearing. Powders were checked with a Hirox optical microscope (Model KH 1300) to assure particles were in the 5-10 μm range.

4.2.5 Scanning Electron Microscopy & Wave Dispersive Spectrometry

The electron microprobe is an instrument very similar to a standard scanning electron microscope (SEM), but instead of focusing on the imaging of samples, the microprobe is designed primarily for chemical analysis. The electron microprobe has an electron column that consists of an electron source, typically a tungsten filament (but also lanthanum hexaboride is used), and focusing magnetic lenses and apertures. The column is held at a vacuum of 1×10^{-4} to 1×10^{-5} Pa. An electron beam is focused on the sample with a spot size of 0.1 to 1 μm. Electron energies can be adjusted from 5-50 keV. The sintered bentonite samples were run at 15 keV and 20 nA to obtain elemental data, while most of the backscattered electron images we acquired at 15 keV and 3 nA. When electrons strike the sample a series of electron interactions occur and secondary, backscattered, and auger electrons are emitted. Some electrons are absorbed, and they create heat, visible light and also x-rays. These x-rays can be created by two mechanisms. The bombarding electron may be decelerated when interacting with the nucleus of the atoms in the sample or the electrons surrounding the nucleus. The energy lost results in the emission of an x-ray of a continuous energy range up to the accelerating potential of electron beam. The beam electron may also interact with an inner shell electron transferring its energy to the inner shell electron ejecting it from the atom, or raising the electron to a higher energy shell. This last type of interaction results in the energized electron falling back into the vacant inner shell, resulting in either another electron being ejected with energy related to electon transition, or the emission of an x-ray photon with the energy equal to the difference between the electron shells. These characteristic x-rays are useful for elemental determination, and are responsible for energy dispersive spectroscopy (EDS) and wave dispersive spectroscopy (WDS).

Most electron microscopes have an energy dispersive spectrometers, but the electron microprobe also has a series of wave dispersive spectrometers. These spectrometers consist of a rotatable, oriented diffraction crystal coupled with a proportional

gas-filled ionization detector. These two are arranged in a geometric relationship according to Bragg's Law (4.5)

$$n\lambda = 2d\sin\theta \tag{4.5}$$

where n is the order of diffraction, λ is the wavelength of the characteristic x-ray (Å), d is the atomic spacing of the diffracting crystal (Å), and θ is the angle of incidence. Depending on the angle of incidence the x-rays will combine constructively or destructively. The choice of crystal, the arrangement of the crystal, and detector is determined by the element of concern's characteristic x-ray wavelength. X-ray detectors are usually Li-drifted silicon or a high-purity germanium.

This system allows for the resolution of peaks about an order of magnitude better than EDS, and an improved peak/background ratio by an order of magnitude.

WDS system is also capable of quantitative analysis. A series of detectors are set to count for separate elements during a scan of a sample, providing ratios of each element found. There are several issues that will affect accuracy and precision of the instrument that must be considered, such as interferences between various characteristic x-rays that need to be accounted. For a full description, see the source reference [87].

WDS Sample Preparation

Samples were mounted in epoxy (Buehler Ltd), from resin and hardener (Epo-Kwick). Mounts were allowed to set over night. Polishing was done with sandpaper up to 1200 grit for low sintering temperatures 700 - 1000°C. Samples sintered from 1100 to 1200°C were also polished with 3μm diamond spray followed by 1/4 μm spray, then ultrasonically cleaned in 100% ethanol. The mounted samples were sputter coated with ~15nm of carbon.

Acquisition Settings

The accelerating voltage was set at 15kV and 20nA to produces an electron spot size of approximately 0.5μm. The electrons excite a tear drop shaped area ~ 1μm in diameter and ~ 1.25μm deep from which characteristic x-rays are produced. The x-ray detectors were arranged at a distance multiple of the wavelength of the characteristic x-ray of the elements of concern. The crystals were chosen depending on the particular x-ray of interest (Table 4.3).

Table 4.3
WDS crystal types and associated elements (TAP: thallium acid phthalate, PET: pentaerythritol, LIF: lithium fluoride)

Element	Line	Crystal	Standard
Na	K-α	TAP	albite
Rb	L-α	TAP	RbI
Mg	K-α	TAP	hornblende
Al	K-α	TAP	albite
Si	K-α	PET	hornblende
Ca	K-α	PET	hornblende
Sr	L-α	PET	$SrTiO_3$
Fe	K-α	LIF	hornblende
Cs	L-α	LIF	CsBr
Ba	L-α	LIF	$BaSO_4$

4.2.6 Neutron Activation Analysis

Neutron Activation Analysis (NAA) was done at the Texas A&M Triga Mark I research reactor. The reactor is pool-type, with sample port tubes for sample

irradiation. Samples were exposed to 10.0×10^{13} neutrons/cm^{2}s at 100 kW. Known quantities of representative standards were run under identical conditions, then compared to unknown samples and quantified using the ratio method. Analysis was done with Genie 2000 software (Canberra Inc.).

Due to the presence of cesium, in our samples short exposures (60 seconds) and long exposures (1 hour) were required. Cesium's very high activation rate hid any signal due to strontium over long exposures. Short exposures were necessary to detect the strontium signal. For short runs samples are pneumatically inserted and pneumatically removed allowing samples to be removed from the neutron flux quickly. Samples were then counted after being removed from the reactor.

4.2.7 Toxicity Characteristic Leach Procedure

The Toxicity Characteristic Leach Procedure (TCLP) is a protocal that is defined very specifically under the Resource Conservation and Recovery Act [88]. Samples under analysis are exposed to an acetic acid solution for a predetermined amount of time while mixed. The liquid is then analyzed to quantify the concentration of various listed substances. If the concentration of any listed toxin is above guideline limits the waste is considered hazardous. If the waste fails the TCLP it must be disposed in a hazardous waste facility.

A simplified TCLP was performed on the sintered clay samples as a baseline leachability test. This is not a definitive leach resistance test, but only used to compare between the different sinterings and loadings of these particular samples.

TCLP reagent and sample preparation

Each sample of sintered bentonite clay was ground to a powder by mortar and pestle and sifted through # 100 sieve to $\leq 150\mu$m. The simplified TCLP required 5 grams of powder added to 96.5 mL DIW in a 500 mL beaker. The simplified TCLP

differs from the regulatory procedure and is only for comparison of our samples to each other, passing the simplified TCLP has no legal consequence.

Steps of Simplified TCLP [89]

1. Place 5 grams of sample powder in a 500 mL beaker, add 96.5 mL DIW, cover with a watch glass, stir vigorously on a magnetic stirrer for 5 minutes. Measure and record the solution's pH.

2. For pH <5 got to step #3. For pH >5, go to step #4.

3. Prepare fluid #1: Add 5.7 mL glacial acetic acid to 500 mL DIW, add 64.3 mL of 1 N NaOH, then dilute to a volume of 1 L. The resulting pH should be 4.93 ± 0.05. Procede to step #6.

4. For pH >5, add 3.5 mL of 1 N HCl, slurry briefly, cover with a watch glass, heat to 50 °C and hold at 50 °C for 10 minutes. Allow the solution to cool to room temperature and record pH. If pH is <5, proceed to step #3. If pH is >5, proceed to step #5.

5. Prepare fluid #2: Dilute 5.7 mL glacial acetic acid with DIW to a volume of 1 L. The resulting pH should be 2.88 ± 0.05. Proceed to step #6.

6. Transfer 50 grams fo powder (100 mesh) into 2.2 L polyethylene bottle, add 1000 grams of fluid specified above and seal bottle tightly with teflon tape.

7. Agitate bottle at 30 ± 2 rpm for 18 ± 2 hours.

8. Filter leachate thruogh 0.7 μm filter.

9. Add 20 mL of extract to each of two labeled sample vials. Measure the pH of the two vials.

10. Add 100 mL of the extract to another two labeled vials for cation analysis. Add 1 mL of concentrated HNO_3 to each vial to ensure a pH <2.

11. Save additional leachate for analyses if needed.

Leachate solutions were anayzed with iductively coupled plasma mass spectroscopy (ICP-MS) either at Texas A&M Trace Element Laboratory for samples sintered at 700, 800 and 1000 °C, or Argonne National Laboratory for samples sintered at 1100 and 1200 °C.

4.3 Waste Form Heat Generation Model

Calculations with experimental data collected in this study were input to a model described by Kaminski [90]. The model will determine waste form radius, assuming a right cylinder with an input maximum centerline temperature. The model accounted for the different isotopes and only required the wt% of cesium and strontium, thermal conductivity, density, and a maximum center-line temperature. The model assumes passive cooling with air at 90°C with natural convection. The waste form was assumed to be inside a stainless steel canister 0.02 m thick. The spent fuel was assumed to be 4.25 enriched uranium, with burn-up at 50GWD/ton, and 20 years of cooling. The isotopic composition of the spent fuel was determined from ORIGEN simulations by J. Stillman (ANL).

5. RESULTS

Upon sintering at higher temperatures the clay color transformed from a reddish brown at 700°C to a pale yellow at 1200°C (5.3). The samples at lower sinterings were brittle and pulverized easily, while those sintered at ≤1000 °C became very hard and were much more difficult to pulverize.

5.1 Bulk Properties

Sinterings ranged from 700°C to 1400 °C, but at 1400 °C the samples melted completely. The lowest waste loading, ~15 wt% waste, became bloated when sintered at 1200°C resulting in a pumice-like porous mass. When the waste loading was increased to 18 and 21% wt% the samples distorted less severly, swelling and cracking slightly, loadings above 21 wt% had a smooth texture and uniform coloration (Figure 5.1).

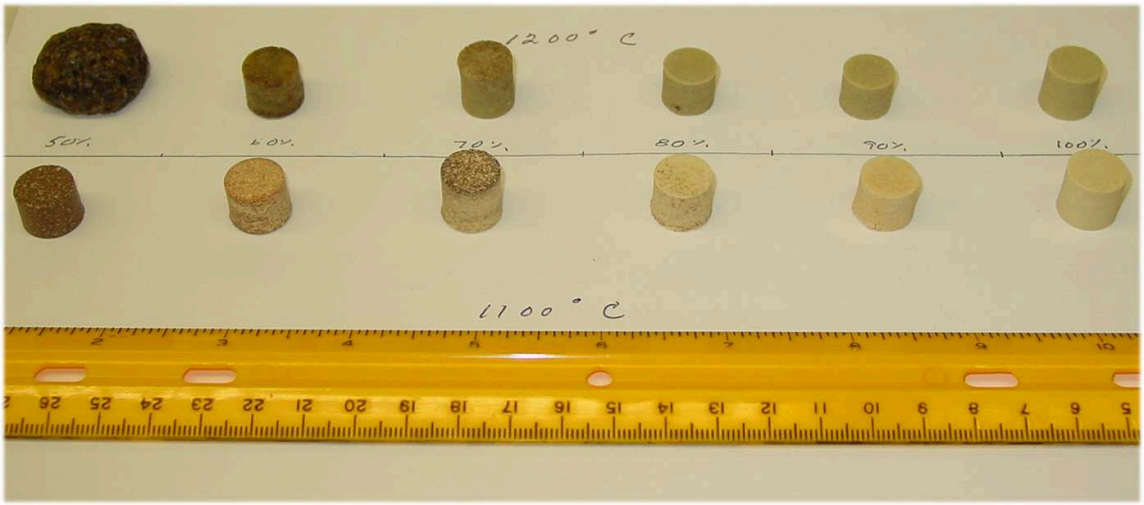

Fig. 5.1. 1100 °C and 1200 °C sintered bentonite clay various loadings.

At sintering temperatures ≤1000°C the color transformed from a reddish brown at the lowest sintering temperatures to a pale yellow at the highest. The color of the samples sintered at temperatures 800 through 1000 °C resulted mottled combinations. Lower loadings at 700, 800, and 1000°C sintering temperatures displayed darker coloration than the 100% loaded samples (Figure 5.2), the ceramics had the lightest coloration at 1100°C at loadings >80% and the 1200°C became darker (Figure 5.3). The bentonite tranformed from a brick colored, rough texture 700°C to a pale yellow, hard glassy ceramic at 1200°C (Figure 5.3).

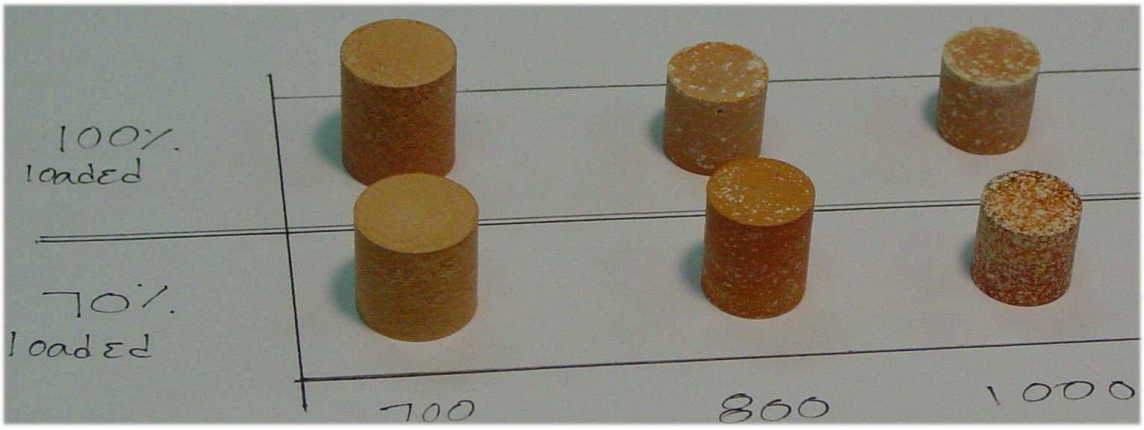

Fig. 5.2. 700, 800, and 1000 °C sintered bentonite clay with 24%-32% waste loadings.

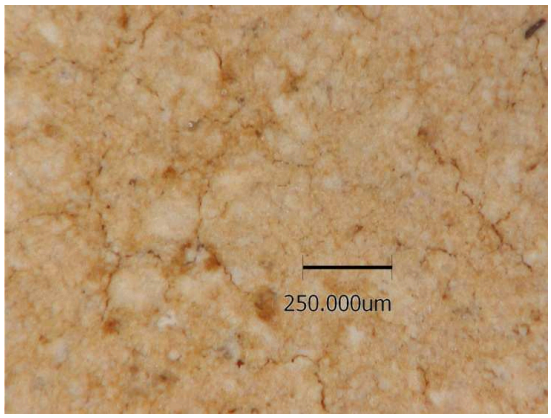

(a) 700°C 32wt% waste

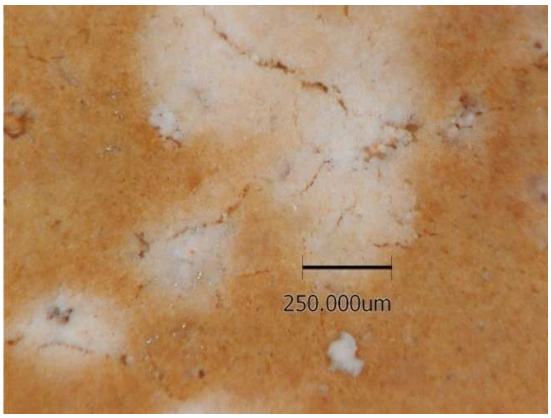

(b) 800°C 24wt% waste

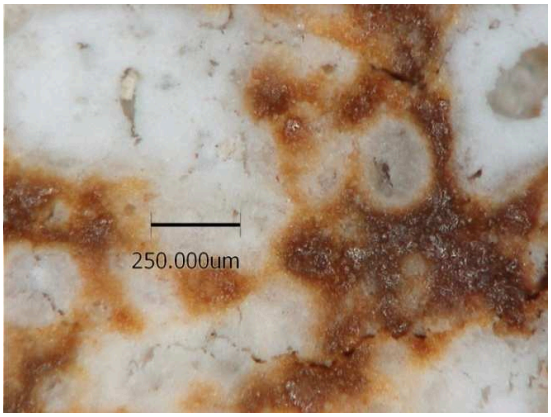

(c) 1000°C 26 wt% waste.

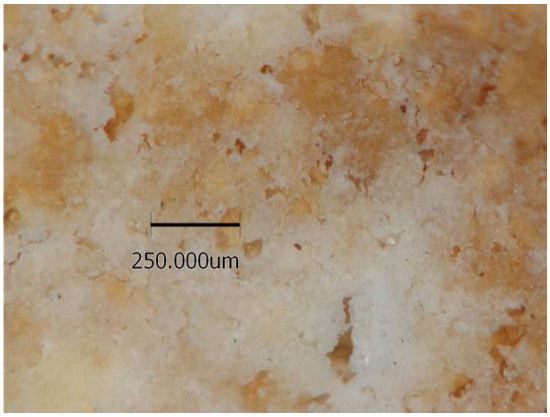

(d) 1000°C 31wt% waste.

(e) 1100°C 21wt% waste

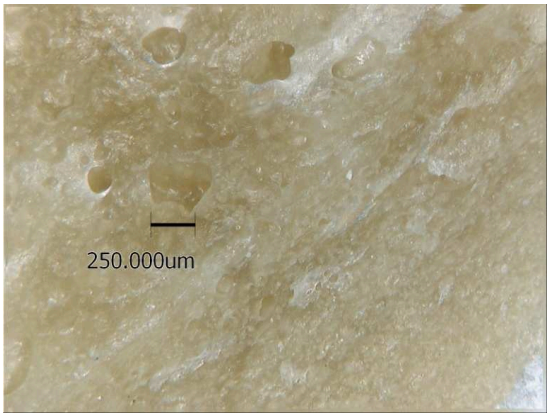

(f) 1200°C 21wt% waste

Fig. 5.3. Bentonite clay sintered at 700, 800, 1000, 1100, and 1200 °C with various waste concentrations

5.1.1 Density

The bulk density trends were variable, generally increasing with loading and sintering temperature. At 700, 1000, and 1100°C there was a drop in bulk density at the highest loadings (Table 5.1).

Table 5.1
Bulk densities of sintered bentonite as a function of maximum theoretical loading.

Bulk density g/cm^3					
	Sintering Temperature °C				
Loading (% of max)	700	800	1000	1100	1200
100	1.21	1.78	1.84	2.18	2.53
90				3.03	2.51
80				2.95	2.55
70	1.24	1.76	2.02	2.94	2.41
60				2.89	2.12
50				2.73	

5.1.2 Porosity

The porosity of the samples was reduced with increasing sintering temperature. The lowest porosity was at the highest sintering temperature of 1200 °C at 100% loading with 4.7%. The porosity 1100°C was higher than at 1000°C at 70% loadings of the theoretical maximum. The lowest sintering temperature of 700°C resulted in ceramics with greater than 50% porosity (Table 5.2).

The porosity of the clay varied substantially from sintering to sintering. When plotted with thermal conductivity on the Y-axis and porosity on the X-axis (Figure

5.4) we have the relationship predicted by Coble and Kingery [91]. The higher density at the higher sintering temperatures will produce a higher thermal conductivity.

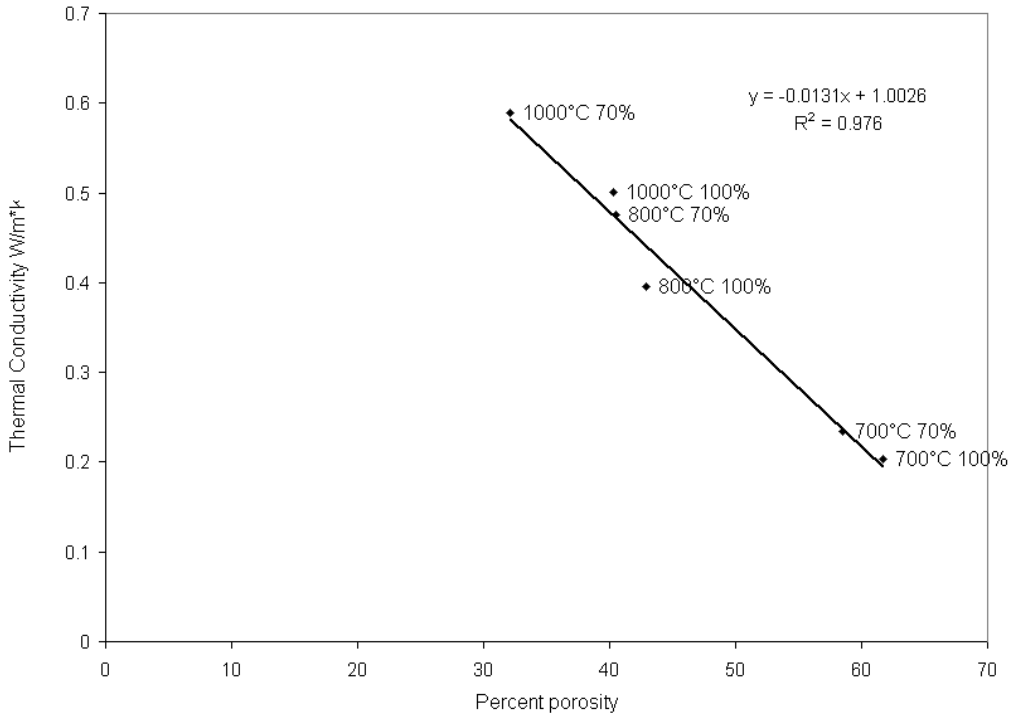

Fig. 5.4. Porosity effects on thermal conductivity of bentonite sintered at 700, 800, and 1000 °C waste loadings at 70 and 100% of theoretical maximum.

Table 5.2
Open porosity of sintered bentonite clay loaded with Cs, Sr, Ba, and Rb ions.

Open porosity %			
	Loading (% of max)		
Sintering Temperature °C	70%	90%	100%
1200	14.4		4.7
1100	33.6	32.7	
1000	32.1		40.3
800	40.5		43.0
700	58.5		61.7

5.2 Differential Scanning Calorimetry and Thermal Gravimetric Analysis

Thermal Gravimetric Analysis (TGA) records the mass changes under heating. Differential Scanning Calorimetry (DSC) measures the thermodynamic heat flux as a function of temperature. In these plots exothermic heat flux is positive, and endothermic heat flow is negative. DSC-TGA was applied simultaneously to the various unsintered bentonite clay loadings. The results are qualitative only showing trends and onset temperatures. A sample of pure bentonite clay was analyzed as well to document the baseline clay behavior. The pure bentonite has an exothermic bloating reaction accompanied by a small mass loss at 950°C (Figure 5.5). This bloating is attributed to the release of oxygen during the reduction of various oxides in the clay [92]. A similar exotherm occurs >1200°C when the 16% loaded bentonite bloats, but without a detectable mass loss (top left Figure 5.1, and 5.6).

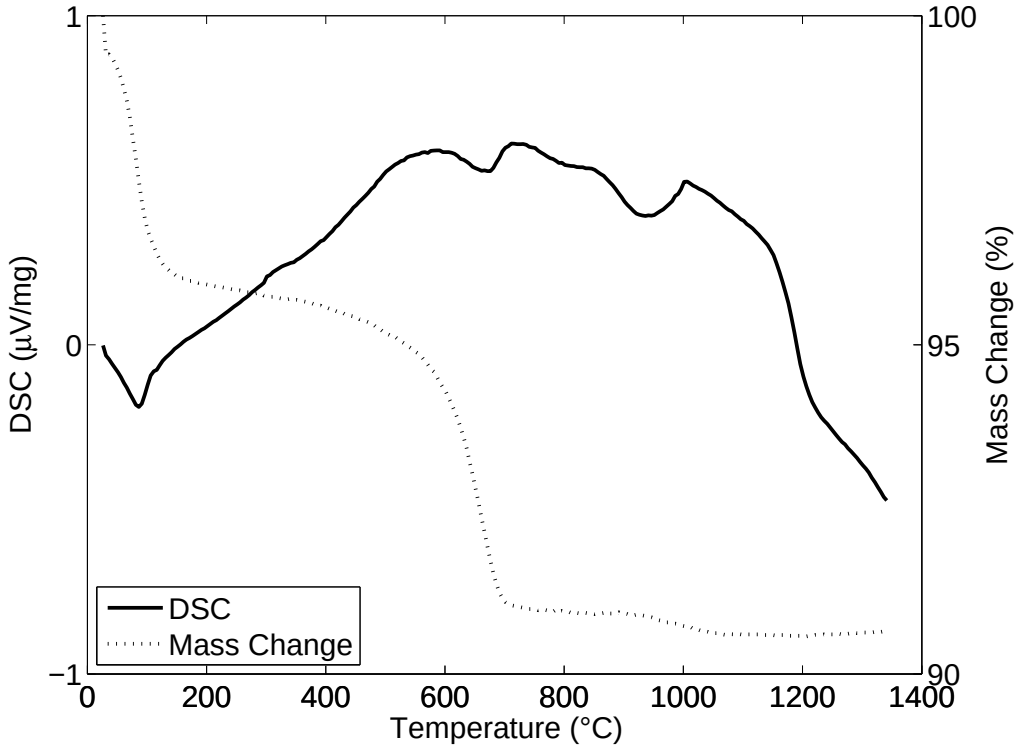

Fig. 5.5. Pure bentonite combined differential calorimetry and thermal gravometry displaying high temperature bloating effects

Each of the loaded bentonite clay samples started with a sharp drop in mass upon initial heating with one exception, the 16 mass percent waste loaded sample (Figure 5.6). This sample was stored in a dessicator prior to analysis and during this time the powder lost most of the loosely bound water.

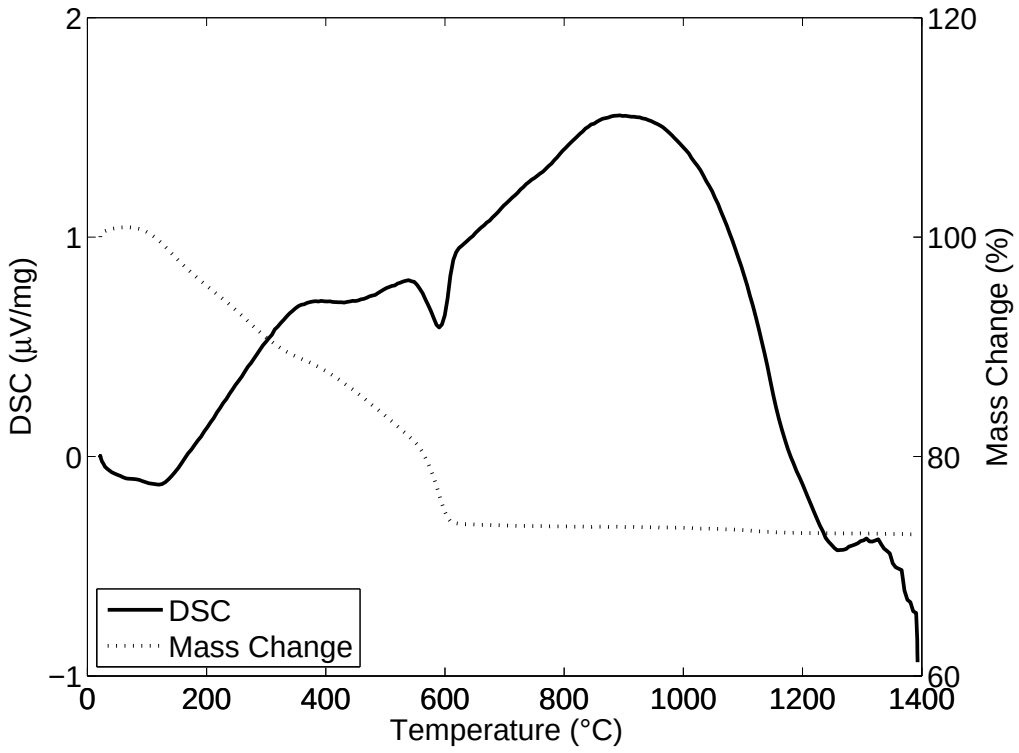

Fig. 5.6. 16 mass percent waste loaded bentonite combined differential calorimetry and thermal gravometry

The dehydration process in montmorillonite has been documented by Onal and Sarikaya [93]. The mass loss rates due to water release coincide with how tightly bound the water is to the clay. Once the heating begins the early steep mass loss is due to the drying of interparticle water. This water comes off quickly then concludes at ≤200 °C (Figures 5.7, 5.7). This mass loss has an associated endotherm visible as a negative slope ~150°C.

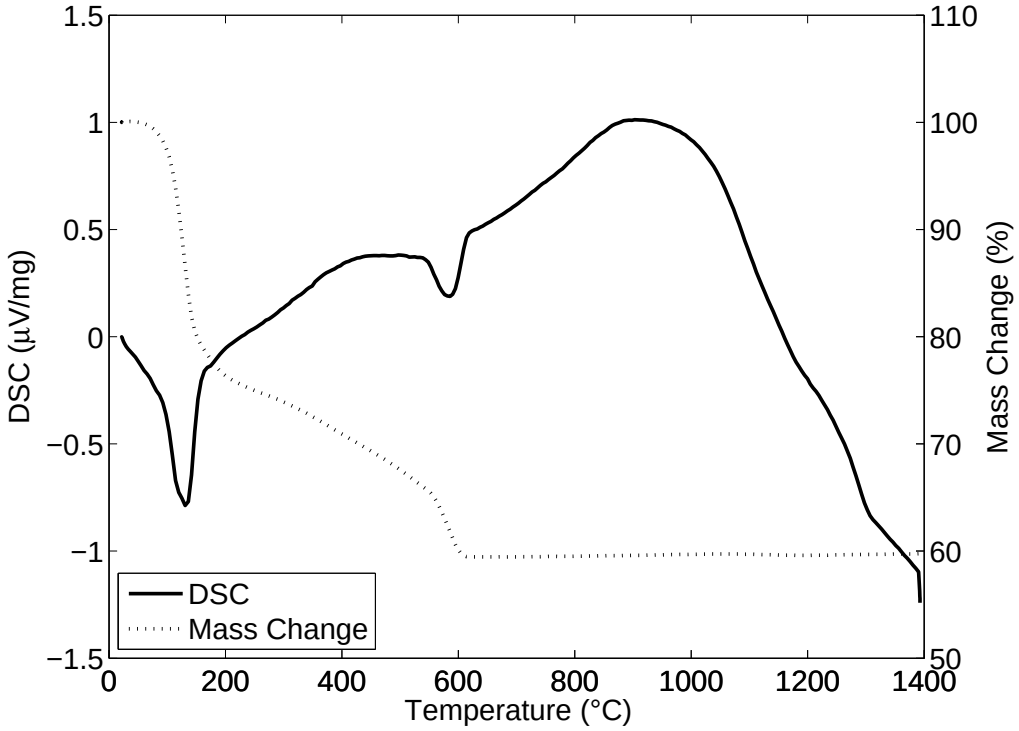

Fig. 5.7. 22 mass percent waste loaded bentonite combined differential scanning calorimetry and thermal gravometry plot

The second mass loss step, with a gentler slope becomes evident once the interparticle water is exhausted. This mass loss is due to adsorbed water and interlayer water. The heat flux is exothermic during this process, seen as a upward trend from 150–200°C concluding at 400–500°C with a plateau (Figures 5.6, 5.7). The interlayer water is held much more tightly than the interparticle water due to cations that also occupy spaces between the clay layers. The cations and the water create partial bonds amongst themselves and with the oxygen attached to the silica tetrahedrals. As the heating continues the mass loss rate transitions to another rapid decline. This final dehydration step is due to dehydroxylation water losses which set in ~500°C in the clay loaded with waste ions, the mass loss concludes ~600°C (Figures 5.6, 5.7) which differs from the pure bentonite at 700°C (Figure 5.5). Onal [93] and Grim [94]

found dehydroxylation mass loss concluded ~800°C. Balek observed when bentonite was saturated with different cations dehydroxylation concluded at 700°C [95].

The heat flux which was flat during the interparticle water drying, becomes sharply endothermic during dehydroxylation reaching an inflection at ~575°C (Figures 5.7, 5.6). The dehydroxylation water release in bentonite clay requires the highest temperature. This is due to hydroxyl groups being molecularly bound within the clay structure. When hydroxylation occurs the lattice of the clay becomes porous and amorphous. This structural damage concludes from 600 to 650°C. Each of these stages is visible in the 16 and 22 mass percent waste loaded bentonite (Figures 5.6, 5.7) as well as the pure bentonite (Figure 5.5). The heat flux returns to an increasing exothermic trend peaking at ~900°C, then becoming endothermic. This endotherm continues until pure bentonite and 50% loadings bloat (Figures 5.5, 5.6), at 1000 and 1200°C respectively. Higher loading ceramics eventually melt at >1300°C. This is known from a glass-like coating on the bottom of the DSC-TGA crucibles.

The onset temperatures for each of mass loss steps are consistent across the samples (Figure 5.8). The first dehydration step is dependent on the amount of initial water in sample which can vary substantially from sample to sample, the ion saturated bentonite is very hygroscopic. All samples lost water continuously until the completion of dehydroxylation step. During this dehydroxylation phase, ~600°C, is also where nitrates are exhausted as reported by Kaminski *et al* [2].

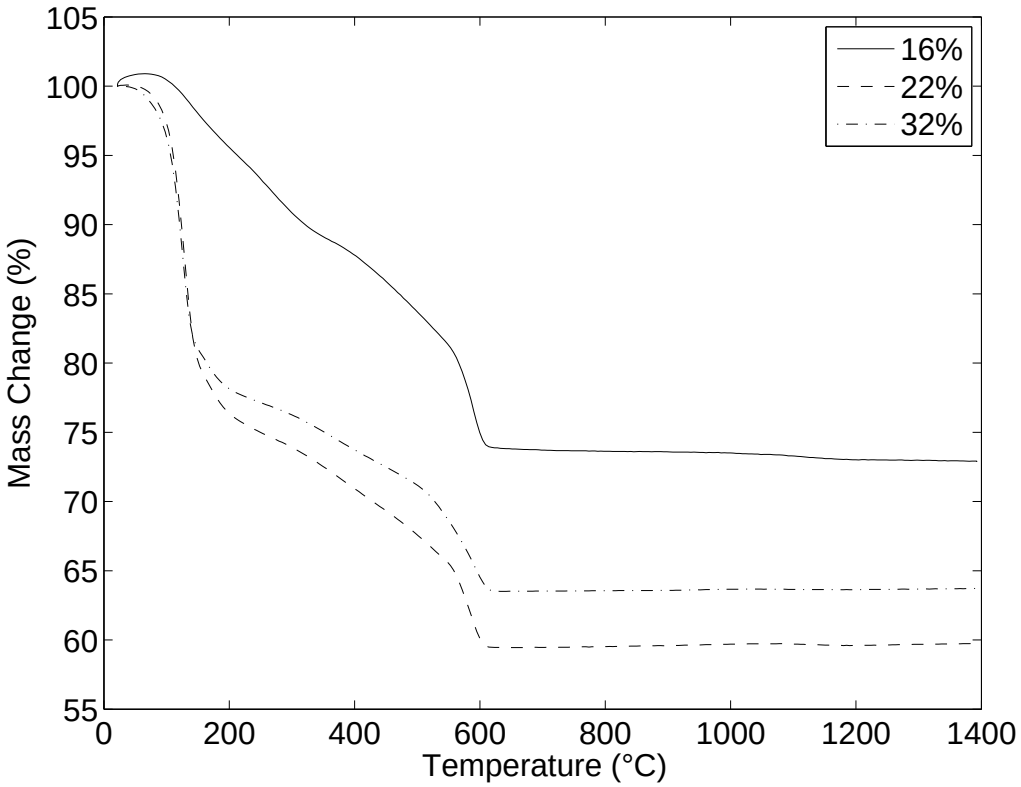

Fig. 5.8. Mass changes upon heating of bentonite clay at various concentrations of waste.

5.3 Light Flash Analysis

Samples sintered at 700°C had the lowest thermal diffusivities that do not exceed 0.24 mm^2/s, with the higher loading slightly higher than the lower 70% waste loading. The specific heat was higher for the lower loading with a maximum at 1.06 J/g·K at 300 K (Figure 5.9). The 700°C 100% loaded bentonite specific heat falls between that of pollucite and Sr-feldspar, but the lower loading exceeds that of both minerals at temperatures >125°C.

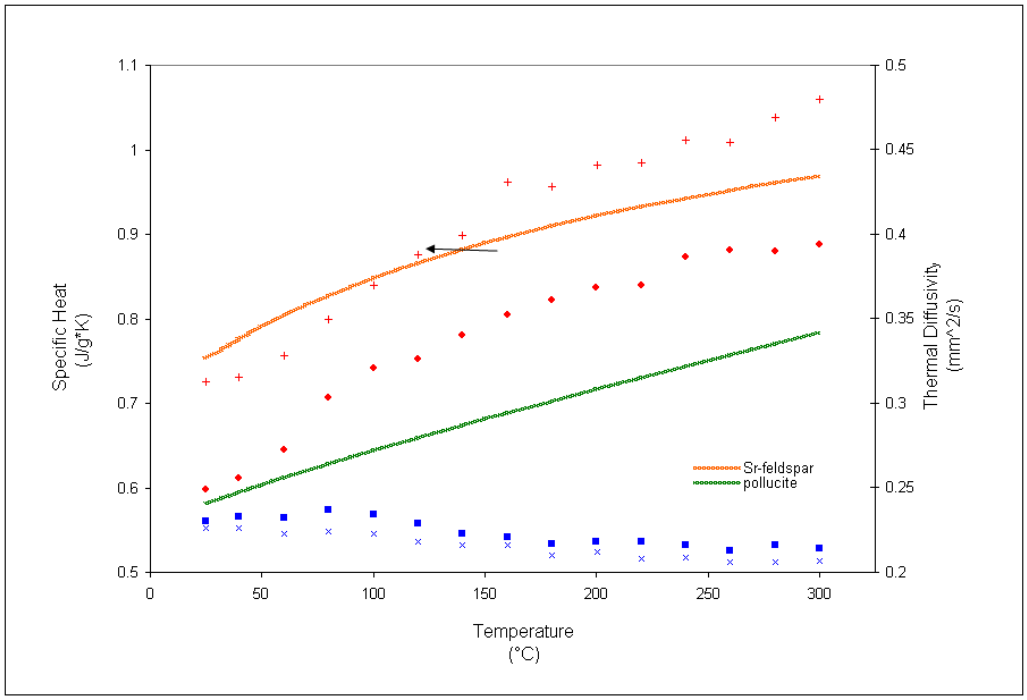

Fig. 5.9. Sintered bentonite, 700 °C where × refers to thermal diffusivity of 70% loaded bentonite; and ▪ refers to the thermal diffusivity of 100% loaded bentonite; + refers to the specific heat of 70% loaded bentonite; • refers to the specific heat of 100% loaded bentonite; green line is the specific heat of pollucite *Ogorodova, 2003*; and the orange line is the specific heat of Sr-feldspar *Chernyshova, 1991.*

At 800°C sinterings the thermal diffusivities continued to increase from 0.33 at to 0.38 from room temperature to 300°C also with higher thermal diffusivities for higher loadings. Specific heat on the other hand was higher for the lower waste loading reaching a maximum at 0.99 J/g·K at 300°C. The higher loading's specific heat coincides with that of pollucite at temperatures >125°C, the lower 70% loading specific heat was closer to that of Sr-felspar at temperatures >200°C (Figure 5.10).

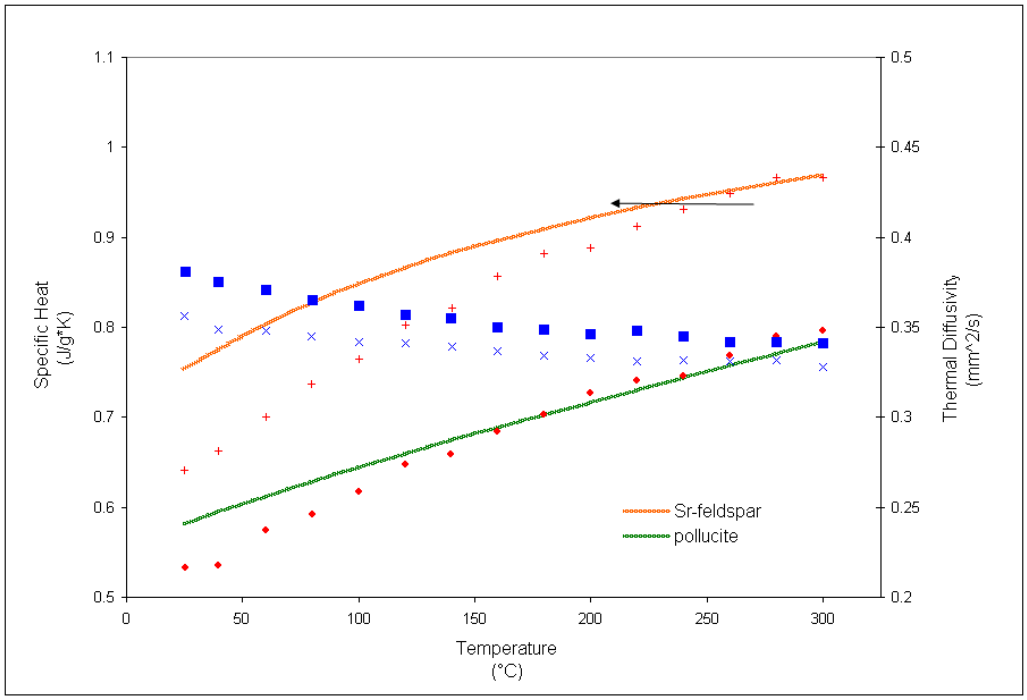

Fig. 5.10. Sintered bentonite, 800 °C where × refers to thermal diffusivity of 70% loaded bentonite; and ▪ refers to the thermal diffusivity of 100% loaded bentonite; + refers to the specific heat of 70% loaded bentonite; • refers to the specific heat of 100% loaded bentonite; green line is the specific heat of pollucite *Ogorodova, 2003*; and the orange line is the specific heat of Sr-feldspar *Chernyshova, 1991.*

At 1000°C sinterings the thermal diffusivity increased to a maximum of 0.50 mm^2/s at room temperature for the 70% theoretical maximum waste loading. For this case the lower loading had a higher thermal diffusivity than the higher loading. Specific heat was higher for the lower loading but the difference was relatively small with 0.83 J/g·K for a 70 % loading and 0.77 J/g·K at the 90% loading, both values coincide well with the specific heat of Sr-feldspar (Figure 5.11). The specific heat of the loaded bentonite was higher for samples with lower waste concentrations at each temperature tested (Figures 5.9, 5.10, and 5.11). Overall thermal diffusivity increased with sintering temperature. As thermal diffusivity increases, the ceramic can

change temperature more quickly, thus improving thermal conductivity. Sintering at 700 and 800°C higher waste loading resulted in higher thermal diffusivities (Figures 5.9 and 5.10). Sintering at 1000°C the thermal diffusivity for the lower loading was higher than the theoretical maximum loading (Figure 5.11).

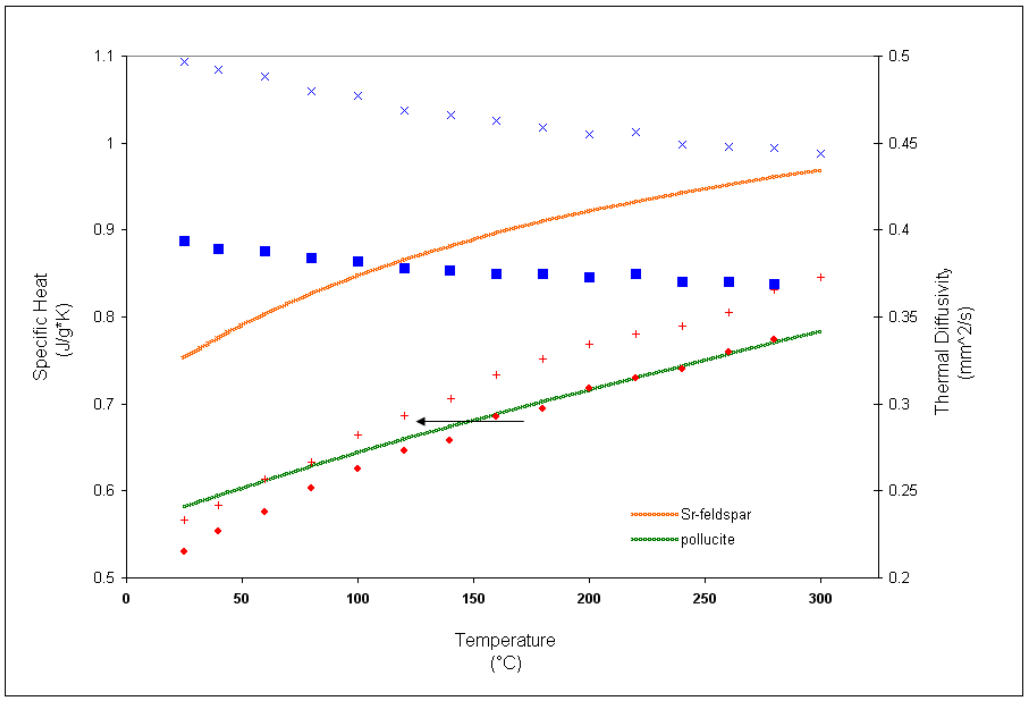

Fig. 5.11. Sintered bentonite, 1000 °C where × refers to thermal diffusivity of 70% loaded bentonite; and ▪ refers to the thermal diffusivity of 100% loaded bentonite; + refers to the specific heat of 70% loaded bentonite; • refers to the specific heat of 100% loaded bentonite; green line is the specific heat of pollucite *Ogorodova, 2003*; and the orange line is the specific heat of Sr-feldspar *Chernyshova, 1991.*

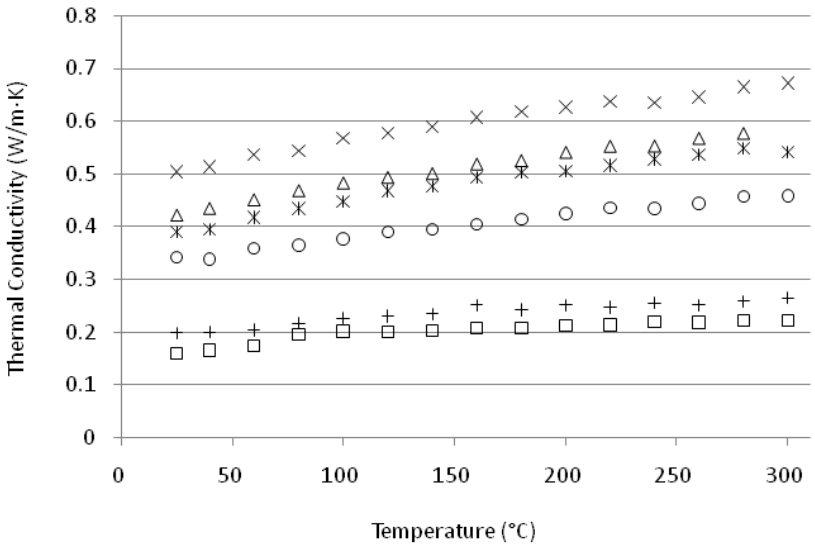

Fig. 5.12. Thermal conductivity of sintered bentonite where + refers to 70% loaded bentonite sintered at 700°C; □ refers to 100% loaded bentonite also sintered at 700 °C; ∗ refers to 70% loaded bentonite sintered at 800°C; ∘ refers to 100% loaded bentonite sintered at 800°C; × refers to 70% loaded bentonite sintered at 1000°C; and ▽ refers to 100% loaded bentonite sintered at 1000°C. Measured in air.

Thermal conductivity was calculated from the bulk density (Figure 5.1), thermal diffusivity, and specific heat (measured in air). The higher sintering temperatures resulted in higher thermal conductivities and the lower waste loadings had higher thermal conductivities at each sintering temperature. The highest thermal conductivity was for 70% theoretical maximum loaded bentonite, or 26 mass percent waste ions sintered at 1000°C at 0.68 W/m·K at 275°C (Figure 5.12).

When compared to porosity data, the lower thermal conductivities for the higher loadings coincide with the higher porosity in these samples.

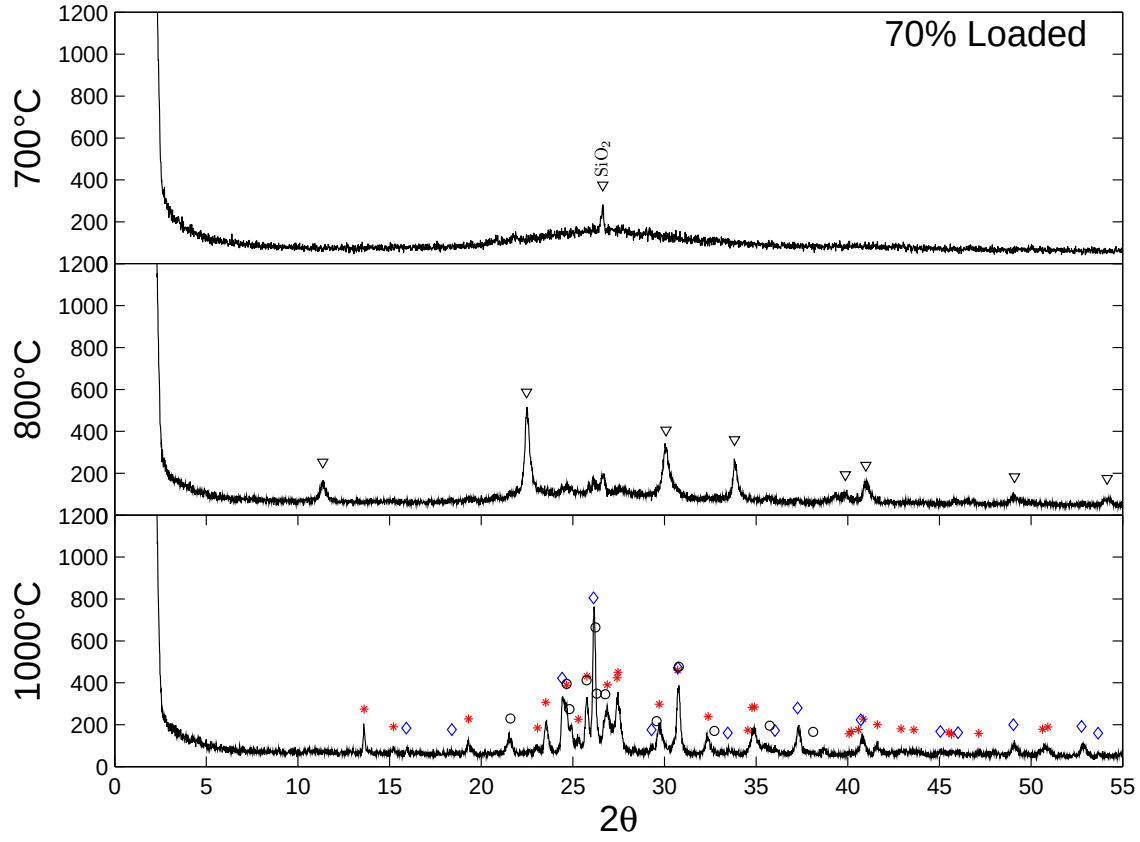

Fig. 5.13. XRD of 70% theoretical waste loaded bentonite. Where ▽ barium aluminum silicate $Ba(Al_2Si_2Si_2O_8)$ PDF 1-088-1048; ◊ refers to cesium aluminum silicate (pollucite) $CsAlSiO_4$ PDF 47-0471; ⋆ refers to barium strontium aluminum silicate $Ba_{0.5}Sr_{0.5}Al_2Si_2O_8$ PDF 38-1452; ∘ cesium aluminum silicate $Cs_4Al_4Si_{20}O_{48}$ PDF 41-0569.

Bentonite clay loaded with ions to 70% of the theoretical maximum, approximately 25 mass percent waste, sintered at 700 °C displayed an amorphous hump, and a low intensity peak due to quartz which is present in bentonite as an impurity (top of Figure 5.13). The quartz peak at 26.6 2θ (Figure A.11) remains as crystals

up to 10μm unitl 1000°C sinterings (Figures 5.27, 5.28). ty XRD peak is visible up to 800°C (5.13, 5.14).

As the sintering temperature was increased to 800 °C a barium aluminosilicate structure appears, $Ba(Al_2Si_2Si_2O_8)$. At the 1000 °C three phases become apparent; cesium aluminum silicate (pollucite) $CsAlSiO_4$, a 50:50 barium strontium aluminum silicate $Ba_{0.5}Sr_{0.5}Al_2Si_2O_8$, and a high silica content cesium aluminum silicate $Cs_4Al_4Si_{20}O_{48}$.

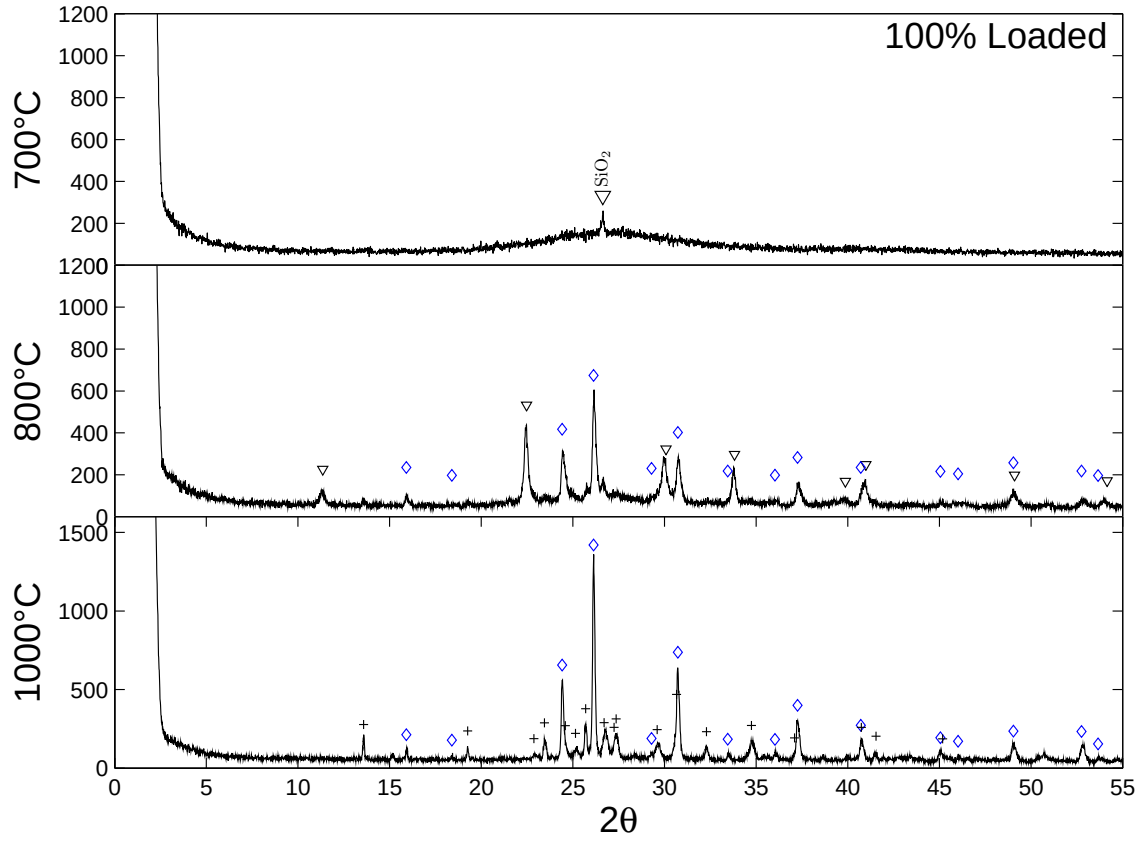

Fig. 5.14. XRD of 100% theoretical waste loaded bentonite. Where ▽ barium aluminum silicate $Ba(Al_2Si_2O_8)$ PDF 1-088-1048; ◊ refers to cesium aluminum silicate (pollucite) $CsAlSiO_4$ PDF 47-0471; + refers to barium strontium aluminum silicate $Ba_{.75}Sr_{.25}Al_2Si_2O_8$ PDF 38-1451.

At approximately 32 mass percent waste ions, or 100% loaded bentonite the 700°C sintering resulted in the a very similar situation observed with the lower loading, only a quartz peak and a amorphous hump was visible in the XRD scan. Sintering at 800°C also displays the same barium alumino silicate as before $Ba(Al_2Si_2O_8)$, but also pollucite appears, cesium aluminum silicate $CsAlSiO_4$. At 1000°C we see two phases. These are pollucite $CsAlSiO_4$ and a 75:25 barium strontium aluminosilicate $Ba_{.75}Sr_{.25}Al_2Si_2O_8$ (Figure 5.14).

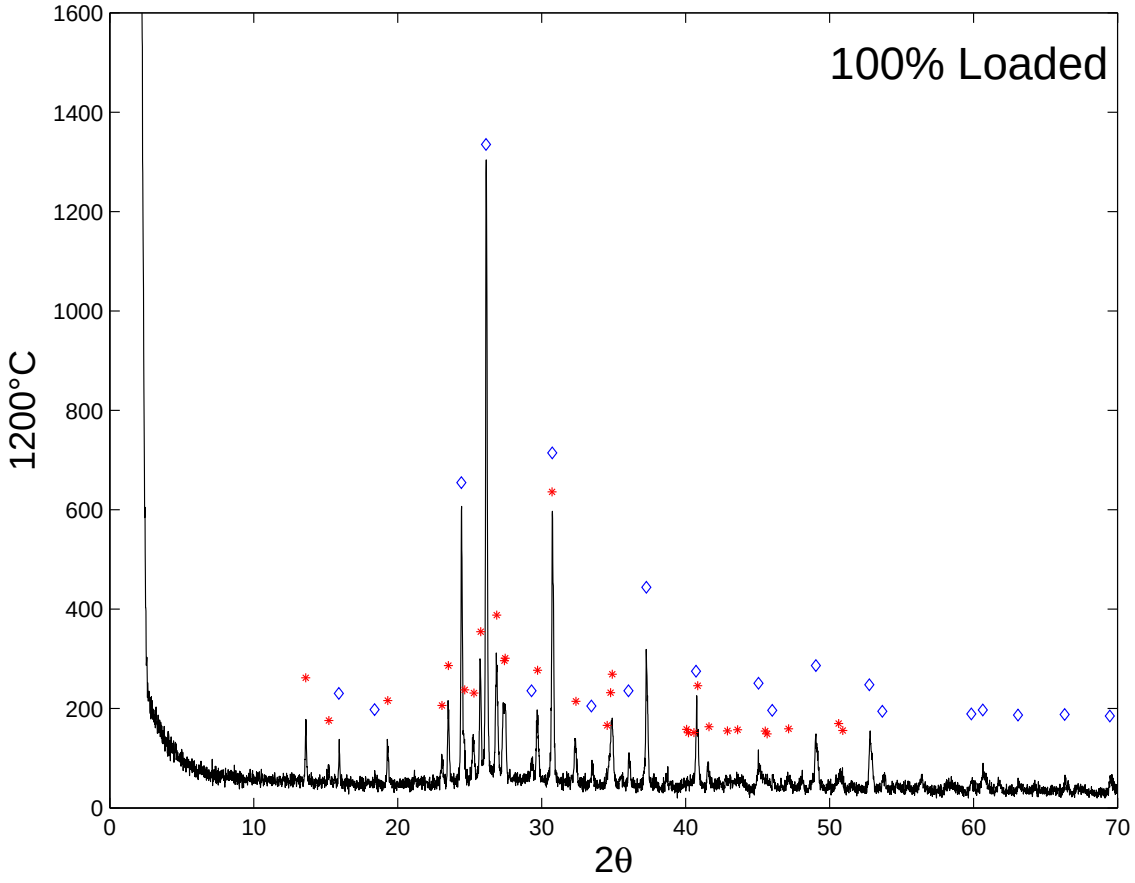

Fig. 5.15. XRD of 100% theoretical waste loaded bentonite sintered at 1200°C. Where ◊ refers to cesium aluminum silicate (pollucite) $CsAlSiO_4$ PDF 47-0471; ⋆ refers to barium strontium aluminum silicate $Ba_{0.5}Sr_{0.5}Al_2Si_2O_8$ PDF 38-1452.

Sintering the maximum loading at 1200 °C resulted in two apparent phases. The pollucite is still prominent and displays very sharp high peaks, the other is the 50:50 barium aluminosilicate Figure 5.15.

5.5 Scanning Electron Microscopy and Wave Dispersive Spectroscopy

Samples sintered at 700, 800, 1000, 1100, and 1200 °C were analyzed and elemental maps were produced. In addition to the elemental maps backscattered electron images of the selected areas were also created to reference the location and topography of the mapped areas. The elemental map images are gray scale where lighter areas refer to higher concentrations of a particular element. The concentrations are not transferable from image to image or element to element. The overall concentration of each component was determined with neutron activation analysis, and most images are only qualitative. Quantitative analysis was reserved for the sample sintered 1200°C. The relative intensity of the signal is only relevant within each individual image. For clarity contrast and brightness may have been modified. Bright white areas are only a local high concentrations and should not be considered absolute maximums, or that no other elements are present. The location of each of the mappings was chosen primarily for its lack of porosity, to focus on the mineral phases present, flat areas were chosen over cracks and voids.

The lowest sintering temperature of 700°C produced a very course texture. Strontium in the higher loading appears to be concentrated in small areas, and the cesium in the lower loading is concentrated in some regions more than others. But overall the four elements Cs, Sr, Ba, and Rb are distributed homogeneously (Figures 5.16, 5.17). The central dark region in the lower loading (70 % theoretical) is void of the four elements in this figure is probably quartz that has not dissolved during sintering. The region has a high silicon concentration (Appendix D).

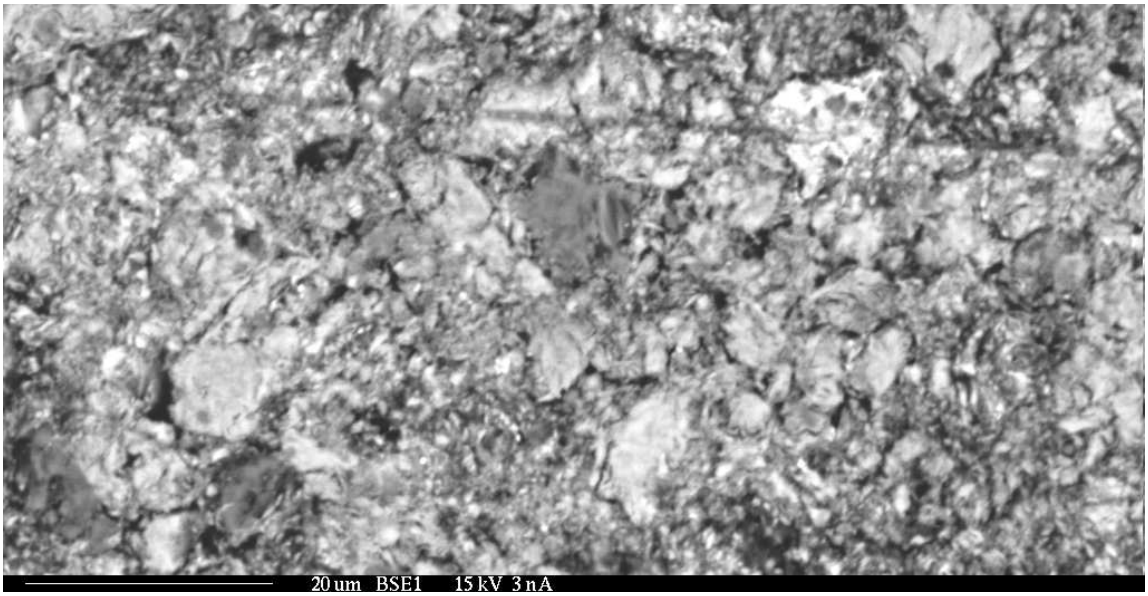

(a) Backscattered image at 1000X of 700 °C sintered bentonite 25% waste metals

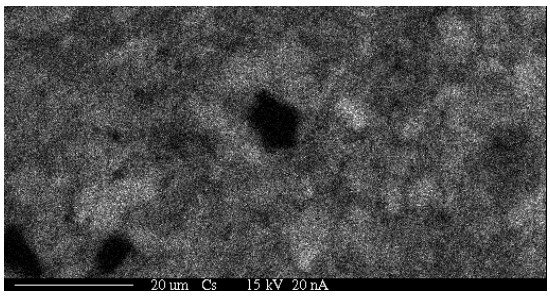

(b) Cs relative concentration

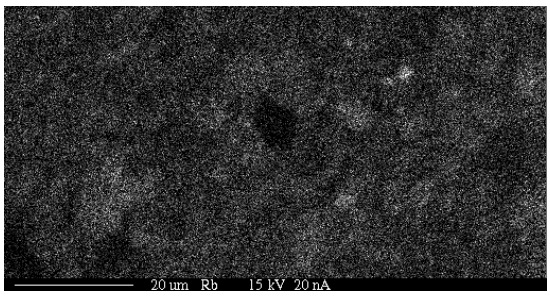

(c) Rb relative concentration

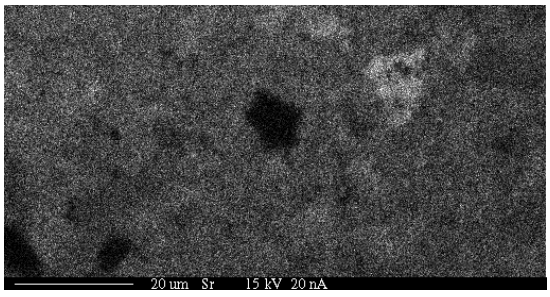

(d) Sr relative concentration

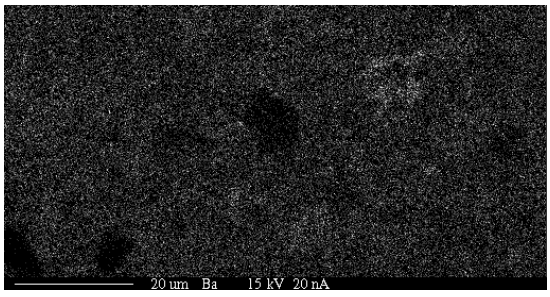

(e) Ba relative concentration

Fig. 5.16. 700 °C sintered bentonite, 25 mass pct. waste ions; backscattered image (top) and element maps where light areas refer to higher concentration (bottom).

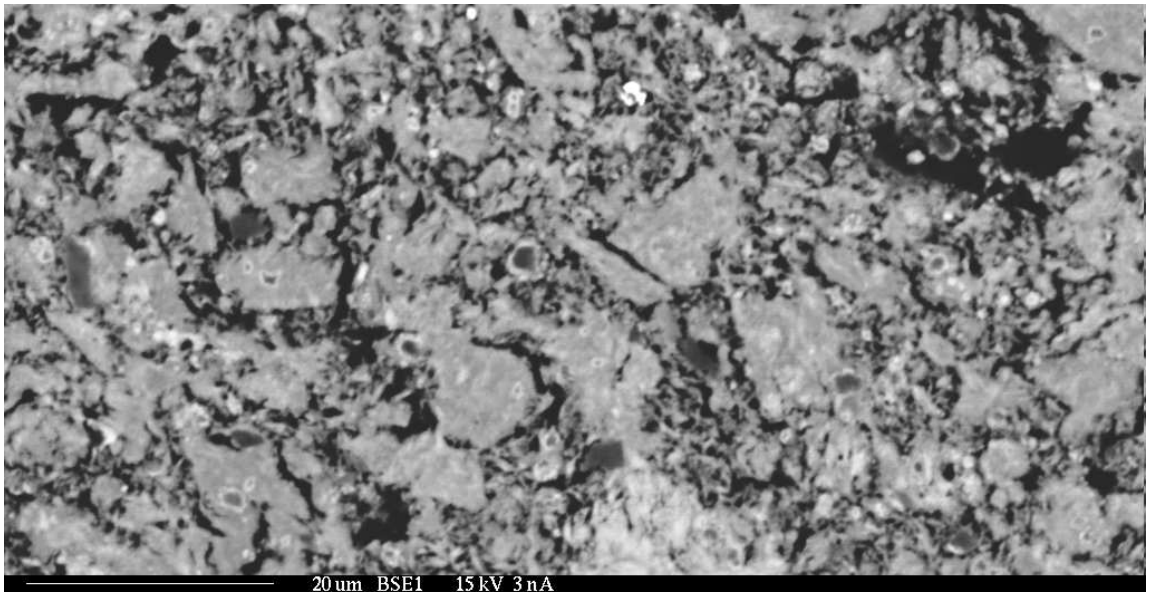

(a) Backscattered image at 1000X of 700 °C sintered bentonite 32% waste metals

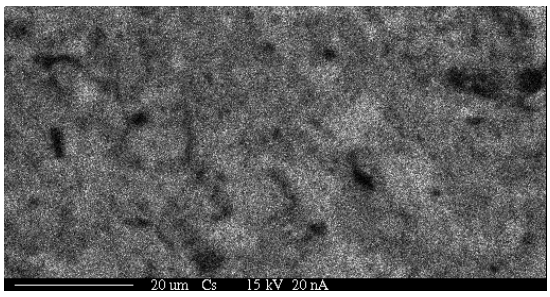

(b) Cs relative concentration

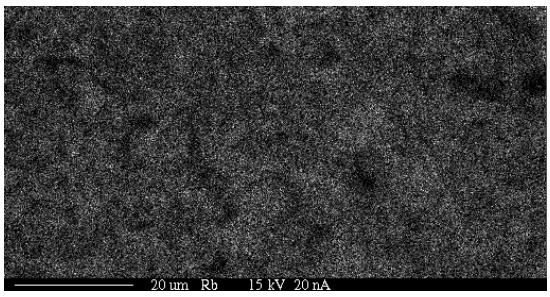

(c) Rb relative concentration

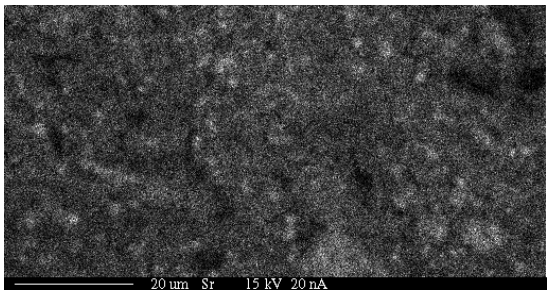

(d) Sr relative concentration

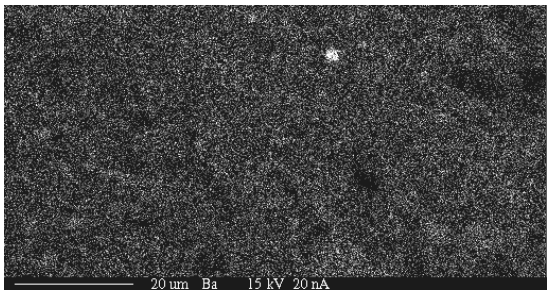

(e) Ba relative concentration

Fig. 5.17. 700 °C sintered bentonite, 32 mass pct. waste ions; backscattered image (top) and element maps where light areas refer to higher concentration (bottom).

At 800°C sintering the surfaces are smoother, with larger continuous flat areas. The elements cesium and strontium have areas of high concentration similar to the 700°C sintering. Rubidium and barium in the higher waste loaded bentonite also display small regions of high concentration (Figures 5.18, 5.19).

In bentonite sintered at 1000 °C and loaded to 70% of the theoretical maximum (~26 mass percent) the waste ions are distributed in a similar manner to the 800°C sinterings, with areas of higher concentration (Figure 5.20). Bentonite loaded to 100% (~31 mass percent) at 1000°C displays a transition from lower temperature sinterings, and the 70% loading (Figure 5.21). Up to this point the surfaces have been rough and porous. In the backscattered image of the 1000°C 100%loading three distinct regions are visible, a very rough dark area, and a flat region with bright spots and a slightly darker grey area. Within the elemental maps a very clear segregation is evident. The cesium and strontium have become concentrated in much smaller areas within the sample, and the barium and rubidium also have become concentrated to separate regions in the sample. The cesium and rubidium are occuping the same areas, while the barium is in the opposing regions. The strontium has become very concentrated in isolated small spots. The silicon has become homogenously distributed, and no longer in small high concentration clumps (Appendix D).

The backscattered image of bentonite sintered at 1100°C shows are very large flat area with interdispersed dark holes. Within the flat area three different regions are visible. There is a grey matrix that encompasses two brighter phases, a very bright region and a light grey area. The elemental maps show that the bright area is high in cesium as well as rubidium. The grey area is rich in barium and strontium (Figure 5.22).

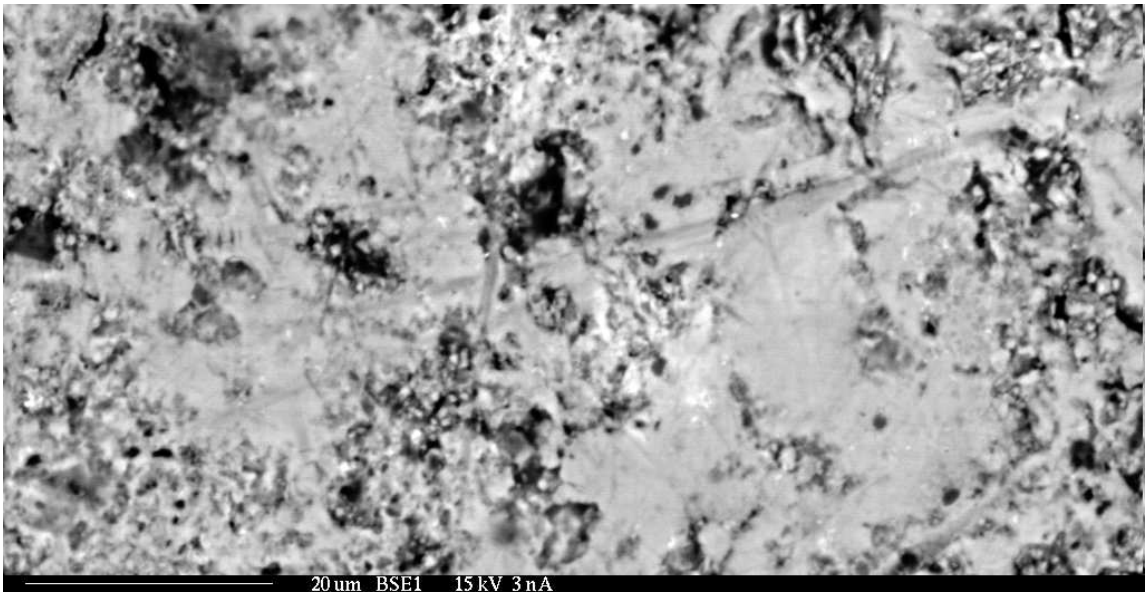

(a) Backscattered image at 1000X of 800 °C sintered bentonite 24% waste metals

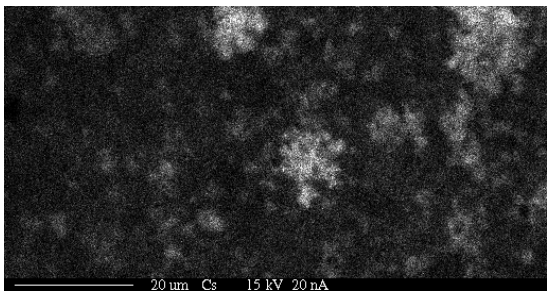

(b) Cs relative concentration

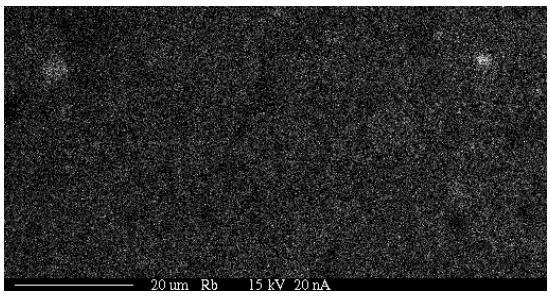

(c) Rb relative concentration

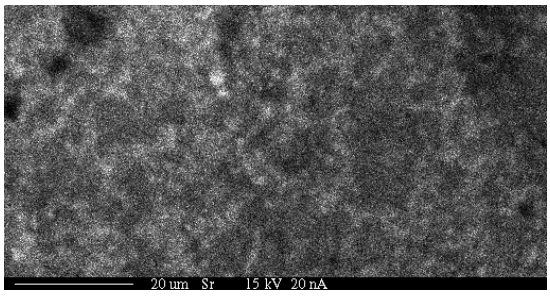

(d) Sr relative concentration

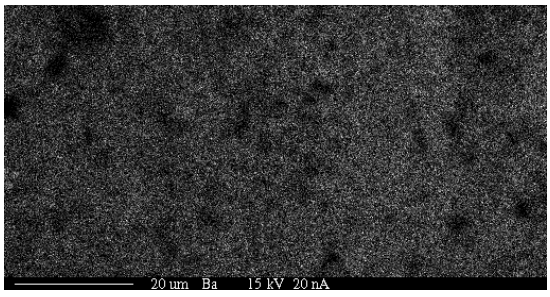

(e) Ba relative concentration

Fig. 5.18. 800 °C sintered bentonite, 24 mass pct. waste ions; backscattered image (top) and element maps where light areas refer to higher concentration (bottom).

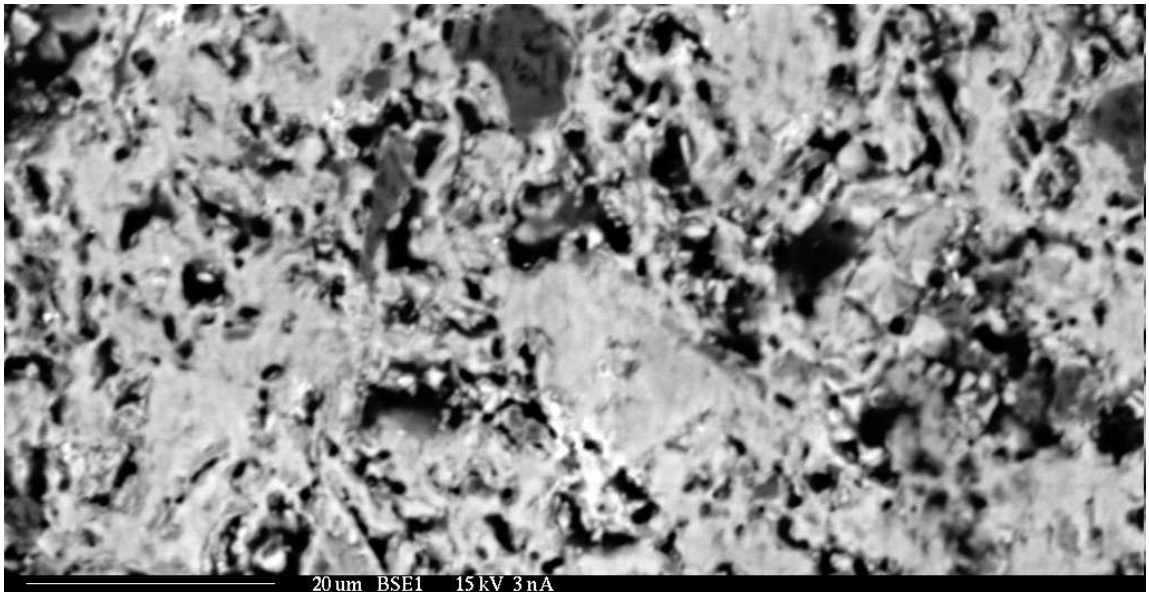

(a) Backscattered image at 1000X of 800 °C sintered bentonite 32% waste metals

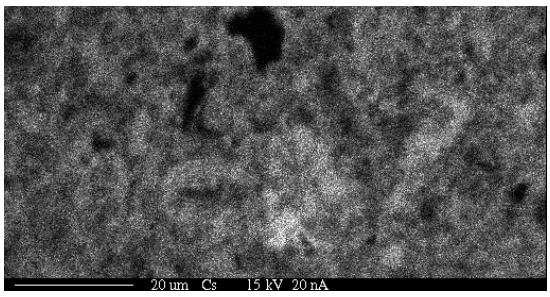

(b) Cs relative concentration

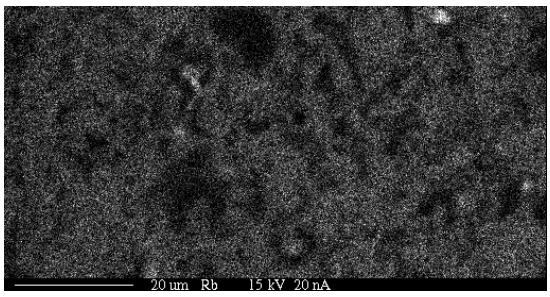

(c) Rb relative concentration

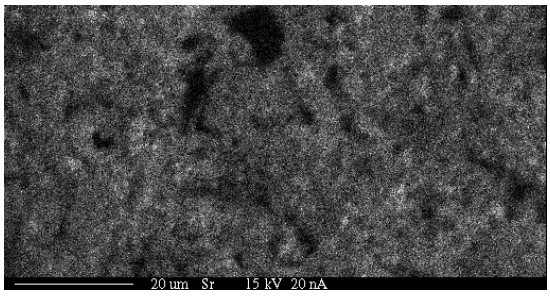

(d) Sr relative concentration

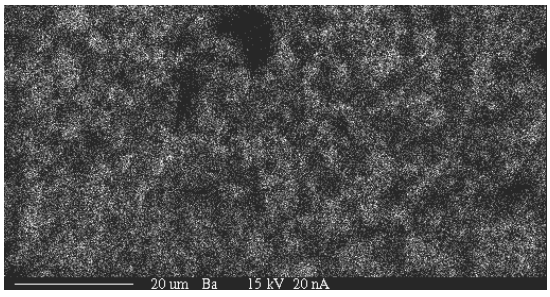

(e) Ba relative concentration

Fig. 5.19. 800 °C sintered bentonite, 32 mass pct. waste ions; backscattered image (top) and element maps where light areas refer to higher concentration (bottom).

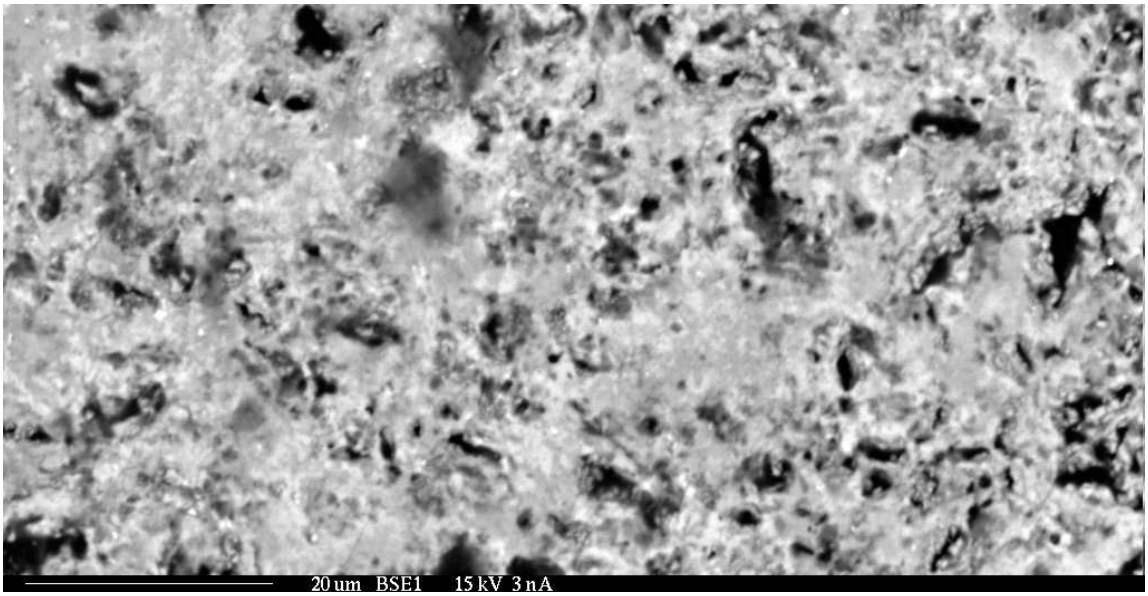

(a) Backscattered image at 1000X of 1000 °C sintered bentonite 26% waste metals

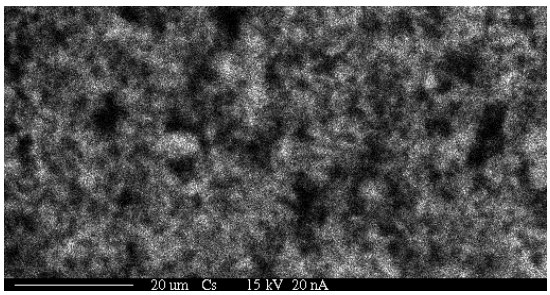

(b) Cs relative concentration

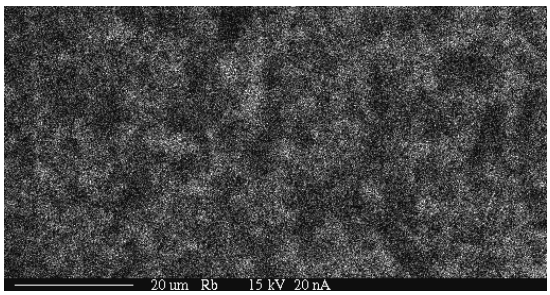

(c) Rb relative concentration

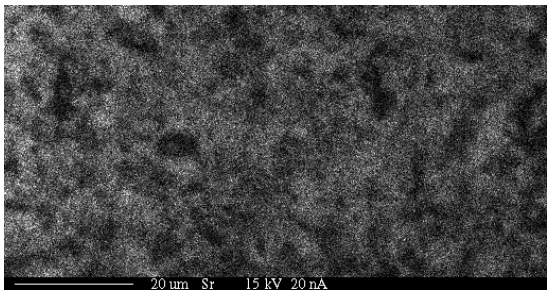

(d) Sr relative concentration

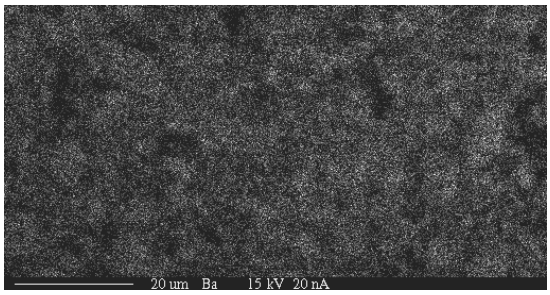

(e) Ba relative concentration

Fig. 5.20. 1000 °C sintered bentonite, 26 mass pct. waste ions; backscattered image (top) and element maps where light areas refer to higher concentration (bottom).

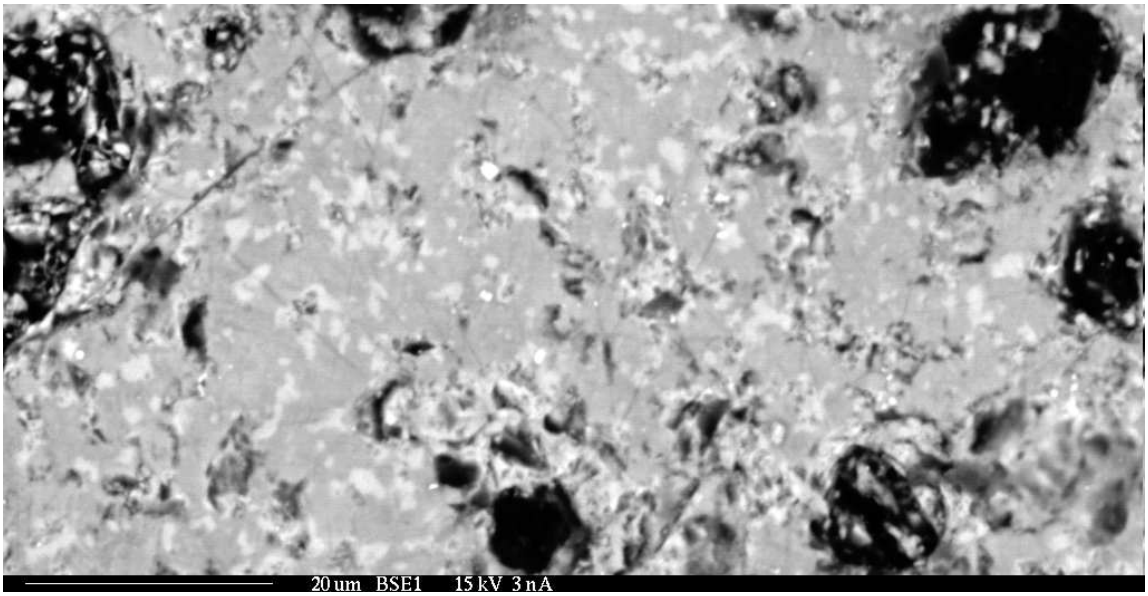

(a) Backscattered image at 1000X of 1000 °C sintered bentonite 31% waste metals

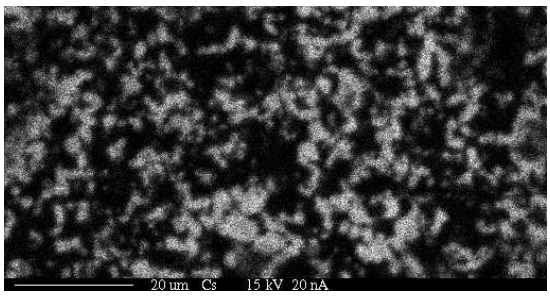

(b) Cs relative concentration

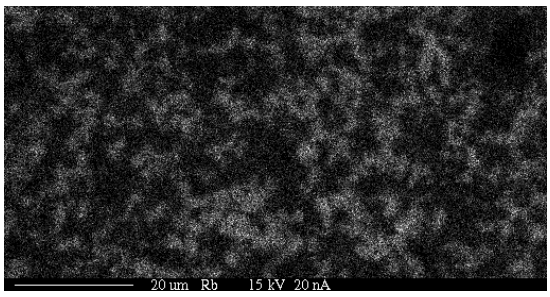

(c) Rb relative concentration

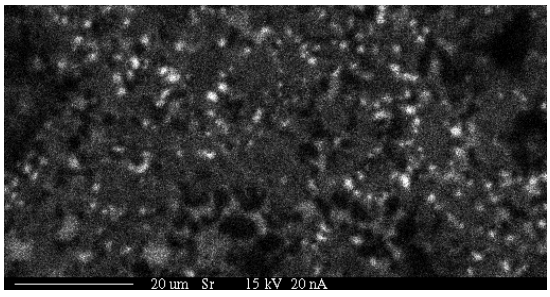

(d) Sr relative concentration

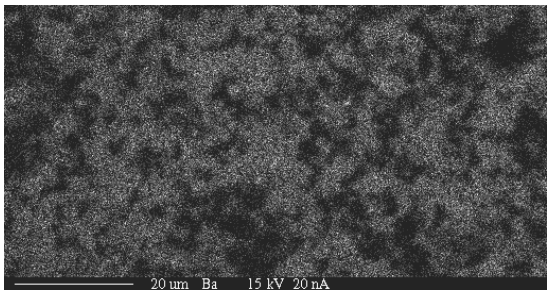

(e) Ba relative concentration

Fig. 5.21. 1000 °C sintered bentonite, 31 mass pct. waste ions; backscattered image (top) and element maps where light areas refer to higher concentration (bottom).

Sintering at 1200 °C resulted in a very drastic development visible in the backscattered image. Crystals are visible throughout the sample. Two distinct types of crystals easily noticeable, light areas (representative of larger atomic mass) with crystals of indeterminant structure, and long rectangular grey crystals. Both crystals are embedded in a dark phase. The rectangular crystals are indicative of celsian, or barium feldspar [96] appear in small groups of micrometer to submicrometer size, as well as crystals over 10 μm long but less than 1μm wide. The light crystals tend to be larger with width to length ratios much closer to unity (Figure 5.23). This sample was re-analyzed with spectroscopy focused on quantification in specific regions, and added a wider spectrum of elements.

At 1200°C the appearance of crystals motivated a quantitative analysis. The three regions visible were samples for analysis. In addition to the cesium, strontium, rubidium and barium, the elements aluminum, calcium, silicon, iron, magnesium, and sodium were included in the analysis.

The grey lath crystal phase had slightly higher levels of barium than the rest of sample, the dark region is higher in strontium (Figure 5.24). The needles have the highest levels of aluminum, and lower levels of silicon and calcium than the surrounding dark phase (Figure 5.25).

Elemental maps show a progressive segregation of the cesium and rubidium from the strontium and barium. As the sintering temperature is increased the back scattered image transitions from coarse nondescript texture to one with three distinct regions. Very little difference is visible between the samples until 1000°C where the 26 mass percent sample appears similar to the lower sintering temperatures, but at 31 mass percent waste ions the elemental segregation and phase definition starts to appear. This trend continues as the sintering temperatures were increased.

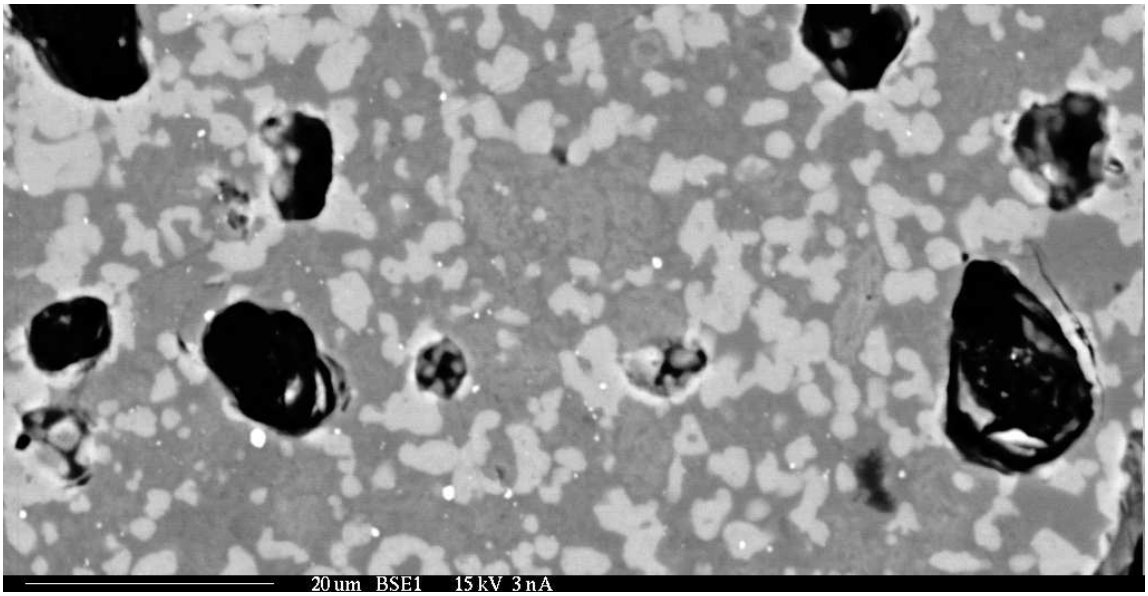

(a) Backscattered image at 1000X of 1100 °C sintered bentonite 30% waste metals

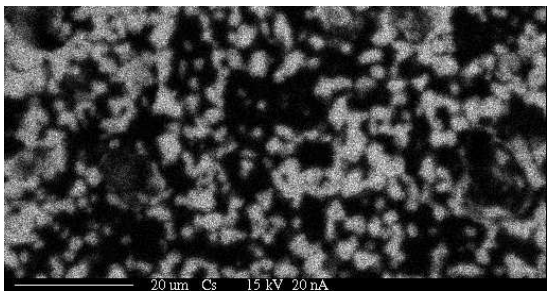

(b) Cs relative concentration

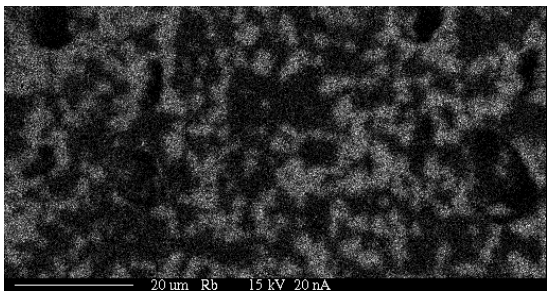

(c) Rb relative concentration

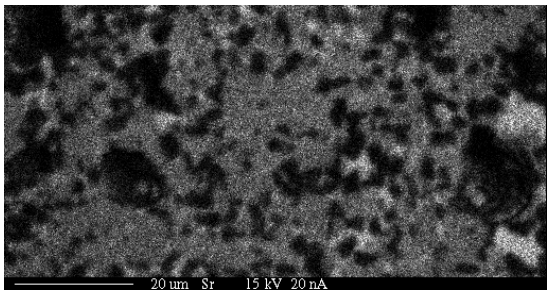

(d) Sr relative concentration

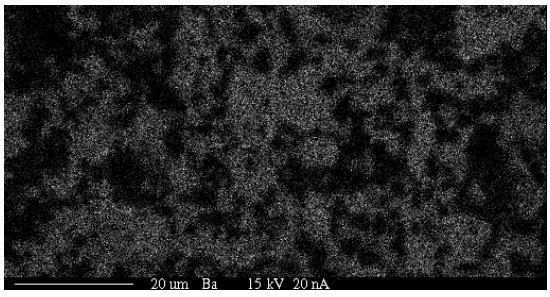

(e) Ba relative concentration

Fig. 5.22. 1100 °C sintered bentonite, 30 mass pct. waste ions; backscattered image (top) and element maps where light areas refer to higher concentration (bottom).

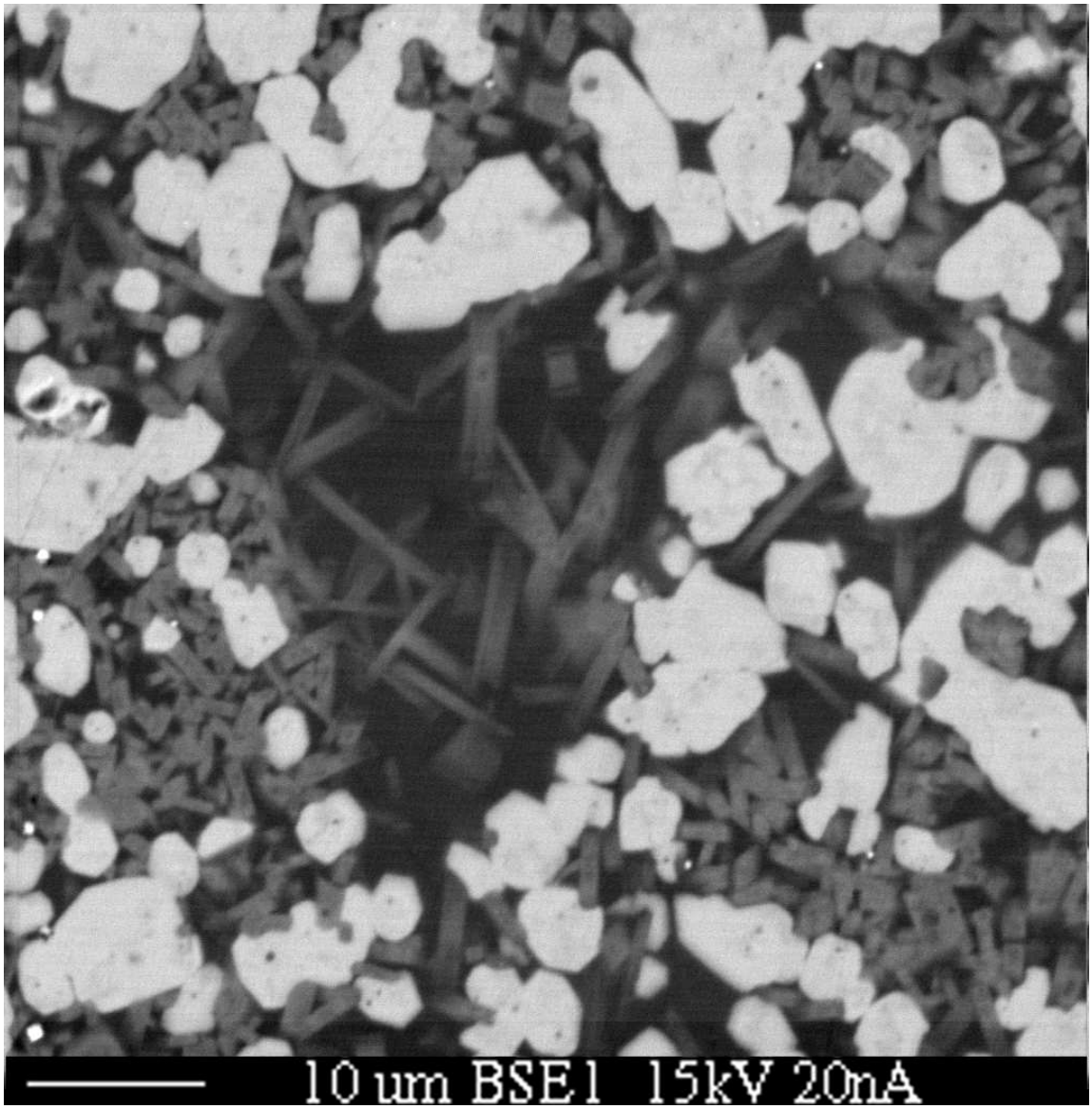

Fig. 5.23. BSE 1500X of 1200 °C sintered 100% loaded bentonite; needle shape crystals consistent with Barium/Strontium-alumino silicates celsian.

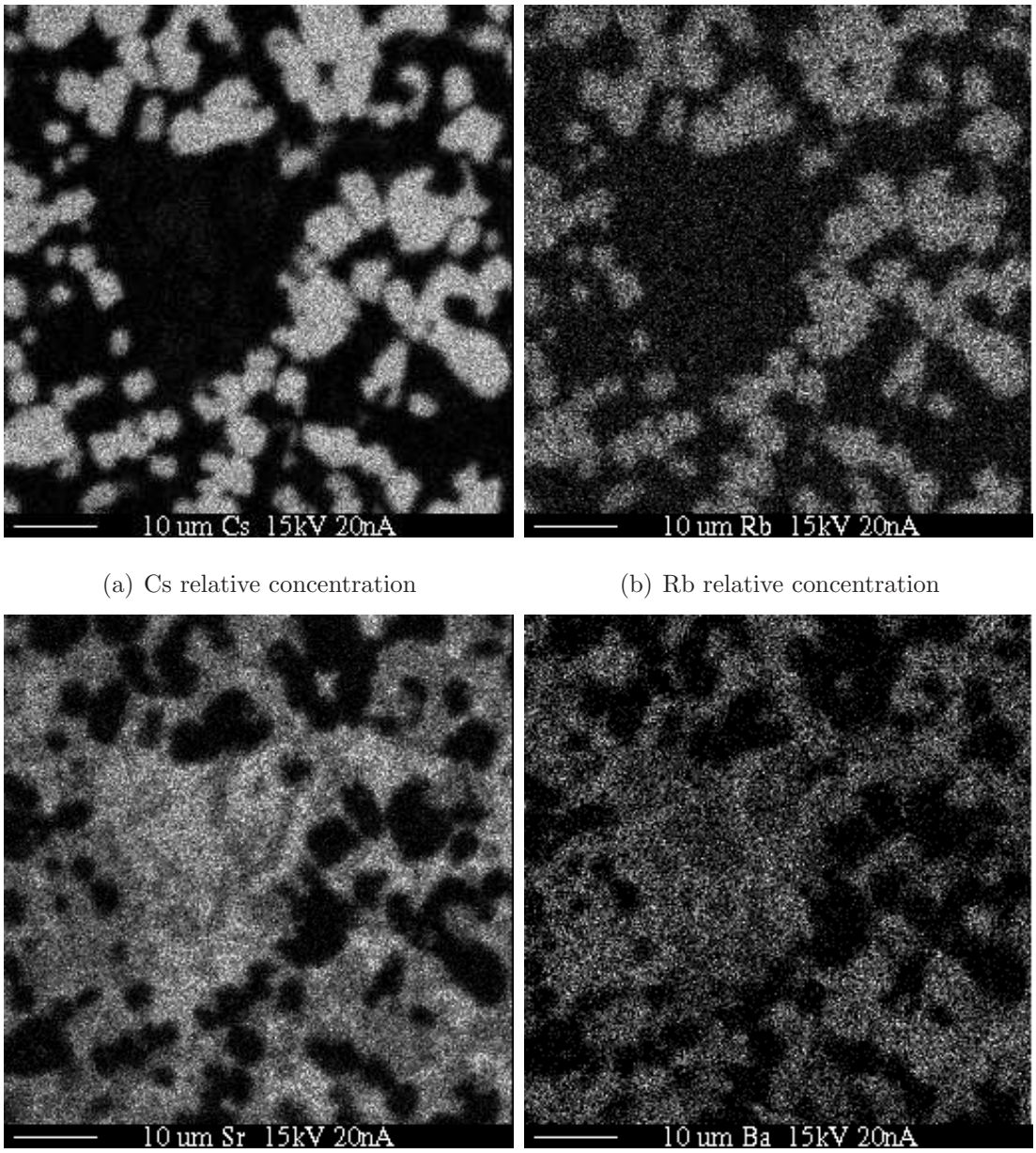

(a) Cs relative concentration

(b) Rb relative concentration

(c) Sr relative concentration

(d) Ba relative concentration

Fig. 5.24. 1200 °C sintered bentonite, 30 mass pct. waste ions; backscattered image (top) and element maps where light areas refer to high concentration (bottom).

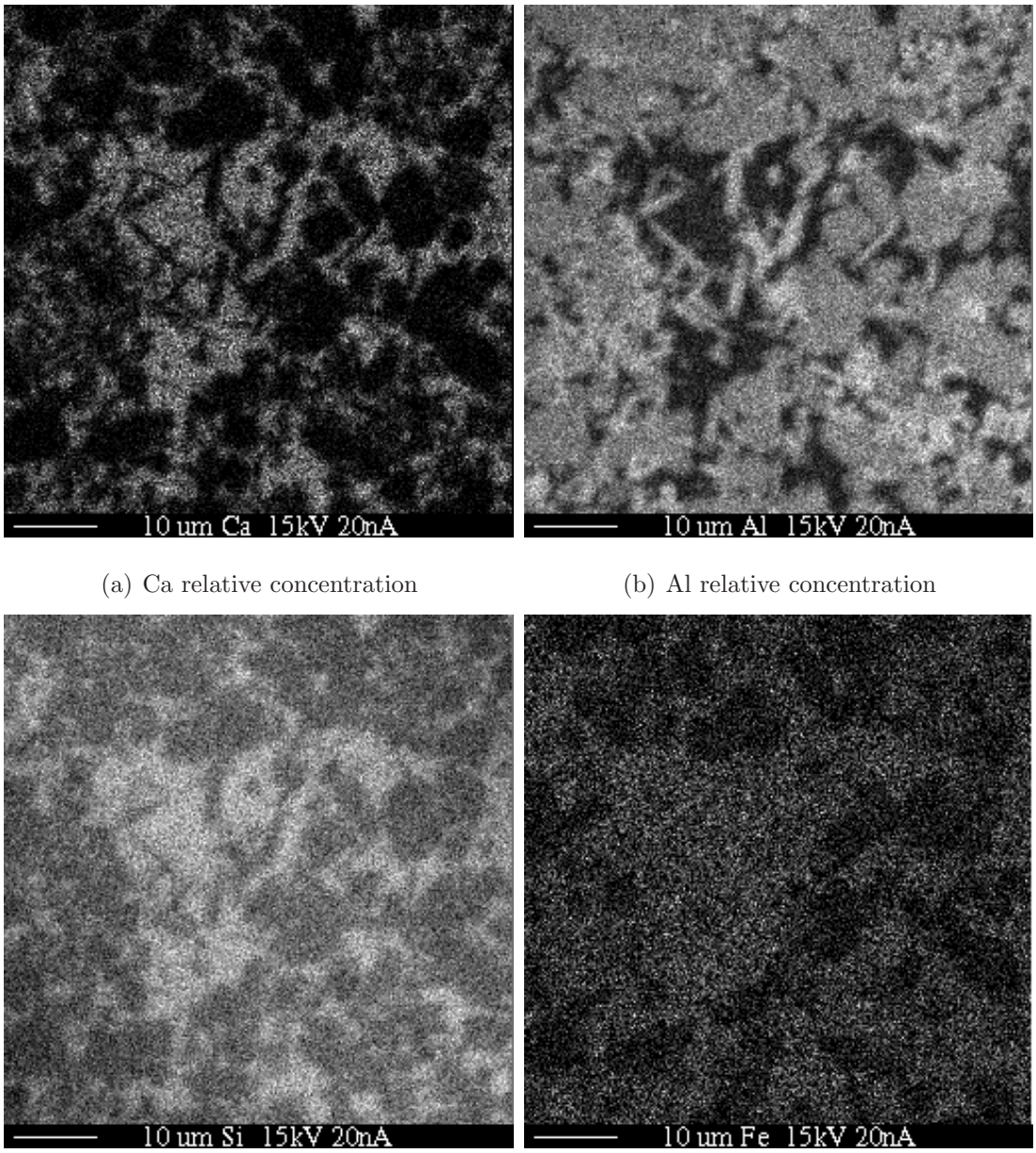

(a) Ca relative concentration

(b) Al relative concentration

(c) Si relative concentration

(d) Fe relative concentration

Fig. 5.25. 1200 °C sintered bentonite, 30 mass pct. waste ions; backscattered image (top) and element maps where light areas refer to high concentration (bottom).

The brightest areas have high cesium and rubidium concentrations, and low to undetectable levels of strontium and barium, low levels of iron, magnesium, and sodium, and moderate concentrations of aluminum and silicon. The dark regions hold barium, the highest levels of strontium, calcium, silicon, sodium, magnesium, and iron (Figures 5.24, 5.25). Points were selected for quantitative elemental analysis by x-ray counting (5.26). The results show that the needle shaped crystals are >4% barium, the highest barium concentration of all other areas. The bright areas are ~7.4% cesium and ~1.8% ruddidium, both higher than the other areas. The dark area has the highest concentration of strontium and silicon, at ~2.85% and ~22.3% percent respectively as well as the highest levels of calcium, iron, magnesium, and sodium (Table 5.3). Silicon maps have been isolated to highlight the dissolution of quartz grains >1000°C (Figures 5.27,5.28)

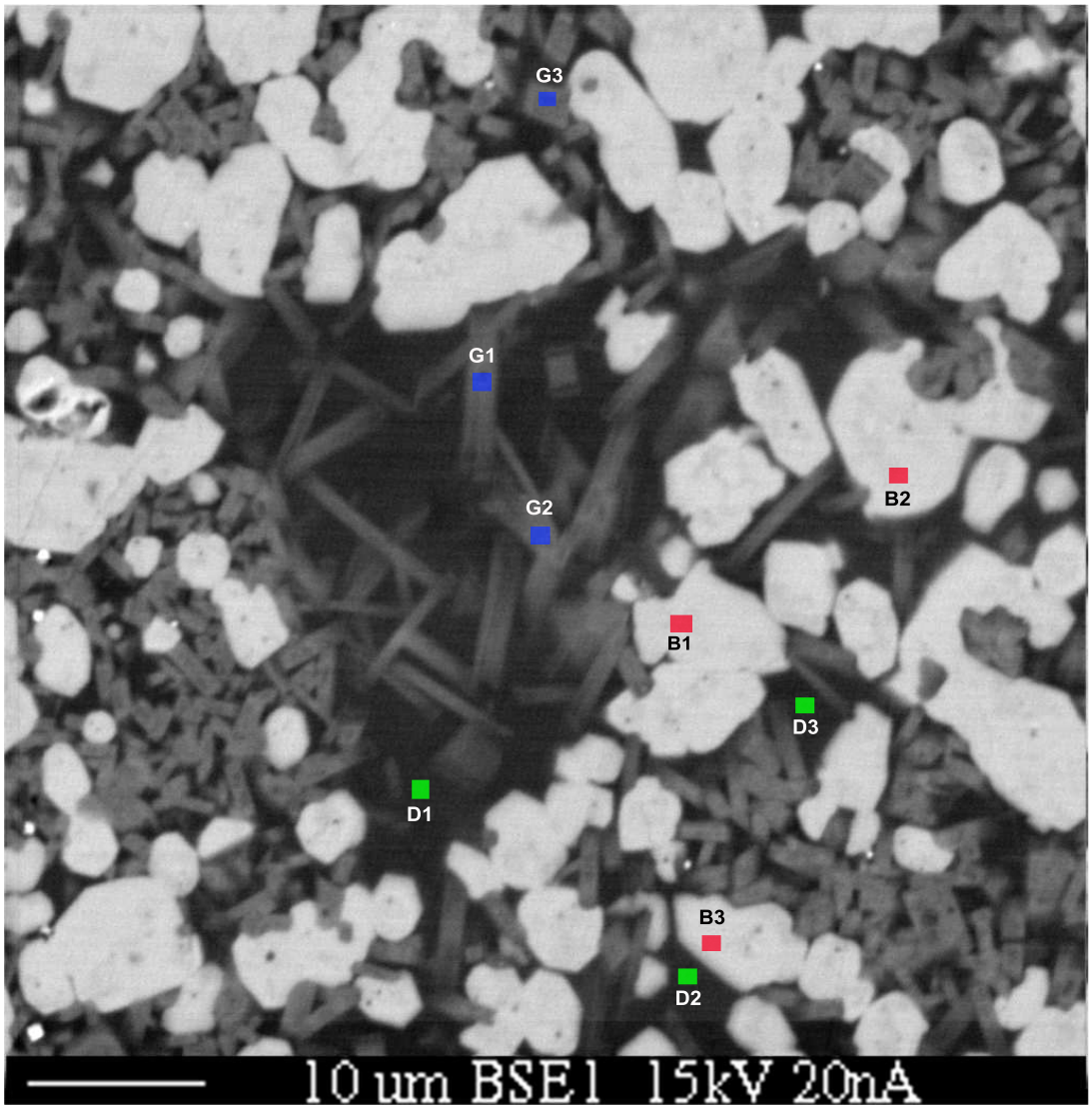

Fig. 5.26. Points selected for quantitative analysis in 1200 °C sintered bentonite. ■ bright areas; ■ gray areas; ■ dark areas.

Table 5.3
Elemental concentrations of selected points in 1200 °C sintered bentonite assuming simple oxides.

Location	Cs	Sr	Ba	Rb	Al	Ca	Si	Fe	Mg	Na	O	Total (atom %)
Dark 1	0.44	2.87	2.14	0.20	2.79	1.74	22.43	1.32	2.83	1.98	61.26	99.999
Dark 2	0.38	2.81	2.18	0.18	3.05	1.68	22.31	1.28	2.78	2.12	61.25	99.999
Dark 3	0.38	2.87	2.28	0.18	3.12	1.67	22.13	1.30	2.81	2.08	61.18	99.999
Bright 1	7.40	0.00	0.17	1.82	9.07	0.01	20.52	0.51	0.05	0.31	60.14	100.001
Bright 2	7.58	0.00	0.15	1.79	9.18	0.02	20.35	0.49	0.08	0.33	60.05	100
Bright 3	7.36	0.06	0.22	1.77	9.24	0.03	20.32	0.51	0.07	0.33	60.10	99.999
Grey 1	0.11	1.67	4.13	0.24	10.02	0.20	18.71	1.00	0.93	1.62	61.37	100.001
Grey 2	0.12	1.67	4.41	0.21	10.62	0.18	18.24	0.99	0.85	1.37	61.35	99.999
Grey 3	0.15	1.67	4.18	0.25	10.09	0.21	18.65	0.91	0.98	1.53	61.37	100

Detection limits and basis oxides in APPENDIX B.

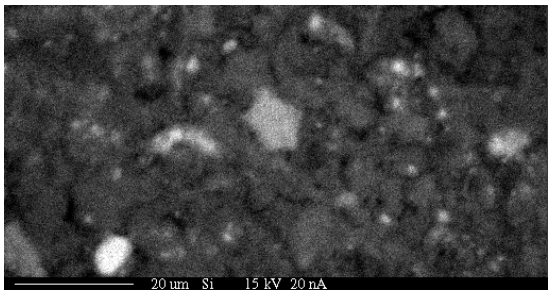

(a) Si concentration in 70% loaded bentonite 700°C

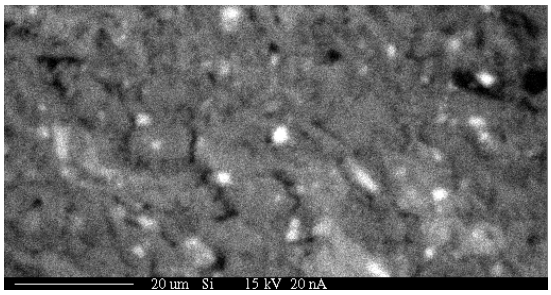

(b) Si concentration in 100% loaded bentonite 700°C

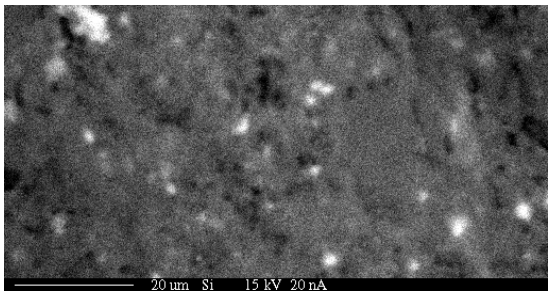

(c) Si concentration in 70% loaded bentonite 800°C

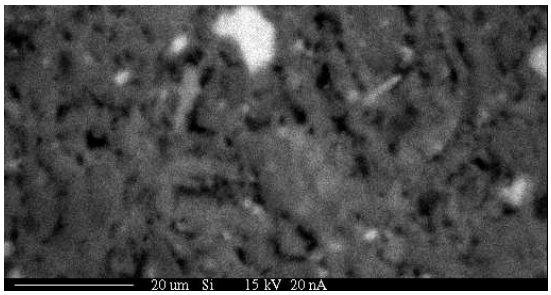

(d) Si concentration in 100% loaded bentonite 800°C

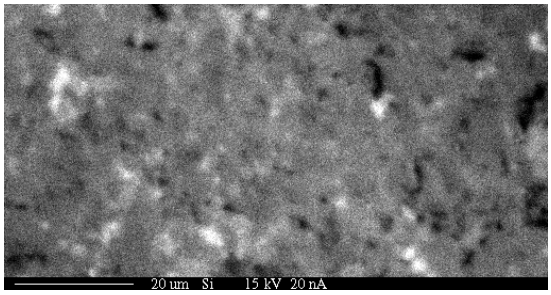

(e) Si concentration in 70% loaded bentonite 1000°C

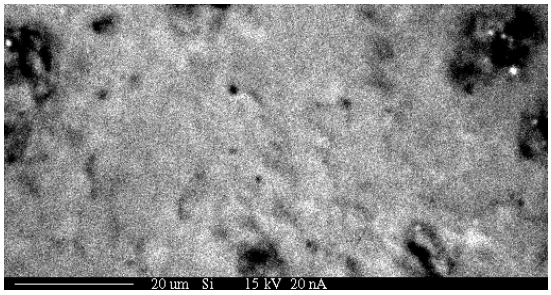

(f) Si concentration in 100% loaded bentonite 1000°C

Fig. 5.27. Silicon elemental maps across 700-1000°C sinterings at 70% and 100% loadings, where white refers to a local high concentration at 1000X.

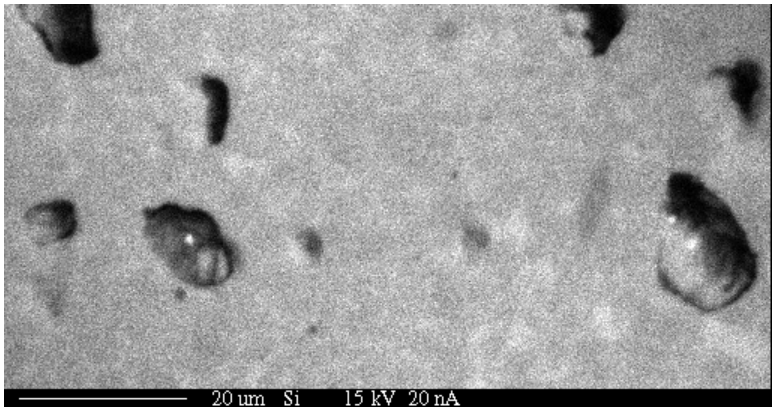

(a) Si concentration in 100% loaded bentonite 1100°C

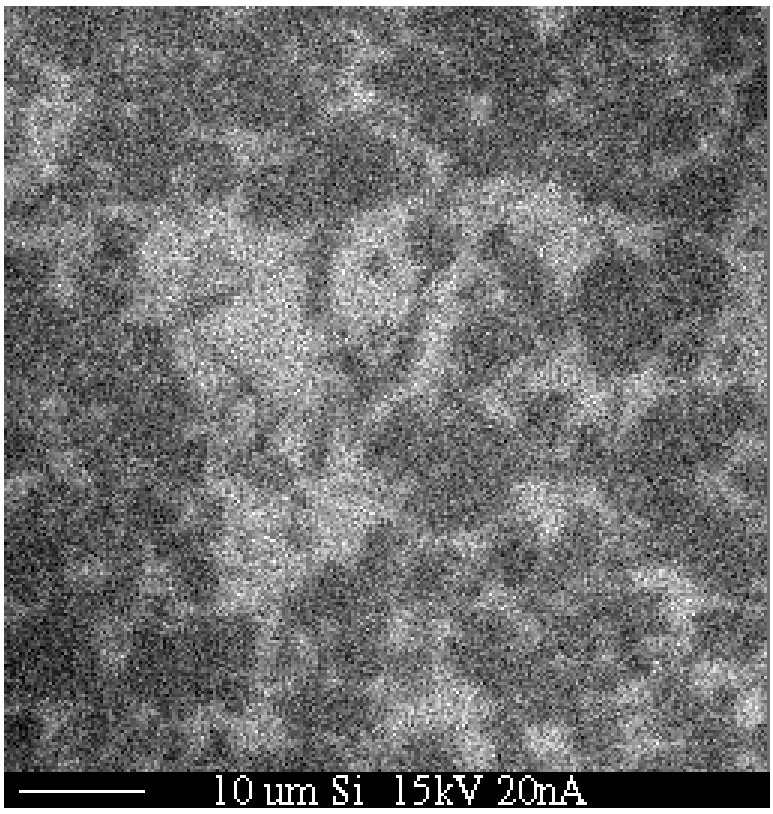

(b) Si concentration in 100% loaded bentonite 1200°C

Fig. 5.28. Silicon elemental maps of 1100 and 1200°C sinterings, where white refers to a local high concentration at 1000X.

5.6 Neutron Activation Analysis

Bentonite clay loaded with FPEX raffinate ions was analyzed with Neutron Activation Analysis (NAA). Bentonite loaded to 70% of the theoretical maximum and sintered at 700, 800, and 1000 °C averaged 10.96 mass% cesium, 3.49 mass% strontium, 8.93 mass% barium, and 1.54 mass% rubidium. Bentonite clay loaded to 100 % of the theoretical mass had 13.70 mass% cesium, 4.37 mass% strontium, 11.66 mass% barium, and 2.06 mass% rubidium (Table 5.4). NAA details for each element in the bentonite sintered at 700, 800, and 1000°C at each theoretical mass concentration are in Appendix D.

Table 5.4
Elemental mass% of each element across all sinterings from NAA

	Average mass% across all sinterings			
Element	70% loaded	std dev	100% loaded	std dev
Cesium	10.96	0.18	13.70	0.22
Strontium	3.49	0.28	4.37	0.35
Barium	8.93	1.22	11.66	1.20
Rubidium	1.54	0.14	2.06	0.14

5.7 Toxicity Characteristic Leach Procedure

Sintered bentonite powders ≤ 150μm in size with ions of cesium, strontium, barium and rubidium were mixed with an acetic acid solution for 18 hours. The leachate was then analyzed by ICP-MS. There are numerous types of hazardous waste. One reason waste is classified as hazardous is if the barium concentration in its TCLP leachate is above 100 ppm.

Bentonite sintered at 700 °C with 70 % and 100 % theoretical waste concentrations had 442 and 961 ppm barium concentrations in their leachate solutions respectively. Sintered at 800 °C and loaded to 70% of the theoretical maximum passed at 34.3 ppm, but the 100% laoded bentonite failed at 172 ppm. Both loadings, 70% and 100%; passed when sintered at 1000 °C with 18 and 63.1 ppm barium in the leachate respectively. 1100 °C sintering resulted in very low leach rates in the 70% loaded bentonite, with the highest concentration for barium at 12.6 ppm; at the 100% loading strontium increases to 78 ppm which is just below the regulation limit. At 1200 °C all element concentrations are below 10 ppm at both loadings. All ion leach rates went down as the sintering temperature was increased with the exception of strontium. Strontium leach rates were relatively high for the 100% loaded bentonite at all sintering temperatures except 1200 °C Figure 5.29.

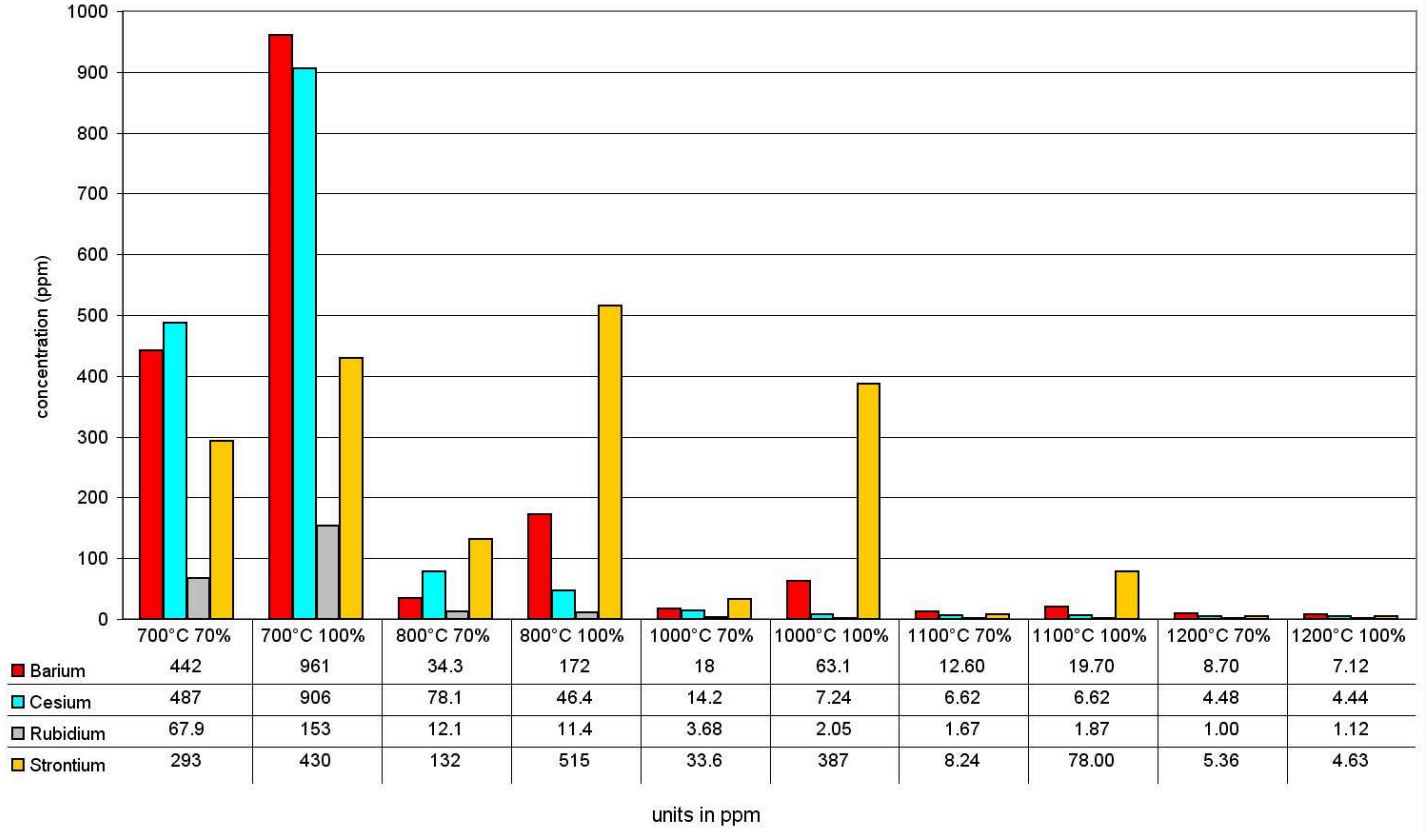

Fig. 5.29. TCLP Results 700, 800, 1000, 1100 and 1200 °C 70% and 100% loaded bentonite clay (ppm)

5.8 Heat Generation Model

Data collected in this study was input to the model, and compared to a borosilicate waste glass with cesium, strontium, and the lanthanides (Table 5.6). The glass was developed under the AFCI at Pacific Northwest National Laboratory [97].

Our ceramic waste form center-line temperature was limited to a maximum 1053°C, based on the observed stability at 1200°C, with an additional safety factor (90%). Thermal conductivity has been shown to increase linearly with sintering temperature [**?**], this was used to extrapolate for the unknown thermal conductivities. An initial thermal conductivity was assumed, and input into the model. The model generated a center-line temperature and edge temperatures, the average of the two was used to extrapolate for the thermal conductivity. The new thermal conductivity was entered into the model to re-calculate the center-line and cladding temperatures. The center-line temperature for the borosilicate glass was limited to the glass transition temperature of 719°C.

Waste form diameter size was found comporable to the borosilicate glass(Table 5.5).

Table 5.5
Wasteform diameter for sintered bentonite and CSLN-7C borosilicate glass

Waste form	radius (m)	Diameter (in)
70% bentonite	0.192	15.09
100% bentonite	0.169	13.31
CSLN-7C glass	0.164	12.9

burn-up=50 GWD/ton; 4.25 enrichment; 20 yr cooled

As the waste form radius is increased, the cladding surface and centerline temperatures will increase (5.30).

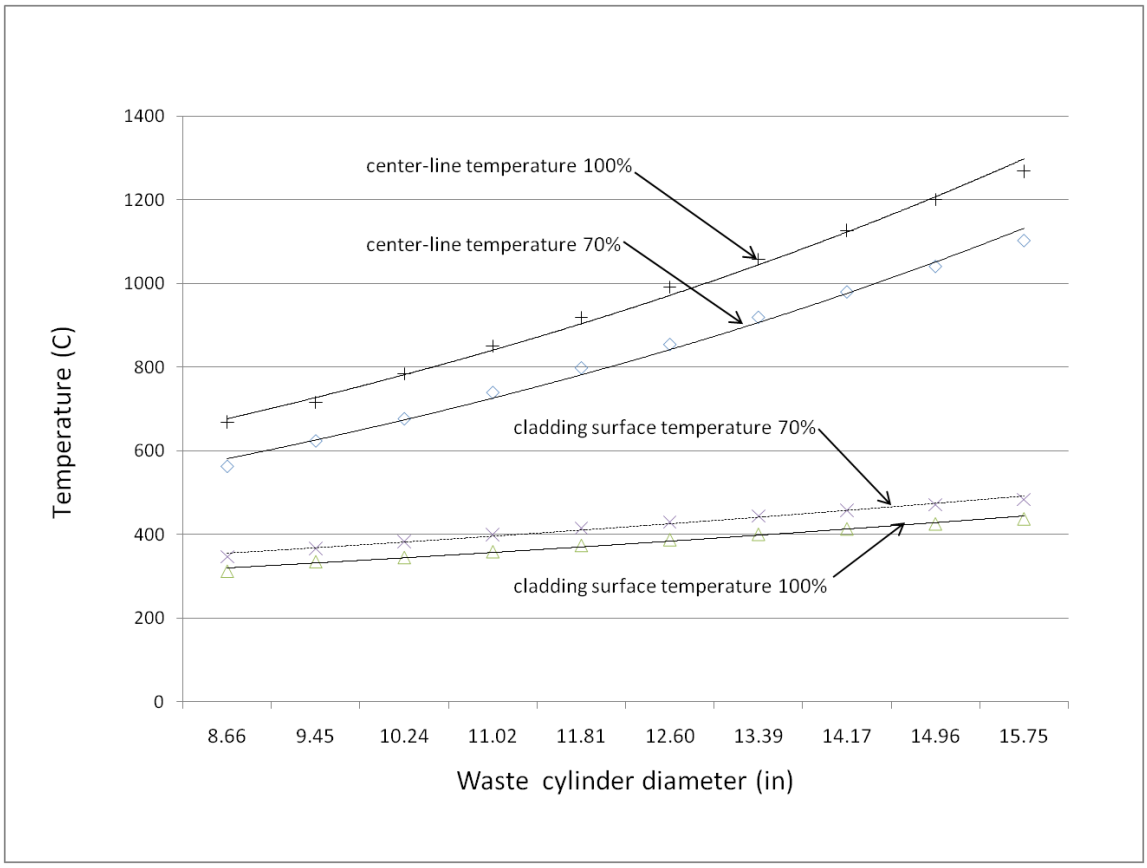

Fig. 5.30. Center-line temperature and cladding surface temperature as a function of waste form diameter; where + refers to 100% loaded bentonite center-line temperature, ◊ 70% loaded bentonite center-line temperature, × 100% loaded bentonite cladding surface temperature, △ 70% loaded bentonite cladding surface temperature

Table 5.6

Glass Composition

Cs Sr Lanthanide Glass (CSLN-7C)

	Measured	Target	Element %
Al2O3	18.07	17	
B2O3	10.5	10	
BaO	6.02	5.71	5.11%
CeO2	7.77	7.04	
Cs2O	5.45	5.98	5.36%
Eu2O3	0.4	0.41	
Gd2O3	0.48	0.46	
La2O3	3.58	3.59	
Nd2O3	11.34	11.86	
Pr2O3	3.26	3.28	
Rb2O	0.79	0.77	0.69%
SiO2	29.48	28	
Sm2O3	2.59	2.49	
SrO	2.09	1.98	1.77%
Y2O3	1.44	1.43	1.28%
Total	103.27	100	
Density (g/cm^3)	3.36		
T_g (°C)	719		

6. DISCUSSION

Ions in a nitric acid solution were added to the bentonite clay. As the moisture is driven off the clay, the solution becomes increasingly concentrated with lower and lower pH. The effect of low pH on the cation exchange capacity is to lower it. Typical cation exchange values for bentonite are ~1 meq/g or lower [98]. Strontium (Sr^{2+}) cation exchange capacity as a function of pH onto a pillared aluminum montmorillonite was reported by Papachristodoulou *et al* [25] to be approximately 0.1 meq/g at a pH of 3.5, 0.64 meq/g at a pH 7.0 and 0.82 meq/g at pH 8.5. Delgado suggested the following Na^+-H^+ exchange reaction for sodium montmorillonite.

$$\text{Na-montmorillonite} + H_2O \leftrightharpoons \text{H-montmorillonite} + NaOH$$

He suggested the penetration of H^+ into the lattice were responsible for the decomposition of the montmorillonite, via release of exchangeable Al^{3+} and Mg^{2+} as ions [99]. Avena described the equilibrium between the hydrogen of the solution and the hydroxyl groups attached to the particle edges more generally as

$$SO^- + H^+ \rightleftharpoons SOH$$

and

$$SOH + H^+ \rightleftharpoons SOH_2{}^+$$

where the S represents any surface site [100]. In our case this may be occurring, but in our system the water is eventually completely driven off leaving all of the Cs, Ba, Sr, Rb, as well as the original Na, Ca, Fe, and Mg cations to precipitate onto the bentonite surfaces. In our bentonite, magnesium, iron, calcium, and sodium initially reside between the layers of silica and alumina sheets. These ions and the additional waste ions saturate the anion sites as well as precipitate on the bentonite surfaces.

6.1 Waste Form Consolidation

Porcelain is a ceramic usually produced by mixing kaolinite clay with quartz and feldspars. Approximate proportions are 50 wt% kaolin, 25 wt% fluxing agents, and 25 wt% quartz. Fluxing agents are typically potash feldspar ($K_2O{\cdot}Al_2O_3{\cdot}0.6SiO_2$), soda feldspar ($Na_2O{\cdot}Al_2O_3{\cdot}0.6SiO_2$), and lime feldspar ($CaO{\cdot}Al_2O_3{\cdot}0.2SiO_2$). The process of converting these raw materials to porcelain proceeds in an abbreviated form as follows: (1) Dehydroxylation breaks down the clay structure, converting kaoline to metakaoline. (2) α- to β-quartz inversion, a reversible transition from a trigonal to hexagonal crystal structure at 573°C. (3) Sanidine forms, which is a homogeneous mixure of alkali feldspars, at 700-1000°C. (4) Metakaolin transforms to a spinel-type structure and releases free amorphous silica at 950-1000°C. (5) Free silica forms a eutectic with the feldspar and alumina K_2O-Al_2O_3-SiO_2. The temperature depends on the type of feldspar, the concentration, and other components present. (6) As the temperature rises porosity is eliminated through viscous phase sintering. (7) The unstable spinel transforms to mullite at ~1000°C. (8) At ~1200°C the melt becomes saturated with silica quartz, and the quartz to cristobalite transformation begins. (9) Above 1200°C prismatic mullite crystals grow into the feldspar grains. (10) Cooling begins, the semi-solid nature of the glass phase prevents residual stresses into the glass transition temperature. (11) Cooling through the quartz inversion temperature at 573°C reduces quartz particle volume by 2% (this can crack the porcelain if not managed properly). (12) At 250 - 225°C, β to α-cristobalite inversion occurs, but less sudden than the quartz inversion, which makes this less of a fracture issue [101,102]. Ohya and others found quartz grains cause cracking in porcelain due to a large thermal expansion differences between the crystalline quartz ($\alpha \approx 23 \times 10^{-6}K^{-1}$) and the glassy phase ($\alpha \approx 3 \times 10^{-6}K^{-1}$) in the temperature range 20- 750°C [103].

In our case we have a very similar composition, but the process feed has a different form. The total silica may be comparable, but the source in the raw feed for porcelain is quartz. Quartz dissolution does not occur until >1200°C. The porcelain feed is

~25% feldspar mineral, which has silica and alumina, but our system is comprised of bentonite saturated with up to 30 wt% alkali and alkaline earth metal ions. Thus the ions are consuming the alumina and silica to produce the feldspars and pollucite, omitting the alumina polymorphs that occur in porcelain. Despite these differences there are similarities in the crytalization process of porcelain with our system:

(1) At 550°C DSC shows an endotherm, and simultaneous mass loss, evident of dehydroxylation (Figure 5.6. 5.7) The hydroxyl groups attached to the alumina layers are driven off causing a collapse of the layered bentonite structure (600-800 °C), similar to what has been reported for pure bentonite [94], as well as bentonite saturated with cations [95]. The XRD scans show an amorphous hump which confirms the lack of crystal structure (Figures 5.13, 5.14). The montmorillonite becomes meta-montmorillonite after dehydroxylation, as reported by Malek [104]. Meta-montmorillonite is a porous amorphous material confirmed by the density at 700°C which is the lowest we recorded, over 50% for both 70% and 100% loadings (Figure 5.1). Balek reported that the cations move into the vacancies of the meta-montmorillonite that remain after dehydroxylation [95]. We see that the cations are easily leached from the structure that remains after sintering to 700°C, with leach rates over 900 ppm for cesium and barium at the 100% loading (Figure 5.29). The remaining water is lost at this step, the nitrate has been shown to be released at this stage as well [2].

(2) At 800°C the amorphous structure begins to crystallize, instead of the metakaolin in porcelain, we see the appearance of hexacelsian ($BaAl_2Si_2O_8$) and pollucite ($CsAlSiO_4$) in the XRD scans (Figures 5.13, 5.14). Hexacelsian is the first phase visible in the XRD at 800°C and 70% loading, pollucite also appears but in the 100% loaded sample also at 800°C. The leach rates determined by our simplified TCLP decrease for all elements tested, with the smallest change of 2.2 times less for strontium at 800°C than the 700°C sintering (Figure 5.29). We also see the Group I and Group II elements begin to segregate into distinct separate regions 800°C (Figure 5.19).

(3) 1000°C hexacelsian is no longer visible and has been replaced by monoclinic forms with variable strontium to barium ratios (Figures 5.14, 5.13). For this transition to occur, from hexagonal to monoclinic, from a planar to three dimensional structure Al-O and Si-O bonds must be broken. Bansal reported the energy required, for strontium as 527 kJ/mol [105]. In our DSC plots this is visible as a peak at ~900°C that becomes endothermic due to this transformation, which continues downward as the ceramic eventually melts (Figures 5.6, 5.7). These celsian crystal structures that form exist in various ratios of barium to strontium. Our samples show a 50:50 Ba to Sr crystal phase at 1000°C at the 70% loading (bottom of Figure 5.13) as well as at 1200°C with a 100% loading (Figure 5.15). A separate 25:75 Ba to Sr ratio feldspar is detected at 1000°C and 100% loading (bottom of Figure 5.14). As the monoclinic feldspars grow, so does the pollucite phase. In the higher loading (100%) the pollucite XRD peaks double in intensisty from 800 to 1000°C sinterings (Figure 5.14). The crystals grow in separate regions as the separation of the alkali, and alkaline earths continues. The segeration is visible as separate phases growing in the backscattered image of the 100% loaded bentonite, as well as the concentration of elements in the elemental maps (Figure top 5.20). The leach rates have decreased to <100 ppm for all elements except strontium which is still high at 387 ppm.

(4) At 1100°C the backscattered image shows a uniform grey colored matrix with a dark phase within, and a larger white region throughout. The white is typical of high Z elements, such as cesium. The DSC has a steep downward slope at 1100°C indicative of energy consumption during melting. The grains of silica are no longer visible, and silica has become homogeneously distributed (Figure 5.28). The density has increased from 1.84 g/cm^3 at 1000°C to 2.18 g/cm^3 indicative of viscous sintering. The different structured phases embedded within the silica rich region indicate a eutectic has formed (Figure 5.22).

(5) 1200°C a high silica phase has formed and is filled with Sr- and Ba-feldspar crystals, and cesium has formed monoclinic crystals up to 10 μm wide (Figure 5.23).

The ceramic is a light colored glassy structure, uniform in color and texture (Figure top right 5.1, and bottom right 5.3). Leach rates have dropped appreciably, the 700°C at the 100% loading leached >200 times more than in the 1200°C sinterings (Figure 5.29). The rubidium we can assume has done the same due to very similar chemistry, as well as rubidium's location in the elemental maps which overlap that of cesium (Figure 5.24, and Table 5.3). XRD plots are inconclusive with respect to rubidium, the low concentration 1.54–2.06 wt% (Table 5.4) coupled with overlapping peaks make confirmation difficult (Table 6.1). The bentonite is allowed to cool after sintering, I will forgo the steps and speak about cooling with respect to the phases present.

During sintering at ~800°C, crystallization begins with the appearance of a hexagonal barium alumino-silicate in the XRD (Figure 5.13). This compound has been found to be unstable [105]. Sorrell suggested perhaps the hexagonal celsian appears during rapid crystallization only to be consumed by the monoclinic feldspar [5]. Our XRD plots support this. The hexagonal celsian (barium alumino-silicate) is present at 800°C but not at 1000 or 1200°C (Figures 5.13, 5.14, and 5.15). The hexagonal celsian, or hexacelsian as it is known, has a transition from hexagonal to orthorhombic at ~300°C accompanied by a large volume change [106]. This property makes it undesirable in most applications where degradation is an issue to be avoided.

Bentonite sintered to ≤1000°C when cooled, contracts unevenly. It is evident in the discontinuous grains and rough cracked texture (Figure 5.3). By 1000°C the hexacelsian phase is no longer detectable by XRD and the monoclinic barium and strontium feldspars become prevalent (Figure 5.13, 5.14). The leach rates go down (Figure 5.29) as well as porosity (Table 5.2), and the bentonite becomes more dense (Table 5.1).

As the strontium and barium form crystals, so do cesium and rubidium. The cesium forms pollucite, a body centered cubic structure. In our samples it is first visible in the XRD plot at 800°C sintered bentonite with a 100% loading (center of

Table 6.1
Peak proximity in XRD scans of body centered cubic Cs and Rb aluminosilicates, truncated full data can be found in Figures A.3, A.10.

$CsAlSiO_4$		$RbAl(SiO_3)_2$	
2θ	intensity	2θ	intensity
15.915	6	15.898	2
18.395	2	18.392	3
24.415	44	24.435	29
26.13	100	26.166	100
29.29	4	29.327	3
30.729	44	30.797	33
32.136	1	33.562	5
33.455	4		
36.025	6	36.131	2
37.265	22	37.361	14
40.715	12	40.836	4
45.054	6	45.163	2
46.016	5	46.159	1
48.061	1	48.158	1
49.037	10	49.184	4
52.758	12	52.979	5
53.656	3	53.854	4

Figure 5.14). The phase is prevalent in all samples sintered above 800°C, and develops strong XRD peaks by 1200°C (Figures 5.13, 5.14, 5.15). A minor high silica content cesium alumino-silicate ($CsAlSi_5O_{12}$) becomes visible in the 70% loaded bentonite at 1000°C (the ∘ in Figure 5.13). This phase is a base centered orthorhombic that has been reported to have anisotropic thermal expansion characteristics, with a higher thermal expansion below 500°C than above 500°C [107]. In high concentrations this could cause cracking during cooling. The bentonite sintered at 1000°C (Figure 5.3 center) has a mottled coloration as well as holes, and some with inclusions. This base centered monoclinic phase may have contributed to the rough texture by contracting at a different rate during cooling than the surrounding matrix. Also at 1000°C quartz has not yet dissolved, adding a phase with a volume change during cooling (α to β inversion).

The high silica cesium alumino silicate phase is not detected at 1200°C (Figure 5.15), neither is the hexagonal barium feldspar or quartz. With these gone the porosity reaches a minimum at 1200°C sinterings with 14.4% for the 70% loading and 4.7% for the 100%. The densities also increase to values above 2 g/cm^3 at sinterings over 1100°C (Table 5.1). As the minerals transform to phases with consistent thermal expansion behaviour, the bentonite ceramic becomes more dense and has lower porosity. The porosity is 33.6%, and 32.7% for 70% and 90% loadings at 1100°C, and 14.4% and 4.7% for 70% and 100% loadings at 1200°C (Table 5.2). This decrease in porosity (~57% for 70%) is greater than the decrease from 700°C to 1100°C (43% for the 70% loading). The decrease in porosity is due to viscous sintering.

During sintering a liquid phase forms, this liquid wets the grain surfaces and capillary forces quickly spread the liquid through the pores, eliminating porosity in the process. The solid's solubility in the liquid will determine the extent and effectiveness of viscous phase sintering. If the solid is soluble the porosity is eliminated as the grains grow to minimize surface energy. The compact density increases as the viscous solid reacts to capillary action filling pores and cracks [108].

Bahat did a study [3] focused on the heterogeneous nucleation in alkaline earth feldspars. The study analyzed the effects different nucleating agents had on glass, primarily oxides. The systems were BaO-Al_2O_3-SiO_2, SrO-Al_2O_3-SiO_2 and CaO-Al_2O_3-SiO_2. Although working with glass, these observations have parallels with our case. Our nucleating oxides come from impurities in the bentonite, and although we do not begin with feldspars, they are created in our process. Bahat found barium would nucleate into feldspar crystals readily producing good quality glasses with a variety of oxide co-reactants. He noted strontium and calcium glass systems produced metastable fields, with hexagonal and orthorhombic structures, as well as stable triclinic orientations, but to a lesser extent. The barium nucleation product was limited to the metastable hexacelsian crystal phase. The hexacelsian nucleated from more oxide agents than any of the other crystals. These nucleating agents are used in small amounts typically less than 1%. When iron oxide was used as a nucleating agent the crystal growth was fast, forming a fine-grained ceramic. Bahat found the ratio of FeO/Fe_2O_3 did not affect nucleation rate.

Our samples have 4.85 wt% iron oxide (Fe_2O_3) according to the supplier. In our quantitative element analysis iron in the dark phase is at its highest concentration, at ~1.3% (Table 5.3). Alumina and silica as well as the alkaline earths metal ions are also in the dark phase. We observe the hexagonal barium structure before any other crystal phase, at the lower loading of 70% at 800°C (Figure 5.13). The presence of iron oxide may act as a nucleating agent accelerating the favored hexagonal barium feldspar as reported by Bahat [3].

What has occurred is the barium crystallized faster than the strontium; nucleated by the various impurities in the bentonite, the hexacelsian formed quickly. Due to the limited alumina, the strontium was not able to form crystals before the alumina was consumed by the other reactants, and was left in the silica phase. Alumina is the limiting reactant during the formation of the alumino-silicates. If we assume a 1 kg basis, and all the alkali, and alkaline earth metals are to be converted to alumino-

silicates 1.55 moles of alumina are required for bentonite with 25 wt% waste, and 1.98 moles for the 32 wt% waste loading. If the remainder of the material is dry and dehydroxylated bentonite (750.7 g for the 25 wt% waste, and 680.9 g for the 32 wt% waste) only 1.52 and 1.38 moles of alumina are available at 25 and 32 wt% loadings, respectively. There is a 0.03 mole deficiency for the 25 wt% waste loading, and 0.6 mole deficiency for the 32 wt% waste loading (calculations in Appendix C).

During the SEM analysis of the 1200°C sintered bentonite, the feldspar crystals appeared to be protruding from a depression. Upon closer inspection, the surface was found to be flat. The back-scattered image intensity is determined by the number of electrons that bounce off the target, larger nuclei deflect better than light nuclei. Silicon and aluminum are light elements compared to the alkali and alkaline earths. The result is the light elements appear dark, and the heavy ones appear bright. As the electron gun bombards the ceramic surface with electrons they penetrate until they hit an atom and are elastically scattered back to the detector. The electrons are deflecting off of the feldspar crystals after going through various amounts of silicon, the intensity of the signal is decreased as the silicon thickness increases, creating an illusion of a three dimensional surface.

The TCLP leachate had high concentrations of strontium up to 1100°C. The strontium unable to form crystals leached easily. The strontium was not completely immobilized until the temperature of the silica was high enough to melt, then viscous sintering could occur. Melting is visible in the silica element maps at 1100°C where silica becomes homogeneously distributed (Figure 5.28). The silica is no longer present as quartz crystals at temperatures >1000°C, but has melted and spread throughout the ceramic, visible as a disappearance of large areas absent of all elements except silicon (Figures 5.27, 5.28).

Optical images of sintered bentonite at temperatures <1100°C show pores and cracking (Figure 5.3). Two contributing factors to the porosity and cracking are differences in thermal expansion coefficients of the various phases, and if viscous

phase sintering is occurring or not. In the XRD scans at lower temperatures hexacelsian is present, which has a an orthorhombic transition with a volume change at ~300°C [106]. Bansal reports that both the barium $BaAl_2Si_2O_8$ and strontium $SrAl_2Si_2O_8$ celsian go through a hexacelsian phase before transitioning to the monoclinic form. The transition for barium hexacelsian to the monoclinic is very slow, while the strontium analog occurs rapidly. Our sinterings were held for 12 hours, so this is not an issue. Bansal also stated the two form solid solutions across the entire composition range [109]. If there were enough alumina both barium and strontium could form crystals, and mix within the glass phase.

At 1000°C and 70% loading $CsAlSi_5O_{12}$ is observed in the XRD (Figure 5.14), this compound also displays anisotropic thermal expansion characteristics, at temperatures <500°C it exists as an orthorhombic rather than the body-centered cubic at higher temperatures [107]. As the sintered bentonite cools areas with high concentrations of these phases will separate from phases with lower thermal expansion coefficients. Other sources of porosity are incomplete consolidation of the green pucks, and pores that remain after dehydroxylation. Porosity is high before liquid phase sintering has developed, and before the high thermal expansion polymorths have transitioned to their stable counterparts. In the optical images of the 1000°C sintered bentonite at 26wt% and 31wt% waste (Figure 5.3), small crystal inclusions are visible inside the holes. These may be crystals that shrunk quickly relative to the surrounding matrix, or solid quartz crystals which have separated from the surrounding material. To limit porosity the sintering must be carried out until the silica melts, and the monoclinic forms are allowed to develop. The thermal conductivity is maximized at low porosity (Figure 5.4).

In our system sintering should be carried out to at least 1100°C. The leach testing shows strontium concentration in the leachate <100 ppm after sintering to 1100°C, but to lower the porosity substantially sintering to 1200°C is required, thus increasing thermal conductivity. The waste loadings should not be lower than 21 wt% waste,

waste concentrations <21 wt% have a detrimental effect on the ceramic's material properties. Samples loaded with 15 wt% waste bloated at 1200°C, and loadings with 21 wt% waste and above had smooth textures and uniform coloration when sintered at >1100°C (Figure 5.1).

6.2 Engineering Considerations

The FPEX solution will require careful planning and engineering to ensure safety and reliable processing. The steps must be minimized to reduce sources of failure. In this study we dried liquid and clay solution ignoring the off-gas losses, this will not be possible in a full scale operation. Each step will require careful accounting to keep track of all losses.

In our experiments an intermediate step produced a powder. From a nonproliferation and safety perspective this is serious matter. The dry powder may be an integral processing step, but the amount of powder available at any given time must be minimized as much as possible. This can be accomplished by continuous, rather than batch processing as well as low volumetric flow rates. This has the added advantage of reducing shielding requirements for downstream operations.

Engineering and design of the facility must consider each potential problem, such as high pressure lines, or plumbing to be routed with adequate separation from high risk areas. The choice of equipment will require careful cost analysis, due to contamination replacing parts is undesirable, although at times unavoidable.

If volitization is unavoidable an engineering remedy is necessary. In vitrification operations a cold cap on the melt reduces the losses. The cold cap is a layer of solid glass that is allowed on top of the glass melt surface. In a ceramic process, perhaps the monolith could be continuously grown in a manner that keeps the heated region sealed, and only the relatively cool ceramic allowed to be exposed. Engineering such a system would be difficult due to the large amount of acidic off-gases to manage.

Temperatures greater than 1000°C are necessary to pass TCLP for this process, perhaps greater to improve porosity, and therefore thermal conductivity. Grinding and re-sintering could improve porosity substantially, but introducing an addition step that requires producing a powder is highly undesirable. A preferred method would be to reach the optimum density in one continuous step. The size of the final wasteform will be determined by the centerline temperature, which will have to fall below the melting point of the waste form matrix. The limiting factor will be the melting point of the glassy phase. How far below the melting point will require an engineering decision. Typically a temperature below the glass transition temperature is chosen for glass waste forms, safety factor is also applied, 90% of the glass transition temperature for example.

Once the waste form is created the durability will need to be assessed. Radiation damage can manifest itself in Frenkel defects, where an interstitial is paired with a vacancy. These defects can either cluster and grow into defect loops, or combine and annihilate each other [110]. Pollucite has been analyzed after Cs-137 has decayed and displayed small volume increases [41], in our system we also have strontium to contend with in two separate phases. How this complex structure responds to radiation will require testing. Sickafus has shown radiation resistance of each material will depend on ion charge and size, as well as ease of defect movement in the structure [111].

REFERENCES

[1] J. D. Law, T. G. Garn, R. S. Herbst, D. H. Meikrantz, D. R. Peterman, C. L. Riddle, T. A. Todd, and J. L. Tripp. Development of cesium and strontium separation and immobilization technologies in support of an advanced nuclear fuel cycle. Technical report, Idaho National Laboratory, 2006.

[2] M. D. Kaminski, C. J. Mertz, M. Ferrandon, N. L. Dietz, and G. Sandi. Physical properties of an alumino-silicate waste form for cesium and strontium. *Journal of Nuclear Materials*, 2009.

[3] D. Bahat. Heterogeneous nucleation of alkaline earth feldspars in glasses. *Journal of Materials Science*, 4(10):847–854, 1969.

[4] Advanced fuel cycle initiative (”‘afci”’) program plan. Technical report, DOE, May 2005.

[5] CA Sorrell. Solid state formation of barium, strontium and lead feldspars in clay-sulfate mixtures. *Am. Mineral*, 47(3-4):291–298, 1962.

[6] VI Spitsyn and VV Gromov. A study of the systematic adsorption of radioactive strontium by montmorillonite and its fixation by roasting. *Atomic Energy*, 5(4):1341–1347, 1959.

[7] D. M. Strachan and W. W. Schulz. Glass and ceramic materials for the immobilization of megacurie-amounts of pure cesium-137. In *78. annual meeting of the American Ceramic Society*, volume 3, 1976.

[8] D.M. Strachan and W.W. Schulz. Characterization of pollucite as a material for long-term storage of cesium-137. *American Ceramic Society Bulletin*, 58(9), 1979.

[9] ER Vance, BE Scheetz, MW Barnes, and BJ Bodnar. Studies of pollucite. *The Scientific Basis for Nuclear Waste Management, Stephen V. Topp, editor, Elsevier Science Publishing Co. Inc*, 1982.

[10] N.J. Hess, F.J. Espinosa, S.D. Conradson, and W.J. Weber. Beta radiation effects in ^{137}Cs-substituted pollucite. *Journal of Nuclear Materials*, 281(1):22 – 33, 2000.

[11] R.C. Ewing and F.N. von Hippel. Nuclear Waste Management in the United States–Starting Over. *Science*, 325(5937):151, 2009.

[12] *Alternatives to Direct SNF Disposal: Advanced Nuclear Fuel Cycles*, February 2003.

[13] C. W. Forsberg. Rethinking high-level waste disposal: Separate disposal of high-heat radionuclides ^{90}Sr and ^{137}Cs. *Nuclear Technology*, 131(2):252 – 268, 2000.

[14] RA Wigeland, TH Bauer, TH Fanning, and EE Morris. Spent Nuclear Fuel Separations and Transmutation Criteria for Benefit to a Geologic Repository. *Waste Management*, 2004.

[15] G.F. Vandegrift, M.C. Regalbuto, S. Aase, A. Bakel, T.J. Battisti, D. Bowers, J.P. Byrnes, M.A. Clark, J.W. Emery, J.R. Falkenberg, et al. Designing and Demonstration of the UREX+ Process Using Spent Nuclear Fuel. In *presentation at the International Conference on Advances for Future Nuclear Fuel Cycles, Nîmes, France*, pages 21–24, 2004.

[16] MC Thompson. Demonstration of the UREX Solvent Extraction Process with Dresden Reactor Fuel Solution. Technical report, WSRC-TR-2002-00444, Savannah River Site (US), 2002.

[17] C. L. Riddle, J. D. Baker, J. D. Law, C. A. McGrath, D. H. Meikrantz, B. J. Mincher, D. R. Peterman, and T. A. Todd. Fission product extraction (fpex): Development of a novel solvent for the simultaneous separation of strontium and cesium from acidic solutions. *Solvent Extraction and Ion Exchange*, 23(3):449–461, 2005.

[18] J.D. Law, R.S. f, D.R. Peterman, R.D. Tillotson, and T.A. Todd. Development of a cobalt dicarbollide/polyethylene glycol solvent extraction process for separation of cesium and strontium to support advanced aqueous reprocessing. *Nuclear technology*, 147(2):284–290, 2004.

[19] T. A. Todd, T. A. Batcheller, J. D. Law, and R. S. Herbst. Cesium and strontium separation technologies literature review. Technical Report INEEL/EXT-04-01895, Idaho National Engineering and Environmental Laboratory, March 2004.

[20] M. Benedict, T. H. Pigford, and H. W. Levi. *Nuclear Chemical Engineering Second Edition*. McGraw-Hill Inc., New York NY, 1981.

[21] L. P. Hatch. Ultimate disposal of radioactive wastes. Technical report, BNL-1345, Brookhaven National Lab., 1953.

[22] Scott G. Barney. Fixation of radioactive waste by hydrothermal reaction with clays. Technical report, U. S. Atomic Energy Commission, 1974.

[23] P. Pusch. Use of bentonite for isolation of radioactive waste products. *Clay Minerals*, 27:353–361, 1992.

[24] U Bartl and K Czurda. Migration and retention phenomena of radionuclides in clay-barrier systems. *Applied Clay Science*, 6(3):195–214, 1991.

[25] C Papachristodoulou. "'a new approach for enhancing sr^{2+} retention by an al-pilc in acidic solutions"'. *Microporous and Mesoporous Materials*, 39(1-21-2):367–379, 2000.

[26] J.L. Kulp. Geologic Time Scale Isotopic age determinations on rocks of known stratigraphic age define an absolute time scale for earth history. *Science*, 133(3459):1105–1114, 1961.

[27] I. MacLaren, J. Cirre, and C.B. Ponton. Hydrothermal synthesis of pollucite (CsAlSi2O6) powders. *Journal of the American Ceramic Society*, 82(11):3242–3244, 1999.

[28] N. Miyagawa, N. Shinohara, and M. Okumiya. Synthesis and fabrication of pollucite glass-ceramics by using arc melting technique. *Journal of the Ceramic Society of Japan*, 107(1248):762–765, 1999.

[29] H. Fryda, G. Vetter, and P. Boch. High-Alumina Cement/Silica Fume Materials for Caesium Trapping. In *Third ECers. Proc. 3 rd European Ceramic Society Conf.*, volume 3, pages 213–218, 1993.

[30] Marsha J. Lambregts and Steven M. Frank. Characterization of cesium containing glass-bonded ceramic waste forms. *Microporous and Mesoporous Materials*, 64(1-31-3):1–9, 2003.

[31] J.-L. Rehspringer, J. Balencie, S. Vilminot, D. Burger, a. Boos, and C. Estourns. Confining caesium in expanded natural perlite. *Journal of the European Ceramic Society*, 27(2-32-3):619–622, 2007.

[32] EE Konovalov, OV Starkov, EM Glagovskii, MP Myshkovskii, AV Kuprin, LP Pelevin, LS Gudkov, and AK Nardova. Immobilization of Silica Gel Fixed Cesium and Strontium into Mineral-Like Matrices in the SHS Mode. *Radiochemistry*, 44(4):420–422, 2002.

[33] C. Pereira. A method for synthesizing pollucite from chabazite and cesium chloride, 1997.

[34] N. G. Vasil'eva, N. N. Anshits, O. M. Sharonova, M. V. Burdin, and A. G. Anshits. Immobilization of cesium and strontium radionuclides in framework aluminosilicates with the use of porous glass-ceramic matrices based on coal fly ash cenospheres. *Glass Physics and Chemistry*, 31(5):637–647, 2005.

[35] H. Mimura, K. Akiba, and M. Ozawa. Preparation of Ceramic Solid Forms Immobilizing Cesium and/or Strontium and Evaluation of their Physical and Chemical Properties. In *Proc. Int. Conf. Nuclear Energy for New Europe*, pages 9–12, 2002.

[36] V. I. Bogdanova, B. A. Fursenko, I. A. Belitskij, L. M. Predeina, G. I. Galaj, V. S. Pavlyuchenko, and I. V. Drobot. Cesium and strontium immobilization using zeolite-containing rocks and high temperature treatment. *Vopr. Materialoved.*, 3:31–40, 1997.

[37] E Zimmer, K Scharf, and S. O. Schmidt. A stable ceramic matrix for fixation of fission products. *Waste Management*, 201:320–325, 1993.

[38] K. Yanagisawa, M. Nishioka, and N. Yamasaki. Immobilization of cesium into pollucite structure by hydrothermal hot-pressing. *Journal of Nuclear Science and Technology*, 24(1):51–60, 1987.

[39] James L. Anchell, Julia C. White, Michael R. Thompson, and Anthony C. Hess. "'an ab initio periodic hartree-fock study of group ia cations in ana-type zeolites"'. *The Journal of Physical Chemistry*, 98(1616):4463–4468, 1994.

[40] RM Barrer and LVC Rees. Self-diffusion of alkali metal ions in analcite. *Transactions of the Faraday Society*, 56:709–721, 1960.

[41] Jeffrey A. Fortner. Determination of transmutation effects in crystalline waste forms. Technical report, Argonne, IL, 1999.

[42] L. P. Ogorodova, L. V. Melchakova, I. A. Kiseleva, and I. A. Belitsky. Thermochemical study of natural pollucite. *Thermochimica Acta*, 403(2):251–256, 2003.

[43] Elsevier Science Publishers B V, I V Chernyshova, V M Agoshov, M Gambino, P Gaune, and J P Bros. Thermodynamic properties and barium feldspars of strontium. *Science*, 175:119–127, 1991.

[44] Ikuo Yanase, Sachiko Tamai, and Hidehiko Kobayashi. Sintering of pollucite using amorphous powder and its low thermal expansion property. *Journal Of The Ceramic Society Of Japan*, 111(8):533–536, 2003.

[45] A.Q. Tool. Relation Between Inelastic Deformability and Thermal Expansion of Glass in its Annealing Range*. *Journal of the American Ceramic Society*, 29(9):240–253, 1946.

[46] G.H. Beall. Refractory glassceramics based on alkaline earth aluminosilicates. *Journal of the European Ceramic Society*, 29(7):1211–1219, 2009.

[47] D.F. Bickford, A. Applewhite-Ramsey, C.M. Jantzen, and K.G. Brown. Control of Radioactive Waste Glass Melters: I, Preliminary General Limits at Savannah River. *Journal of the American Ceramic Society*, 73(10):2896–2902, 1990.

[48] J. H. Saling and A. W. Fentiman. *Radioacitve Waste Management 2nd Edition*. Taylor & Francis, New York NY, 2002.

[49] D.J. Wronkiewicz, J.K. Bates, S.F. Wolf, and E.C. Buck. Ten-year results from unsaturated drip tests with UO2 at 90 C: implications for the corrosion of spent nuclear fuel. *Journal of Nuclear Materials*, 238(1):78–95, 1996.

[50] H. Zimmermann. Investigations on swelling and fission gas behaviour in uranium dioxide. *Journal of Nuclear Materials*, 75(1):154–161, 1978.

[51] I. Zacharie, S. Lansiart, P. Combette, M. Trotabas, M. Coster, and M. Groos. Thermal treatment of uranium oxide irradiated in pressurized water reactor: Swelling and release of fission gases. *Journal of Nuclear Materials*, 255(2-3):85–91, 1998.

[52] J.C.S. Long and R.C. Ewing. Yucca Mountain: Earth-science issues at a geologic repository for high-level nuclear waste. *Annual Review of Earth and Planetary Sciences*, 2004.

[53] J. L. McElroy, W. J. Bjorklund, and W. F. Bonner. Waste vitrification: A historical perspective. In *The treatment and handling of radioactive wastes*, pages 171–177, Richland, Wash., April 1982.

[54] D. F. Bickford and R. Schumacher. Vitrification of hazardous and radioactive wastes. *Ceramic Engineering and Science Proceedings*, 16(2):1 – 10, 1995.

[55] R. Nakaoka, G. Veazey, et al. Vitrification system for the treatment of plutonium-bearing waste at Los Alamos National Laboratory. In *Conference: GLOBAL 2001, PARIS (FR)*, 2001.

[56] GW Becker Jr, J.M. McKibben, S.R. Site, and N. Reno. Vitrification of Rocky Rats Ash Followed by Encapsulation in the Defense Waste Processing Facility. Technical report, Savanah River Site, 1997.

[57] *Volatilization of cesium and ruthenium from high-level waste glass*, Las Vegas, NV, USA, 1990.

[58] N.E. Bibler, T.L. Fellinger, S.L. Marra, R.J. O'driscoll, J.W. Ray, and W.T. Boyce. Tc-99 and Cs-137 volatility from the DWPF production melter during vitrification of the first macrobatch of HLW sludge at the Savannah River site. *Materials Research Society Symposium - Proceedings*, 608:697 – 702, 2000.

[59] MJ Plodinec and BG Kitchen. Establishing the acceptability of Savannah River site waste glass. Technical report, Westinghouse Savanah River Co., 1990.

[60] *Design of a high-level waste pretreatment process for the purpose of vitrification*, Tucson, AZ, USA, 1986.

[61] T. N. Jr. Sargent, T. J. Overcamp, D. F. Bickford, and C. A. Cicero-Herman. Vitrification of cesium-laden organic ion-exchange resin in a stirred melter. *Nuclear Technology*, 123(1):60 – 66, 1998.

[62] M. K. Andrews. Glass formulation development and testing for the vitrification of cesium-loaded (CST). *Proceedings of the Air & Waste Management Association's Annual Meeting & Exhibition*, 1997.

[63] D. G. Bennett, J. J. W. Higgo, and S. M. Wickman. Review of waste immobilization matrices. Technical Report 0126-1, Galson Sciences Limited, December 2001.

[64] J.V. Hanna, L.P. Aldridge, and E.R. Vance. Cs speciation in cements. *Materials Research Society Symposium - Proceedings*, 663:89 – 96, 2001.

[65] R. Neilson Jr., P. Kalb, M. Fuhrmann, and P. Colombo. Solidification of Ion Exchange Resin Wastes in Hydraulic Cement. In *The treatment and handling of radioactive wastes*, pages 497–503, Richland, WA, April 1982.

[66] DS Perera, MG Blackford, ER Vance, JV Hanna, KS Finnie, and CL Nicholson. Geopolymers for the immobilization of radioactive waste. In *Materials research society symposium proceedings*, volume 824, pages 607–612. Warrendale, Pa.; Materials Research Society; 1999, 2004.

[67] D.S. Perera, E.R. Vance, Z. Aly, J. Davis, and C.L. Nicholson. Immobilization of Cs and Sr in geopolymers with Si/Al molar ratio of˜ 2. *Ceramic Transactions*, 176:91–96, 2005.

[68] N. V. Elizondo, E. Ballesteros, and B. I. Kharisov. Cleaning of liquid radioactive wastes using natural zeolites. *Applied Radiation and Isotopes*, 52:27–30, 2000.

[69] J. Yoo, T. Shinagawa, J. P. Wood, W. P. Linak, D. A. Santoianni, C. J. King, Y. Seo, and J. O. L. Wendt. High-temperature sorption of cesium and strontium on dispersed kaolinite powders. *Environmental Science and Technology*, 39:5087–5094, 2005.

[70] G. N. Brown, K. J. Bontha, J. R.and Carson, R. J. Elovich, and J. R. DesChane. Comparison of inorganic ion exchange materials for removing cesium, strontium, and transuranic elements from k-basin water. Technical Report PNNL-11746, Pacific Northwest National Laboratory, October 1997.

[71] H. Mimura, T. Hirabayashi, and M. Ozawa. Leachability and thermal properties of ceramic solid forms immobilizing cesium and/or strontium. In *International Conference - Nuclear Energy for New Europe, Proceedings*, pages 615 – 622, Portoroz, Slovenia, 2003.

[72] K.D. Reeve and A.E. Ringwood. The SYNROC process for immobilizing high-level nuclear wastes. *Radioactive Waste Management. Proceedings of an International Conference*, pages 307 – 24, 1984.

[73] I. W. Donald, B. L. Metcalfe, and R. N. J. Taylor. Review the immobilization of high level radioactive wastes using ceramics and glasses. *Journal of Materials Science*, 32:5851–5887, 1997.

[74] ML Carter, ER Vance, and H. Li. Hollandite-rich ceramic melts for the immobilization of Cs. In *Scientific Basis for Nuclear Waste Management XXVII: Materials Research Society Symposium Proceedings*, volume 807, pages 249–254, 2004.

[75] *HIPed Tailored Ceramic Waste Forms for the Immobilization of Cs, Sr and Tc*. INL/CON-07-12875, Idaho National Laboratory (INL), 2007.

[76] J. Tripp and V. Maio. Evaluation of the use of synroc to solidify the cesium and strontium separations product from advanced aqueous reprocessing of spent nuclear fuel. Technical report, INL/EXT-06-01377, Idaho National Laboratory (INL), 2006.

[77] CM Jantzen. Characterization and Performance of Fluidized Bed Steam Reforming (FBSR) Product as a Final Waste Form. *Ceramic Transactions*, 155:319–329, 2004.

[78] M. Cowen, J. Bradley Mason, K. Ryan, and D. Schmoker. Steam reforming technology for denitration and immobilization of DOE tank wastes. *Ceramic Transactions*, 176:99 – 110, 2006.

[79] Carol M. Jantzen, John M. Pareizs, Troy H. Lorier, and James C. Marra. "'durability testing of fluidized bed steam reforming (fbsr) products"'. *Ceramic Transactions*, 176:121 – 137, 2006.

[80] J. B. Mason and D. Bradbury. Patent: Process for the treatment of radioactive graphite, September 2003.

[81] G. E. Voelker, W. G. Steedman, and R. R. Chandran. Steam reforming of low-level mixed waste. Technical Report DOE/MC/32091-97/C0789, ThermoChem Inc., December 1996.

[82] *Steam Reforming Solidification of Cesium and Strontium Separations Product from Advanced Aqueous Processing of Spent Nuclear Fuel*, 2006.

[83] A.K. Herbst. Optimization of Hydraulic Cement Ad Mixture Waste Forms for Sodium-Bearing, High Aluminum, and High Zirconium Wastes. In *18 th Annual US Department of Energy Low-Level Radioactive Waste Management Conference Proceedings*, 1997.

[84] Yun Bao, S. Kwan, D.D. Siemer, and M.W. Grutzeck. Binders for radioactive waste forms made from pretreated calcined sodium bearing waste. *Journal of Materials Science*, 39(2):481 – 488, 2004.

[85] Candido Pereira, 2005.

[86] W. J. Parker, R. J. Jenkins, C. P. Butler, and G. L. Abbott. Flash method of determining thermal diffusivity, heat capacity, and thermal conductivity. *Journal of Applied Physics*, 32(9):1679–1684, 1961.

[87] Renald N. Guillemette. Methods of soil analysis. part 5. mineralogical methods. In L. Richard Drees April L. Ulery, editor, *Methods of Soil Analysis*, volume 5. Soil Science Society of America, Inc, Madison, Wisconsin, USA, 2008.

[88] Environmental Health & Safety Online. The epa tclp: Toxicity characteristic leaching procedure and characteristic wastes (d-codes), http://www.ehso.com/cssepa/TCLP.htm 2009.

[89] Michael D. Kaminski. Simplified "'tclp"', February 2009.

[90] M.D. Kaminski. Engineering product storage under the advanced fuel cycle initiative. Part I: An iterative thermal transport modeling scheme for high-heat-generating radioactive storage forms. *Journal of Nuclear Materials*, 347(1-2):94–103, 2005.

[91] RL Coble and WD Kingery. Effect of porosity on physical properties of sintered alumina. *Journal of the American Ceramic Society*, 39(11):377–385, 1956.

[92] RE Grim. *International Series in the Earth Sciences: Applied Clay Mineralogy*, pages 352–355. McGraw-Hill: New York, 1962.

[93] M. Onal and Y. Sarikaya. Thermal behavior of a bentonite. *Journal of Thermal Analysis and Calorimetry*, 90(1):167–172, 2007.

[94] RE Grim and WF Bradley. Investigation of the effect of heat on the clay minerals illite and montmorillonite . *Journal of the American Ceramic Society*, 23(8):242–248, 1940.

[95] V. Balek, Z. Malek, S. Yariv, and G. Matuschek. Characterization of montmorillonite saturated with various cations. *Journal of Thermal Analysis and Calorimetry*, 56(1):67–76, 1999.

[96] B. Yoshiki and K. Matsumoto. High-temperature modification of barium feldspar. *J. Am. Ceram. Soc*, 34(9):283–86, 1951.

[97] J. V. Crum, A. L. Billings, J. Lang, J. C. Marra, C. Rodriguez, J. V. Ryan, and J. D. Vienna. Baseline glass development for combined fission products waste streams. Technical report, PNNL, 2009.

[98] ND Hutson, MJ Hoekstra, and RT Yang. Control of microporosity of Al2O3-pillared clays: effect of pH, calcination temperature and clay cation exchange capacity. *Microporous and Mesoporous Materials*, 28(3):447–459, 1999.

[99] A. Delgado, F. Gonzalez-caballero, and J. M. Bruque. On the zeta potential and surface charge density of montmorillonite in aqueous electrolyte solutions. *Journal of Colloid and Interface Science*, 113(1):203–211, 1986.

[100] M.J. Avena, R. Cabrol, and C.P. De Pauli. Study of some physicochemical properties of pillared montmorillonites; acid-base potentiometric titrations and electrophoretic measurements. *Clays and clay minerals*, 38(4):356–362, 1990.

[101] W.M. Carty and U. Senapati. Porcelain-raw materials, processing, phase evolution, and mechanical behavior. *Journal of the American Ceramic Society*, 81(1):3–20, 1998.

[102] Y. Iqbal and W.E. Lee. Microstructural evolution in triaxial porcelain. *Journal of The American Ceramic Society*, 83(12):3121–3127, 2000.

[103] Y. Ohya, Y. Takahashi, M. Murata, Z. Nakagawa, and K. Hamano. Acoustic emission from a porcelain body during cooling. *Journal of the American Ceramic Society*, 82(2):445–448, 1999.

[104] Z. Malek, V. Balek, D. Garfinkel-Shweky, and S. Yariv. The study of the dehydration and dehydroxylation of smectites by emanation thermal analysis. *Journal of Thermal Analysis and Calorimetry*, 48(1):83–92, 1997.

[105] N. Bansal, C. Drummond, and III E S H. Kinetics of hexacelsian-to-celsian phase transformation in SrAl 2 Si 2 O 8. *American Ceramic Society, Journal*, 76(5):1321–1324, 1993.

[106] L. Barbeeri, A.B. Corradi, C. Leonelli, T. Manfredini, M. Romagnoli, and C. Siligardi. The microstructure and mechanical properties of sintered celsian and strontium-celsian glass-ceramics. *Materials Research Bulletin*, 30(1):27–41, 1995.

[107] Martin Fisch, Thomas Armbruster, and Boris Kolesov. Temperature-dependent structural study of microporous "'csalsi$_5$o$_{12}$"'. *Journal of Solid State Chemistry*, 181(3):423–431, 2008.

[108] R.M. German. *Liquid phase sintering*. Plenum Pub Corp, 1985.

[109] NP Bansal. Solid state synthesis and properties of monoclinic celsian. *Journal of Materials Science*, 33(19):4711–4715, 1998.

[110] KE Sickafus, L. Minervini, RW Grimes, JA Valdez, M. Ishimaru, F. Li, KJ McClellan, and T. Hartmann. Radiation tolerance of complex oxides. *Science*, 289(5480):748–751, 2000.

[111] K.E. Sickafus, R.W. Grimes, J.A. Valdez, A. Cleave, M. Tang, M. Ishimaru, S.M. Corish, C.R. Stanek, and B.P. Uberuaga. Radiation-induced amorphization resistance and radiation tolerance in structurally related oxides. *Nature Materials*, 6(3):217–223, 2007.

APPENDIX A
XRD REFERENCE PDFS

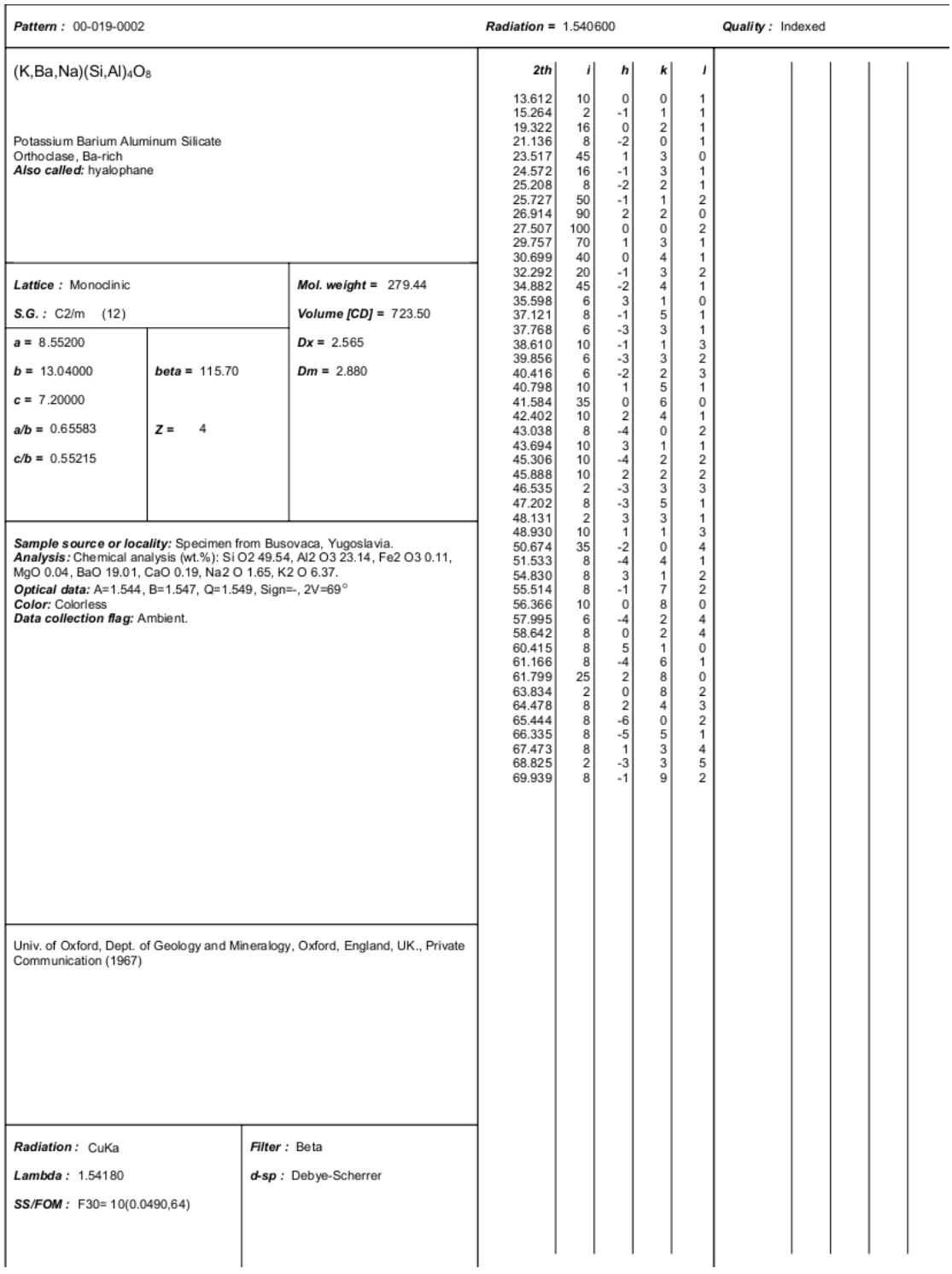

Pattern : 00-019-0002 ***Radiation =*** 1.540600 ***Quality :*** Indexed

$(K,Ba,Na)(Si,Al)_4O_8$

Potassium Barium Aluminum Silicate
Orthoclase, Ba-rich
Also called: hyalophane

Lattice : Monoclinic
S.G. : C2/m (12)

a = 8.55200
b = 13.04000
c = 7.20000
a/b = 0.65583
c/b = 0.55215

beta = 115.70
Z = 4

Mol. weight = 279.44
Volume [CD] = 723.50
Dx = 2.565
Dm = 2.880

Sample source or locality: Specimen from Busovaca, Yugoslavia.
Analysis: Chemical analysis (wt.%): Si O2 49.54, Al2 O3 23.14, Fe2 O3 0.11, MgO 0.04, BaO 19.01, CaO 0.19, Na2 O 1.65, K2 O 6.37.
Optical data: A=1.544, B=1.547, Q=1.549, Sign=-, 2V=69°
Color: Colorless
Data collection flag: Ambient.

Univ. of Oxford, Dept. of Geology and Mineralogy, Oxford, England, UK., Private Communication (1967)

Radiation : CuKa
Lambda : 1.54180
SS/FOM : F30= 10(0.0490,64)

Filter : Beta
d-sp : Debye-Scherrer

2th	i	h	k	l
13.612	10	0	0	1
15.264	2	-1	1	1
19.322	16	0	2	1
21.136	8	-2	0	1
23.517	45	1	3	0
24.572	16	-1	3	1
25.208	8	-2	2	1
25.727	50	-1	1	2
26.914	90	2	2	0
27.507	100	0	0	2
29.757	70	1	3	1
30.699	40	0	4	1
32.292	20	-1	3	2
34.882	45	-2	4	1
35.598	6	3	1	0
37.121	8	-1	5	1
37.768	6	-3	3	1
38.610	10	-1	1	3
39.856	6	-3	3	2
40.416	6	-2	2	3
40.798	10	1	5	1
41.584	35	0	6	0
42.402	10	2	4	1
43.038	8	-4	0	2
43.694	10	3	1	1
45.306	10	-4	2	2
45.888	10	2	2	2
46.535	2	-3	3	3
47.202	8	-3	5	1
48.131	2	3	3	1
48.930	10	1	1	3
50.674	35	-2	0	4
51.533	8	-4	4	1
54.830	8	3	1	2
55.514	8	-1	7	2
56.366	10	0	8	0
57.995	6	-4	2	4
58.642	8	0	2	4
60.415	8	5	1	0
61.166	8	-4	6	1
61.799	25	2	8	0
63.834	2	0	8	2
64.478	8	2	4	3
65.444	8	-6	0	2
66.335	8	-5	5	1
67.473	8	1	3	4
68.825	2	-3	3	5
69.939	8	-1	9	2

Fig. A.1. Potassium Barium Aluminum Silicate, Orthoclase-Barium rich

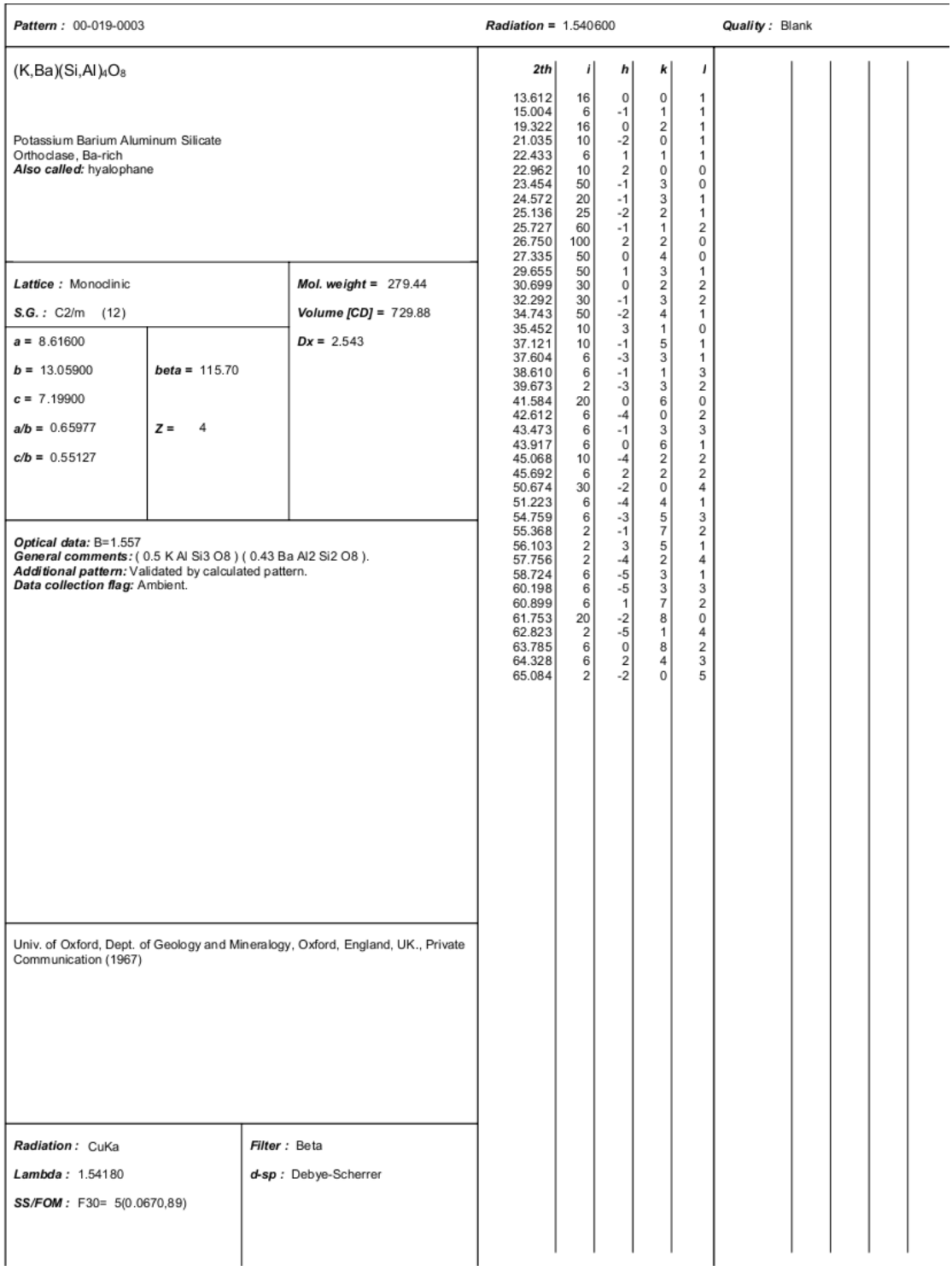

Pattern : 00-019-0003 **Radiation =** 1.540600 **Quality :** Blank

$(K,Ba)(Si,Al)_4O_8$

Potassium Barium Aluminum Silicate
Orthoclase, Ba-rich
Also called: hyalophane

Lattice : Monoclinic
S.G. : C2/m (12)

a = 8.61600
b = 13.05900
c = 7.19900
a/b = 0.65977
c/b = 0.55127

beta = 115.70
Z = 4

Mol. weight = 279.44
Volume [CD] = 729.88
Dx = 2.543

Optical data: B=1.557
General comments: (0.5 K Al Si3 O8) (0.43 Ba Al2 Si2 O8).
Additional pattern: Validated by calculated pattern.
Data collection flag: Ambient.

Univ. of Oxford, Dept. of Geology and Mineralogy, Oxford, England, UK., Private Communication (1967)

Radiation : CuKa
Lambda : 1.54180
SS/FOM : F30= 5(0.0670,89)

Filter : Beta
d-sp : Debye-Scherrer

2th	i	h	k	l
13.612	16	0	0	1
15.004	6	-1	1	1
19.322	16	0	2	1
21.035	10	-2	0	1
22.433	6	1	1	1
22.962	10	2	0	0
23.454	50	-1	3	0
24.572	20	-1	3	1
25.136	25	-2	2	1
25.727	60	-1	1	2
26.750	100	2	2	0
27.335	50	0	4	0
29.655	50	1	3	1
30.699	30	0	2	2
32.292	30	-1	3	2
34.743	50	-2	4	1
35.452	10	3	1	0
37.121	10	-1	5	1
37.604	6	-3	3	1
38.610	6	-1	1	3
39.673	2	-3	3	2
41.584	20	0	6	0
42.612	6	-4	0	2
43.473	6	-1	3	3
43.917	6	0	6	1
45.068	10	-4	2	2
45.692	6	2	2	2
50.674	30	-2	0	4
51.223	6	-4	4	1
54.759	6	-3	5	3
55.368	2	-1	7	2
56.103	2	3	5	1
57.756	2	-4	2	4
58.724	6	-5	3	1
60.198	6	-5	3	3
60.899	6	1	7	2
61.753	20	-2	8	0
62.823	2	-5	1	4
63.785	6	0	8	2
64.328	6	2	4	3
65.084	2	-2	0	5

Fig. A.2. Potassium Barium Aluminum Silicate II, Orthoclase-Barium rich

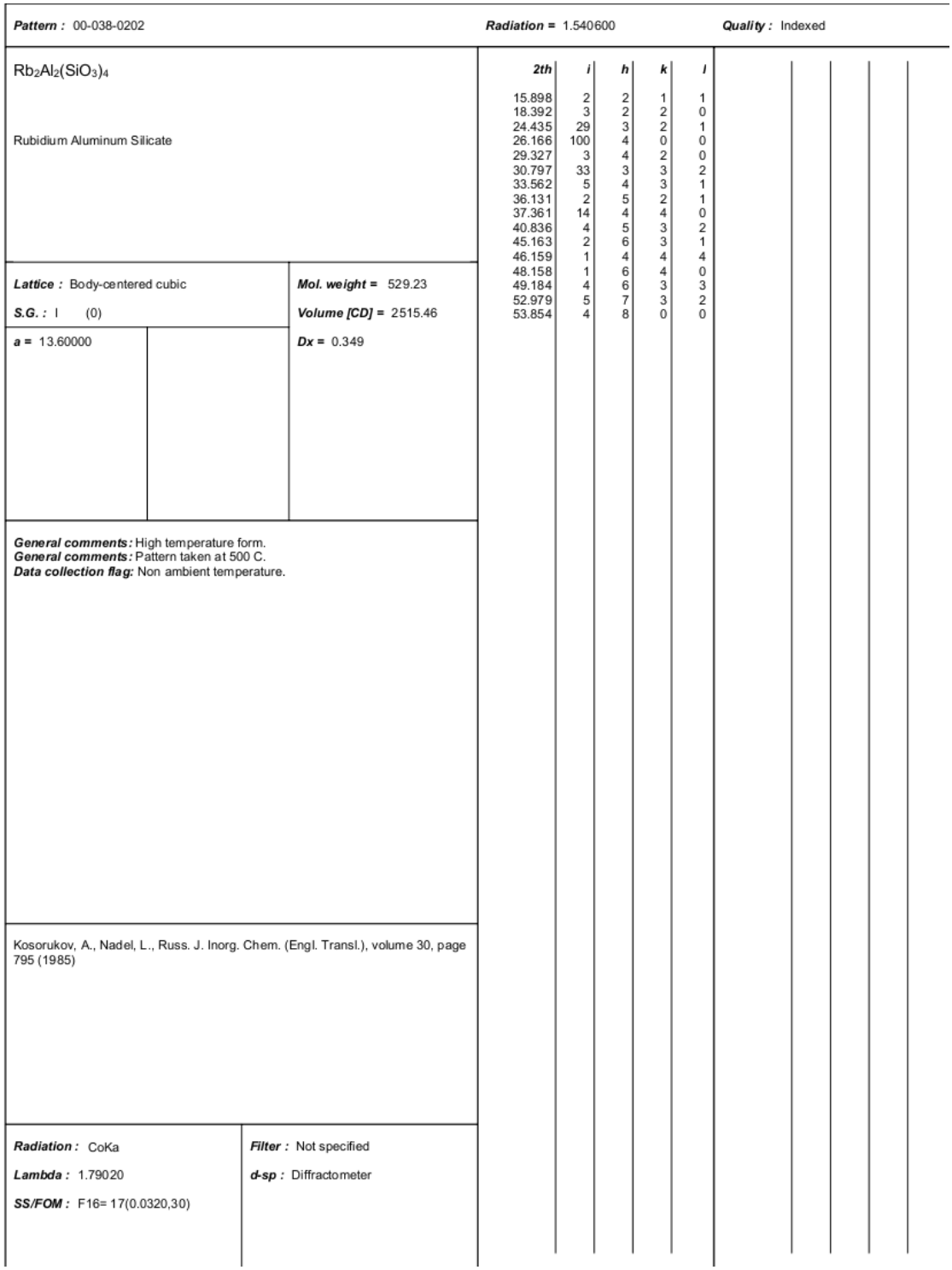

Pattern : 00-038-0202 ***Radiation =*** 1.540600 ***Quality :*** Indexed

$Rb_2Al_2(SiO_3)_4$

Rubidium Aluminum Silicate

Lattice : Body-centered cubic
S.G. : I (0)
a = 13.60000
Mol. weight = 529.23
Volume [CD] = 2515.46
Dx = 0.349

General comments: High temperature form.
General comments: Pattern taken at 500 C.
Data collection flag: Non ambient temperature.

Kosorukov, A., Nadel, L., Russ. J. Inorg. Chem. (Engl. Transl.), volume 30, page 795 (1985)

Radiation : CoKa
Lambda : 1.79020
SS/FOM : F16= 17(0.0320,30)
Filter : Not specified
d-sp : Diffractometer

2th	i	h	k	l
15.898	2	2	1	1
18.392	3	2	2	0
24.435	29	3	2	1
26.166	100	4	0	0
29.327	3	4	2	0
30.797	33	3	3	2
33.562	5	4	3	1
36.131	2	5	2	1
37.361	14	4	4	0
40.836	4	5	3	2
45.163	2	6	3	1
46.159	1	4	4	4
48.158	1	6	4	0
49.184	4	6	3	3
52.979	5	7	3	2
53.854	4	8	0	0

Fig. A.3. Rubidium Aluminum Silicate

Pattern : 00-038-1450 **Radiation =** 1.540600 **Quality :** High

$BaAl_2Si_2O_8$

Barium Aluminum Silicate
Celsian, syn

Lattice : Monoclinic
S.G. : C2/m (12)

a = 8.64110
b = 13.04700
c = 7.20310
a/b = 0.66231
c/b = 0.55209

beta = 115.07
Z = 4

Mol. weight = 375.46
Volume [CD] = 735.55
Dx = 3.390
Dm = 3.380

Sample preparation: The sample was prepared by Talmy, I., and Haught, D., of the Naval Surface Weapons Center, Silver Spring, Maryland, USA, by mixing stoichiometric quantities of Ba C2 O4, Si O2 gel and Al2 O3. Ten percent monoclinic Ba Al2 Si2 O8 was added as seed. The mixture was heated at 1250 C for 5 hours and at 1350 C for 5 hours.
Temperature of data collection: The mean temperature of data collection was 25.8 C.
Color: Colorless
Structure: Unit cell data was reported by Bruno et al. (1). Current work indicates all reflections are indexable on a cell with c-dimension, half of that given by Bruno (c=14.401, S.G.='I2/a').
Polymorphism: Other polymorphs reported are hexagonal (26-137) and monoclinic (10-352).
Optical data: A=1.5835, B=1.589, Q=1.594, Sign=+
Additional pattern: To replace 18-153 and 19-90.
Additional pattern: See ICSD 25836 (PDF 74-377).
Data collection flag: Ambient.

Wong-Ng, W., McMurdie, H., Paretzkin, B., Hubbard, C., Dragoo, A., NBS, Gaithersburg, MD, USA., ICDD Grant-in-Aid (1986)

CAS Number: 1302-50-7

Radiation : CuKa1
Lambda : 1.54060
SS/FOM : F30= 94(0.0070,46)

Filter : Monochromator crystal
d-sp : Diffractometer
Internal standard : Si FP

2th	i	h	k	l
13.563	64	0	2	0
15.097	24	-1	1	1
19.231	34	0	2	1
22.160	9	1	1	1
22.702	29	2	0	0
23.386	35	-1	3	0
24.536	28	-1	3	1
25.025	48	-2	2	1
25.645	74	-1	1	2
26.544	100	-2	2	0
27.160	51	-2	0	2
27.319	39	0	4	0
29.507	58	1	3	1
30.626	30	0	4	1
32.243	41	-1	3	2
34.168	25	2	2	1
34.370	43	-3	1	2
34.665	64	-2	4	1
35.049	14	-3	1	0
35.824	3	-2	4	0
37.050	11	-1	5	1
37.439	6	-3	3	1
38.563	19	-1	1	3
39.665	13	-3	3	2
39.902	10	1	3	2
40.314	10	-3	3	0
40.645	14	1	5	1
41.499	23	0	6	0
41.936	13	2	4	1
42.179	9	-4	0	1
42.581	11	-4	0	2
42.748	16	-1	5	2
42.984	18	3	1	1
43.460	9	-1	3	3
43.853	11	0	6	1
44.526	8	-4	2	1
44.926	16	-4	2	2
45.226	9	2	2	2
46.392	16	4	0	0
46.938	7	-3	5	1
47.492	10	-4	0	3
48.434	7	1	1	3
48.857	9	-3	5	2
49.059	8	1	5	2
49.358	4	-3	5	0
50.382	20	0	4	3
50.655	20	-2	0	4
50.986	11	-4	4	1
52.070	1	-1	5	3
52.690	3	-2	2	4
53.512	3	-5	1	2
53.911	4	3	1	2
54.702	7	-3	5	3
55.464	5	-1	7	2
55.654	12	3	5	1
56.384	8	0	8	0
56.397	8	2	0	3
57.921	10	-4	2	4
58.274	13	0	8	1
58.494	6	-2	4	4
59.417	1	-5	1	0
60.138	11	0	6	3
60.667	9	-4	6	1
60.818	12	-2	8	1
61.552	11	-2	8	0
62.830	7	-5	1	4
63.046	6	-5	3	0

Fig. A.4. Barium Aluminum Silicate, Celsian

Pattern : 00-038-1453 **Radiation =** 1.540600 **Quality :** High

$Ba_{0.25}Sr_{0.75}Al_2Si_2O_8$

Barium Strontium Aluminum Silicate

Lattice : Monoclinic
S.G. : C2/m (12)

a = 8.45020
b = 12.99210 **beta =** 115.23
c = 7.15140
a/b = 0.65041 **Z =** 4
c/b = 0.55044

Mol. weight = 338.18
Volume [CD] = 710.22
Dx = 3.163

Sample preparation: The sample was prepared by I. Talmy and D. Haught of the Naval Surface Weapons Center, Silver Spring, Maryland, USA, by mixing stoichiometric quantities of Ba C2 O4, Sr C2 O4, fused-Si O2, and Al2 O3. The mixture was heated at 1350 C for 2 hours. The Sr C2 O4 and Ba C2 O4 were coprecipitated from the mixture of Sr (N O3)2 and Ba (N O3)2 with (N H4)2 C2 O4.
Color: Colorless
Temperature of data collection: The mean temperature of data collection was 25.8 C.
Structure: The initial cell parameters were obtained based on those of the end-members Sr Al2 Si2 O8 and Ba Al2 Si2 O8.
Data collection flag: Ambient.

Wong-Ng, W., McMurdie, H., Paretzkin, B., Hubbard, C., Dragoo, A., NBS (USA)., ICDD Grant-in-Aid (1986)

Radiation : CuKa1
Lambda : 1.54060
SS/FOM : F30= 94(0.0063,51)

Filter : Monochromator crystal
d-sp : Diffractometer
Internal standard : Si FP

2th	i	h	k	l
13.619	41	0	2	0
15.253	16	-1	1	1
19.339	26	0	2	1
21.353	6	-2	0	1
23.260	23	2	0	0
23.591	44	-1	3	0
24.702	25	-1	3	1
25.415	31	-2	2	1
25.825	70	-1	1	2
27.048	100	-2	2	0
27.545	79	0	0	2
29.827	48	1	3	1
30.781	29	0	4	1
32.445	39	-1	3	2
34.760	24	2	2	1
35.033	67	-2	4	1
35.875	7	-3	1	0
36.505	1	-1	5	0
37.249	10	-1	5	1
38.095	11	-3	3	1
38.849	9	-1	1	3
40.241	11	-3	3	2
40.706	9	-2	2	3
40.965	13	1	5	1
41.684	17	0	6	0
42.536	8	2	4	1
42.985	7	-1	5	2
43.258	7	-4	0	1
43.738	9	-1	3	3
43.919	14	3	1	1
44.062	15	0	6	1
45.540	8	-4	2	1
45.801	12	-4	2	2
45.942	13	2	2	2
46.918	5	-3	3	3
47.304	8	-2	6	1
47.559	12	4	0	0
48.381	10	3	3	1
49.005	6	1	1	3
49.399	8	-3	5	2
49.495	8	1	5	2
50.116	1	-3	5	0
50.646	8	-2	6	2
50.813	13	0	4	3
51.060	18	-2	0	4
51.962	7	-4	4	1
52.408	1	-1	5	3
53.089	1	-2	2	4
54.821	3	-5	1	2
54.971	4	3	1	2
55.216	6	-3	5	3
55.762	3	-1	7	2
56.503	5	3	5	1
56.635	9	0	8	0
56.903	5	0	0	4
57.524	1	-5	1	3
58.660	9	-5	3	2
58.776	11	0	2	4
58.916	10	-2	4	4
59.146	3	2	2	3
60.544	2	0	6	3
61.270	10	-5	3	3
61.588	6	-4	6	1
62.046	11	-2	8	0
63.847	4	-5	1	4

Fig. A.5. Barium (0.25) Strontium (0.75) Aluminum Silicate

Pattern : 00-038-1452 ***Radiation =*** 1.540600 ***Quality :*** High

$Ba_{0.5}Sr_{0.5}Al_2Si_2O_8$

Barium Strontium Aluminum Silicate

Lattice : Monoclinic
S.G. : C2/m (12)

a = 8.51000
b = 13.01040
c = 7.16970
a/b = 0.65409
c/b = 0.55107

beta = 115.13
Z = 4

Mol. weight = 350.60
Volume [CD] = 718.66
Dx = 3.240

Sample preparation: The sample was prepared by I. Talmy and D. Haught of the Naval Surface Weapons Center of Silver Spring, Maryland, USA, by mixing stoichiometric amounts of Sr C2 O4, Ba C2 O4, fused-Si O2, and Al2 O3 at 1350 C for 2 hours. The Sr C2 O4 and Ba C2 O4 were coprecipitated from the mixture of Sr (N O3)2 and Ba (N O3)2 with (N H4)2 C2 O4.
Color: Colorless
Temperature of data collection: The mean temperature of data collection was 26.5 C.
Structure: The initial cell parameters were obtained based on those of the end members Sr Al2 Si2 O8 and Ba Al2 Si2 O8.
Data collection flag: Ambient.

Wong-Ng, W., McMurdie, H., Paretzkin, B., Hubbard, C., Dragoo, A., NBS (USA)., ICDD Grant-in-Aid (1986)

Radiation : CuKa1
Lambda : 1.54060
SS/FOM : F30= 92(0.0072,45)

Filter : Monochromator crystal
d-sp : Diffractometer
Internal standard : Si FP

2th	i	h	k	l
13.615	55	0	2	0
15.213	16	-1	1	1
19.313	23	0	2	1
21.228	1	-2	0	1
23.073	21	2	0	0
23.523	42	-1	3	0
24.651	21	-1	3	1
25.295	32	-2	2	1
25.765	61	-1	1	2
26.875	100	-2	2	0
27.409	64	0	4	0
27.466	63	0	0	2
29.718	43	1	3	1
30.724	26	0	4	1
32.384	35	-1	3	2
34.550	13	2	2	1
34.779	47	-3	1	2
34.905	66	1	1	2
35.603	7	-3	1	0
36.119	2	-2	4	0
36.419	1	-1	5	0
37.169	9	-1	5	1
37.868	8	-3	3	1
38.750	8	-1	1	3
40.070	11	-3	3	2
40.191	11	1	3	2
40.578	4	-2	2	3
40.842	13	1	5	1
41.614	19	0	6	0
42.348	8	2	4	1
42.907	11	-1	5	2
43.364	6	2	0	2
43.606	12	-1	3	3
43.981	8	0	6	1
45.217	4	-4	2	1
45.521	10	-4	2	2
45.661	10	2	2	2
46.770	5	-3	3	3
47.151	11	4	0	0
48.074	8	3	3	1
48.776	4	1	1	3
49.226	8	-3	5	2
49.338	7	1	5	2
49.857	2	-3	5	0
50.627	12	0	4	3
50.918	15	-2	0	4
51.642	7	-4	4	1
52.269	1	-1	5	3
52.945	2	-2	2	4
54.421	2	-5	1	2
54.613	2	3	1	2
55.025	5	-3	5	3
55.658	3	-1	7	2
56.195	5	-4	4	3
56.552	5	0	8	0
56.693	4	0	0	4
58.389	6	-4	2	4
58.565	9	0	2	4
58.824	5	2	2	3
60.406	3	0	6	3
61.013	7	-3	7	2
61.285	6	-4	6	1
61.877	9	-2	8	0
63.672	3	-1	7	3

Fig. A.6. Barium (0.50) Strontium (0.50) Aluminum Silicate

Pattern : 00-038-1451 **Radiation =** 1.540600 **Quality :** High

$Ba_{0.75}Sr_{0.25}Al_2Si_2O_8$

Barium Strontium Aluminum Silicate

Lattice : Monoclinic
S.G. : C2/m (12)

a = 8.58020
b = 13.03140
c = 7.18920
a/b = 0.65843
c/b = 0.55168

beta = 115.15
Z = 4

Mol. weight = 363.03
Volume [CD] = 727.62
Dx = 3.314

Sample preparation: The sample was prepared by Talmy, I., Haught, D., Naval Surface Weapons Center, Silver Spring, Maryland, USA, by mixing stoichiometric amounts of Ba C2 O4, Sr C2 O4, fused-Si O2, and Al2 O3 at 1500 C for 2 hours. The Sr C2 O4 and Ba C2 O4 were coprecipitated from the mixture of Sr (N O3)2 and Ba (N O3)2 with (N H4)2 C2 O4.
Color: Colorless
Temperature of data collection: The mean temperature of data collection was 25.0 C.
Structure: Initial cell parameters of the solid solution were deduced based on those of the end-members Sr Al2 Si2 O8 and Ba Al2 Si2 O8.
Data collection flag: Ambient.

Wong-Ng, W., McMurdie, H., Paretzkin, B., Hubbard, C., Dragoo, A., NBS (USA)., ICDD Grant-in-Aid (1986)

Radiation : CuKa1
Lambda : 1.54060
SS/FOM : F30= 88(0.0076,45)

Filter : Monochromator crystal
d-sp : Diffractometer
Internal standard : Si FP

2th	i	h	k	l
13.582	57	0	2	0
15.155	21	-1	1	1
19.262	30	0	2	1
22.281	6	1	1	1
22.879	23	2	0	0
23.454	40	-1	3	0
24.585	21	-1	3	1
25.148	40	-2	2	1
25.700	62	-1	1	2
26.700	100	-2	2	0
27.253	44	-2	0	2
27.360	49	0	4	0
29.599	67	1	3	1
30.662	30	0	4	1
32.290	45	-1	3	2
34.386	17	2	2	1
34.552	47	-3	1	2
34.747	64	-2	4	1
35.322	11	-3	1	0
35.960	4	-2	4	0
36.348	2	-1	5	0
37.101	14	-1	5	1
37.622	10	-3	3	1
38.646	12	-1	1	3
39.842	11	-3	3	2
40.060	13	1	3	2
40.517	9	-3	3	0
40.746	14	1	5	1
41.538	22	0	6	0
42.149	12	2	4	1
42.521	9	-4	0	1
42.830	11	-1	5	2
43.280	14	3	1	1
43.522	9	-1	3	3
43.918	10	0	6	1
44.857	8	-4	2	1
45.181	14	-4	2	2
45.448	11	2	2	2
46.595	11	-3	3	3
46.733	13	4	0	0
47.012	5	-2	6	1
47.764	10	3	3	1
48.605	6	1	1	3
49.031	8	-3	5	2
49.180	9	1	5	2
49.596	4	-3	5	0
50.394	16	-2	6	2
50.500	18	0	4	3
50.763	20	-2	0	4
51.306	8	-4	4	1
52.153	1	-1	5	3
52.802	3	-2	2	4
53.944	2	-5	1	2
54.266	3	3	1	2
54.863	7	-3	5	3
55.549	5	-1	7	2
55.908	8	-4	4	3
56.440	7	0	8	0
56.588	4	-3	3	4
58.112	8	-4	2	4
58.420	11	0	2	4
58.595	8	-2	4	4
59.917	3	-5	1	0
60.242	5	0	6	3
60.501	9	-5	3	3
60.939	10	1	7	2
61.698	12	-2	8	0
63.100	5	-5	1	4
63.580	7	1	1	4

Fig. A.7. Barium (0.75) Strontium (0.25) Aluminum Silicate

Pattern : 00-041-0569 ***Radiation =*** 1.540600 ***Quality :*** Calculated

$Cs_4Al_4Si_{20}O_{48}$

Cesium Aluminum Silicate
Also called: Aluminosilicate, (Cs)

Lattice : Base-centered orthorhombic
S.G. : Ama2 (40)

a = 16.77600
b = 13.82800
c = 5.02100
a/b = 1.21319
c/b = 0.36310

Mol. weight = 1969.23
Volume [CD] = 1164.76
Dx = 2.807

Data collection flag: Ambient.

von Ballmoos, R., Higgins, J., Collection of Simulated XRD Powder Patterns For Zeolites, volume 10, page 366S (1990)

Radiation : CuKa
Lambda : 1.54180
SS/FOM : F30=336(0.0029,31)

Filter : Not specified
d-sp : Calculated spacings

2th	i	h	k	l	2th	i	h	k	l
10.542	1	2	0	0	56.392	1	10	2	0
12.790	2	0	2	0	56.612	3	3	6	2
16.607	1	2	2	0	57.091	1	5	7	1
18.785	2	0	1	1	57.191	1	8	0	2
19.525	4	1	1	1	57.851	8	3	1	3
20.414	1	3	2	0	58.140	3	8	5	1
21.163	1	4	0	0	58.330	5	10	1	1
21.593	50	2	1	1	58.869	3	8	2	2
24.661	100	3	1	1	58.919	1	1	3	3
24.810	52	4	2	0	59.559	1	8	6	0
25.750	21	0	4	0	59.759	3	2	3	3
26.229	18	0	3	1					
26.299	23	1	4	0					
26.769	39	1	3	1					
27.898	5	2	4	0					
28.337	7	2	3	1					
28.447	3	4	1	1					
29.566	10	5	2	0					
30.376	8	3	4	0					
30.785	14	3	3	1					
31.984	5	6	0	0					
32.724	19	5	1	1					
33.573	4	4	4	0					
33.943	7	4	3	1					
34.582	5	6	2	0					
35.741	10	0	0	2					
37.080	9	0	5	1					
37.320	6	5	4	0					
37.350	7	6	1	1					
*37.360	4	2	0	2					
37.480	4	1	5	1					
37.660	4	5	3	1					
38.109	13	0	2	2					
38.499	3	1	2	2					
38.659	7	2	5	1					
39.058	1	0	6	0					
39.438	1	1	6	0					
39.648	2	2	2	2					
39.778	1	7	2	0					
40.557	2	3	5	1					
41.506	5	3	2	2					
*41.506	5	6	4	0					
41.816	7	6	3	1					
41.906	6	4	0	2					
42.265	3	7	1	1					
42.385	7	3	6	0					
43.095	1	4	5	1					
*43.105	9	8	0	0					
43.994	2	4	2	2					
44.573	1	0	4	2					
44.843	5	4	6	0					
44.913	2	1	4	2					
45.932	5	2	4	2					
46.052	1	7	4	0					
46.182	2	5	5	1					
46.332	2	7	3	1					
47.041	4	5	2	2					
47.401	1	8	1	1					
47.591	6	3	4	2					
47.850	5	5	6	0					
48.710	6	6	0	2					
49.549	8	0	7	1					
49.768	2	6	5	1					
49.839	7	4	4	2					
49.869	1	1	7	1					
50.578	3	6	2	2					
50.808	1	2	7	1					
51.157	5	8	3	1					
52.346	3	3	7	1					
52.626	2	5	4	2					
52.766	3	9	1	1					
53.765	4	7	5	1					
53.965	1	0	6	2					
54.134	3	2	8	0					
54.264	1	1	6	2					
54.454	2	4	7	1					
54.534	2	7	2	2					
55.903	1	6	4	2					
56.003	1	9	4	0					
56.252	2	9	3	1					

Fig. A.8. Cesium Aluminum Silicate, Si rich

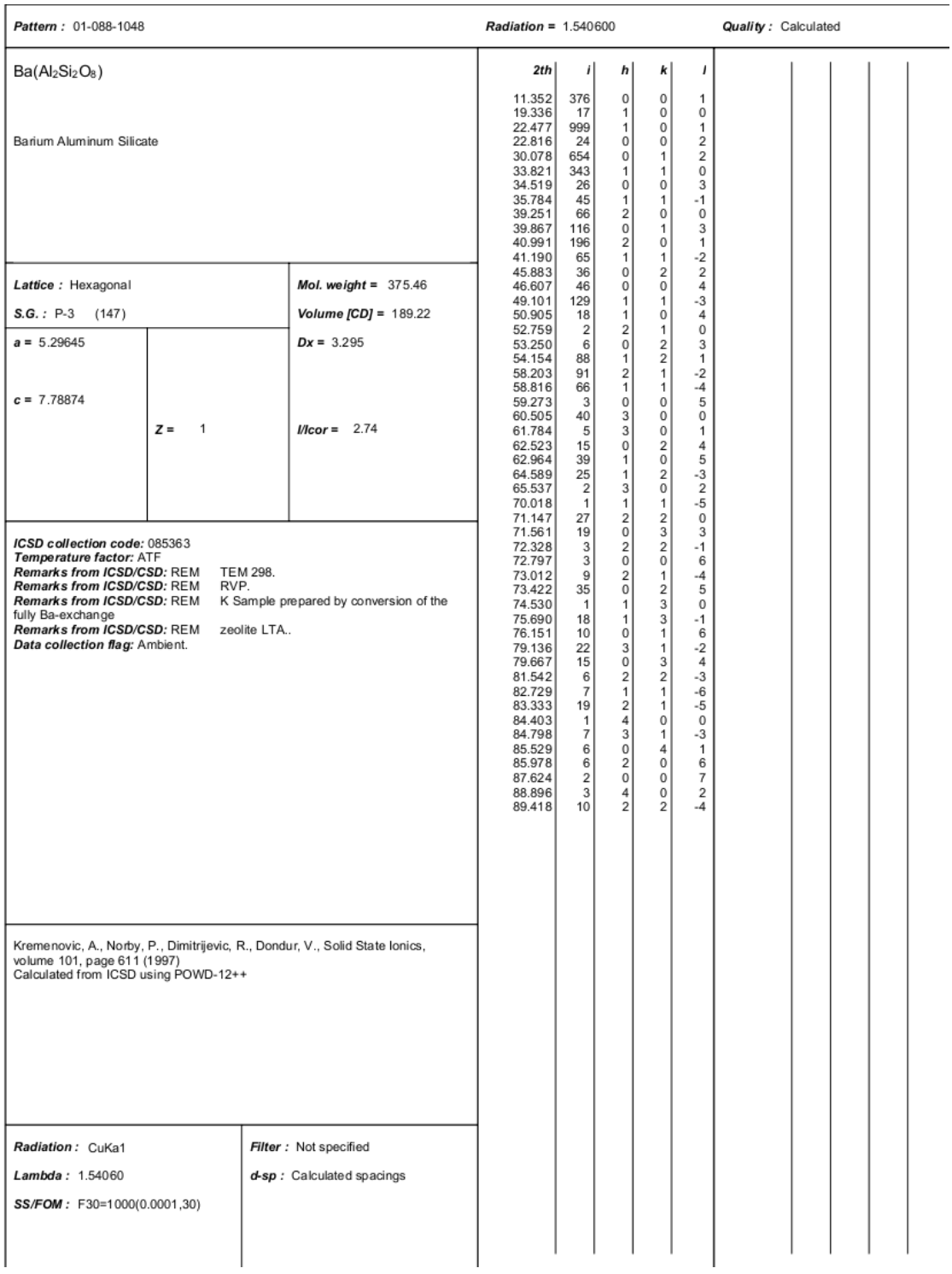

Pattern : 01-088-1048 ***Radiation =*** 1.540600 ***Quality :*** Calculated

$Ba(Al_2Si_2O_8)$

Barium Aluminum Silicate

Lattice : Hexagonal
S.G. : P-3 (147)
a = 5.29645
c = 7.78874
Z = 1
Mol. weight = 375.46
Volume [CD] = 189.22
Dx = 3.295
I/Icor = 2.74

ICSD collection code: 085363
Temperature factor: ATF
Remarks from ICSD/CSD: REM TEM 298.
Remarks from ICSD/CSD: REM RVP.
Remarks from ICSD/CSD: REM K Sample prepared by conversion of the fully Ba-exchange
Remarks from ICSD/CSD: REM zeolite LTA..
Data collection flag: Ambient.

Kremenovic, A., Norby, P., Dimitrijevic, R., Dondur, V., Solid State Ionics, volume 101, page 611 (1997)
Calculated from ICSD using POWD-12++

Radiation : CuKa1
Lambda : 1.54060
SS/FOM : F30=1000(0.0001,30)
Filter : Not specified
d-sp : Calculated spacings

2th	i	h	k	l
11.352	376	0	0	1
19.336	17	1	0	0
22.477	999	1	0	1
22.816	24	0	0	2
30.078	654	0	1	2
33.821	343	1	1	0
34.519	26	0	0	3
35.784	45	1	1	-1
39.251	66	2	0	0
39.867	116	0	1	3
40.991	196	2	0	1
41.190	65	1	1	-2
45.883	36	0	2	2
46.607	46	0	0	4
49.101	129	1	1	-3
50.905	18	1	0	4
52.759	2	2	1	0
53.250	6	0	2	3
54.154	88	1	2	1
58.203	91	2	1	-2
58.816	66	1	1	-4
59.273	3	0	0	5
60.505	40	3	0	0
61.784	5	3	0	1
62.523	15	0	2	4
62.964	39	1	0	5
64.589	25	1	2	-3
65.537	2	3	0	2
70.018	1	1	1	-5
71.147	27	2	2	0
71.561	19	0	3	3
72.328	3	2	2	-1
72.797	3	0	0	6
73.012	9	2	1	-4
73.422	35	0	2	5
74.530	1	1	3	0
75.690	18	1	3	-1
76.151	10	0	1	6
79.136	22	3	1	-2
79.667	15	0	3	4
81.542	6	2	2	-3
82.729	7	1	1	-6
83.333	19	2	1	-5
84.403	1	4	0	0
84.798	7	3	1	-3
85.529	6	0	4	1
85.978	6	2	0	6
87.624	2	0	0	7
88.896	3	4	0	2
89.418	10	2	2	-4

Fig. A.9. Barium Aluminum Silicate

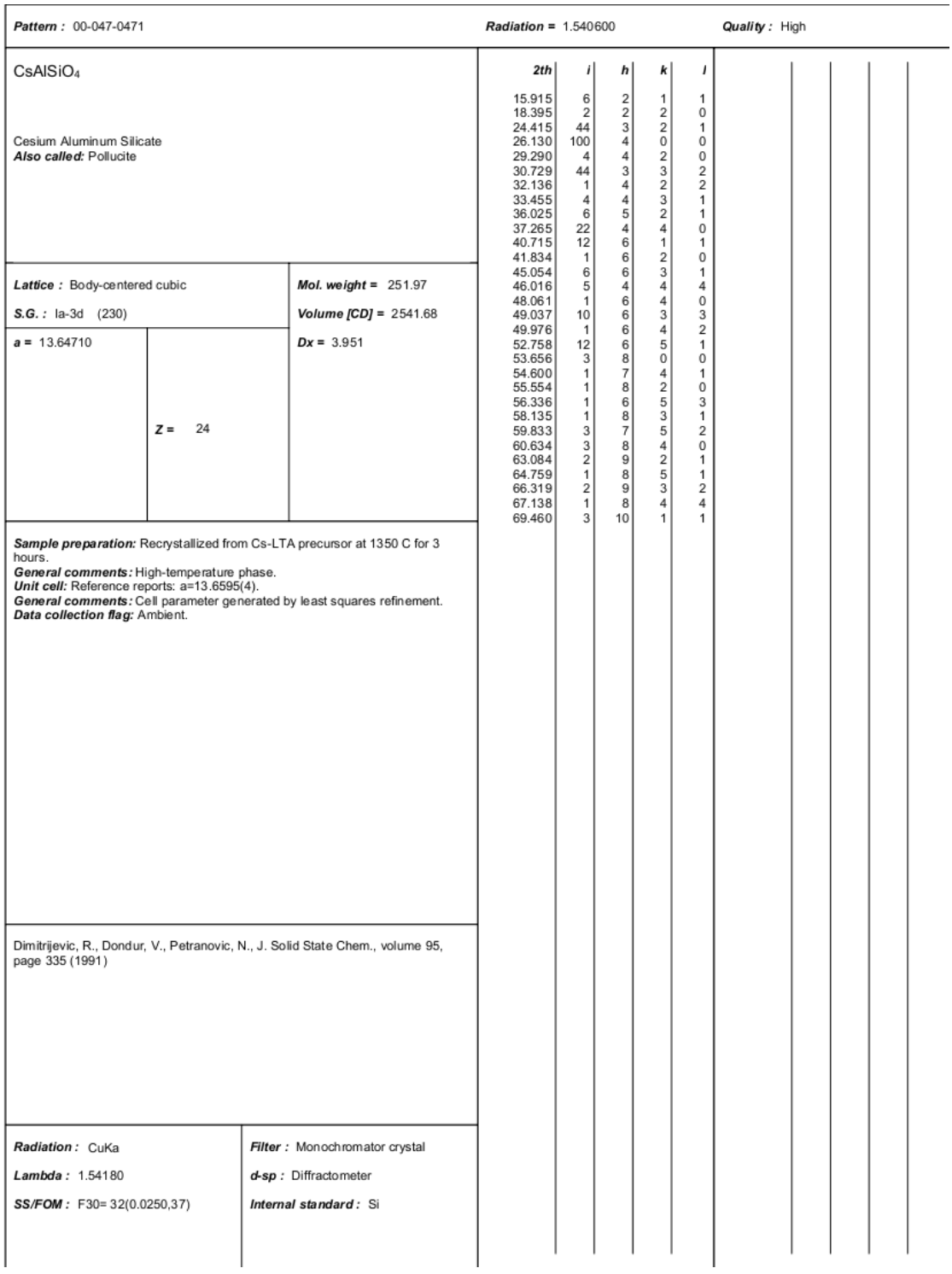

Pattern : 00-047-0471 ***Radiation =*** 1.540600 ***Quality :*** High

$CsAlSiO_4$

Cesium Aluminum Silicate
Also called: Pollucite

Lattice : Body-centered cubic
S.G. : Ia-3d (230)
a = 13.64710
Z = 24
Mol. weight = 251.97
Volume [CD] = 2541.68
Dx = 3.951

Sample preparation: Recrystallized from Cs-LTA precursor at 1350 C for 3 hours.
General comments: High-temperature phase.
Unit cell: Reference reports: a=13.6595(4).
General comments: Cell parameter generated by least squares refinement.
Data collection flag: Ambient.

Dimitrijevic, R., Dondur, V., Petranovic, N., J. Solid State Chem., volume 95, page 335 (1991)

Radiation : CuKa
Lambda : 1.54180
SS/FOM : F30= 32(0.0250,37)
Filter : Monochromator crystal
d-sp : Diffractometer
Internal standard : Si

2th	i	h	k	l
15.915	6	2	1	1
18.395	2	2	2	0
24.415	44	3	2	1
26.130	100	4	0	0
29.290	4	4	2	0
30.729	44	3	3	2
32.136	1	4	2	2
33.455	4	4	3	1
36.025	6	5	2	1
37.265	22	4	4	0
40.715	12	6	1	1
41.834	1	6	2	0
45.054	6	6	3	1
46.016	5	4	4	4
48.061	1	6	4	0
49.037	10	6	3	3
49.976	1	6	4	2
52.758	12	6	5	1
53.656	3	8	0	0
54.600	1	7	4	1
55.554	1	8	2	0
56.336	1	6	5	3
58.135	1	8	3	1
59.833	3	7	5	2
60.634	3	8	4	0
63.084	2	9	2	1
64.759	1	8	5	1
66.319	2	9	3	2
67.138	1	8	4	4
69.460	3	10	1	1

Fig. A.10. Cesium Aluminum Silicate, Pollucite

Pattern : 01-088-2487 ***Radiation =*** 1.540600 ***Quality :*** Calculated

SiO_2

Silicon Oxide
Quartz low

Lattice : Hexagonal
S.G. : P3221 (154)

a = 4.93000
c = 5.38500

Z = 3

Mol. weight = 60.08
Volume [CD] = 113.35
Dx = 2.641
I/Icor = 3.00

ICSD collection code: 041672
ICSD space group comment: ICSD SG: P3221S IT is: 154 SG short form: P3221
Remarks from ICSD/CSD: REM THE.
Remarks from ICSD/CSD: REM M PDF 46-1045.
Remarks from ICSD/CSD: REM M Calculated with pseudo-potential total-energy method.
Remarks from ICSD/CSD: REM M Experimental cell: 4.916, 5.4054.
Test from ICSD: No R value given.
Test from ICSD: At least one TF missing.
Remarks from ICSD/CSD: REM PRE Mentioned.
Data collection flag: Non ambient pressure.

Tse, J.S., Klug, D.D., Allan, D.C., Phys. Rev. B: Condens. Matter, volume 51, page 16392 (1995)
Calculated from ICSD using POWD-12++

Radiation : CuKa1
Lambda : 1.54060
SS/FOM : F28=1000(0.0001,29)

Filter : Not specified
d-sp : Calculated spacings

2th	*i*	*h*	*k*	*l*
20.788	212	1	0	0
26.623	999	0	1	1
36.419	74	1	1	0
39.538	72	1	0	2
40.202	31	1	1	-1
42.303	49	2	0	0
45.680	27	2	0	1
50.134	104	1	1	-2
50.826	4	0	0	3
54.838	33	0	2	2
55.488	14	0	1	3
57.024	2	1	2	0
59.777	77	2	1	-1
64.127	14	1	1	-3
65.538	3	3	0	0
67.630	44	1	2	2
68.089	40	0	3	1
68.206	57	2	0	3
73.733	17	1	0	4
75.500	21	3	0	2
77.363	10	2	2	0
79.865	22	1	2	-3
81.160	21	1	3	0
81.379	25	1	1	-4
83.526	11	3	1	-1
85.135	2	2	0	4
86.842	1	2	2	-2
87.377	2	3	0	3

Fig. A.11. Quartz

APPENDIX B

QUANTITATIVE WDS DETECTION LIMITS & BASIS OXIDES

Table B.1
Quantitative WDS detection limits of selected locations in 1200 °C sintered bentonite and basis oxides.

	Na	Rb	Mg	Al	Si	Ca	Sr	Fe	Cs	Ba
Detection limits										
Dark 1	0.0125	0.0203	0.0084	0.0089	0.0248	0.015	0.0874	0.0394	0.1318	0.1378
Dark 2	0.0123	0.0203	0.0084	0.0089	0.0207	0.015	0.0846	0.0393	0.1282	0.1477
Dark 3	0.0123	0.0204	0.0084	0.0089	0.0257	0.0146	0.0867	0.04	0.129	0.1359
Bright 1	0.0132	0.023	0.0098	0.0108	0.0272	0.0156	0.0894	0.0421	0.2113	0.1325
Bright 2	0.013	0.0226	0.0098	0.0106	0.0276	0.0154	0	0.0415	0.1936	0.1293
Bright 3	0.0137	0.0225	0.0099	0.0107	0.0291	0.0152	0.0843	0.0418	0.1999	0.125
Grey 1	0.0125	0.021	0.0087	0.0104	0.0247	0.0147	0.0829	0.0406	0.1311	0.1518
Grey 2	0.0126	0.0204	0.0088	0.0105	0.0246	0.0145	0.0813	0.0424	0.12	0.1499
Grey 3	0.0124	0.0202	0.0087	0.0105	0.0228	0.0142	0.0862	0.0413	0.1216	0.1439
Basis Oxides	Na_2O	Rb_2O	MgO	Al_2O_3	SiO_2	CaO	SrO	FeO	Cs_2O	BaO

APPENDIX C
STOICHIOMETRY CALCULATIONS

	STOICHIOMETRY													
MASS														
AVERAGES-- across all sinterings		70% loaded			100% loaded									
	Cesium	10.9605			Cesium	13.703		pollucite	CsAlSiO4	feldspar	Ba or Sr Al2Si2O8			
	Strontium	3.49362			Strontium	4.373		for each mole Cs or Rb 1 mole Al and 1 mole Si						
	Barium	8.93453			Barium	11.658		for each mole Sr or Ba 2 moles Al and 2 moles Si						
	Rubidium	1.54017			Rubidium	2.056								
waste mass %	total	24.9288			total	31.7913								
clay mass %	left=clay	75.0712			left=clay	68.209								
							moles we need to make feldspars/pollucite							
1000 gram basis			70% laoded		100% loaded		70%		100%					
	grams	MW	moles		moles		Al2O3	SiO2	Al2O3	SiO2				
Cs	137.03	132.906	0.82468		1.0310333		0.41234004	0.82468	0.51552	1.031033328				
Sr	43.73	87.62	0.39872		0.499087		0.3987245	0.79745	0.49909	0.998173933				
Ba	116.58	137.327	0.6506		0.8489226		0.65060282	1.30121	0.84892	1.697845289				
Rb	20.56	85.4678	0.1802		0.2405584		0.09010249	0.1802	0.12028	0.240558433				
						total	1.55176985	3.10354	1.98381	3.967610983				
Bentonite Composition		%	MW	70% loading leaves 75.07g of clay	moles 70%	100% loading 68.09g of clay	moles 100%		at our 70% and 100% loading we are lacking alumina					
	SiO2	0.6956	60.0843	750.7	8.6909046	680.9	7.8828253		this is not counting losses to Mg, Ca, Na, K etc.					
	Al2O3	0.2069	101.961		1.5233214		1.38168315							
	MgO	0.027	40.3044		0.5028955		0.4561363		excess silica in all		100% loaded		70%	
	Fe2O3	0.0485	159.69		0.2279977		0.20679848			%	0.30352		0.01833	
	CaO	0.013	56.077		0.1740304		0.15784903			moles lack	0.60212		0.02845	
	Na2O	0.0243	61.9789		0.2943261		0.26695972							
	K2O	0.003	94.2		0.0239076		0.02168471							

Fig. C.1. Stoichiometry calculations, alumina deficiencies

APPENDIX D

NEUTRON ACTIVATION DETAILS

Table D.1

Strontium concentration in sintered bentonite loaded with 100% & 70% theoretical waste ion concentrations; irradiated at 10 X 10^{13} neutrons/s·cm^2 for 60 sec, counted for 300 sec.

		Specific Activity of Sr-87			
Sintering Temp. °C	mass (g)	Wt. Mean	Standard Dev.	Strontium mass %	Std. Dev.
		100% Theoretical Loading			
700	0.1002	2.72E+01	1.55E+00	4.115	3.28E-01
800	0.1001	2.95E+01	1.68E+00	4.466	3.56E-01
1000	0.1004	3.00E+01	1.70E+00	4.539	3.62E-01
		70% Theoretical Loading			
700	0.1000	2.31E+01	1.31E+00	3.497	2.79E-01
800	0.1002	2.29E+01	1.30E+00	3.464	2.76E-01
1000	0.1002	2.32E+01	1.32E+00	3.520	2.81E-01

Table D.2

Cesium concentration in sintered bentonite loaded with 100% & 70% theoretical waste ion concentrations; irradiated at 10 X 10^{13} neutrons/s·cm^2 for 3600 sec, counted for 1200 sec.

		Specific Activity of Cs-134			
Sintering Temp. °C	mass (g)	Wt. Mean	Standard Dev.	Cesium mass %	Std. Dev.
		100% Theoretical Loading			
700	0.5	1.78E+01	2.08E-01	13.915	2.2E-01
800	0.5003	1.76E+01	2.06E+00	13.774	2.2E-01
1000	0.5003	1.72E+01	1.99E+00	13.422	2.1E-01
		70% Theoretical Loading			
700	0.5004	1.40E+01	1.82E-01	10.933	1.9E-01
800	0.5003	1.40E+01	1.68E+00	10.933	1.8E-01
1000	0.5003	1.39E+01	1.68E+00	10.847	1.8E-01

Table D.3

Rubidium mass percent in sintered bentonite loaded with 100% & 70% theoretical waste ion concentrations; irradiated at 10 X 10^{13} neutrons/s·cm^2 for 3600 sec, counted for 1200 sec.

		Specific Activity of Rb-86			
Sintering Temp. °C	mass (g)	Wt. Mean	Standard Dev.	Rubidium mass %	Std. Dev.
		100% Theoretical Loading			
700	0.5	2.16E-01	1.43E-02	2.001	1.3E-01
800	0.5003	2.43E-01	1.45E-02	2.251	1.4E-01
1000	0.5003	2.07E-01	1.50E-02	1.918	1.4E-01
		70% Theoretical Loading			
700	0.5004	1.89E-01	1.60E-02	1.751	1.5E-01
800	0.5003	1.50E-01	1.38E-02	1.387	1.3E-01
1000	0.5003	1.60E-01	1.66E-02	1.482	1.5E-01

Table D.4

Barium mass percent in sintered bentonite loaded with 100% & 70% theoretical waste ion concentrations; irradiated at 10 X 10^{13} neutrons/s·cm^2 for 3600 sec, counted for 1200 sec.

		Specific Activity of Ba-131			
Sintering Temp. °C	mass (g)	Wt. Mean	Standard Dev.	Barium mass %	Std. Dev.
		100% Theoretical Loading			
700	0.5	1.52E-01	1.07E-02	12.155	8.7E-01
800	0.5003	1.46E-01	1.79E-02	11.675	1.4E+01
1000	0.5003	1.40E-01	1.51E-02	11.195	1.2E+01
		70% Theoretical Loading			
700	0.5004	1.12E-01	1.65E-02	8.980	1.3E+00
800	0.5003	1.00E-01	1.50E-02	7.996	1.2E+00
1000	0.5003	1.23E-01	1.39E-02	9.828	1.1E+00